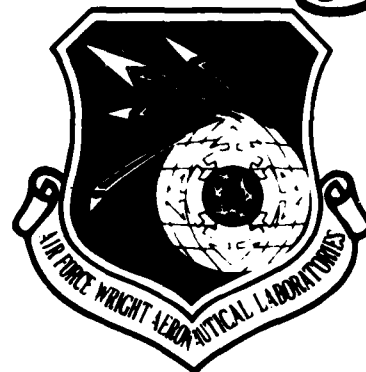AFWAL-TR-85-3102

AD-A165 891

INTRODUCTION TO ROBUST MULTIVARIABLE CONTROL

D. BRETT RIDGELY, CAPTAIN, USAF
SIVA S. BANDA

CONTROL DYNAMICS BRANCH
FLIGHT DYNAMICS LABORATORY

FEBRUARY 1986

FINAL REPORT FOR PERIOD - OCTOBER 1983 TO SEPTEMBER 1985

DTIC
ELECTE
MAR 2 5 1986
E

DTIC FILE COPY

APPROVED FOR PUBLIC RELEASE; DISTRIBUTION UNLIMITED

FLIGHT DYNAMICS LABORATORY
AIR FORCE WRIGHT AERONAUTICAL LABORATORIES
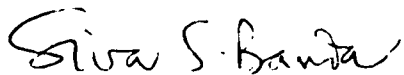**AIR FORCE SYSTEMS COMMAND**
WRIGHT-PATTERSON AIR FORCE BASE, OH 45433

86

NOTICE

When Government drawings, specifications, or other data are used for any purpose other than in connection with a definitely related Government procurement operation, the United States Government thereby incurs no responsibility nor any obligation whatsoever; and the fact that the government may have formulated, furnished, or in any way supplied the said drawings, specifications, or other data, is not to be regarded by implication or otherwise as in any manner licensing the holder or any other person or corporation, or conveying any rights or permission to manfacture use, or sell any patented invention that may in any way be related thereto.

This report has been reviewed by the Office of Public Affairs (ASD/PA) and is releasable to the National Technical Information Service (NTIS). At NTIS, it will be available to the general public, including foreign nations.

This technical report has been reviewed and is approved for publication.

SIVA S. BANDA
Project Engineer
Control Dynamics Branch

DAVID K. BOWSER, Chief
Control Dynamics Branch
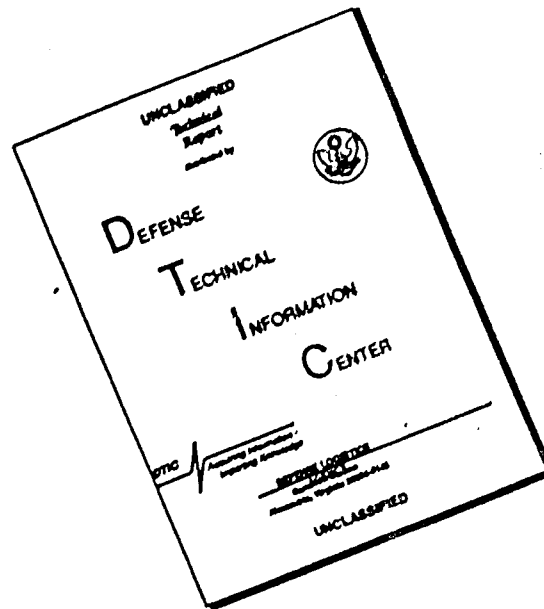Flight Control Division

FOR THE COMMANDER

H. MAX DAVIS, Assistant for
Research and Technology
Flight Control Division
Flight Dynamics Laboratory

DISCLAIMER NOTICE

THIS DOCUMENT IS BEST
QUALITY AVAILABLE. THE COPY
FURNISHED TO DTIC CONTAINED
A SIGNIFICANT NUMBER OF
PAGES WHICH DO NOT
REPRODUCE LEGIBLY.

SECURITY CLASSIFICATION OF THIS PAGE

AD-A165891

REPORT DOCUMENTATION PAGE

1a. REPORT SECURITY CLASSIFICATION	1b. RESTRICTIVE MARKINGS
Unclassified	
2a. SECURITY CLASSIFICATION AUTHORITY	3. DISTRIBUTION/AVAILABILITY OF REPORT
	Approved for Public Release;
2b. DECLASSIFICATION/DOWNGRADING SCHEDULE	Distribution unlimited.
4. PERFORMING ORGANIZATION REPORT NUMBER(S)	5. MONITORING ORGANIZATION REPORT NUMBER(S)
AFWAL-TR-85-3102	

6a. NAME OF PERFORMING ORGANIZATION	6b. OFFICE SYMBOL (If applicable)	7a. NAME OF MONITORING ORGANIZATION
Flight Dynamics Laboratory	AFWAL/FIGC	
6c. ADDRESS (City, State and ZIP Code)		7b. ADDRESS (City, State and ZIP Code)
Wright-Patterson AFB, OH 45433-6553		

8a. NAME OF FUNDING/SPONSORING ORGANIZATION	8b. OFFICE SYMBOL (If applicable)	9. PROCUREMENT INSTRUMENT IDENTIFICATION NUMBER

8c. ADDRESS (City, State and ZIP Code)	10. SOURCE OF FUNDING NOS.			
	PROGRAM ELEMENT NO.	PROJECT NO.	TASK NO.	WORK UNIT NO.
	61102F	2304	N3	17

11. TITLE (Include Security Classification) INTRODUCTION TO ROBUST MULTIVARIABLE CONTROL

12. PERSONAL AUTHOR(S)
Capt D. Brett Ridgely and Siva S. Banda

13a. TYPE OF REPORT	13b. TIME COVERED	14. DATE OF REPORT (Yr., Mo., Day)	15. PAGE COUNT
Final Report	FROM Oct 83 TO Sept 85	86 February	458

16. SUPPLEMENTARY NOTATION

17.	COSATI CODES		18. SUBJECT TERMS (Continue on reverse if necessary and identify by block number)
FIELD	GROUP	SUB. GR.	Linear Control Systems, Robust Control, Multivariable Control
17	01		Optimal Control, Loop Transfer Recovery, Robustness Analysis,
			Roll Attitude Control, Singular Values, LQG/LTR

19. ABSTRACT (Continue on reverse if necessary and identify by block number)
Linear multiple-input multiple-output (multivariable) control systems are considered. The intent of this report is to familiarize the working engineers with some of the developments in the area of robust multivariable control theory that have occurred in the past 10 years. The concepts of singular values are used to systematically develop robust control systems analysis and design techniques. The advantages and limitations of these techniques are discussed. Examples are used to illustrate the methods.

20. DISTRIBUTION/AVAILABILITY OF ABSTRACT	21. ABSTRACT SECURITY CLASSIFICATION
UNCLASSIFIED/UNLIMITED ☐ SAME AS RPT ☒ DTIC USERS ☐	Unclassified

22a. NAME OF RESPONSIBLE INDIVIDUAL	22b. TELEPHONE NUMBER (Include Area Code)	22c. OFFICE SYMBOL
SIVA S. BANDA	(513) 255-8677	AFWAL/FIGC

DD FORM 1473, 83 APR   EDITION OF 1 JAN 73 IS OBSOLETE.   UNCLASSIFIED

FOREWORD

TABLE OF CONTENTS

1. INTRODUCTION

This technical report is a set of lecture notes for a course taught by the authors during the spring of 1985, to engineers in the Flight Dynamics Laboratory and students at the Air Force Institute of Technology. The intent of this course was to familiarize the working engineers with some of the developments in the area of robust multivariable control theory that have occurred in the past 10 years. To the knowledge of the authors, there is no textbook or single report in the open literature covering all the material contained in this report.

The emphasis of this report (and the course) is on robustness analysis and design techniques for multiple-input, multiple-output control systems. Chapter 2 is divided into two parts. The first part gives the necessary mathematical background, including the notion of singular values. In the second part, some of the required fundamentals from linear systems theory are reviewed. Chapter 3 discusses robustness analysis methods given the information about the plant and the controller. The concepts of singular values are used in Chapter 4 to define good multivariable control loop shapes; performance limitations for multivariable systems are discussed in Chapter 5. The material discussed in Chapters 3, 4, and 5 is independent of the techniques that one may use in designing the controllers.

The remainder of the report concentrates on developing and applying the Linear Quadratic Gaussian with Loop Transfer Recovery (LQG/LTR) methodology, which is one particular robust control design method. Since this method is based upon optimal control theory, a brief review of necessary key concepts is given in Chapter 6. The underlying ideas

of LQG/LTR are explained in Chapters 7 and 8. Chapters 9 and 10 utilize the background material from Chapters 4-8 and formally present the LQG/LTR methodology. A method of matching the singular values of the loop transfer matrix and a formal procedure for loop shaping are discussed in Chapter 11. The mathematical relationship between the LQG/LTR method and L_2/H_2 optimization is explained in detail in Chapter 12. Several controllers are designed for lateral attitude control of a drone aircraft using LQG/LTR methodology in Chapter 13. Summary and conclusions are contained in Chapter 14.

The material contained in Chapters 3 and 13 is claimed to be the original work of the authors and their colleagues. The rest of the material in this report was collected and compiled from various journal articles, conference papers, and textbooks. The reference material that was used in preparing a particular chapter is given at the end of each chapter. It is needless to say that there are numerous other publications in this area of controls research that are not brought up in this report.

In preparing this report, special emphasis was placed on using a uniform notation. This report is only intended to serve as an introduction to the topic of robust multivariable control. It is not possible to treat each and every design method and analysis tool in this area of research comprehensively in a single report. Finally, even though most of the material in this report comes from publications of various researchers, the authors accept responsibility for any inaccuracies in this report.

2. MATHEMATICAL PRELIMINARIES AND INTRODUCTION

TO LINEAR SYSTEMS

We divide this chapter into two sections, the first on mathematical preliminaries and the second an introduction to linear systems. These sections are by no means comprehensive. We have made an attempt to cover almost all the prerequisites that one needs to follow the rest of the chapters. In the first section we explain the properties of matrices, eigenvalues, eigenvectors, singular values, singular vectors and norms of vectors and matrices. In the second section we explain some of the basic linear systems analysis tools both in the time and frequency domains. There is no single textbook that gives all the information contained in this chapter. We have used several texts and journal papers in preparing this material. A list of these references and a few other suggested readings are given at the end of this chapter.

2.1 Mathematical Preliminaries

2.1-1 Matrix Operations, Properties, and Forms

Principal Diagonal - consists of the m_{ii} elements of a square matrix M.

Diagonal Matrix - a square matrix in which all elements off the principal diagonal are zero.

Trace - sum of all the elements on the principal diagonal of a square matrix

$$\text{trace } M = \sum_{i=1}^{n} m_{ii} \tag{2.1}$$

Determinant - denoted by det|M| or $|M|$, definition given in any linear algebra book.

Singular matrix - a square matrix whose determinant is zero.

Minor – the minor M_{ij} of a square matrix M is the determinant formed after the ith row and jth column are deleted from M.

Principal Minor – a minor whose diagonal elements are also diagonal elements of the original matrix.

Cofactor – a signed minor given by

$$c_{ij} = (-1)^{i+j} M_{ij} \tag{2.2}$$

Adjoint Matrix – the adjoint of M, denoted by adj[M], is the transpose of the cofactor matrix. The cofactor matrix is formed by replacing each element of M by its cofactor.

Inverse Matrix – inverse of M is denoted by M^{-1}, has the property $MM^{-1} = M^{-1}M = I$, and is given by

$$M^{-1} = \text{adj}[M]/\,|M| \tag{2.3}$$

Rank of a Matrix – the rank r of a matrix M (not necessarily square) is the order of the largest square array contained in M which has nonzero determinant.

Transpose of a Matrix – denoted by M^T, it is the original matrix with its rows and columns interchanged, i.e. $m'_{ij} = m_{ji}$.

Symmetric Matrix – a matrix containing only real elements which satisfies $M = M^T$.

Transpose of a product of matrices –

$$(AB)^T = B^T A^T \tag{2.4}$$

Inverse of a product of matrices –

$$(AB)^{-1} = B^{-1}A^{-1} \tag{2.5}$$

(Complex) Conjugate – the conjugate of a scalar $a = \alpha + j\beta$ is $a^* = \alpha - j\beta$. The conjugate of a vector or matrix simply replaces each element of the vector or matrix with its conjugate, denoted by m^* or M^*.

Hermitian matrix – a matrix which satisfies

$$M = M^H \tag{2.6}$$

where superscript H stands for Hermite. The operation of Hermite is simply complex conjugate transposition - usually, * is used in place of H.

Unitary Matrix - a complex matrix U is unitary if $U^H = U^{-1}$.

Orthogonal Matrix - a real matrix R is orthogonal if $R^T = R^{-1}$.

2.1-2 Eigenvalues and Eigenvectors

Let A be an $(n \times n)$ matrix, and v_i be an $(n \times 1)$ vector. The eigenvalue problem is

$$[\lambda_i I - A] v_i = 0 \tag{2.7}$$

Solution of

$$\det[\lambda I - A] = 0 \tag{2.8}$$

gives the eigenvalues $\lambda_1, \lambda_2, \ldots, \lambda_n$. Given λ_i, the non-trivial solution v_i of (2.7) is called an eigenvector. We also refer to $v_1, v_2, \ldots, v_n$ as right eigenvectors. These are said to lie in the null space of the matrix $[\lambda_i I - A]$. The eigenvectors obtained from

$$v_i^T [\lambda_j I - A] = 0 \tag{2.9}$$

are referred to as left eigenvectors. Left and right eigenvectors are orthogonal to each other, that is,

$$v_i^T v_j = \begin{cases} 1 & \text{for } i = j \\ 0 & \text{for } i \neq j \end{cases} \tag{2.10}$$

If the eigenvalues of A are distinct, then A can be written as

$$A = T \Lambda T^{-1} \tag{2.11}$$

where Λ is a diagonal matrix containing the eigenvalues. This is called an eigenvector decomposition (EVD). T is called a modal matrix.

The columns of T are the right eigenvectors v_i and the rows of T^{-1} are the left eigenvectors w_i^T. Thus

$$T = [\, v_1 \quad v_2 \ldots v_n \,], \qquad T^{-1} = [\, w_1^T \quad w_2^T \ldots w_n^T \,]^T$$

Note that (2.10) is true since we know $T^{-1}T = I$. Finding T for the case of repeated eigenvalues is omitted here (for more information see ref [2-1]).

Some properties of eigenvalues

    1. All the eigenvalues of a Hermitian matrix are real.

    2. All the eigenvalues of a unitary matrix have unit magnitude.

    3. If a matrix A is Hermitian, then the modal matrix T in (2.11) is unitary. EVD is then

$$A = U \Lambda U^H \qquad (2.12)$$

since $U^{-1} = U^H$.

    4. If A is Hermitian, then

$$\min_{x \neq 0} \frac{x^H A x}{x^H x} = \lambda_{\min}(A) \qquad (2.13)$$

and

$$\max_{x \neq 0} \frac{x^H A x}{x^H x} = \lambda_{\max}(A) \qquad (2.14)$$

The quantity $\frac{x^H A x}{x^H x}$ is called the Rayleigh's quotient. Sometimes we are not interested in the complete solution of the eigenvalue problem (i.e. all the eigenvalues and eigenvectors). We may want an estimate of the first mode. One of the nice properties of Rayleigh's quotient is that it is never smaller than $\lambda_{\min}(A)$. Also, the minimum of the left-hand side of (2.13) is achieved when x is the eigenvector corresponding to $\lambda_{\min}$. Similarly, the maximum is achieved in (2.14) when x is the eigenvector corresponding to $\lambda_{\max}(A)$. Eq (2.13) is particularly useful

in the modal analysis of structures represented by finite element
models.

Some more properties (see Ref [2-12])

1. If A is (rxm) and B is (mxn) , then

   AB is (nxn) and is singular if $n > m$ (2.15)

2. If A is (nxm), B is (mxp) and C is (pxn), then

   ABC is (nxn) and is singular if $n > m$ or $n > p$ (2.16)

3. A is singular iff $\lambda_i(A) = 0$ for some i (2.17)

4. $\lambda(A) = 1/ \lambda(A^{-1})$ (2.18)

5. $\lambda(\alpha A) = \alpha \lambda(A)$, α is scalar (2.19)

6. $\lambda(I+A) = 1+ \lambda(A)$ (2.20)

2.1-3 Some useful matrix identities (see Ref [2-13])

1. $[I_n + C_2 C_1 H_2 H_1]^{-1} C_2 C_1 = C_2 [I_m + C_1 H_2 H_1 C_2]^{-1} C_1$

$$= C_2 C_1 [I_r + H_2 H_1 C_2 C_1]^{-1}$$

$$= C_2 C_1 - C_2 C_1 H_2 [I_p + H_1 C_2 C_1 H_2]^{-1} H_1 C_2 C_1 \qquad (2.21)$$

where C_1 is (mxr), C_2 is (nxm), H_1 is (pxn), and H_2 is (rxp).
For the following three identities, the dimensions of matrices P, K, and
C are: I is (nxn), K is (nxr) and C is (rxn)

2. $(P^{-1} + KC)^{-1} = P - PK(I + CPK)^{-1} CP$ (2.22)

3. $(I + KCP)^{-1} = I - K(I + CPK)^{-1} CP$ (2.23)

4. $(I + PKC)^{-1} = I - PK(I + CPK)^{-1} C$ (2.24)

2.1-4 Definiteness of Matrices

If all the real parts of the eigenvalues of matrix A are >0, then A is
said to be positive definite.

If all the real parts of the eigenvalues of matrix A are ≥ 0, then A is
said to be positive semidefinite.

If all the real parts of the eigenvalues of $-A$ are >0, then A is said to be _negative definite_.

If all the real parts of the eigenvalues of $-A$ are $\geqslant 0$, then A is said to be _negative semidefinite_.

If some of the real parts of the eigenvalues of A are positive and some negative, then A is said to be _indefinite_.

2.1-5 Singular values

Let us first define inner product and norms of vectors.

Inner Product – The inner product is also called a scalar (or dot) product since it yields a scalar function. The inner product of complex vectors x and y is defined by

$$\langle x,y \rangle = (x^*)^T y = y^T x^* = x_1^* y_1 + x_2^* y_2 + \ldots + x_n^* y_n = \sum_{i=1}^{n} x_i^* y_i \quad (2.25)$$

where $(.)^*$ indicates complex conjugate of the vector in parenthesis.

If x and y are real, then

$$\langle x,y \rangle = \sum_{i=1}^{n} x_i y_i = x_1 y_1 + x_2 y_2 + \ldots + x_n y_n \quad (2.26)$$

Note that when x and y are complex $\langle x,y \rangle = y^T v^*$. However, when x and y are real

$$\langle y,y \rangle = x^T v = v^T x = \langle v,x \rangle \quad (2.27)$$

Norm or Length of a vector – The length of a vector x is called the Euclidean norm and is (also known as ℓ_2 norm)

$$\|x\|_F = \|x\|_2 = \sqrt{\langle x,x \rangle} = \sqrt{x_1^2 + x_2^2 + \ldots + x_n^2} \quad (2.28)$$

Definition of spectral norm or ℓ_2 norm of a matrix is given by

$$\|A\|_2 = \max_{x \neq 0} \frac{\|Ax\|_2}{\|x\|_2} \qquad \text{where } A \in C^{m \times n} \quad (2.29)$$

It turns out that

$$\|A\|_2 = \max_i \sqrt{\lambda_i(A^H A)} \quad , \quad i=1,2,\ldots,r$$
$$= \max_i \sqrt{\lambda_i(AA^H)} \quad , \quad i=1,2,\ldots,m \quad (2.30)$$

2-6

Note that $A^H A$ and AA^H are Hermitian and positive semidefinite and hence eigenvalues of $A^H A$ and AA^H are always real and non-negative. If A is nonsingular, $A^H A$ is positive definite, and the eigenvalues of $A^H A$ and AA^H are all positive.

We now introduce the notion of <u>singular values</u> of complex matrices. These are denoted by the symbol σ. If $A \in C^{n \times n}$, then

$$\sigma_i(A) = \sqrt{\lambda_i(A^H A)} = \sqrt{\lambda_i(AA^H)} \geq 0 \qquad i=1,2,\ldots,n \qquad (2.31)$$

and they are all non-negative since $A^H A$ and AA^H are Hermitian. If A is non-square, i.e., $A \in C^{m \times n}$, then

$$\sigma_i(A) = \sqrt{\lambda_i(A^H A)} = \sqrt{\lambda_i(AA^H)} \qquad (2.32)$$

for $1 \leq i \leq k$, where k = number of singular values = $\min(m,n)$ and $\sigma_1(A) \geq \sigma_2(A) \geq \ldots \geq \sigma_k(A)$. From (2.30) and (2.31), we have

$$\sigma_{max}(A) = \max_{x \neq 0} \frac{\|Ax\|_2}{\|x\|_2} = \|A\|_2 \qquad (2.33)$$

It can be shown that

$$\sigma_{min}(A) = \min_{x \neq 0} \frac{\|Ax\|_2}{\|x\|_2} = \frac{1}{\|A^{-1}\|_2} \qquad (2.34)$$

provided A^{-1} exists. Thus the maximum singular value of A, $\sigma_{max}(A)$ is simply the spectral norm of A. The spectral norm of A^{-1} is the inverse of $\sigma_{min}(A)$, the minimum singular value of A. The spectral norm is also known as the ℓ_2 norm. Usually we will write $\bar{\sigma}(A)$ and $\underline{\sigma}(A)$ to indicate $\sigma_{max}(A)$ and $\sigma_{min}(A)$.

It follows that

$$\sigma_{max}(A^{-1}) = \|A^{-1}\|_2 = 1/\sigma_{min}(A) \qquad (2.35)$$

$$\sigma_{min}(A^{-1}) = 1/\|A\|_2 = 1/\sigma_{max}(A) \qquad (2.36)$$

$$\sigma_{min}(A) = 0 \qquad \text{if A is singular.} \qquad (2.37)$$

Let us now introduce the <u>singular value decomposition</u> (SVD). Given any (nxn) complex matrix A, there exist unitary matrices U and V such that

$$A = U \Sigma V^H = \sum_{i=1}^{n} \sigma_i(A) \, u_i v_i^H \tag{2.38}$$

where Σ is a diagonal matrix containing the singular values $\sigma_i(A)$ arranged in descending order, u_i are the column vectors of U, i.e.,

$$U = [u_1, u_2, \ldots, u_n] \tag{2.39}$$

and v_i are the column vectors of V, i.e.,

$$V = [v_1, v_2, \ldots, v_n] \tag{2.40}$$

The v_i are called the <u>right singular vectors of A</u> or the right eigenvectors of $A^H A$ because

$$A^H A v_i = \sigma_i^2(A) v_i \tag{2.41}$$

The u_i are called the <u>left singular vectors of A</u> or the left eigenvectors of $A^H A$ because

$$u_i^H A^H A = \sigma_i^2(A) u_i^H \tag{2.42}$$

For completeness let us also state the SVD for non-square matrices. If A is an (mxn) complex matrix, then the SVD of A is given by:

$$A = U \Sigma V^H = \sum_{i=1}^{k} \sigma_i(A) u_i v_i^H \tag{2.43}$$

where

$$U = [u_1, u_2, \ldots, u_m] \tag{2.44}$$

$$V = [v_1, v_2, \ldots, v_n] \tag{2.45}$$

and Σ contains a diagonal nonnegative definite matrix Σ_1 of singular values arranged in descending order in the form

$$\Sigma = \begin{bmatrix} \Sigma_1 \\ 0 \end{bmatrix} \quad \text{if } m > n \tag{2.46}$$

$$[\Sigma_1 \quad 0] \quad \text{if } m < n$$

Let us digress momentarily now and point out an important property of unitary matrices. Recall that a complex matrix A is defined to be unitary if $A^H = A^{-1}$. Then $AA^H = AA^{-1} = I$. Therefore, $\lambda_i(AA^H) = 1$ for all i, and

$$\|A\|_2 = \bar{\sigma}(A) = \underline{\sigma}(A) = 1 \qquad (2.47)$$

Therefore, the (ℓ_2) norm of a unitary matrix is unity. Thus, <u>unitary matrices are norm invariant</u> (if we multiply any matrix by a unitary matrix, it will not change the norm of that matrix).

Finally, the <u>condition number</u> of a matrix A is given by

$$\text{cond}(A) = \underline{\sigma}(A) / \bar{\sigma}(A) \qquad (2.48)$$

If the condition number of a matrix is close to zero, it indicates the ill-conditioning of that matrix, which implies inversion of A may produce erroneous results.

<u>2.1-6 Some useful singular value properties</u>

1. If $A, E \in C^{m \times n}$, and $\det(A+E) > 0$, then $\bar{\sigma}(E) < \underline{\sigma}(A)$ $\qquad$ (2.49)

2. $\sigma_i(\alpha A) = |\alpha| \, \sigma_i(A)$, $\alpha \in C$, $A \in C^{m \times n}$ $\qquad$ (2.50)

3. $\bar{\sigma}(A + B) \leq \bar{\sigma}(A) + \bar{\sigma}(B)$, $A, B \in C^{m \times m}$ $\qquad$ (2.51)

4. $\bar{\sigma}(AB) \leq \bar{\sigma}(A)\bar{\sigma}(B)$, $A \in C^{m \times k}$, $B \in C^{k \times n}$ $\qquad$ (2.52)

5. $\underline{\sigma}(AB) \geq \underline{\sigma}(A)\underline{\sigma}(B)$, $A \in C^{m \times k}$, $B \in C^{k \times n}$ $\qquad$ (2.53)

6. $\left| \underline{\sigma}(A) - \underline{\sigma}(B) \right| \leq \sigma(A-B)$, $A, B \in C^{m \times n}$ $\qquad$ (2.54)

7. $\underline{\sigma}(A) - 1 \leq \underline{\sigma}(I + A) \leq \underline{\sigma}(A) + 1$, $A \in C^{n \times n}$ $\qquad$ (2.55)

8. $\underline{\sigma}(A) \leq \left| \lambda_i(A) \right| \leq \bar{\sigma}(A)$, $A \in C^{n \times n}$ $\qquad$ (2.56)

9. $\underline{\sigma}(A) - \bar{\sigma}(B) \leq \underline{\sigma}(A + B) \leq \underline{\sigma}(A) + \bar{\sigma}(B)$, $A, B \in C^{n \times n}$ $\qquad$ (2.57)

10. $\left| \underline{\sigma}(A) - \underline{\sigma}(B) \right| \leq \bar{\sigma}(A + B)$, $A, B \in C^{m \times n}$ $\qquad$ (2.58)

11. $\underline{\sigma}(A) - \bar{\sigma}(B) \leq \underline{\sigma}(A - B) \leq \underline{\sigma}(A) + \bar{\sigma}(B)$ $\qquad$ (2.59)

12. Rank (A) = the number of nonzero singular values of A $\qquad$ (2.60)

13. $\sigma_i(A^H) = \sigma_i(A)$, $A \in C^{m \times n}$ $\qquad$ (2.61)

14. $\bar{\sigma}(A) \leq \sqrt{\text{trace}(A^H A)} \leq \sqrt{n}\ \bar{\sigma}(A),\ A \in C^{mxn}$ (2.62)

15. $\text{trace}(A^H A) = \sum_{i=1}^{k} \sigma_i^2(A),\ k = \min(m,n),\ A \in C^{mxn}$ (2.63)

16. $\det(A^H A) = \prod_{i=1}^{k} \sigma_i^2(A),\ k = \min(m,n),\ A \in C^{mxm}$ (2.64)

17. $\sigma_i(AB) \neq \sigma_i(BA)$ in general for all i

$$A \in C^{nxn},\ B \in C^{nxm}$$ (2.65)

18. $\bar{\sigma}(A)\underline{\sigma}(B) \leq \bar{\sigma}(AB)$ for $A \in C^{mxn}$, $B \in C^{nx\ell}$, $n \leq \ell$ only (2.66)

19. $\underline{\sigma}(A)\bar{\sigma}(B) \leq \bar{\sigma}(AB)$ for $A \in C^{mxn}$, $B \in C^{nx\ell}$, $n \leq m$ only. (2.67)

20. $\underline{\sigma}(AB) \leq \bar{\sigma}(A)\underline{\sigma}(B)$ for $A \in C^{mxn}$, $B \in C^{nx\ell}$

and no restrictions on m, n, and ℓ (2.68)

21. $\underline{\sigma}(AB) \leq \underline{\sigma}(A)\bar{\sigma}(B)$ for $A \in C^{mxn}$, $B \in C^{nx\ell}$

and no restrictions on m, n, and ℓ (2.69)

From the above formulas, the following four inequalities can be deduced.

22. $\left|\underline{\sigma}(A) - \underline{\sigma}(B)\right| \leq \bar{\sigma}(A + B) \leq \bar{\sigma}(A) + \bar{\sigma}(B)$ (2.70)

23. $\left|\underline{\sigma}(A) - \underline{\sigma}(B)\right| \leq \bar{\sigma}(A - B) \leq \bar{\sigma}(A) + \bar{\sigma}(B)$ (2.71)

24. If B is square or has more columns than rows,

$$\underline{\sigma}(A)\underline{\sigma}(B) \leq \underline{\sigma}(AB) \leq \bar{\sigma}(A)\underline{\sigma}(B) \leq \bar{\sigma}(AB) < \bar{\sigma}(A)\bar{\sigma}(B)$$ (2.72)

25. If A is square or has more rows than columns,

$$\underline{\sigma}(A)\underline{\sigma}(B) \leq \underline{\sigma}(AB) \leq \underline{\sigma}(A)\bar{\sigma}(B) \leq \bar{\sigma}(AB) \leq \bar{\sigma}(A)\bar{\sigma}(B)$$ (2.73)

So far, we have stated many properties without proofs. For a change, let us give few properties with proofs.

Later in these notes we will see several robustness tests for multi-input multi-output control systems involving the quantities $\underline{\sigma}(I+G(jw))$ and $\underline{\sigma}(I+G^{-1}(jw))$, where $G(jw)$ is a loop transfer matrix (later we will use $G(jw)K(jw)$). First let us prove the following matrix identity for any square complex matrix $G(jw)$

$$(I + G)^{-1} + (I + G^{-1})^{-1} = I,\ G \in C^{nxn}$$ (2.74)

To prove (2.74), consider the identity

$$I + G = G + G$$

$$I + G = G(I + G^{-1})$$

$$(I + G)(I + G^{-1})^{-1} = G$$

$$I + (I + G)(I + G^{-1})^{-1} = I + G$$

$$(I + G)(I + G)^{-1} + (I + G)(I + G^{-1})^{-1} = I + G$$

$$(I + G)^{-1} + (I + G)^{-1}(I + G)(I + G^{-1})^{-1} = I$$

$$(I + G)^{-1} + (I + G^{-1})^{-1} = I$$

which is (2.74).

We can now prove the following useful inequalities.

$$\bar{\sigma}[(I + G)^{-1}] + \bar{\sigma}[(I + G^{-1})^{-1}] \geq 1 \tag{2.75}$$

$$\bar{\sigma}[(I + G)^{-1}] + 1 \geq \bar{\sigma}[(I + G^{-1})^{-1}] \tag{2.76}$$

$$\bar{\sigma}[(I + G^{-1})^{-1}] + 1 \geq \bar{\sigma}[(I + G)^{-1}] \tag{2.77}$$

$$\bar{\sigma}(G) \geq \underline{\sigma}(I + G) / \underline{\sigma}(I + G^{-1}) \geq \underline{\sigma}(G) \tag{2.78}$$

To prove (2.75), recall from (2.51) that

$$\bar{\sigma}(A) + \bar{\sigma}(B) \geq \bar{\sigma}(A + B)$$

Letting $A = (I + G)^{-1}$ and $B = (I + G^{-1})^{-1}$, and noting that $A + B = I$ from (2.74), we get (2.75).

To prove (2.76), recall from (2.71) that

$$\bar{\sigma}(A - B) \leq \bar{\sigma}(A) + \bar{\sigma}(B)$$

Letting $A = I$ and $B = (I + G)^{-1}$, plus the fact that $A - B = I - (I + G)^{-1} = (I + G^{-1})^{-1}$ from (2.74), we get (2.76).

Letting $A = I$ and $B = (I + G^{-1})^{-1}$, the argument above proves (2.77).

To prove (2.78), first notice that the terms in the center of the inequality relate to the terms in (2.75)-(2.77) through the relation

$$\underline{\sigma}(A) = 1 / \bar{\sigma}(A^{-1}) \tag{2.79}$$

which is obvious from (2.34) and (2.35). Looking at the left inequality, we may prove it by considering (2.69) in the form

$$\bar{\sigma}(B) \geqslant \underline{\sigma}(AB) / \underline{\sigma}(A)$$

Letting $A = (I + G^{-1})$ and $B = G$, and realizing that

$AB = (I + G^{-1})G = I + G$, we have the left side. For the right, consider

(2.53) in the form

$$\underline{\sigma}(AB) / \underline{\sigma}(A) \geqslant \underline{\sigma}(B)$$

Using A and B as above, we have the right-hand side.

2.1-7 Other Norms

The following table summarizes various norms, such as ℓ_1, ℓ_2, ℓ_∞, L_2 and L_∞ for vectors and matrices. The L_2 and L_∞ norms are also referred to as H_2 and H_∞ norms.

Table 2.1

NORM TYPE	VECTOR $x(jw)$	MATRIX $G(jw)$
ℓ_1	$\sum_i \lvert x_i \rvert$	$\max_j \sum_i \lvert g_{ij} \rvert$ (max col sum of $\lvert G \rvert$)
ℓ_2	$\left[\sum_i \lvert x_i \rvert^2 \right]^{\frac{1}{2}}$	$\bar{\sigma}(G)$
ℓ_∞	$\max_i \lvert x_i \rvert$	$\max_i \sum_j \lvert g_{ij} \rvert$ (max row sum of $\lvert G \rvert$)
L_2 or H_2	$\left[\frac{1}{2\pi} \int_{-\infty}^{\infty} \sum_i \lvert x_i \rvert^2 \, dw \right]^{\frac{1}{2}}$	$\left[\frac{1}{2\pi} \int_{-\infty}^{\infty} \text{trace}(G*G) \, dw \right]^{\frac{1}{2}}$
L_∞ or H_∞	$\left[\sup_\omega \sum_i \lvert x_i \rvert^2 \right]^{\frac{1}{2}}$	$\sup_\omega \bar{\sigma}(G)$

It is useful to know that the ℓ_2 norm of matrices is also known as the spectral norm or Hilbert norm. Obviously, for a given matrix, different norms give different values. However, it can be shown that any norm of a matrix cannot be smaller than the spectral radius of that matrix, that is,

2-12

$$\left\|A\right\|_{\text{any norm}} \geq \rho(A) \tag{2.80}$$

where

$$\rho(A) = \text{spectral radius of } A$$
$$= \max_i \left|\lambda_i(A)\right| \tag{2.81}$$

2.2 Linear System Fundamentals

2.2-1 State Variables

One way of constructing a mathematical model for a physical system is to use a state variable description. Typically, for aerospace systems we use positions, velocities, angular positions and angular rates as state variables. The mathematical models we obtain using state variables are called state models or state space models.

There are other ways of constructing math models for physical processes. For example, we can use 1) impulse response models, 2) step response models, 3) high order differential equation models relating system inputs and outputs, or 4) transfer function representations of the models (limited to linear time-invariant systems).

State variable descriptions are valid for linear or nonlinear, time-invariant or time-variant systems. They have become popular because most of modern system theory, i.e., optimal control theory and estimation theory, relies heavily upon state variable representation. The transfer function approach (better known as the frequency domain approach) is also very elegant, in that many of the classical design specifications (such as the bandwidth and shaping of the loop-transfer function) are very explicit in the frequency domain. These specifications are not easily represented in the state variable approach (better known as the time-domain approach). On the other hand, the state space approach handles multiple-input multiple-output systems with ease,

2-13

whereas classical frequency domain approaches do not. Therefore, knowledge of both time domain and frequency domain approaches is essential to take advantage of the best of both worlds, thus resulting in the best designs.

2.2-2 Solution of State Equations

Consider the following linear time-invariant state space model

$$dx(t)/dt = \dot{x}(t) = Ax(t) + Bu(t) \qquad (2.82)$$

$$y(t) = Cx(t) \qquad (2.83)$$

where x, u and y represent the state, input and output vectors respectively. A, B and C are constant matrices and are referred to as the plant matrix, input distribution matrix and output distribution matrix, respectively. The dimensions of these vectors and matrices will be shown explicitly when needed. For right now, let's just say that all the dimensions are compatible. Equation (2.82) is called the state equation and (2.83) is called the output equation. In general, a deterministic state model may contain an additional term $Du(t)$ in (2.83). Also, we may have an additional equation such as $z(t) = Hx(t)$ representing measurements. The output variables y (sometimes known as response variables) may need to be controlled with u even though the available measurements are z. For our discussion, we will assume that we can measure all the response variables that we wish to control. A stochastic state space model may contain two noise terms, one in the state equation and another in the measurement equation. These noise terms are known as process and measurement noise, respectively. We will ignore these noise terms for right now.

Before we obtain the complete solution of the state equation (2.82), we must first obtain the homogeneous solution. The state equation without the forcing function (i.e., $u = 0$) is

$$\dot{x} = Ax \qquad (2.84)$$

For notational brevity we will not show the independent variable t from now on, unless it is necessary. Analogous to the solution of a scalar differential equation $\dot{x} = ax$, we can write the solution of (2.84) as

$$x = e^{A(t-t_0)}x(t_0) \qquad (2.85)$$

If we let

$$\phi(t) = e^{At} \qquad (2.86)$$

then (2.85) becomes

$$x = \phi(t-t_0)x(t_0) \qquad (2.87)$$

The matrix ϕ in (2.86) is known as the state transition matrix because it describes the change in the states from one time to another time. Some of the properties of the state transition matrix are as follows:

$$\phi(t_2-t_1)\phi(t_1-t_0) = \phi(t_2-t_0) \qquad (2.88)$$

$$\phi(t)\phi(t)\ldots\phi(t) = \phi^q(t) = \phi(qt) \qquad (2.89)$$

$$\phi^{-1}(t) = \phi(-t) \qquad (2.90)$$

$$\phi(0) = I \qquad (2.91)$$

$$\det(\phi(t)) \neq 0 \qquad \forall \text{ finite } t \qquad (2.92)$$

To obtain the complete solution of (2.82), consider

$$d/dt(e^{-At}x) = e^{-At}(-A)x + e^{-At}\dot{x}$$
$$= e^{-At}(\dot{x} - Ax) \qquad (2.93)$$

Substituting (2.82) into (2.93) we get

$$d/dt(e^{-At}x) = e^{-At}(Ax + Bu - Ax)$$
$$= e^{-At}Bu$$

Integrating, we get

$$e^{-At}x = \int_{t_0}^{t} e^{-A\tau}Bu \, d\tau + K \qquad (2.94)$$

where K is an arbitrary constant matrix of integration. The lower limit on the integral is the initial time at which $u(t)$ is applied. We will assume the initial time to be zero. To evaluate K, we let $t = 0$ in (2.94), which gives $K = x(0)$. We can rearrange (2.94) as

$$x(t) = e^{At}x(0) + \int_{0}^{t} e^{A(t-\tau)}Bu(\tau) \, d\tau \qquad (2.95)$$

$$= \phi(t)x(0) + \int_{0}^{t} \phi(t-\tau)Bu(\tau) \, d\tau \qquad (2.96)$$

$$= \phi(t)x(0) + \int_{0}^{t} \phi(\beta)Bu(t-\beta) \, d\beta \qquad (2.97)$$

Referring to the right-hand side of (2.96), the first term is the homogeneous solution (or zero input response, i.e., $u = 0$) and the second term is the particular solution (or zero state response, i.e., $x(0) = 0$).

Substituting (2.96) into (2.83) we get

$$y(t) = C\phi(t)x(0) + C \int_{0}^{t} \phi(t-\tau)Bu(\tau) \, d\tau \qquad (2.98)$$

The equations (2.96) and (2.98) give the complete solution to the state space model of (2.82) and (2.83) in terms of the system matrices (A, B, and C), the input $u(t)$ and the initial conditions of the states $x(t_0)$. The first term in (2.98) is the transient response and the second term is the steady state output response.

Questions such as how to evaluate the state transition matrix of (2.86) and how to evaluate the convolution integral in (2.98) will not be addressed here. They can be found in any text book on classical control theory.

As mentioned before, (2.98) describes the output $y(t)$ in terms of A, B, C, u and $x(t_0)$. We can also describe the output y in terms of eigenvalues and eigenvectors of the matrix A. This gives further insight into the output response, i.e., it will tell us how the

2-16

eigenvalues and eigenvectors of the plant will affect the output time response.

Consider the state space model (2.82) and (2.83) again. The characteristic equation is given by

$$\det(\lambda I - A) = \lambda^n + a_{n-1}\lambda^{n-1} + \ldots + a_1\lambda + a_0 = 0 \qquad (2.99)$$

The eigenvalues of this equation are λ_1, λ_2, $\ldots$, λ_n. When all the eigenvalues are distinct, recall that the eigenvector decomposition of A gives us

$$A = T\Lambda T^{-1} \qquad (2.100)$$

where T is the modal matrix. The eigenvectors v_i are the columns of T and satisfy the equation

$$[\lambda_i I - A]v_i = 0 \qquad (2.101)$$

The rows of T^{-1} are the row vectors w_i^T and satisfy the equation

$$w_i^T[\lambda_i I - A] = 0 \qquad (2.102)$$

From linear algebra we know that e^{At} can be represented as

$$e^{At} = I + At + A^2 t^2/2! + A^3 t^3/3! + \ldots \qquad (2.103)$$

Using (2.100) in (2.103) we get

$$e^{At} = I + (T\Lambda T^{-1})t + (T\Lambda T^{-1})^2 t^2/2! + (T\Lambda T^{-1})^3 t^3/3! + \ldots$$

$$= T(I + \Lambda t + \Lambda^2 t^2/2! + \Lambda^3 t^3/3! + \ldots)T^{-1}$$

$$= Te^{\Lambda t}T^{-1} \qquad (2.104)$$

Note that

$$e^{\Lambda t} = \operatorname{diag}(e^{\lambda_1 t}, e^{\lambda_2 t}, e^{\lambda_3 t} \ldots, e^{\lambda_n t}) \qquad (2.105)$$

Substituting (2.104) into (2.98), we get

$$y(t) = CTe^{\Lambda t}T^{-1}x(0) + C\int_0^t Te^{\Lambda(t-\tau)}T^{-1}Bu(\tau)\, d\tau \qquad (2.106)$$

The state transition matrix can be written as

$$e^{At} = \sum_{i=1}^{n} v_i e^{\lambda_i t} w_i^T \qquad (2.107)$$

Substituting (2.107) into (2.98), we get

$$y(t) = \sum_{i=1}^{n} Cv_i e^{\lambda_i t} w_i^T x(0)$$

$$+ \sum_{j=1}^{m} \sum_{i=1}^{n} Cv_i w_i^T b_j \int_0^t e^{\lambda_i t} u_j (t-\tau) \, d\tau \qquad (2.108)$$

It is evident from (2.108) that the <u>entire eigenstructure</u> (i.e., all the eigenvalues and eigenvectors) determines the output time response of the system. By selecting the eigenvalues and eigenvectors, it is possible to design a feedback control law $u(t)$ that will shape the output response so that it is close to the desired response.

2.2-3 Transfer Matrices

Taking the Laplace transform of the state space model, we obtain the Transfer Function Matrix (TFM) $G(s)$ as follows

$$G(s) = C(sI-A)^{-1}B \qquad (2.109)$$

This equation is a mathematical model (in the frequency domain) of the plant from the input-output viewpoint. Note that the matrix $G(s)$ can also be viewed as the matrix consisting of the Laplace transform of impulse responses, that is, the transfer function $g_{ij}(s)$ is the Laplace transform of the output y_j when the input u_j is a unit impulse function. $G(s)$ is called the plant transfer matrix. The dimension of the matrix $G(s)$ is given by : (the number of outputs by number of inputs). Obviously, $G(s)$ may be a square or a non-square matrix.

Let's call the controller matrix $K(s)$ and assume that it is given. Figure 2.1 shows the closed-loop block diagram assuming unity feedback.
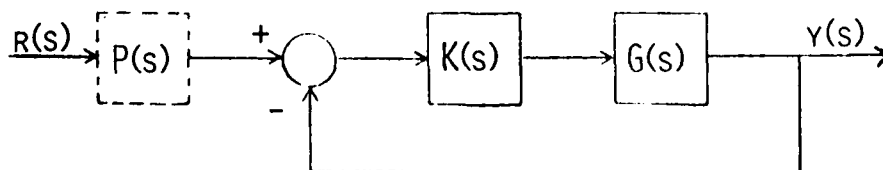
Fig 2.1   Closed-Loop Block Diagram.

We chose this kind of structure for the block diagram because if we have
a controller (or compensator) matrix in the feedback loop, a block
diagram equivalent to Fig 2.1 can be obtained through block diagram
manipulation. The transfer matrix $P(s)$ is called a pre-compensator
matrix. We will ignore $P(s)$ for the time being since it does not effect
the closed-loop stability. It is sufficient to know that we
use $P(s)$ to shape the command inputs to achieve desired performance.
For stability analysis we need to study how the loops behave. This
requires calculation of loop transfer matrices, which we get by breaking
the loop either at the input to the plant $G(s)$ or at the output of the
plant $G(s)$. If we break the loop at the input, the loop transfer matrix
(or open-loop matrix) is KG and if we break the loop at the output it is
GK. The matrices GK and KG are always square. In a SISO system GK = KG,
whereas in a MIMO system GK $\neq$ KG, in general. The matrix $(I + KG)$ or
$(I + GK)$ is called the return difference matrix, and the matrix
$(I + KG)^{-1}$ or $(I + GK)^{-1}$ is called the inverse return difference matrix.
We will see later on that the closed-loop stability is directly related
to the return difference matrix. Finally, the matrices $(I + GK)^{-1}$ and
$GK(I + GK)^{-1}$ are called the (output) sensitivity matrix, S, and the
(output) complimentary sensitivity matrix, T, respectively. Similarly,
(input) sensitivity and (input) complimentary sensitivity matrices can
be written by replacing GK with KG above. We will see that the sum of
the matrices S and T is equal to the identity matrix and will learn how
to use the matrices S and T in control system design to achieve good
command following, disturbance rejection and robustness to high
frequency modelling errors.

Ignoring $P(s)$, the closed-loop transfer matrix G_{CL} between v and r from Fig 2.1 can be written in several different forms as follows

$$G_{CL} = GK[I + GK]^{-1} \tag{2.110}$$

$$= [I + GK]^{-1}GK \tag{2.111}$$

$$= G[I + KG]^{-1}K \tag{2.112}$$

Equations (2.110 - 2.112) are proved in Appendix 2A.

2.2-4 Relationship Between the Closed-Loop and Open-Loop

Characteristic Polynomials
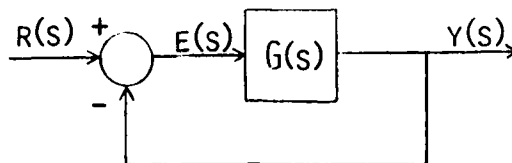
Fig 2.2 Block Diagram of MIMO Feedback System

Consider the MIMO closed-loop block diagram shown in Fig 2.2. Here $G(s)$ is an open-loop transfer matrix, i.e., $G(s)$ contains both the plant transfer matrix and the controller matrix. We have selected this block diagram configuration to derive the relationship between closed-loop and open-loop characteristic polynomials because it is simple and easy to derive the relationships we are after.

Let us now proceed with Fig 2.2. First let ϕ_{OL} and ϕ_{CL} denote the open-loop and closed-loop characteristic polynomials respectively. The state space description of Fig 2.2 is as follows

$$\dot{x}(t) = Ax(t) + Be(t) \tag{2.113}$$

$$y(t) = Cx(t) \tag{2.114}$$

$$e(t) = r(t) - y(t) \tag{2.115}$$

The relationship between $G(s)$ and the state space description is

$$G(s) = C(sI - A)^{-1}B \tag{2.116}$$

2-20

The open-loop characteristic polynomial $\phi_{OL}(s)$ is

$$\phi_{OL}(s) = \det(sI - A) \tag{2.117}$$

To obtain an expression for the closed-loop characteristic polynomial ϕ_{CL}, let us manipulate (2.113 - 2.115) to obtain

$$\dot{x}(t) = (A - BC)x(t) + Br(t) \tag{2.118}$$

Let $G_{CL}(s)$ represent the closed-loop transfer matrix. The relationship between $G_{CL}(s)$ and the state space description is

$$G_{CL}(s) = C(sI - A + BC)^{-1}B \tag{2.119}$$

The closed-loop characteristic polynomial $\phi_{CL}(s)$ is

$$\phi_{CL}(s) = \det(sI - A + BC) \tag{2.120}$$

or

$$\phi_{CL}(s) = \det(sI - A_{CL}) \tag{2.121}$$

where

$$A_{CL} = A - BC \tag{2.122}$$

The closed-loop system will be stable if and only if all the eigenvalues of A_{CL} are in the open left-half s-plane. To rephrase: the closed-loop system will be stable if and only if all the roots of $\phi_{CL}(s)$ are in the open left-half s-plane. These roots are also the closed-loop poles.

The relationship between $\phi_{CL}(s)$ and $\phi_{OL}(s)$ is as follows

$$\phi_{CL}(s) = \phi_{OL}(s) \cdot \det[I + G(s)] \tag{2.123}$$

Equation (2.123) relates the closed-loop poles to the open-loop poles and the determinant of the return difference matrix. This equation turns out to be very useful in MIMO Nyquist stability criterion. To prove (2.123), we need a few determinant identities which are stated in Appendix 2B. Substituting (2.120) into the left-hand side (LHS) of (2.123) and (2.117) and (2.116) into the right-hand side (RHS) of (2.123), we have

$$\det(sI - A + BC) = \det(sI - A) \cdot \det(I + C(sI - A)^{-1}B) \qquad (2.124)$$

Let us start with the RHS of (2.124) and show that it is equal to its LHS using the identities in Appendix 2B. The RHS can be written (using (2B.2)) as

$$\text{RHS} = \det \begin{bmatrix} sI - A & B \\ -C & I \end{bmatrix} \qquad (2.125)$$

Using (2B.4) on (2.125), we have

$$\text{RHS} = \det(I) \cdot \det(sI - A + BI^{-1}C)$$

$$= \det(sI - A + BC)$$

$$= \text{LHS of } (2.124)$$

Before we close this discussion on closed-loop characteristic polynomials, let us specialize (2.123) to SISO systems and show that it holds. Let the open-loop transfer function (i.e., it includes the plant and the controller transfer functions) be $g(s)$. Let $n(s)$ and $d(s)$ denote numerator and denominator polynomials of $g(s)$, respectively, that is

$$g(s) = n(s)/d(s) \qquad (2.126)$$

$$\therefore \quad \phi_{OL}(s) = d(s) \qquad (2.127)$$

We also know that the closed-loop transfer function $g_{CL}(s)$ is given by

$$g_{CL}(s) = g(s)/[1 + g(s)]$$

$$= n(s)/[n(s) + d(s)]$$

$$\therefore \quad \phi_{CL}(s) = n(s) + d(s) \qquad (2.128)$$

Now, according to (2.123), we must have

$$\phi_{CL}(s) = \phi_{OL}(s) \cdot [1 + g(s)]$$

$$= d(s) \cdot [1 + n(s)/d(s)]$$

$$= n(s) + d(s)$$

$$= \phi_{CL}(s)$$

which is correct.

If one is interested in treating the controller and plant matrices separately, the algebra is a bit tedious and is shown completely in Appendix 2C.

2.2-5 Zeros of MIMO Systems and Their Meaning

The poles of a MIMO system are simple and straight-forward to calculate. We know that the open-loop poles are simply the roots of the open-loop characteristic equation, $\det(sI - A) = 0$. The closed-loop poles are given by the closed-loop characteristic equation, $\det(sI - A_{CL}) = 0$, where A_{CL} is given by (2.119). They can also be calculated using (2.123). What about the zeros of a transfer matrix? Are the zeros of a transfer matrix the same as the zeros of the individual transfer functions in the matrix? The answer is no, in general.

First let's consider the meaning of the zeros of a transfer function for a SISO system. A system zero absorbs the energy of a complex exponential signal at a frequency equal to the zero's frequency. For example, consider the following transfer function

$$\frac{y(s)}{u(s)} = \frac{(s+2)}{(s+3)(s+4)}$$

Let the input signal be

$$u(t) = u_0 e^{-2t}$$

Then

$$y(t) = u_0 e^{-3t} - u_0 e^{-4t}$$

Obviously, the output does not contain any terms of the form e^{-2t}. Thus, the system has blocked all input signals with a frequency equal to the

location of the zero. We would like to preserve this intuitive idea even for MIMO systems.

For a MIMO System, if we have what we will define as a <u>transmission zero</u> at $s = z_k$, and if the input vector $u(t)$ has the form

$$u(t) = u_0 e^{z_k t}$$

where u_0 is a real constant vector (note that u_0 indicates the direction of the input vector), then we want the output vector $y(t)$ not to contain any signals of the form $e^{z_k t}$. This concept must be refined a bit, which involves the direction u_0. Let us explain this with the help of the following simple example.

$$y(s) = \begin{bmatrix} \dfrac{s+1}{s^2} & 0 \\[2ex] 0 & \dfrac{s+2}{s^2} \end{bmatrix} u(s) \tag{2.129}$$

For this system, it turns out that we have transmission zeros at $s = -1$ and $s = -2$. If we apply a general input vector $u(t)$ to the system, of the form

$$u(t) = u_0 e^{-t}$$

where u_0 is also a vector, then the output $y_1(t)$ will not contain a term e^{-t}, but the output $y_2(t)$ will. Therefore, in a multivariable sense, the 2-dimensional output vector $y(t)$ will contain the zero frequency exponential term e^{-t}. Similarly, if we apply an input vector of the form

$$u(t) = u_0 e^{-2t}$$

to the system (2.129), then $y_2(t)$ will not contain the frequency e^{-2t}, but $y_1(t)$ will.

The above argument indicates that we cannot use an arbitrary direction u_0. This simple example suggests that we retain the

2-24

energy-absorbing property only by using an input vector of a specific direction. In the example, if we consider the inputs

$$u(t) = \begin{bmatrix} 1 \\ 0 \end{bmatrix} e^{-t}$$

and

$$u(t) = \begin{bmatrix} 0 \\ 1 \end{bmatrix} e^{-2t}$$

we can see that the output vector $y(t)$ will not contain terms at either zero's frequency.

Thus, we arrive at the time domain interpretation of transmission zeros of MIMO systems. If a system $G(s)$ has a transmission zero at $s = z_k$, and if we apply an input vector

$$u(t) = u_k e^{z_k t}$$

where u_k is an appropriate input direction associated with the transmission zero at $s = z_k$, then the output vector $y(t)$ will not contain the (complex) exponential $e^{z_k t}$ in any of its components.

So far we have not addressed the problem of how to find the transmission zeros. There are many methods available to calculate them, but we will study only a few. Furthermore, we have not discussed the fact that there are other types of zeros, namely decoupling zeros and invariant zeros. For a completely controllable and observable system (definition in Section 2.2-9), the set of system zeros is just the set of transmission zeros. Since we usually deal with controllable and observable systems, we only need to know how to calculate the transmission zeros. For more on other types of zeros, the reader is referred to Ref [7].

2.2-6 Calculation of transmission zeros

One method of calculating transmission zeros is to arrange the

plant matrix G(s) into Smith-McMillan form. We do this by finding two

unimodular matrices M(s) and N(s) (unimodular matrix means that the

determinant of the matrix is independent of the variable s) such that

$$G_1(s) = M(s)G(s)N(s) \tag{2.130}$$

where $G_1(s)$ has the form

$$G_1(s) = \begin{bmatrix} \frac{\varepsilon_1(s)}{\psi_1(s)} & 0 & \cdots & 0 & 0 & \cdots & 0 \\ 0 & \frac{\varepsilon_2(s)}{\psi_2(s)} & \cdots & 0 & 0 & \cdots & 0 \\ \vdots & \vdots & & \vdots & \vdots & & \vdots \\ 0 & 0 & \cdots & \frac{\varepsilon_p(s)}{\psi_p(s)} & 0 & \cdots & 0 \\ 0 & 0 & \cdots & 0 & 0 & \cdots & 0 \\ \vdots & \vdots & & \vdots & \vdots & & \vdots \\ 0 & 0 & \cdots & 0 & 0 & \cdots & 0 \end{bmatrix} \tag{2.131}$$

In (2.131), $\varepsilon_i(s)$ and $\psi_i(s)$ are relatively prime polynomials (see

Appendix 2D for the definition of relatively prime polynomials).

Moreover, the ε_i's and ψ_i's have to satisfy the following:

$$\varepsilon_1(s) \,\big|\, \varepsilon_2(s) \,\big|\, \varepsilon_3(s) \,\big|\, \ldots \,\big|\, \varepsilon_p(s) \tag{2.132}$$

and

$$\psi_p(s) \,\big|\, \psi_{p-1}(s) \,\big|\, \psi_{p-2}(s) \,\big|\, \ldots \,\big|\, \psi_1(s) \tag{2.133}$$

Where $a|b|c$ means that a divides b without remainder and b divides c

without remainder. When all these are satisfied, $G_1(s)$ is said to be in

the Smith-McMillan form of G. If we define the transmission zero

polynomial z(s) as

$$z(s) = \prod_{i=1}^{p} \varepsilon_i(s) \tag{2.134}$$

then the roots of $z(s) = 0$ are the transmission zeros. If we start with

the <u>system matrix</u> P(s), where

$$P(s) = \begin{bmatrix} sI-A & -B \\ C & 0 \end{bmatrix} \qquad (2.135)$$

and arrange it in Smith-McMillan form, the resulting polynomial (2.134) will yield <u>all</u> zeros of the system (that is, both the transmission zeros *and decoupling zeros*).

<u>Example 2.2-1</u>

This example will illustrate the method of obtaining the transmission zeros by arranging the transfer matrix into Smith-McMillan form.

Suppose $G(s)$ is given by

$$G(s) = \frac{1}{d(s)} P(s)$$

where

$$d(s) = (s+1)(s+2)$$

and

$$P(s) = \begin{bmatrix} 1 & 1 \\ s^2+s-4 & 2s^2-s-8 \\ s^2-4 & 2s^2-8 \end{bmatrix}$$

We obtain the matrices $M(s)$ and $N(s)$ in (2.130) as follows:

Because $P(s)$ has 2 columns and 3 rows we append a (2x2) and a (3x3) identity matrix to it both below and to the right:

$$\begin{bmatrix} 1 & -1 \\ s^2+s-4 & 2s^2-s-8 \\ s^2-4 & 2s^2-8 \end{bmatrix} \quad \begin{bmatrix} 1 & 0 & 0 \\ 0 & 1 & 0 \\ 0 & 0 & 1 \end{bmatrix}$$

$$\begin{bmatrix} 1 & 0 \\ 0 & 1 \end{bmatrix}$$

Performing elementary row operations on the upper 3 by

5 block yields

$$
\begin{bmatrix} 1 & -1 \\ 0 & 3(s^2-4) \\ 0 & 3(s^2-4) \end{bmatrix}
\begin{bmatrix} 1 & 0 & 0 \\ 4-s-s^2 & 1 & 0 \\ 4-s^2 & 0 & 1 \end{bmatrix}
$$

$$
\begin{bmatrix} 1 & 0 \\ 0 & 1 \end{bmatrix}
$$

Performing elementary column operations on the left 5

by 2 block yeilds

$$
\begin{bmatrix} 1 & 0 \\ 0 & s^2-4 \\ 0 & s^2-4 \end{bmatrix}
\begin{bmatrix} 1 & 0 & 0 \\ 4-s-s^2 & 1 & 0 \\ 4-s^2 & 0 & 1 \end{bmatrix}
$$

$$
\begin{bmatrix} 1 & 1/3 \\ 0 & 1/3 \end{bmatrix}
$$

Final row operations give

$$
\begin{bmatrix} 1 & 0 \\ 0 & s^2-4 \\ 0 & 0 \end{bmatrix}
\begin{bmatrix} 1 & 0 & 0 \\ 4-s-s^2 & 1 & 0 \\ s & -1 & 1 \end{bmatrix}
$$

$$
\begin{bmatrix} 1 & 1/3 \\ 0 & 1/3 \end{bmatrix}
$$

Thus,

$$
M(s) = \begin{bmatrix} 1 & 0 & 0 \\ 4-s-s^2 & 1 & 0 \\ s & -1 & 1 \end{bmatrix}
\qquad
N(s) = \begin{bmatrix} 1 & 1/3 \\ 0 & 1/3 \end{bmatrix}
$$

and the Smith-McMillan form $G_1(s)$ of $G(s)$ is

2-28

$$G_1(s) = \frac{1}{(s+1)(s+2)} \begin{bmatrix} 1 & 0 \\ 0 & s^2-4 \\ 0 & 0 \end{bmatrix}$$

$$= \begin{bmatrix} \dfrac{1}{(s+1)(s+2)} & 0 \\ 0 & \dfrac{s-2}{s+1} \\ 0 & 0 \end{bmatrix}$$

Notice that $M(s)$ and $N(s)$ are unimodular matrices, since elementary row and column operations do not affect the determinant (except by a constant when a row or column is multiplied by a constant). The transmission zero from the Smith-McMillan form is at $s = 2$.

Obviously, it may be difficult to arrange a matrix into Smith-McMillan form, mainly because we have to do algebraic manipulation of polynomial matrices, which is difficult to do by hand and even more difficult on the computer (unless you have an algebraic manipulation language). There is a computer program called "zeros" available at WPAFB that calculates all the zeros by posing the problem as a generalized eigenvalue problem and solving it using Q-Z algorithms. We will not study the details of that technique; rather, we will study the following technique, which is based upon right-coprime factorizations (r.c.f.) or left-coprime factorizations (l.c.f.). For the definition of r.c.f. and l.c.f. see Appendix 2E.

Suppose that we have a right-coprime factorization of $G(s)$ as

$$G(s) = N_r(s)[D_r(s)]^{-1} \qquad (2.136)$$

Then we can state the following:

2-29

-- If $G(s)$ is square and nonsingular, then the transmission zeros are the roots of $\det[N_r(s)] = 0$.

-- If $G(s)$ is non-square, then the transmission zeros are given by the frequencies at which the rank of $N_r(s)$ drops below its normal rank (normal rank is the largest rank that the matrix can have).

Similar statements can be made for a l.c.f. of $G(s)$,

$$G(s) = [N_\ell(s)]^{-1} D_\ell(s). \tag{2.137}$$

How do we find a r.c.f. or l.c.f. of $G(s)$ as shown in (2.136) or (2.137)? To answer that, we state the following method:

Consider the state space model

$$\dot{x} = Ax + Bu$$

$$y = Cx + Du \tag{2.138}$$

so that

$$G(s) = C(sI - A)^{-1}B + D \tag{2.139}$$

Suppose that the system described by (2.138) is stabilizable and detectable (we will discuss stabilizability and detectability later in these notes). Select matrices F and K such that all the eigenvalues of the matrices $A_0 = A - BK$ and $\bar{A}_0 = A - FC$ have negative real parts. Then we will have

$$G(s) = N_r(s)[D_r(s)]^{-1} = [D_\ell(s)]^{-1} N_\ell(s) \tag{2.140}$$

and

$$\begin{bmatrix} Y_r(s) & X_r(s) \\ -N_\ell(s) & D_\ell(s) \end{bmatrix} \begin{bmatrix} D_r(s) & -X_\ell(s) \\ N_r(s) & Y_\ell(s) \end{bmatrix} = I \qquad \text{for all } s \tag{2.141}$$

if we define

$$N_\ell(s) = C(sI - \bar{A}_0)^{-1}(B - FD) + D \tag{2.142}$$

$$D_\ell(s) = I - C(sI - \bar{A}_0)^{-1}F \tag{2.143}$$

$$N_r(s) = (C - DK)(sI - A_0)^{-1}B + D \tag{2.144}$$

$$D_r(s) = I - K(sI - A_0)^{-1}B \qquad (2.145)$$

$$X_r(s) = K(sI - \overline{A}_0)^{-1}F \qquad (2.146)$$

$$Y_r(s) = I + K(sI - \overline{A}_0)^{-1}(B - FD) \qquad (2.147)$$

$$X_\ell(s) = K(sI - A_0)^{-1}F \qquad (2.148)$$

$$Y_\ell(s) = I + (C - DK)(sI - A_0)^{-1}F \qquad (2.149)$$

The equation (2.141) is called the generalized Bezout identity. The only nontrivial step needed so far is to find matrices K and F such that the matrices A_0 and $\overline{A}_0$ have eigenvalues with negative real parts. This can be accomplished by solving Riccati equations; i.e., select arbitrary positive definite matrices Q_1, Q_2, R_1 and R_2 of appropriate dimensions, and solve the equations

$$Q_1 + MA + A^T M - MBR_1^{-1}B^T M = 0 \qquad (2.150)$$

$$Q_2 + LA^T + AL - LC^T R_2^{-1}CL = 0 \qquad (2.151)$$

for the unknown matrices M and L. Then define

$$K = R_1^{-1}B^T M \qquad\qquad F = LC^T R_2^{-1} \qquad (2.152)$$

The rationale behind this is given in Chapter 6 of this notes. The main advantage of this method is that it deals with manipulation of real numbers, not polynomials. Basically, it requires two computer programs, one to solve Riccati equations and the other to do complex matrix inversion, $(sI - A)^{-1}$.

Now let us show a couple of simple examples and make a few comments.

Example 2.2-2

Consider the system:

$$A = \begin{bmatrix} -2 & 0 \\ 0 & 0 \end{bmatrix} \qquad\qquad B = \begin{bmatrix} -2 & 0 \\ 0 & 2 \end{bmatrix}$$

$$C = \begin{bmatrix} 1 & 0 \\ 0 & 1 \end{bmatrix} \qquad D = \begin{bmatrix} 1 & 0 \\ 0 & 1 \end{bmatrix}$$

so that

$$G(s) = C(sI - A)^{-1}B + D = \begin{bmatrix} \dfrac{s}{s+2} & 0 \\ 0 & \dfrac{s+2}{s} \end{bmatrix}$$

Choosing

$$Q_1 = Q_2 = R_1 = R_2 = \begin{bmatrix} 1 & 0 \\ 0 & 1 \end{bmatrix}$$

and solving (2.150) and (2.151), then substituting the resulting M and L matrices into (2.152) yields

$$K = \begin{bmatrix} -0.4142 & 0 \\ 0 & 1 \end{bmatrix} \qquad F = \begin{bmatrix} 0.2361 & 0 \\ 0 & 1 \end{bmatrix}$$

We really only need one factorization, so we'll choose the l.c.f. Also note that we only need N_ℓ from (2.142), but we will calculate D_ℓ as well for completeness. The X and Y matrices are not needed at all here but are useful in other applications (see Chapter 17). Next we need $\overline{A}_0$, which is given by

$$\overline{A}_0 = A - FC = \begin{bmatrix} -2.2361 & 0 \\ 0 & -1 \end{bmatrix}$$

Substituting all these quantities into (2.142) and (2.143) yields

$$N_\ell(s) = C(sI - \overline{A}_0)^{-1}(B - FD) + D$$

$$= \begin{bmatrix} 1 & 0 \\ 0 & 1 \end{bmatrix} \begin{bmatrix} s+2.2361 & 0 \\ 0 & s+1 \end{bmatrix}^{-1} \left\{ \begin{bmatrix} -2 & 0 \\ 0 & 2 \end{bmatrix} - \begin{bmatrix} 0.2361 & 0 \\ 0 & 1 \end{bmatrix} \begin{bmatrix} 1 & 0 \\ 0 & 1 \end{bmatrix} \right\} + \begin{bmatrix} 1 & 0 \\ 0 & 1 \end{bmatrix}$$

$$= \begin{bmatrix} \dfrac{s}{s+2.2361} & 0 \\ 0 & \dfrac{s+2}{s+1} \end{bmatrix}$$

2-32

$$D_\ell(s) = I - C(sI - \bar{A}_0)^{-1}F$$

$$= \begin{bmatrix} 1 & 0 \\ 0 & 1 \end{bmatrix} - \begin{bmatrix} 1 & 0 \\ 0 & 1 \end{bmatrix} \begin{bmatrix} s + 2.2361 & 0 \\ 0 & s + 1 \end{bmatrix}^{-1} \begin{bmatrix} 0.2361 & 0 \\ 0 & 1 \end{bmatrix}$$

$$= \begin{bmatrix} \dfrac{s+2}{s+2.2361} & 0 \\ 0 & \dfrac{s}{s+1} \end{bmatrix}$$

It is trivially obvious that $G(s) = [D_\ell(s)]^{-1}N_\ell(s)$ for this example. Since $G(s)$ is square, to find the transmission zeros we must find the roots of

$$\det[N_\ell(s)] = \frac{s(s+2)}{(s+1)(s+2.2361)} = 0$$

which are $s = 0$ and $s = -2$.

Quite often, r.c.f.'s and l.c.f.'s are defined in terms of polynomial matrices rather than transfer function matrices (see Ref. [2-3]). Looking at the previous example, it is obvious that

$$G(s) = \begin{bmatrix} s+2 & 0 \\ 0 & s \end{bmatrix}^{-1} \begin{bmatrix} s & 0 \\ 0 & s+2 \end{bmatrix}$$

since the denominators of the corresponding individual elements of $N_\ell(s)$ and $D_\ell(s)$ are the same. The denominators will always share this property. Therefore, let's look at an example where the l.c.f. is already given in polynomial form.

Example 2.2-3

Consider the l.c.f.

$$G(s) = \begin{bmatrix} \dfrac{s}{s+2} & 0 & \dfrac{s+1}{s+2} \\ 0 & \dfrac{s+1}{s^2} & \dfrac{1}{s} \end{bmatrix} = [D_\ell(s)]^{-1}N_\ell(s)$$

$$= \begin{bmatrix} s+2 & 0 \\ 0 & s^2 \end{bmatrix}^{-1} \begin{bmatrix} s & 0 & s+1 \\ 0 & s+1 & s \end{bmatrix}$$

2-33

We note that $G(s)$ is a non-square matrix and the normal rank of $N_\ell(s)$ is two. There is no frequency for which the rank of $N_\ell(s)$ is less than two, i.e., for all values of s, there are always two columns that are linearly independent. Therefore, there are no transmission zeros for this system. Notice that had we tried to guess the transmission zeros by inspecting the individual transfer functions of $G(s)$, we would have been in trouble. Also notice that, typically, rectangular systems do not have transmission zeros because it is unlikely that all minors of size less than or equal to the normal rank will be simultaneously zero.

From the above two examples, we see that the transmission zeros of $G(s)$ exhibit some phenomena which do not exist in the SISO case. A transmission zero may appear as a pole of the same $G(s)$ (note that in Example 2.2-2 the poles are also at $s = 0$ and $s = -2$). Even though individual elements of $G(s)$ have zeros, the matrix $G(s)$ may not have zeros. Despite all these differences, the interpretation of zeros of MIMO systems is still the same as the zeros of SISO systems from the time-response point of view (as explained at the beginning of section 2.2-5).

2.2-7 Nonminimum Phase Systems

In section 2.2-5 and 2.2-6 we discussed a great deal about zeros. Why are we so concerned about zeros? Because systems with zeros in the right-half of the s-plane cause considerable difficulty to the control system designer. This type of system is called a nonminimum phase system. Zeros have a dramatic influence on the nature of the time response. Whenever there is a zero in the right-half s-plane, the initial time response of the system is negative even though the steady-state value is positive. This type of initial response (typical

to both SISO and MIMO systems) presents a difficult control problem. Imagine trying to drive a car in which every time you turned the wheel to the left, the initial response moved the car to the right before it eventually came back to the left. This is the type of behavior one must contend with in a nonminimum phase system.

The zeros of the open-loop system are the same as the zeros of the closed-loop system under unity feedback for both SISO and MIMO systems, whether they are controllable and observable or not. If we think of feedback design for SISO systems using root locus, we know that all the branches of the loci start at the open-loop poles and end at the zeros. The closed-loop poles lie somewhere on the root locus and their location depends upon the gain that is selected. Naturally, if we have a zero in the right-half plane, the closed-loop system will go unstable provided the gain is sufficiently increased. This is true for MIMO systems also. The root locus for a MIMO system starts at the open-loop poles. Some of the branches of the loci end at the (finite) transmission zeros and the others end at (conceptually) the transmission zeros at infinity. If there is a transmission zero in the right-half plane, the closed-loop system will go unstable for a high enough value of gain.

Among other concerns, we will see later that when we use the control system design procedure LQG/LTR (Linear Qaudratic Gaussian with Loop Transfer Recovery), we may not be able to achieve robustness to high frequency modeling errors or achieve good performance at low frequencies, depending upon whether the right-half plane transmission zeros are above or below the cross-over frequency of the uncertainty profile.

Before we close this section on zeros, we should remember that nonminimum phase behavior is a modeling problem, not the real system's problem. That is, the zero locations depend upon where we mount the actuators and sensors. We can change the pattern of zero locations and hence change the nonminimum phase behavior of the model by rearranging the control distribution and/or measurement distribution as represented by the matrices B and C in the state space model. However, with a given set of actuator and sensor locations, we may be stuck with nonminimum phase behavior.

2.2-8 The Multivariable Nyquist Stability Criterion

Nyquist stability criterion gives a YES or NO type answer to the question of stability of a feedback system, i.e., does the closed-loop system have any poles in the right half s-plane or not. Before digital computers became popular, it was not a trivial task to find the roots of the characteristic equation by hand, in order to find closed-loop stability. Nyquist criterion was, however, relatively easy to apply by hand for SISO design and analysis. Today, the question of YES or NO stability is relatively easy; all one needs to do is to write the state space description of the closed-loop system and calculate (using canned digital computer subroutines) the eigenvalues of the closed-loop system matrix. This leads to the question of why we study Nyquist criterion for MIMO systems. We study it because of the following reasons:

1) It does still provide a YES or NO type answer to MIMO closed-loop stability.

2) For systems that contain time delay terms of the form $e^{-s\tau}$, state space methods are very awkward since the system is infinite-dimensional. The Nyquist theorem is very useful for such systems.

2-36

3) Most importantly, it forms the basis for closed-loop robustness analysis for modeling errors and for closed-loop robust control design using loop-shaping techniques.

Consider the block diagram of Fig 2.2. Recall that the closed loop characteristic polynomial is given by

$$\phi_{CL} = \phi_{OL} \cdot \det[I + G(s)] \tag{2.153}$$

where

$$\phi_{OL} = \det(sI - A) \tag{2.154}$$

We now need some basics from complex variable theory.
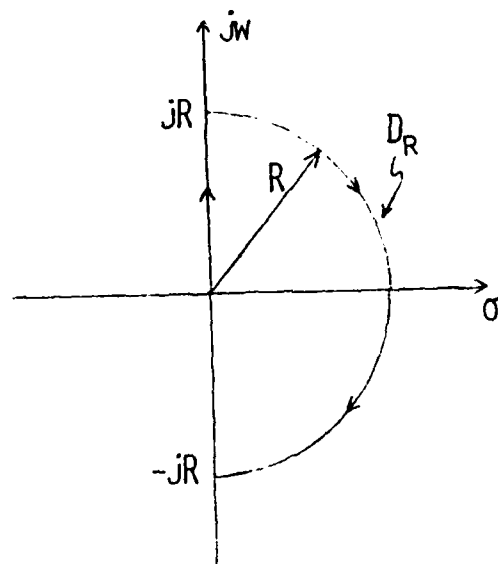
Fig 2.3. The Nyquist Contour D_R in the s-Plane

Let us define a closed contour D_R as shown in Fig 2.3. The clockwise contour D_R, as $R \to \infty$, is called the Nyquist contour and encloses the entire right-half s-plane. The closed-loop system of Fig 2.2 will be stable if and only if the Nyquist contour D_R does not encircle any of the roots of the closed-loop characteristic polynomial $\phi_{CL}(s)$ given in (2.153). This is simply a restatement of "no closed-loop poles in the right-half s-plane". Before we find the Nyquist stability criteria, let

us first state without proof what is called "the principle of the argument" from complex variable theory.

The principle of the argument: Let C be a closed clockwise contour in the s-plane (note that D_R is a particular closed contour). Let $f(s)$ be a complex valued function (for us $f(s)$ may be ϕ_{CL}). Suppose that:

  1) $f(s)$ is analytic on the contour C (i.e., df/ds exists for every point on C).

  2) $f(s)$ has Z zeros inside C.

  3) $f(s)$ has P poles inside C.

   If we plot $f(s)$ in the complex s-plane by evaluating it at every point on C, then what we get is called the image of the clockwise contour C under the mapping $f(s)$. The principle of the argument states that this image encircles the origin in the complex plane $Z - P$ times in a clockwise sense.

   Let the notation $N(A, f(s), C)$ denote the number of clockwise encirclements of the point A in the complex plane by the image of the clockwise contour C under the mapping $f(s)$. Using this notation, we can write the principle of the argument as

$$N(0, f(s), C) = Z - P \qquad (2.155)$$

   One useful property that we will need later is as follows. Suppose that $f(s)$ can be written as

$$f(s) = f_1(s)f_2(s) \qquad (2.156)$$

Also suppose that there are no pole-zero cancellations between $f_1(s)$ and $f_2(s)$. Then the principle of argument yields

$$N(0, f_1(s)f_2(s), C) = N(0, f_1(s), C) + N(0, f_2(s), C) \qquad (2.157)$$

If $f_1(s)$ has Z_1 zeros and P_1 poles inside the contour C, and if $f_2(s)$ has Z_2 zeros and P_2 poles inside the contour C, then (2.157) means that

$$Z - P = (Z_1 - P_1) + (Z_2 - P_2) \tag{2.158}$$

We are now ready to deduce the closed-loop stability of Fig 2.2 using the principle of the argument that we just discussed. Recall that the roots of the characteristic equation shown in (2.153) are the poles of the closed-loop system. Also recall that ϕ_{CL} can be written using a state space description as follows (see (2.120) and the development surrounding it)

$$\phi_{CL} = \det(sI - A + BC) \tag{2.159}$$

Note that ϕ_{CL} in (2.159) is an nth degree polynomial with n zeros and no poles. It may be confusing, but we should remember that the n zeros of the polynomial in (2.159) are the n closed-loop poles. We should also note that the term $\det[I + G(s)]$ is, in general, a numerator polynomial divided by a denominator polynomial. But this denominator polynomial will get cancelled when multiplied by ϕ_{OL} (you can check it quickly by taking any simple MIMO example). This is why ϕ_{CL} given by (2.153) is also a nth degree polynomial with n zeros and no poles.

If we apply the principle of the argument to $\phi_{CL}(s)$ using the Nyquist contour, $f(s) = \phi_{CL}(s)$ and $C = D_R$. Since $\phi_{CL}(s)$ has no poles, $P = 0$. For stability, there must be no zeros of $\phi_{CL}(s)$ in the right-half s-plane, that is, $Z = 0$. Therefore, (2.155) becomes

$$N(0, \phi_{CL}(s), D_R) = 0 \tag{2.160}$$

if and only if the closed-loop system is stable. Substituting (2.153) into (2.160) we have

$$N(0, \phi_{OL} \cdot \det(I + G), D_R) = 0 \tag{2.161}$$

if and only if the closed-loop system is stable. Using (2.157), we can write (2.161) as

$$N(0, \phi_{OL}(s) \det(I + G), D_R)$$

$$= N(0, \phi_{OL}(s), D_R) + N(0, \det(I + G), D_R) = 0 \qquad (2.162)$$

Note that $\phi_{OL}(s)$ is a polynomial (see (2.154)) with n zeros and no

poles. These zeros correspond to the open-loop poles of the transfer

matrix $G(s)$. Let $P_{U,OL}$ denote the number of unstable open-loop poles of

$G(s)$. The principle of the argument applied to $\phi_{OL}(s)$ then gives

$$N(0, \phi_{OL}(s), D_R) = P_{U,OL} \qquad (2.163)$$

Substituting (2.163) into (2.162), we have

$$P_{U,OL} + N(0, \det(I + G), D_R) = 0$$

or

$$N(0, \det(I + G), D_R) = -P_{U,OL} \qquad (2.164)$$

Hence, the closed-loop system of Fig 2.2 is stable if and only if

(2.164) is satisfied. Let us rephrase this. The closed-loop system of

Fig 2.2 is stable if and only if the number of <u>counter-clockwise</u>

encirclements of the origin by the image of the clockwise Nyquist

contour D_R under the mapping $\det(I + G)$ equals the number of unstable

open-loop poles of the open-loop transfer matrix $G(s)$.

Now let's look at the Nyquist stability criteria for the SISO case.

Since the determinant of a scalar is itself, (2.164) reduces to

$$N(0, 1 + g(s), D_R) = -P_{U,OL} \qquad (2.165)$$

It is also easy to see that

$$N(0, 1 + g(s), D_R) = N(-1, g(s), D_R) \qquad (2.166)$$

The reason is that if we plot the image of D_R under the mapping $1 + g(s)$

then by shifting every point of $1 + g(s)$ by -1, we obtain the image of

D_R under the mapping $g(s)$. That is, (2.166) states that the number of

encirclements of the origin by the image of D_R under the map $1 + g(s)$ is

the same as the number of encirclements of -1 by the image of D_R under

the map $g(s)$. Assuming that Fig 2.2 stands for a SISO system, the closed-loop system is stable if and only if

$$N(-1, g(s), D_R) = -P_{U,OL} \qquad (2.167)$$

Unfortunately, (2.164) can not be simplified any further (that is, removing the determinant operator or shifting the origin to -1) for an arbitrary __matrix__ $G(s)$. The only further simplification possible is for the special case where G is a diagonal matrix, that is

$$G(s) = diag[\ g_1(s),\ g_2(s),\ \ldots,\ g_n(s)] \qquad (2.168)$$

which means we are dealing with n decoupled SISO systems (this is a trivial multivariable case). In this case

$$det[I + G(s)] = \prod_{i=1}^{n} [1 + g_i(s)] \qquad (2.169)$$

and (2.164) can be written as (see the property shown in (2.157) also)

$$\sum_{i=1}^{n} N(0,\ 1 + g_i(s),\ D_R) = -P_{U,OL} \qquad (2.170)$$

Notice that the nice thing about the Nyquist stability criteria is that in order to determine closed-loop stability we don't need to solve for closed-loop eigenvalues. We can find closed-loop stability based on open-loop information. In the SISO case, we use either $g(s)$ or $1 + g(s)$ as shown in (2.167) or (2.165). In the MIMO case, we have to use the determinant of the return difference, $det[I + G(s)]$, and we cannot simplify it to the form of (2.167) unless $G(s)$ is completely decoupled. This does increase the difficulty in using the technique, but for time-delay systems we really have no choice. For robustness analysis (see Chapter 3), our stability tests will be based on the Nyquist criteria, but we will not actually have to plot $det[I + G(s)]$. As one final comment, if a compensator matrix $K(s)$ is present in the system, we can simply replace $G(s)$ with $G(s)K(s)$ through the relationship given in Appendix 2C (substitute equation (2C.26) into (2.160)).

2.2-9 Controllability, Observability, Stabilizability and

Detectability

In this section we briefly explain what we mean by controllability, observability, stabilizability and detectability. These concepts (determined only from state space models) are important to design techniques using optimal control theory, eigenstructure assignment, pole placement, etc.

A linear system described by the state space model

$$\dot{x}(t) = Ax(t) + Bu(t) \tag{2.171}$$

is said to be <u>completely controllable</u> if and only if the system can be transferred from any initial state x_o at any initial time t_o to any final state $x(t_f) = x_f$ within a finite time $t_f - t_o$. If the system is <u>not</u> completely controllable (i.e., <u>uncontrollable</u>), then no matter how much control energy we put into the system, there are certain states in the state space that can not be reached. From a pole-placement viewpoint, a completely controllable system implies that we can move all the poles of the system (using feedback) whether those poles are in the left-half or right-half s-plane.

A simple test to determine complete controllability for the linear system of (2.171) is to first form the so-called controllability matrix, denoted by M_C, given by

$$M_C = [B \mid AB \mid A^2B \mid \ldots \mid A^{n-1}B] \tag{2.172}$$

where n is the number of states. If the rank of M_C is equal to n, then the system is completely controllable. If this rank is less than n, the system is uncontrollable. The rank defect of M_C (i.e., n minus the actual rank of M_C) tells us how many modes (poles) are uncontrollable.

When the eigenvalues of A are distinct, the uncontrollable modes have the property

$$\text{Rank}[\ \lambda_u I - A,\ B] = g < n \qquad (2.173)$$

Equation (2.173) gives us a way to find which modes are uncontrollable. If the eigenvalue λ_u is uncontrollable, then it is also called an input decoupling zero.

There is another way to describe controllability. Consider the system of (2.171), and assume all eigenvalues of A are distinct. Define a transformation of state variables by

$$x(t) = Tz(t) \qquad (2.174)$$

where $z(t)$ is the transformed state, and T is a transformation matrix whose columns are the eigenvectors of the A matrix. Then (2.171) can be rewritten as

$$\dot{z}(t) = T^{-1}ATz(t) + T^{-1}Bu(t) = \Lambda z(t) + B^1 u(t) \qquad (2.175)$$

where Λ is a diagonal matrix with the eigenvalues as the diagonal elements. If B^1 does not have a zero row, then the system is completely controllable; otherwise, it is not completely controllable, and the eigenvalues corresponding to the zero rows are the uncontrollable modes.

If all the unstable modes (poles or eigenvalues) are controllable, then that system is said to be stabilizable. This tells us that stabilizability does not imply complete controllability since the stable modes (poles in the left-half plane) may not be controllable (i.e., we may not be able to move them using feedback). However, complete controllability does imply stabilizability.

A system is said to be completely observable if every initial state $x(t_0)$ can be exactly determined from the measurements of the output $y(t)$ over a finite interval of time $t_0 \leqslant t \leqslant t_f$. This implies that

every state $x(t)$ affects the output $y(t)$. If there are any states that do not affect the system response, then it is <u>not</u> a completely observable (i.e., <u>unobservable</u>) system. This means that if the system is not completely observable, then there are certain states that can never be identified or estimated because there are some states that do not influence the output.

A quick way to check if the linear system described by

$$\dot{x}(t) = Ax(t) + Bu(t)$$

$$y(t) = Cx(t) \tag{2.176}$$

is completely observable is to first form the so-called observability matrix M_o given by

$$M_o = [C^T \mid A^T C^T \mid (A^T)^2 C^T \mid \ldots \mid (A^T)^{n-1} C^T] \tag{2.177}$$

If the rank of M_o is n, where n is the size of A matrix, then the system in (2.176) is completely observable; otherwise, it is unobservable. The rank defect of M_o is equal to the number of unobservable modes. Another way to understand complete observability is to use the transformation (assuming nonrepeated eigenvalues) shown in (2.174) on the output equation of (2.176). We have

$$y(t) = Cx(t) = CTz(t) = C^1 z(t) \tag{2.178}$$

If a column of C^1 has all zeros, then one mode is not coupled to any of the outputs and the system is not completely observable. Again, the modes corresponding to the zero columns are unobservable.

If the unobservable modes are in the open left-half s-plane (i.e., stable), then the system is said to be <u>detectable</u>. Obviously, detectability does not imply observability whereas observability does imply detectability.

Finally, a pole-zero cancellation in a transfer function implies that the system is either uncontrollable or unobservable or both. That is why a pole-zero cancellation is not permitted if we are interested in deriving a state space model from the transfer function. Such a cancellation will destroy the information regarding controllability and observability.

Derivation of equations (2.110 - 2.112)

Consider the following MIMO block diagram
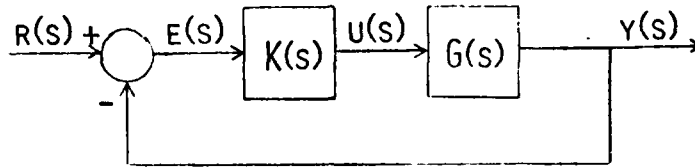
Fig 2A-1   MIMO Block Diagram

We have

$$e = r - y \tag{2A.1}$$

$$y = Gu \tag{2A.2}$$

$$u = Ke \tag{2A.3}$$

To get (2.110), start with (2A.1) and simplify as shown

$$e = r - y$$

$$= r - Gu$$

$$= r - GKe$$

Solving for e, we get

$$e = (I + GK)^{-1}r \tag{2A.4}$$

But

$$y = GKe \tag{2A.5}$$

so that substituting (2A.4) into (2A.5) yields

$$y = GK(I + GK)^{-1}r$$

$$\therefore \quad G_{CL} = GK (I + GK)^{-1} \tag{2.110}$$

To get (2.111), start with (2A.2) and simplify as shown

$$y = Gu$$

$$= GKe$$

$$= GK(r - y)$$

$$= GKr - GKy$$

Solving for y, we get

$$y = (I + GK)^{-1}GKr$$

$$\therefore \qquad G_{CL} = (I + GK)^{-1}GK \qquad\qquad (2.111)$$

To get (2.112), start with (2A.3) and simplify as shown

$$u = Ke$$

$$= K(r - y)$$

$$= K(r - Gu)$$

$$= Kr - KGu$$

Solving for u we get

$$u = (I + KG)^{-1}Kr \qquad\qquad (2A.6)$$

But

$$y = Gu \qquad\qquad (2A.7)$$

so that substituting (2A.6) into (2A.7), we have

$$y = G(I + KG)^{-1}Kr$$

$$\therefore \qquad G_{CL} = G(I + KG)^{-1}K \qquad\qquad (2.112)$$

There are two more ways of obtaining (2.111) from (2.110). The algebra shown in the following steps is sometimes very useful in matrix manipulation. Recalling that $(AB)^{-1} = B^{-1}A^{-1}$, start with (2.110) and simplify as shown below

$$GK(I + GK)^{-1} = [(I + GK)(GK)^{-1}]^{-1}$$

$$= [(GK)^{-1} + I]^{-1}$$

$$= [(GK)^{-1}(I + GK)]^{-1}$$

$$= (I + GK)^{-1}GK$$

which is (2.111).

The other way is to consider the following matrix identity and follow the steps (remember GK is a square matrix).

2-47

$$GK + (GK)^2 = GK + (GK)^2$$

$$GK(I + GK) = (I + GK)GK$$

$$(I + GK)^{-1}GK(I + GK) = GK$$

$$(I + GK)^{-1}GK = GK(I + GK)^{-1}$$

Appendix 2B

Determinant identities required to prove (2.123)

1. If A_1 and A_2 are square matrices, then

$$\det(A_1 A_2) = \det(A_1) \cdot \det(A_2) \tag{2B.1}$$

2. Let A_1 and A_4 be square matrices and let A_2 and A_3 have appropriate dimensions. Then

$$\det \begin{bmatrix} A_1 & A_2 \\ A_3 & A_4 \end{bmatrix} = \det(A_1) \cdot \det(A_4 - A_3 A_1^{-1} A_2) \tag{2B.2}$$

provided A_1^{-1} exists.

3.
$$\det \begin{bmatrix} A_1 & A_2 \\ A_3 & A_4 \end{bmatrix} = \det \begin{bmatrix} A_4 & A_3 \\ A_2 & A_1 \end{bmatrix} \tag{2B.3}$$

4. Combining equations (2B.2) and (2B.3), we get

$$\det \begin{bmatrix} A_1 & A_2 \\ A_3 & A_4 \end{bmatrix} = \det(A_4) \cdot \det(A_1 - A_2 A_4^{-1} A_3) \tag{2B.4}$$

Appendix 2C

The relationship between closed-loop and open-loop characteristic

polynomials for MIMO systems considering the plant and controller

transfer matrices explicitly
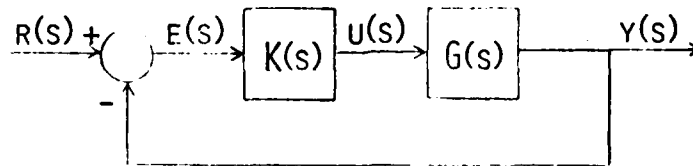
Fig 2C-1   MIMO Block Diagram

Consider the MIMO block diagram shown in Fig 2C-1. Let's derive

the relationship assuming K(s) has poles and zeros in it. Our final

result will hold even if K(s) is a pure gain matrix. First, we need to

write the state space description of the transfer matrices G(s) and

K(s). Let's use the matrices A, B, and C in order to realize G(s) and

the matrices E, F, and D to realize K(s) as shown below.

Plant:

$$\dot{x}(t) = Ax(t) + Bu(t) \tag{2C.1}$$

$$y(t) = Cx(t) \tag{2C.2}$$

$$\therefore \qquad G(s) = C(sI-A)^{-1}B \tag{2C.3}$$

Controller:

$$\dot{z}(t) = Fz(t) + Fe(t) \tag{2C.4}$$

$$u(t) = Dz(t) \tag{2C.5}$$

$$\therefore \qquad K(s) = D(sI - E)^{-1}F \tag{2C.6}$$

We augment the systems represented in (2C.1, 2C.2) with (2C.4, 2C.5) as

shown below by defining a new state vector $(x, z)^T$.

Augmented System:

$$\begin{bmatrix} \dot{x}(t) \\ \dot{z}(t) \end{bmatrix} = \begin{bmatrix} A & BD \\ 0 & E \end{bmatrix} \begin{bmatrix} x(t) \\ z(t) \end{bmatrix} + \begin{bmatrix} 0 \\ F \end{bmatrix} e(t) \tag{2C.7}$$

2-50

$$v(t) = \begin{bmatrix} C & 0 \end{bmatrix} \begin{bmatrix} x(t) \\ z(t) \end{bmatrix}$$

(2C.8)

Note that the BD term in (2C.7) comes from combining (2C.1) and (2C.5).

Let us rewrite this augmented system as:

$$\dot{x}^1(t) = A^1 x^1(t) + B^1 e(t)$$

(2C.9)

$$y(t) = C^1 x^1(t)$$

(2C.10)

where:

$$x^1(t) = [(x(t), z(t)^T]$$

(2C.11)

$$A^1 = \begin{bmatrix} A & BD \\ 0 & E \end{bmatrix}$$

(2C.12)

$$B^1 = \begin{bmatrix} 0 \\ F \end{bmatrix}$$

(2C.13)

$$C^1 = \begin{bmatrix} C & 0 \end{bmatrix}$$

(2C.14)

Let

$$A_1 = I$$

$$A_2 = -C^1$$

$$A_3 = B^1$$

$$A_4 = sI - A^1$$

Then using (2B.4) we have

$$\det \begin{bmatrix} A_1 & A_2 \\ A_3 & A_4 \end{bmatrix}$$

$$= \det(A_4) \cdot \det(A_1 - A_2 A_4^{-1} A_3)$$

$$= \det(sI - A^1) \cdot \det(I + C^1(sI - A^1)^{-1} B^1)$$

$$= \det \begin{bmatrix} sI-A & -BD \\ 0 & sI-E \end{bmatrix} \cdot \det \left\{ I + \begin{bmatrix} C & 0 \end{bmatrix} \begin{bmatrix} sI-A & -BD \\ 0 & sI-E \end{bmatrix}^{-1} \begin{bmatrix} 0 \\ F \end{bmatrix} \right\}$$

(2C.15)

Since $(sI - A)$ and $(sI - E)$ are square matrices, using (2B.2) we have

$$\det \begin{bmatrix} sI - A & -BD \\ 0 & sI - E \end{bmatrix} = \det(sI - A) \cdot \det(sI - E) \qquad (2C.16)$$

It is easy to verify that

$$\begin{bmatrix} sI - A & -BD \\ 0 & sI - E \end{bmatrix}^{-1} = \begin{bmatrix} (sI - A)^{-1} & (sI - A)^{-1}BD(sI - E)^{-1} \\ 0 & (sI - E)^{-1} \end{bmatrix} \qquad (2C.17)$$

Substituting (2C.16) and (2C.17) into (2C.15) and carrying out the

matrix multiplication we have

$$\det \begin{bmatrix} A_1 & A_2 \\ A_3 & A_4 \end{bmatrix}$$

$$= \det(sI - A) \cdot \det(sI - E) \cdot \det[I + C(sI - A)^{-1}BD(sI - E)^{-1}F] \qquad (2C.18)$$

Substituting (2C.3) and (2C.6) into (2C.18) we get

$$\det \begin{bmatrix} A_1 & A_2 \\ A_3 & A_4 \end{bmatrix}$$

$$= \det(sI - A) \cdot \det(sI - E) \cdot \det[I + G(s)F(s)] \qquad (2C.19)$$

From Appendix 2B, we know that (2B.2) and (2B.4) are equal. Let us

start with (2B.2) and simplify as shown

$$\det \begin{bmatrix} A_1 & A_2 \\ A_3 & A_4 \end{bmatrix}$$

$$= \det(A_1) \cdot \det(A_4 - A_3 A_1^{-1} A_2)$$

$$= \det(I) \cdot \det[(sI - A^1) + B^1 I^{-1} C^1]$$

$$= \det \left\{ \begin{bmatrix} sI - A & -BD \\ 0 & sI - E \end{bmatrix} + \begin{bmatrix} 0 \\ F \end{bmatrix} \begin{bmatrix} C & 0 \end{bmatrix} \right\}$$

$$= \det \begin{bmatrix} sI - A & -BD \\ FC & sI - E \end{bmatrix} \qquad (2C.20)$$

Using the result shown in (2B.4), we have

$$\det \begin{bmatrix} sI - A & -BD \\ FC & sI - E \end{bmatrix}$$

$$= \det(sI - E) \cdot \det(sI - A + BD(sI - E)^{-1}FC) \qquad (2C.21)$$

2-52

Substituting (2C.6) and (2C.21) into (2C.20), we have

$$\det(A_1)\cdot\det(A_4 - A_3A_1^{-1}A_2)$$

$$= \det(sI - E)\cdot\det[sI - A + BK(s)C] \qquad (2C.22)$$

Equating (2C.19) and (2C.22), we have

$$\det(sI - E)\cdot\det[sI - A + BK(s)C]$$

$$= \det(sI - A)\cdot\det(sI - E)\cdot\det[I + G(s)K(s)] \qquad (2C.23)$$

Because $K(s)$ is a transfer matrix, the matrices $[sI - A + BK(s)C]$ and $[I + G(s)K(s)]$ in (2C.23) are also transfer matrices, meaning each element of these matrices is a transfer function. Therefore, the determinants of these matrices are transfer functions with poles and zeros. However, the product of $\det(sI - E)$ and $\det[sI - A + BK(s)C]$ is a polynomial because the denominator of $\det[sI - A + BK(s)C]$ gets completely cancelled. Similarly, the denominator of $\det[I + G(s)K(s)]$ also gets completely cancelled when multiplied by $\det(sI - A)$ and $\det(sI - E)$ (you can verify these facts easily with a simple example, if you wish). Thus, both sides of (2C.23) are polynomials.

We know that the poles of the open-loop system are the poles of $G(s)$ and $K(s)$, or in other words, the eigenvalues of the A and E matrices. We define, then

$$\phi_{OL}(s) = \det(sI - A)\cdot\det(sI - E) \qquad (2C.24)$$

Following the derivation done in Section 2.2-4, we realize that

$$\phi_{CL}(s) = \det(sI - E)\cdot\det[sI - A + BK(s)C] \qquad (2C.25)$$

We can now rewrite (2C.23) to show the relationship between $\phi_{CL}(s)$ and $\phi_{OL}(s)$ as

$$\phi_{CL}(s) = \phi_{OL}(s)\cdot\det[I + G(s)K(s)] \qquad (2C.26)$$

2-53

where $\phi_{CL}(s)$ and $\phi_{OL}(s)$ are given in (2C.24) and (2C.25). Because of the definition of $\phi_{OL}(s)$ shown in (2C.24) and to insure both sides are polynomials, we have not cancelled the term $\det(sI - E)$ on both sides of (2C.23). If $K(s)$ is a pure gain matrix, then the realization in (2C.4 - 2C.6) does not exist. If we let $K(s) = K$, then (2C.23) becomes

$$\det(sI - A + BKC) = \det(sI - A) \cdot \det(I + G(s)K) \qquad (2C.27)$$

If K is identity, then (2C.27) becomes

$$\det(sI - A + BC) = \det(sI - A) \cdot \det[I + G(s)] \qquad (2C.28)$$

which is the same result as obtained in Section 2.2-4.

Appendix 2D

A brief explanation of relative primeness of polynomials to understand

equation (2.131)

A <u>monic</u> polynomial is one whose highest degree term has a coefficient equal to one.

Example: Consider the polynomial $f(x)$

$$f(x) = f_n x^n + f_{n-1} x^{n-1} + \ldots + f_o$$

The polynomial $f(x)$ is monic if $f_n = 1$.

A <u>common divisor</u> of polynomials $a_1(x)$, $a_2(x)$, ...,$a_k(x)$ is a polynomial which divides each $a_i(x)$ without remainder.

The <u>greatest common divisor</u> (g.c.d.) is the unique monic common divisor of highest degree, and is itself divisible by any common divisor.

Example: Consider the following factored polynomials:

$$a_1(x) = (x+3)(x+5)(x+10)$$

$$a_2(x) = (x+3)(x+7)(x+9)(x+10)$$

$$a_3(x) = (x+1)(x+3)(x+7)(x+10)(x+13)$$

For this set of polynomials, the common divisors are

$$(x+3), \ (x+10), \text{ and } (x^2 + 13x + 30)$$

The greatest common divisor is $(x^2 + 13x + 30)$, because it has the highest degree, is unique, monic and is itself divisible by any common divisor, such as $(x+3)$, $(x+10)$ or $(x^2 + 13x + 30)$.

A set of polynomials is said to be <u>relatively prime</u> if the g.c.d. has zero order (i.e., equal to unity).

Example: Consider the following factored polynomials

$$a_1(x) = (x+1)(x+3)(x+5)$$

$$a_2(x) = (x+3)(x+9)(x+11)$$

$$a_3(x) = (x+5)(x+11)(x+17)$$

There is no common divisor for all these polynomials except unity. Therefore, the g.c.d. is unity, and $a_1(x)$, $a_2(x)$ and $a_3(x)$ are relatively prime. However, the groups $[a_1(x), a_2(x)]$, $[a_2(x), a_3(x)]$ and $[a_1(x), a_3(x)]$ are not relatively prime, as each has a non-unity g.c.d.

Appendix 2F

Definition of right coprime factorization (r.c.f) to understand equation (2.136)

Suppose $G(s)$ is a transfer function matrix with real coefficients. An ordered pair (N_r, D_r) is called a r.c.f. of $G(s)$ if:

(i) Each element of $N_r(s)$ and $D_r(s)$ is a proper (i.e., the number of poles is greater than or equal to the number of zeros) stable transfer function.

(ii) $D_r(s)$ is square, non-singular and

$$G(s) = N_r(s)[D_r(s)]^{-1}$$

(iii) There exist matrices $X_r(s)$ and $Y_r(s)$ such that

$$X_r(s)N_r(s) + Y_r(s)D_r(s) = I$$

for all s (this is called a Bezout identity).

The left-coprime factorization of $G(s) = [D_\ell(s)]^{-1}N_\ell(s)$ can be defined analogously.

Chapter 2 References

[2-1] J.J. D'Azzo and C.H. Houpis, Linear Control System Analysis and Design, McGraw-Hill, 1981.

[2-2] J.G. Reid, Linear System Fundamentals, McGraw-Hill, 1983.

[2-3] C.T. Chen, Linear System Theory and Design, HRW Series in Electrical and Computer Engineering, 1984.

[2-4] T. Kailath, Linear Systems, Prentice-Hall, 1980.

[2-5] Kwakernaak and Sivan, Linear Optimal Control Systems, Wiley, 1972.

[2-6] M. Athans, Lecture Notes on Multivariable Control Systems, MIT, June 1984.

[2-7] A.G.J. MacFarlane, and N. Karcanias, "Poles and Zeros of Multivariable Systems: A Survey of the Algebraic, Geometric, and Complex Variable Theory", Int. J. of Control, Vol.22, 1975, pp. 657-681.

[2-8] C.N. Nett, C.A. Jacobson, and M.J. Balas, "A Connection Between State Space and Doubly Coprime Fractional Representations", IEEE Trans Auto Control, Vol AC-29, No. 9, Sept 1984, pp 831-832.

[2-9] A.J. Laub, and B.C. Moore, "Calculation of Transmission Zeros Using QZ Techniques", Automatica, Vol. 14, No. 6, Nov. 1978, pp 557-566.

[2-10] V.C. Klema, and A.J. Laub, "The Singular Value Decomposition: Its Computation and Some Applications", IEEE Trans Auto Control, Vol AC-25, No. 2, April 1980, pp 164-176.

[2-11] B.A. Francis, J.W. Helton and G. Zames, "H^{∞} - Optimal Feedback Controllers For Linear Multivariable Systems", IEEE Trans Auto Control, Vol. AC-29, No. 10, Oct 1984, pp 888-901.

[2-12] F.R. Gantmacher, The Theory of Matrices, Volumes One and Two, Chelsea Publishing Co., NY, 1977.

[2-13] W.L. Brogan, Modern Control Theory, Quantum Publishers, Inc, 1974.

Errata for Chapter 2

2.1.4 Definiteness of Matrices

Any matrix A can be written as

$$A = A_s + A_{skew}$$

where A_s is the symmetric portion of the A matrix, given by

$$A_s = \frac{1}{2}(A + A^T)$$

and A_{skew} is the skew-symmetric portion of A, given by

$$A_{skew} = A - A_s$$

When definiteness of a matrix is determined by using eigenvalues, it is based upon only the symmetric portion of the matrix. In the notes, wherever definiteness is defined through eigenvalues, we assume the matrix A has been replaced by the symmetric portion of A.

Appendix 2F

In the last line, $G(s) = [N_\ell(s)]^{-1} D_\ell(s)$ should be $G(s) = [D_\ell(s)]^{-1} N_\ell(s)$.

Chapter 2 References

In Reference 11, "H -Optimal..." should read "H^∞-Optimal...".

3. ROBUSTNESS ANALYSIS

3.1 Introduction

Any mathematical model can only approximate the behavior of a physical system. The problems created by model uncertainties (such as parameter variations, unmodelled or incorrectly modelled dynamics, etc.) have often been either trivialized or ignored in theoretical studies in favor of assuming the alternative of no distinction between models and reality. Stability and good performance in the face of these uncertainties is precisely the issue under study in this chapter.

In designing a feedback compensator, one nominal model must be selected from a class of models that approximate the physical system's behavior, denoted by G . Once a nominal model has been selected, an associated class of modelling errors is defined implicitly by the deviation of any model in G from the nominal design model. When a compensator is designed using this nominal model, the resulting feedback system is said to be robust with respect to the class of modelling errors if it remains stable when the nominal model is replaced by any other model in G. Otherwise, the feedback system is not robust.

The original work in this area was done by Safonov [3-1,3-2], who generalized an approach of Zames [3-3,3-4]. Doyle has since extended the works of Safonov and Zames [3-5,3-6,3-7]. There are many other people who have done excellent work in this area, but are not shown in the reference list of this chapter.

It should be pointed out that there are two types of robustness -- stability robustness and performance robustness. If a closed-loop system remains <u>stable</u> in the face of uncertainties, then that system is

said to possess stability robustness. If the _performance_ of a closed-loop system in the face of uncertainties is acceptable, then that system is said to possess performance robustness.

This chapter addresses the stability robustness problem only. We do this because it doesn't make sense to study various techniques for performance robustness without studying the stability robustness aspects first. Ultimately, the control designer has to make a trade between stability and performance robustness. This trade-off, as well as performance robustness issues, will be addressed starting from Chapter 4.

This chapter highlights four technical papers by Yeh, Banda, Ridgely, and Yedavalli, which were presented at various conferences and are due to appear as Journal articles in 1985. The actual papers appear in Appendices 3A, 3B, and 3C. The reader of these notes is urged to study the material in these Appendices carefully so that he or she can appreciate the techniques. To assist the reader in this regard, sections 3.2 - 3.4 outline some of the major points and discuss the implications and limitations of the results. In these sections, the numbers of the equations, figures, theorems, etc., refer to those in the papers in the corresponding appendices, unless otherwise stated.

3.2 Remarks on Appendix 3A

The most familiar types of errors are probably those of absolute and relative errors. Absolute errors are _additive_ in nature whereas relative errors are _multiplicative_ in nature. One can use both types of errors to derive robustness theorems. Typically, errors in high frequency dynamics (neglected either due to ignorance or due to reduced-order modelling) are characterized by additive perturbations

(Fig 1). Multiplicative perturbations are represented in Fig 2 at the input to the plant and are called input multiplicative perturbations. If these are represented at the output of the plant, then they are called output multiplicative perturbations. Typically, errors in actuator and sensor dynamics are modelled by input and output multiplicative perturbations, respectively. Since the familiar notions of gain and phase margins are associated only with relative errors, multiplicative type perturbations are used to calculate these margins, which will be discussed further in Section 3.3.

Let $G(s)$ indicate the nominal open-loop transfer matrix (i.e., it includes the plant and the controller). Let $\widetilde{G}(s)$ indicate the perturbed open-loop transfer matrix. Also, let $E(s)$ generically denote the particular modelling error under consideration. Then, additive perturbations can be thought of as

$$E(s) = \widetilde{G}(s) - G(s) \tag{3.1}$$

and multiplicative perturbations can be thought of as

$$F(s) = G^{-1}(s)[\widetilde{G}(s) - G(s)] \tag{3.2}$$

or

$$E(s) = [\widetilde{G}(s) - G(s)]G^{-1}(s) \tag{3.3}$$

Suppose that instead of measuring the absolute and relative errors between $\widetilde{G}(s)$ and $G(s)$, we measure the absolute and relative errors between $\widetilde{G}^{-1}(s)$ and $G^{-1}(s)$. In the SISO case, this would correspond to measuring the absolute and relative errors between the nominal and perturbed systems on an inverse Nyquist diagram, in which the inverse loop transfer functions $\widetilde{g}^{-1}(s)$ and $g^{-1}(s)$ are plotted. The inverse Nyquist diagram can also be used to determine stability by counting encirclements of the critical points $(0,0)$ and $(-1,0)$ in the complex

plane. For details see the textbook on control systems by D'Azzo and
Houpis (Ref [3-8]). In this case, the characterization of the error is
referred to as inverse additive (Fig 3) or inverse multiplicative (Fig
4) perturbations. Typically, we model the errors associated with mode
shapes and right-half-plane pole locations using either inverse additive
or inverse multiplicative types of perturbations. The inverse additive
errors $E(s)$ can be thought of as

$$E(s) = \widetilde{G}^{-1}(s) - G^{-1}(s) \tag{3.4}$$

and the inverse multiplicative errors $E(s)$ can be thought of as

$$E(s) = G(s)[\widehat{G}^{-1}(s) - G^{-1}(s)] \tag{3.5}$$

or

$$E(s) = [\widetilde{G}^{-1}(s) - G^{-1}(s)]G(s) \tag{3.6}$$

The merits and demerits of modelling a particular type of error
using one characterization versus another are not well known. For
example, one could model the errors associated with high-frequency
dynamics using multiplicative perturbations instead of additive
perturbations. There are no "rules of thumb" to decide which is the
best way to characterize the uncertainty. This still remains an open
question in current research.

Typically, the robustness tests have the following forms. The
magnitude (or norm) of the modelling error (or uncertainty) is
characterized by a nonnegative frequency-dependent scalar function. The
measure of robustness is also characterized by a nonnegative
frequency-dependent scalar function that represents the magnitude (or
norm) of a certain matrix related to the feedback system. The
robustness tests consist of a comparison of these quantities for all
frequencies on the Nyquist contour.

Let us concentrate on additive and multiplicative perturbations only, since they can be used to represent a large class of uncertainties. The following table summarizes robustness tests for these two types of perturbations (also see equations (1) and (2)).

Table 3.1   Summary of Singular Value Stability Robustness Tests

Type of Perturbation	Error Criterion Perturbed System and Stability Test
Additive	$E(s) = \widetilde{G}(s) - G(s)$ $\widetilde{G}(s) = G(s) + E(s)$ $\bar{\sigma}[E(s)] < \underline{\sigma}[I + G(s)]$
Multiplicative	$E(s) = G^{-1}(s)[\widetilde{G}(s) - G(s)]$ $\widetilde{G}(s) = G(s)[I + F(s)]$ $\bar{\sigma}[E(s)] < \underline{\sigma}[I + G^{-1}(s)]$

The proofs used to derive the stability robustness tests shown in Table 3.1 are based upon Multivariable Nyquist Theory. Interested readers can look into the references listed at the end of this chapter. There are several assumptions made in deriving these results. One of the important assumptions that we will be requiring later is that the nominal closed-loop system must be stable in order to apply these tests. This shouldn't cause too much concern since nominal closed-loop systems are designed to be stable. Implications of this particular assumption will be discussed further in Section 3.3.

Given a plant and given a controller, the loop transfer matrix G(s) is completely known. For additive perturbations, calculation of the minimum singular value of the matrix I + G(s) will give an upper-bound on the uncertainty matrix that the system can tolerate in order for the

3-5

closed-loop system to remain stable. In other words, if the norm of the error matrix $E(s)$ is less than $\underline{\sigma}[I + G(s)]$ for all frequencies, then the closed-loop system is <u>guaranteed</u> to be stable. However, it should also be pointed out that if the norm of the error matrix $E(s)$ is greater than $\underline{\sigma}[I + G(s)]$ (i.e., if the test fails), the test is inconclusive. This means that if the design fails the test, the closed-loop system may or may not be stable and it requires further examination. The reason this happens is that these tests assume the error occurs in the worst possible direction. For multiplicative perturbations, we use $I + G^{-1}(s)$ instead of $I + G(s)$ in the robustness tests.

Because these tests are only sufficient conditions, not necessary <u>and</u> sufficient conditions, they may give overly conservative results for some systems. This should not, however, be looked down upon in general, because these norm-bounded robustness tests give rise to a great deal of theory that answers other important questions. It can, for example, give answers to the questions posed in the example of the paper. These types of questions couldn't have been answered before the development of this theory. In addition, this theory allows us to clearly define and compute multivariable stability margins. Finally, this theory can be extended to give a synthesis procedure that accounts for uncertainties.

We should notice that the tests use only the magnitude of the modelling error and do not exploit any other characteristics or structure of the model error. Hence, they are based on the unstructured part of the model error. In other words, these tests give only a scalar bound on the entire uncertainty matrix. However, it is possible to give bounds on the individual elements of the uncertainty matrix using weighted ℓ_1 and ℓ_∞ norms.

Table 3.2 summarizes some of the results of the paper. The following notation is used in the table. We let

$$A(s) = [I + G^{\pm 1}(s)]^{-1} \qquad (3.7)$$

where $G^{\pm 1}(s)$ refers to $G(s)$ or $G^{-1}(s)$ for additive or multiplicative perturbations, respectively. $|A|$ indicates the magnitude of a_{ij} for all i, j. $\bar{\lambda}(|A|)$ indicates the Perron eigenvalue of the matrix A (the Perron eigenvalue of A is the positive eigenvalue of $|A|$ which is greater than or equal to the magnitude of any other eigenvalue, and the corresponding eigenvector is the only one that has all positive components).

Table 3.2 Some Stability Robustness Tests with Structured Uncertainty	
Theorem number in the paper [comments]	Test
1 [only when F(s) or G(s) is a diagonal matrix]	$\bar{\lambda}[\,|E(s)|\,] < 1/\bar{\lambda}[\,|A(s)|\,]$
2 [only when E(s) and G(s) are triangular matrices]	$\max_i[\,|e_{ii}(s)|\,] < 1/\max_i[\,|a_{ii}(s)|\,]$
3 [any E(s) and G(s)]	$|E(s)| < |A(s)|/\bar{\lambda}^2[\,|A(s)|\,]$
5 [any E(s) and G(s)]	$\max_{i,j}|e_{ij}(s)| < 1/n$ (m.r.s.[m.c.s] of $|A(s)|$)
6 [any E(s) and G(s)]	m.r.s[m.c.s] of $|E(s)|$ < 1/m.r.s.[m.c.s.] of $|A(s)|$

m.r.s. – maximum row sum

m.c.s. – maximum column sum

Notice that Theorem 3 yields bounds on the magnitude of all the elements in the uncertainty matrix $E(s)$. Obviously, this gives a great deal more information about the system when compared to obtaining a single bound on $E(s)$ using singular value tests. Also notice that when $E(s)$ and $G(s)$ have triangular structure, Theorem 2 permits the off-diagonal elements of $E(s)$ to be unrestricted in magnitude. Theorem 3 doesn't impose any restrictions on $F(s)$ or $G(s)$ and is applicable even when $E(s)$ and $G(s)$ are triangular. This is why Theorem 2 gives less conservative (better) results than Theorem 3 when $E(s)$ and $G(s)$ are triangular. Nevertheless, Theorem 3 provides a way to structure $E(s)$ when $G(s)$ is not triangular, which cannot be covered by Theorem 2. To appreciate the use of the theorems shown in Table 3.2, the reader is strongly recommended to carefully study the example given in the paper.

Before we close this section, it must be pointed out that the robustness analysis methods we have discussed so far are for the case where only one uncertainty was considered at a time. In reality we may have multiple uncertainties in a given system. For example, consider a system with both input and output multiplicative perturbations, as shown in Fig 3.1.
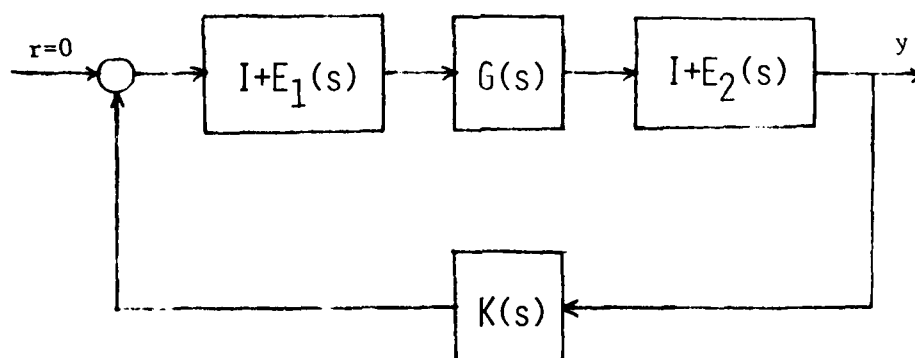
Fig 3.1 An Example of a Block Diagram With Multiple Uncertainties

The analysis of such systems has been done by Doyle using his structured singular value technique as discussed in Ref [3-6]. Consider Fig 3.2 shown below.
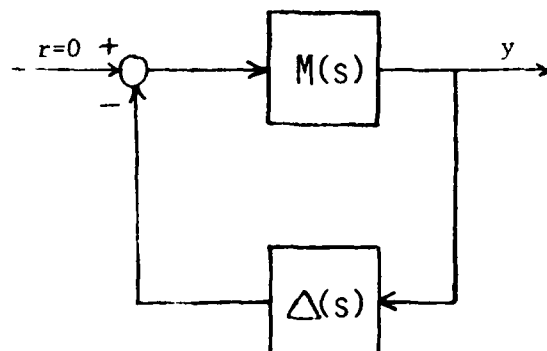
Fig 3.2 An Equivalent Block Diagram to Fig 3.1

Doyle shows that Figs 3.1 and 3.2 are equivalent (for a zero input) if M(s) is chosen, for example, as

$$
M(s) = \begin{bmatrix} (I + KG)^{-1}KG & (I + KG)^{-1}K \\ -(I + GK)^{-1}G & (I + GK)^{-1}GK \end{bmatrix} \tag{3.8}
$$

In other words, Figs 3.1 and 3.2 are equivalent from a closed-loop stability point-of-view if M(s) is selected as shown in (3.8). In Fig 3.2, $\Delta(s)$ is given by

$$
\Delta(s) = \begin{bmatrix} \Gamma_1(s) & 0 \\ 0 & \Gamma_2(s) \end{bmatrix} \tag{3.9}
$$

Similar equivalent block diagrams can be drawn even when we have more than two uncertainties. Doyle shows that the nondestabilizing bounds on the uncertainties $\Gamma_1(s)$ and $\Gamma_2(s)$ are given by a scalar function, μ, which he calls the structured singular value, where

$$
\mu = \inf_D \bar{\sigma}(DMD^{-1}) \tag{3.10}
$$

This formula is good only if the number of uncertainties is less than or equal to three. In (3.10), D is a real diagonal weighting matrix. If

the number of uncertainties is more than three, the formula for μ is much more involved than (3.10), and is not shown here. If only one uncertainty is considered, μ is the same as $\overline{\sigma}$.

Although the structured singular value is a much more versatile tool than those previously discussed in this section, its computation is a different matter. First, note that if the dimension of $G(s)$ is (nxn), then $M(s)$ is (2nx2n), and so is D. Equation (3.10) requires calculation of the infimum of $\overline{\sigma}(DMD^{-1})$ over all D. This requires a search for the optimum D over a 2n-dimensional real space with all possibilities allowed. To the knowledge of the authors of these notes, very few individuals or organizations besides Doyle and his co-workers have the ability to easily calculate μ for a general case. Calculation of μ becomes much more simple, as can be expected, in the case of SISO systems, because then D is (2x2) and a search for the optimum ratio of the two diagonal elements can be done over a 1-dimensional real space easily.

3.3 Remarks on Appendix 3B

This appendix contains two papers on stability margins (i.e., gain and phase margins) for MIMO systems. For SISO systems, single-input multiple-output (SIMO) systems, or multiple-input single-output (MISO) systems, we open one loop at a time and allow the gain or phase to vary in that loop alone. By keeping the value of gain and phase in the other loops at nominal values we can calculate the stability margins for that loop using graphical techniques, like Bode plots, Nyquist plots, etc. However, it is not obvious how to calculate the stability margins for MIMO systems because they not only have multiple loops, but also have cross-feed transfer functions as well. For MIMO systems, what we need

is a method that allows us to vary all the loop gains or loop phases simultaneously in order to calculate the stability margins.

The key to doing this is to assume diagonal perturbations in the stability robustness tests that we discussed in Section 3.2. This diagonal-type perturbation will make the problem tractable and will yield simple-to-use formulas to obtain stability margins. Consider Fig. 1 in the first paper. Let the diagonal perturbation $L(jw)$ be

$$L(jw) = L_1(jw)K(jw) \tag{3.11}$$

where

$$K(jw) = \text{diag}[k_1(jw), k_2(jw), \ldots, k_n(jw)] \tag{3.12}$$

and either

$$L_1(jw) = \text{diag}[\beta_1(w)e^{j\theta_1(w)}, \beta_2(w)e^{j\theta_2(w)}, \ldots, \beta_n e^{j\theta_n(w)}] \tag{3.13}$$

or

$$L_1(jw) = \beta(w)e^{j\theta(w)} I \tag{3.14}$$

Equation (3.13) is used for obtaining independent margins, and equation (3.14) is used for obtaining uniform margins (see paper for definitions of these). The matrix $K(jw)$ shown in equation (3.12) is used to update the nominal system. Before we start the first iteration, we let $K(jw) = I$.

For input multiplicative perturbations, we have the following stability robustness tests

$$\bar{\sigma}[L_1 - I] < \underline{\sigma} [I + (HGK)^{-1}] \tag{3.15}$$

or

$$\bar{\sigma}[L_1^{-1} - I] < \alpha \leqslant \underline{\sigma} [I + HGK] \quad, \alpha \leqslant 1 \tag{3.16}$$

Equation (3.15) is the same as the one shown in Table 3.1, using the notation of Fig. 1 in the first paper of this Appendix. Equation (3.15) is written based on Inverse Nyquist criteria, whereas equation (3.16),

another type of robustness test, is written using Nyquist criteria. We
can also rewrite (3.15-3.16) in terms of eigenvalues as

$$\max_{i} \left| \lambda_i [L_1 - T] \right| < \min_{i} \left| \lambda_i [T + (HGK)^{-1}] \right| \qquad (3.17)$$

or

$$\max_{i} \left| \lambda_i [L_1^{-1} - I] \right| < \alpha \leq \min_{i} \left| \lambda_i [T + HGK] \right| , \quad \alpha \leq 1 \qquad (3.18)$$

The proofs for (3.17-3.18) are given in the first paper. To obtain
independent margins, we use (3.13) in (3.15). If we let
$\theta_1(w) = \theta_2(w) = \ldots = \theta_n(w) = 0$, then we obtain independent gain margins
(IGM), and if we let $\beta_1(w) = \beta_2(w) = \ldots = \beta_n(w) = 1$, then we obtain
independent phase margins (IPM). Similarly, if we substitute (3.14)
into (3.17), it will yield uniform margins. Substitution of $\theta(w) = 0$
gives uniform gain margins (UGM) and $\beta(w) = 1$ gives uniform phase
margins (UPM). Since (3.16) and (3.18) are also stability robustness
tests, substitution of (3.13) and (3.14) into those equations will also
result in independent and uniform stability margins, respectively.
Since (3.15) and (3.16) both yield independent stability margins and
since both of these inequalities are only sufficient conditions, their
union also gives independent stability margins and is less conservative
(i.e., wider margin). Similarly, less conservative uniform stability
margins are given by the union of (3.17) and (3.18).

In what follows, we will show the derivation of the formulas for
IGM and IPM. Substituting (3.13) into (3.15), we get

$$\bar{\sigma}\{diag[(\beta_1 e^{j\theta_1}-1), (\beta_2 e^{j\theta_2}-1),\ldots,(\beta_n e^{j\theta_n}-1)]\} < \underline{\sigma} [I + (HGK)^{-1}] \qquad (3.19)$$

To get IGM, we let

$$\theta_1 = \theta_2 = \ldots = \theta_n = 0 \qquad (3.20)$$

and

$$a_1 = \underline{\sigma} [I + (HGK)^{-1}] \qquad (3.21)$$

Then (3.19) becomes

$$\bar{\sigma}\{\text{diag}[(\beta_1 - 1), (\beta_2 - 1), \ldots, (\beta_n - 1)]\} < a_1 \qquad (3.22)$$

which can be written as

$$\max_i |\beta_i - 1| < a_1 \qquad (3.23)$$

If the largest $|\beta_i - 1|$ is less than a_1, then all of them must be, so that

$$|\beta_i - 1| < a_1 \qquad \forall\ i \qquad (3.24)$$

which may be rewritten as

$$1 - a_1 < \beta_i(w) < 1 + a_1 \qquad \forall\ i \qquad (3.25)$$

The terms $1 + a_1$ and $1 - a_1$ in (3.25) are the upper and lower bounds of the IGM. To get the IPM, we let

$$\beta_1 = \beta_2 = \ldots = \beta_n = 1 \qquad (3.26)$$

Using (3.21) and (3.26) in (3.19), we get

$$\bar{\sigma}\{\text{diag}[(e^{j\theta_1} - 1), (e^{j\theta_2} - 1), \ldots, (e^{j\theta_n} - 1)]\} < a_1 \qquad (3.27)$$

so that

$$\max_i |e^{j\theta_i} - 1| < a_1 \qquad (3.28)$$

This implies

$$|e^{j\theta_i} - 1| < a_1 \qquad \forall\ i \qquad (3.29)$$

which may be rewritten as follows

$$|\cos\theta_i + j\sin\theta_i - 1| < a_1 \qquad \forall\ i \qquad (3.30)$$

$$|(\cos\theta_i - 1) + j\sin\theta_i| < a_1 \qquad \forall\ i \qquad (3.31)$$

$$[\cos^2\theta_i - 2\cos\theta_i + 1 + \sin^2\theta_i]^{\frac{1}{2}} < a_1 \qquad \forall\ i \qquad (3.32)$$

$$[2(1 - \cos\theta_i)]^{\frac{1}{2}} < a_1 \qquad \forall\ i \qquad (3.33)$$

$$\{2[2\sin^2(\theta_i/2)]\}^{\frac{1}{2}} < a_1 \qquad \forall\ i \qquad (3.34)$$

The above equation yields

$$\sin(\theta_i/2) < a_1/2 \qquad \forall\ i \qquad (3.35)$$

or

$$-\sin(\theta_i/2) < a_i/2 \qquad\qquad \forall\ i \qquad\qquad (3.36)$$

Equation (3.35) and (3.36) can be written as

$$\theta_i < 2\sin^{-1}(a_i/2) \qquad\qquad \forall\ i \qquad\qquad (3.37)$$

and

$$\theta_i > -2\sin^{-1}(a_i/2) \qquad\qquad \forall\ i \qquad\qquad (3.38)$$

Equation (3.37) and (3.38) may be combined to give

$$-2\sin^{-1}(a_1/2) < \theta_i(w) < 2\sin^{-1}(a_1/2) \qquad \forall\ i \quad \text{if } a_1 \leqslant 2 \qquad (3.39)$$

and

$$-\pi < \theta_i(w) < \pi \qquad\qquad \forall\ i \quad \text{if } a_1 > 2 \qquad (3.40)$$

Equation (3.40) is true since $2\sin^{-1}(a_i/2)$ lies in between $-\pi$ and π, which are the principal angles. Equations (3.39) and (3.40) give the upper and lower bounds of the IPM.

Substituting (3.13) into (3.16) and doing the algebra shown in (3.22-3.40), we can obtain the IGM and IPM again as

$$\frac{1}{1+\alpha_1} < \beta_i(w) < \frac{1}{1-\alpha_1} \qquad\qquad \forall\ i \qquad\qquad (3.41)$$

$$-2\sin^{-1}(\alpha_1/2) < \theta_i(w) < 2\sin^{-1}(\alpha_1/2) \qquad \forall\ i \qquad (3.42)$$

where

$$\alpha_1 = \underline{\sigma}[I + HGK] \qquad\qquad (3.43)$$

The union of (3.25) and (3.41) will also give IGM (i.e., the larger and smaller numbers of both the upper and lower limits). Similarly, the union of (3.39) and (3.42) will also give IPM.

Recall that for diagonal matrices, singular values and eigenvalues are identical. Substituting (3.14) into (3.17) and (3.18) and following the same algebra as before, we obtain formulas for the UGM and UPM as

$$1 - a_o < \beta(w) < 1 + a_o \qquad\qquad (3.44)$$

$$-2\sin^{-1}(a_o/2) < \theta(w) < 2\sin^{-1}(a_o/2) \qquad \text{if } a_o < 2 \qquad (3.45)$$

$$-\pi < \theta(w) < \pi \qquad\qquad \text{if } a_o > 2 \qquad (3.46)$$

where

$$a_o = \min_i \left| \lambda_i [I + (HGK)^{-1}] \right| \qquad (3.47)$$

and

$$\frac{1}{1 + \alpha_o} < \beta(w) < \frac{1}{1 - \alpha_o} \qquad (3.48)$$

$$-2\sin^{-1}(\alpha_o/2) < \theta(w) < 2\sin^{-1}(\alpha_o/2) \qquad (3.49)$$

where

$$\alpha_o = \min_i \left| \lambda_i [I + HGK] \right| \qquad (3.50)$$

Equations (3.44), (3.48), and their union all give formulas for calculating the UGM. Similarly, equations (3.45), (3.49) and their union all give formulas for calculating the UPM.

Consider Fig 3.3, which doesn't represent any real physical system per se, but helps explain several points.
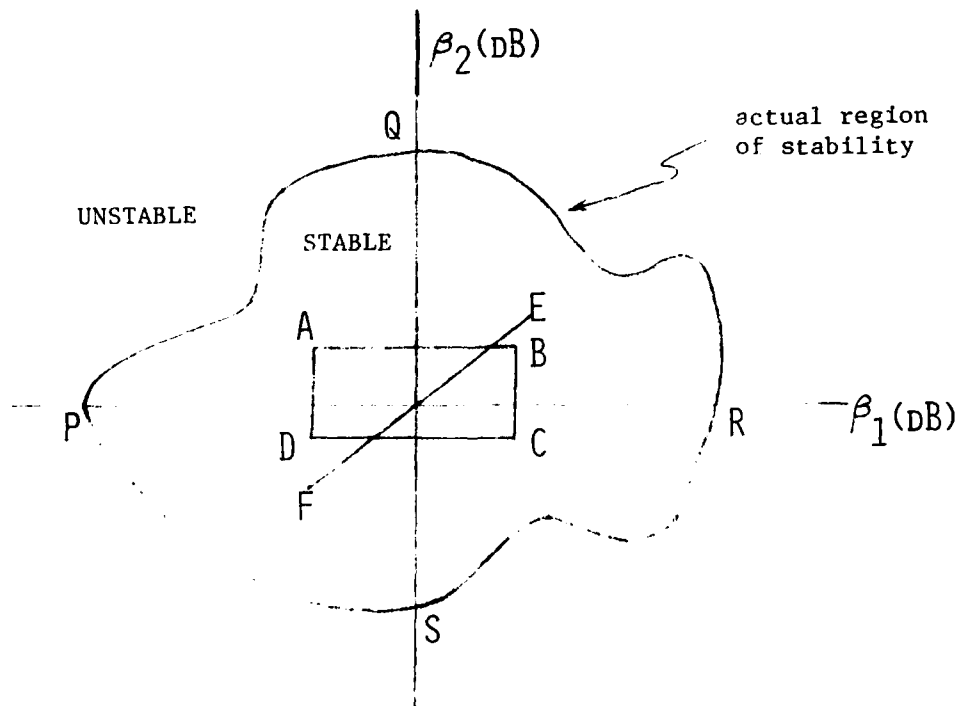
Fig 3.3 Region of Stability in the Gain Space

Let's suppose that the MIMO system Fig 3.3 corresponds to is a 2-input 2-output system. The axes β_1 and β_2 correspond to changes in the loop gains (in dB). Before the system is perturbed (i.e., the nominal system), the loop gains are at their nominal values, which corresponds to the origin in Fig 3.3. Suppose that [a,b] is the TGM in dB using the union of (3.25) and (3.41). This means that as long as the changes in the loop gains β_1 and β_2 lie within the limits [a,b], the closed-loop system is stable. Since by definition of the TGM, β_1 and β_2 can take any value within [a,b] independently and simultaneously, the region of stability is given by the rectangle ABCD. The coordinates of ABCD in terms of a and b are given in Table 3.3.

Table 3.3   Coordinates of ABCD in Fig 3.3

Point	Coordinates
A	(a,b)
B	(b,b)
C	(b,a)
D	(a,a)

Hence, the definition of TGM guarantees that as long as the changes in the loop gains remain within the rectangle ABCD, the closed-loop system is stable. The second paper in this Appendix proves that every point on the boundary of ABCD is also stable, so long as $\underline{\sigma}[I + HGK] \neq 0$ anywhere on the boundary.

Now let us study the line segment EF. Suppose that [c,d] is the UGM in dB using the union of (3.44) and (3.48). This means that as long as each loop gain is changed by the same amount somewhere within [c,d], the closed-loop system is stable. This corresponds to the line segment EF with slope equal to +1 and passing through the nominal operating

point. The slope of this line is +1 because every point on this line corresponds to the same change in loop gains β_1 and β_2. The coordinates of the points E and F are (d,d) and (c,c). The definition of UGM guarantees that every point on the line segment EF is stable. The second paper in Appendix B proves that the end points E and F also correspond to closed-loop stability when $\min_i \left| \lambda_i [I + HGK] \right| \neq 0$ at those points.

Recall that

$$\underline{\sigma}(A) = 1/ \, \overline{\sigma}(A^{-1}) \tag{3.51}$$

and

$$\min_i \left| \lambda_i(A) \right| = 1/ \, \max_i \left| \lambda_i(A^{-1}) \right|$$
$$= 1/ \, \rho(A^{-1}) \tag{3.52}$$

where $\rho(\cdot)$ is the spectral radius of the matrix in the parentheses. The spectral radius of a matrix is always smaller than or equal to any other matrix norm. That is,

$$\rho(A^{-1}) \leqslant \overline{\sigma}(A^{-1}) \tag{3.53}$$

Therefore

$$\min_i \left| \lambda_i(A) \right| > \underline{\sigma}(A) \tag{3.54}$$

If we let

$$A = I + (HGK)^{-1} \tag{3.55}$$

then using the notation of (3.21) and (3.47), we have

$$a_0 \geqslant a_1 \tag{3.56}$$

Using a similar argument we also have (using the notation of (3.43) and (3.50))

$$\alpha_0 \geqslant \alpha_1 \tag{3.57}$$

Therefore, the UGM given by formulas (3.44) and (3.48) will be larger

than or equal to the IGM given by formulas (3.25) and (3.41).

Therefore, the UGM are less conservative than the IGM in a particular direction. However, UGM give only line segments whereas IGM give rectangles covering an area in the gain space. In the case where there are n loops, we will get hypercubes for the IGM, but the UGM will still give 1-dimensional line segments in the n-dimensional space.

Let's refer to Fig 3.3 again. The actual region of stability for the system under consideration may be given by the curve joining the points PQRS as shown in Fig 3.3. As long as changes in the loop gains remain within this region, the closed-loop system is guaranteed to be stable and every point outside this region corresponds to closed-loop instability. Recall that the UGM and IGM formulas are derived from (3.15-3.18), which are only sufficient conditions. This means that the changes in loop gains corresponding to the points outside the rectangle ABCD and off the line segment EF may or may not make the closed-loop system unstable. Our goal is, somehow, to generate the entire actual region of stability PQRS. Since closed-loop stability is guaranteed for every point on the boundary of ABCD, we can do iterative calculations of the UGM and IGM. For example, suppose we choose point A. We know that the changes in loop gains corresponding to that point are (a,b) in dB, and that the system is stable there. This means that we can convert (a,b) into actual magnitudes and use those gains as the diagonal elements in the K matrix in (3.13), i.e., define A as a new nominal operating point. UGM and IGM can then be calculated and plotted using point A as the origin of a new coordinate system. These iterations may be done successively until a_o, a_1, α_o or α_1 becomes (close to) zero.

The formulas for TPM and UPM can be used similarly to generate the entire region of stability in the phase space. See the second paper in Appendix 3B for one possible iteration scheme.

The actual region of stability in the gain or phase space could be obtained, if desired, using independent margins alone (instead of combination of independent and uniform margins). However, since uniform margins are less conservative in a particular direction, the actual boundary of stability will be reached using fewer iterations if uniform margins are used. Generation of regions of stability using only uniform margins is not possible since they generate only 45° lines. Stable regions not on a 45° line couldn't be obtained in an iterative fashion; rather, one would have to first check for nominal closed-loop stability at some other point (recall that these margins are derived from norm-bounded stability robustness tests with the assumption that the nominal closed-loop system is stable). Application of independent and uniform margins together gives an efficient method for computing the entire regions of stability, because the answers from one iteration lead into another iteration, and the number of iterations is minimized.

Finally, it should be noted that after generating the stable regions in the gain and phase spaces, one could double check the boundary in the gain space easily by computing closed-loop eigenvalues at points on the boundary. Such a check is not possible in the phase space since we can't write a transfer function corresponding to a pure phase shift. Also realize that although the method discussed here is good for n-loops, the solution is not tractable graphically for $n > 3$. Additionally, if there are completely detached stable spaces, this method will identify only the one containing the nominal system.

Lastly, a brute force application of SISO gain and phase margin formulas (by successively perturbing the system) will also generate the actual regions of stability, but could take considerably more computations and does not lend itself to computerization very well.

3.4 Remarks on Appendix 3C

This Appendix contains a paper on the area of time-domain robustness analysis. One of the goals in research on robustness analysis is to obtain bounds on the tolerable perturbations (from the stability and performance viewpoint) of the real parameters (such as stability and control derivatives). To meet such a goal, formulation of the problem in the time domain seems appropriate, since in our previously described frequency-domain formulations, information about real parameter variations is imbedded in the singular value bounds on the transfer matrices. However, concepts such as gain and phase margins (which are tolerable loop gain and loop phase variations) can only be handled in the frequency domain.

Time-domain robustness tests give explicit bounds on the real parameter perturbations in the A, B, and C matrices of the state-space model. We will consider three classes of perturbations, as follows:

I) Highly structured perturbations: Perturbation model structure is known and bounds on the individual elements of the perturbation matrix are known.

II) Weekly Structured Perturbations: Perturbation model structure is known, but only a spectral norm bound on the perturbation is known (with no knowledge about the individual element bounds).

III) **Unstructured Perturbations:** Perturbation model structure is not known.

For simplicity, we will use the terms "structured perturbation" for class (I) and "unstructured perturbation" for classes (II) and (III) from now on. For a good discussion on unstructured perturbations, see Ref [3-9]. We are not going to cover that material because we are only interested in obtaining bounds on individual elements of the A, B, and C matrices.

Consider the state space model

$$\dot{x} = Ax + Ex \tag{3.58}$$

where E is the perturbation matrix with structured perturbations

$$|e_{ij}| \leq \epsilon \tag{3.59}$$

The system $A + E$ is stable if

$$|e_{ij}|_{max} = \epsilon < \mu_{\epsilon Y} = 1/\bar{\sigma}[(|P|U_n)_s] \tag{3.60}$$

where P is the solution of Lyapunov matrix equation

$$A^T P + PA + 2I_n = 0 \tag{3.61}$$

and U_n is an (nxn) matrix with all elements equal to unity. The symbol $|\cdot|$ means modulus of every element in the matrix, $(\cdot)_s$ indicates the symmetric portion of the matrix in the parenthesis (i.e., for example, $(A)_s = \frac{1}{2}(A + A^T))$, and $\bar{\sigma}(\cdot)$ indicates the maximum singular value of the matrix $(\cdot)$.

Solution of the Lyapunov equation can be avoided if A is normal, i.e., if $AA^T = A^T A$. Then (see Ref [3-10]) the system $A + E$ is stable if

$$|e_{ij}|_{max} = \epsilon < \mu_{Y\epsilon} = 1/\bar{\sigma}[(|A^{-1}|U_n)_s] \tag{3.62}$$

We can get an even better bound than in (3.60) (or (3.62)) if structured information of the matrix A is taken into consideration. For example, given

$$A = [a_{ij}] \quad , \quad i,j = 1, 2, \ldots, n \tag{3.63}$$

we may have the additional knowledge that some of the elements of A are not subjected to any perturbations, i.e.,

$$e_{ij} = \Delta a_{ij} = 0 \quad \text{for some } i \text{ and } j \tag{3.64}$$

In such a case, a better bound can be obtained by substituting for the matrix U_n (in (3.60) and (3.62)) a matrix U_e whose entries are such that $U_{e_{ij}} = 0$ if the perturbation in a_{ij} is known to be zero (i.e., $e_{ij} = 0$), and $U_{e_{ij}} = 1$ if the perturbation in a_{ij} is known to be non-zero (i.e., $e_{ij} \neq 0$). This means that U_e is a matrix whose entries are normalized with respect to the maximum perturbation $|\Delta a_{ij}|_{max}$ as

$$U_{e_{ij}} = \frac{|\Delta a_{ij}|}{|\Delta a_{ij}|_{max}} \tag{3.65}$$

Thus, the entries will have the values 0 or 1, depending upon the location of the perturbation. Then, (3.60) and (3.62) can be rewritten as

$$|e_{ij}|_{max} = \varepsilon < \mu_{\varepsilon YS} = 1/\overline{\sigma}\left[(|P|U_e)_s\right] \tag{3.66}$$

where P is the solution of (3.61), and

$$|e_{ij}|_{max} = \varepsilon < \mu_{Y\varepsilon S} = 1/\overline{\sigma}\left[(|A^{-1}|U_e)_s\right] \tag{3.67}$$

To apply (3.66), consider an example where

$$A = \begin{bmatrix} -3 & -2 \\ 1 & 0 \end{bmatrix} \tag{3.68}$$

The results are shown in Table 3.3, which clearly indicate that the perturbation location directly influences the perturbation bound.

3-22

Table 3.3 Effect of Structural Information on Perturbation Bound

	Elements of A in which perturbation is assumed														
	all a_{ij}	a_{11} only	a_{12} only	a_{21} only	a_{22} only	a_{11} & a_{12}	a_{11} & a_{22}	a_{11} & a_{21}	a_{12} & a_{21}	a_{12} & a_{22}	a_{21} & a_{22}	a_{11}, a_{12}, a_{21}	a_{11}, a_{12}, a_{22}	a_{11}, a_{21}, a_{22}	a_{12}, a_{21}, a_{22}
U_e	$\begin{bmatrix}1&1\\1&1\end{bmatrix}$	$\begin{bmatrix}1&0\\0&0\end{bmatrix}$	$\begin{bmatrix}0&1\\0&0\end{bmatrix}$	$\begin{bmatrix}0&0\\1&0\end{bmatrix}$	$\begin{bmatrix}0&0\\0&1\end{bmatrix}$	$\begin{bmatrix}1&1\\0&0\end{bmatrix}$	$\begin{bmatrix}1&0\\0&1\end{bmatrix}$	$\begin{bmatrix}1&0\\1&0\end{bmatrix}$	$\begin{bmatrix}0&1\\1&0\end{bmatrix}$	$\begin{bmatrix}0&1\\0&1\end{bmatrix}$	$\begin{bmatrix}0&0\\1&1\end{bmatrix}$	$\begin{bmatrix}1&1\\1&0\end{bmatrix}$	$\begin{bmatrix}1&1\\0&1\end{bmatrix}$	$\begin{bmatrix}1&0\\1&1\end{bmatrix}$	$\begin{bmatrix}0&1\\1&1\end{bmatrix}$
$\mu_{\epsilon YS}$	0.236	1.657	1.657	0.655	0.396	1.0	0.382	0.48	0.5	0.324	0.3027	0.397	0.311	0.273	0.256

These results can be extended to the case of LQ and LQG Regulators. Following the notation used in the paper in Appendix 3C, we have that the perturbed closed-loop system of the LQ Regulator is stable if

$$\left|(\Delta A + \Delta B \cdot |G| + |B + \Delta B| \cdot |\Delta G|)\right|_{ij\max} < \mu_{\epsilon Y}$$
$$= 1/\bar{\sigma}\left[(|P| U_n)_s\right] \tag{3.69}$$

where ΔA, ΔB and ΔG are perturbations in the A, B and (controller gain) G matrices (there is no ΔC term since we assumed full state feedback), and P has to satisfy the Lyapunov equation

$$A_{CL}^{\ T}P + PA_{CL} = -2I_n \tag{3.70}$$

where A_{CL} is the nominal closed-loop system matrix given by

$$A_{CL} = A + BG \tag{3.71}$$

The matrix U_n can be replaced by U_e as before, if the locations of the perturbations in A_{CL} are known. If there are no perturbations in the B and G matrices (i.e., $\Delta B = \Delta G = 0$), then (3.69) gives bounds on the maximum tolerable variations of the real parameters in the A matrix. Similarly, if $\Delta A = \Delta G = 0$, then (3.69) gives bounds on the perturbations in the B matrix, and so on. In the case of the LQG problem, the

nondestabilizing bounds on the real parameters are given by equation
(26) in the paper and will not be repeated here.

Before we close this section, we should note the following. The
robustness tests in the frequency domain are derived based on Nyquist
stability criteria, whereas in the time domain, they are derived based
upon Lyapunov stability criteria. These robustness inequality tests in
both the frequency and time domains are only sufficient conditions,
i.e., if the design passes these tests, the closed-loop system is
guaranteed to be stable; otherwise, no claim can be made regarding
stability. These tests in both domains are conservative. This happens
in the frequency domain because the tests assume that the uncertainty is
in the worst direction (i.e., lack of phase information). In the time
domain, the robustness criteria actually give the conditions under which
perturbed matrix will be negative definite. This is done because all
negative definite matrices are guaranteed to be stable. The problem
with this is that all stable matrices are not necessarily negative
definite. This leads to a conservative result. The criteria in both
domains assume that the nominal closed-loop system (before it is
perturbed) is stable, which should not be a concern.

APPENDIX 3A

(This paper was published in the International Journal of Control, Volume 41,
Number 2, February 1985, pages 365-387.)

STABILITY ROBUSTNESS MEASURES UTILIZING STRUCTURAL INFORMATION

Hsi-Han Yeh[+] , Siva S. Banda*, and Capt D. Brett Ridgely*
AFWAL/FIGC   Flight Dynamics Laboratory
Wright Patterson Air Force Base, OH 45433

Abstract

This paper presents techniques of using weighted ℓ_1 and ℓ_∞ norms to incorporate the structural information of the return difference and the perturbation matrices in the measure of stability robustness of multivariable control systems. The flexibility offered by these norms along with the use of nonnegative matrix theory enables one, in most cases, to reduce the conservatism which has been a typical concern with the use of singular value based stability robustness tests. New stability robustness criteria are derived on the basis of weighted ℓ_1 and ℓ_∞ norms. Examples are given to demonstrate the merits of these methods over singular value tests.

I. Introduction

One of the intriguing problems in the extension of the classical frequency domain analysis and design techniques for single-input, single-output (SISO) feedback systems to multivariable feedback systems is perhaps the measure of relative stability [1-3]. The one-loop-at-a-time stability margins fail to account for the simultaneous variations and crossfeed changes in a multivariable system. Extensions of the Nyquist method to multivariable systems [4-6] also fail to reveal the nearness of a stable multivariable system to instability.

_____

+ On leave from the University of Kentucky under AFOSR resident research program
* Aerospace Engineer

In recent developments [2], [7], the robustness of a multivariable system, i.e., the nearness of a stable multivariable system to instability when subject to plant perturbations or uncertainties, is measured by the singular value of the return-difference of the loop transfer or the inverse loop transfer matrix. For various models of plant perturbations or uncertainties, the robustness criteria may be summarized [8] as either

$$\overline{\sigma}[E(s)] < \underline{\sigma}[I + G(s)] \tag{1}$$

or

$$\overline{\sigma}[E(s)] < \underline{\sigma}[I + G^{-1}(s)] \tag{2}$$

depending upon the modeling of the plant perturbations, where $\underline{\sigma}(\cdot)$ denotes the miniumum singular value, $\overline{\sigma}(\cdot)$ the maximum singular value, E(s) the plant perturbation, G(s) the loop transfer matrix, and I the identity matrix. In some cases, an additional restriction on $\overline{\sigma}[E(s)]$ is required. These conditions impose hard bounds upon the class of plant perturbations that do not destabilize the feedback system. In other words, for each

$$\theta(s) \geqslant \underline{\sigma}[I + G^{\pm}(s)] \tag{3}$$

where $G^{\pm}(s)$ means G(s) or $G^{-1}(s)$ depending upon whether the robustness stability criterion is given by (1) or (2), there always exists an E(s) that satisfies

$$\overline{\sigma}[E(s)] \leqslant \theta(s) \tag{4}$$

3-27

but destabilizes the closed-loop system, provided that the selection of E(s) is unrestricted except in the matrix dimensions. Nevertheless, for a given perturbation E(s), or a class of perturbations for which there is some a priori knowledge about the structure of the multivariable perturbation (i.e., the numerical relationship among the elements of the perturbation matrix E(s)) the robustness tests (1) and (2) are often too conservative. If a perturbation passes the test given by (1) or (2), the perturbed system is stable, if it fails, the test is inconclusive.

The problem of conservatism in the robustness tests for linear feedback control systems has been discussed in several papers [3], [8-13]. Conservatism of these robustness tests may be attributed to the fact that little structural information about a matrix is reflected in its maximum or minimum singular values. In general, if more is known about the uncertainty than just a simple bound on its spectral norm (the maximum singular value), then less conservative stability robustness tests may be formulated. In the extreme case, if the perturbation matrix is completely known, then an eigenvalue test [9] or the Nyquist theorem gives the necessary and sufficient condition for the stability of the perturbed system. A singular value decomposition can be used to reduce the conservatism if there is a significant difference between the smallest and the next smallest singular value of the return difference matrix [8], [11]. The technique of weighting or scaling a matrix in order to obtain a smaller norm has also been employed to reduce the conservatism of robustness criteria [9], [10]. However, the study was essentially for diagonally perturbed systems. It has also been shown that the theory of M-matrices can be used to characterize certain allowable perturbations and thus reduce the conservatism of robustness criteria, in some cases [12].

This paper presents methods of using weighted ℓ_1 and ℓ_∞ norms and the theory of nonnegative matrices to account for the structural information of the perturbation matrix, and to derive less conservative stability robustness criteria. The next section generalizes the singular value inequalities of (1) and (2) into inequalities incorporating general matrix norms. The basic idea of characterizing structural information of a matrix by weighted ℓ_1 and ℓ_∞ norms is developed in Section III and the main results are given in Section IV. Some of the most interesting results, in contrast to the scalar inequalities of (1) and (2), are matrix inequalities bounding the magnitude of each element of the class of nondestabilizing perturbation matrices. Examples are given in Section V to demonstrate the reduction in conservatism of the stability robustness criteria, and conclusions are given in Section VI.

II. General Norm-Bounded Stability Robustness Criteria

Robustness criteria (1) and (2) are special cases of inequalities involving general matrix norms [9-10]. For systems with plant uncertainties modeled as additive or inverse multiplicative perturbations (Fig. 1 and Fig. 4, where $\widetilde{G}(s)$ is the perturbed loop transfer matrix),

$$\widetilde{G}(s) = G(s) + E(s)$$
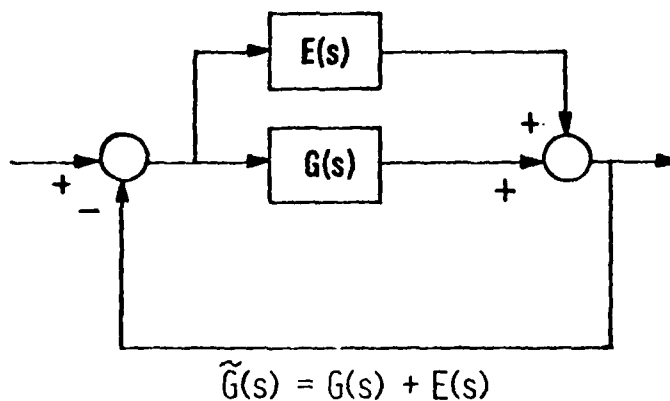
FIG. 1 ADDITIVE PERTURBATION
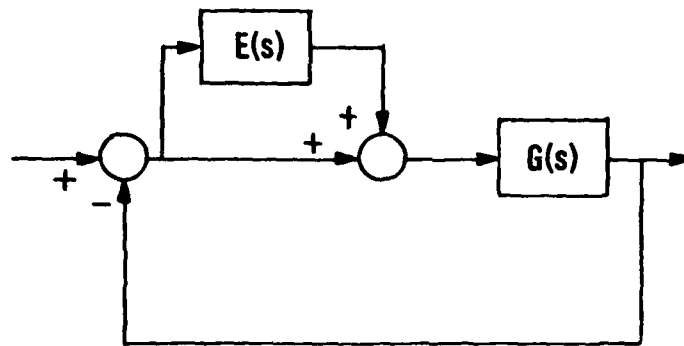
$$\widetilde{G}(s) = G(s)\{I + E(s)\}$$

FIG. 2 MULTIPLICATIVE PERTURBATION
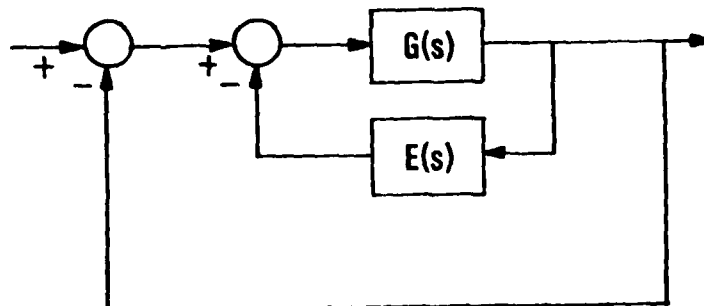
$$\widetilde{G}^{-1}(s) = G^{-1}(s) + E(s) \; ; \; \lambda[E(s)G(s)] \notin (-\infty, -1] \; ; \; s \varepsilon D_R$$

FIG. 3 INVERSE ADDITIVE PERTURBATION
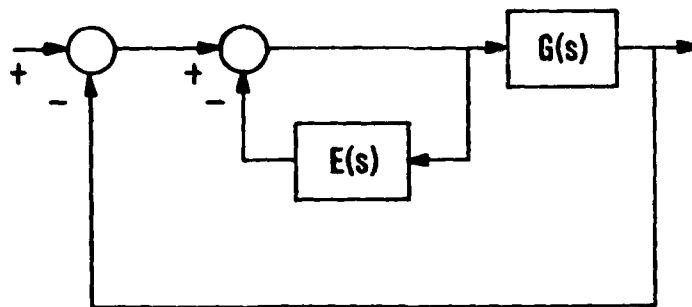
$$\widetilde{G}(s) = G(s) \left\{ I + E(s) \right\}^{-1}$$

FIG. 4 INVERSE MULTIPLICATIVE PERTURBATION

the stability robustness criterion (a sufficient condition) may be generalized as

$$\left\| E(s) \right\| < \frac{1}{\left\| [\ I + G(s)\ ]^{-1} \right\|} \tag{5}$$

except for the inverse multiplicative perturbation (Fig.4) where the additional condition

$$\left\| E(s) \right\| < 1 \tag{6}$$

is imposed. The vertical double bars $\left\| \cdot \right\|$ denote any matrix norm. It is worth noting here that (6) may be replaced by the weaker condition that requires only the eigenvalues of $E(j\omega)$ not belong to the section $(-\infty, -1]$ on the real axis, for all $s \in D_R$. However, for most practical systems, the minimum value of the right-hand side of (5) for $s \in D_R$ is usually smaller

than unity. Therefore, the stronger condition (6) can be used without imposing unnecessary restrictions on the error function E(s). For systems modeled with multiplicative or inverse additive perturbations (Fig.2 and Fig.3), the stability robustness criterion (a sufficient condition) may be generalized as

$$\| E(s) \| < \frac{1}{\| [\ I + G^{-1}(s) \ ]^{-1} \|} \tag{7}$$

Note that for the system of Fig. 3, as stated in the figure, the additional restriction on the eigenvalues of E(s)G(s) must be included. This eigenvalue restriction is implied by $\| E(s)G(s) \| < 1$, which in turn is implied by $\| E(s) \| < 1/ \| G(s) \|$. Thus, a stability robustness criterion for the system of Fig. 3 is the simultaneous satisfaction of the latter and inequality (7). However, in this paper, the development of the robust stability tests of Fig. 3 will be based on (7) only, assuming that the eigenvalue restriction as stated in Fig. 3 is satisfied. Since the derivations of (1)-(2) and (5)-(7) are based on multivariable Nyquist theory, some preliminary conditions on the nominal and perturbed systems must hold, i.e., the open-loop characteristic polynomials of the nominal system and the perturbed system must have the same number of closed right-half plane roots, all imaginary poles of the open-loop perturbed system must also be poles of the open-loop nominal system, and the nominal system must be closed-loop stable. Furthermore, inequalities (1)-(2) and (5)-(7) must hold for all s on the Nyquist contour. The theory here is formulated for n x n square matrices G(s) and unity feedback systems. It can be easily extended to the general case with nonunity feedback.

The general norm inequalities for additively and multiplicatively perturbed systems (Fig.1 and Fig.2) follow from a simple generalization of the derivation given in [7], and has been used in other papers [10], [12]. The general norm inequalities for the inverse additive and inverse multiplicative cases, though not quoted or used elsewhere, can be derived in the same fashion as the derivation of the singular value inequalities in [2]. However, because the perturbation matrix $E(s)$ appears nonlinearly in the convex combination of $\tilde{G}(s)$ and $G(s)$ (Fig.3 and Fig.4), the generalization of the proofs in [2] to the proofs of the inequalities (5)-(7) for the inverse additive and inverse multiplicative perturbation cases is not trivial. The proof of (5) for the inverse multiplicative perturbation case (Fig. 4) is given in another paper [19]. The proof of (7) for the inverse additive perturbation case can then be analogously formulated. The formulation of perturbation models into Figs. 1-4 is attributed to Lehtomaki et al [8].

It is evident from the comparison of (1) and (2) with (5) and (7) that the conservatism of stability robustness criteria can be reduced if norms of the perturbation matrix $E(s)$ and the inverse return difference matrix can be computed to be less than their corresponding maximum singular values (note that $\underline{\sigma}(A) = 1/ \overline{\sigma}(A^{-1})$). Since there are infinitely many ways to compute a matrix norm, the idea of reducing the conservatism in the robustness criteria here is to account for as much structural information of the perturbation matrix and the return difference matrix as possible in order to obtain the smallest possible norms of these matrices.

III. <u>Utilization of Structural Information of Matrices in Weighted</u> ℓ_1 <u>and</u> ℓ_∞ <u>Norms</u>

Structural information of a matrix can be exploited to a considerable extent in weighted ℓ_1 and ℓ_∞ norms. These norms have been used extensively in numerical analysis [14] but are not widely used in control literature. They have been used in calculating the gain margin (uniform for all loops) of diagonally perturbed multivariable feedback systems [10], but their potential in reducing the conservatism of norm-bounded stability robustness tests has not been fully exploited.

A norm of a vector is a function which assigns to every vector a real number $\| \cdot \|$ such that

$$\| \underline{x} \| > 0 \quad \text{unless } \underline{x} = 0 \tag{8}$$

$$\| \alpha \underline{x} \| = | \alpha | \cdot \| \underline{x} \| \quad \text{for any } \alpha \text{ in the field} \tag{9}$$

$$\| \underline{x} + \underline{y} \| \leqslant \| \underline{x} \| + \| \underline{y} \| \tag{10}$$

A norm of a square matrix is defined as a real-valued function $\| \cdot \|$ (the same notation as the vector norm is used because the distinction will be clear in the context) such that for any two square matrices A and B of the same size

$$\| A \| > 0 \quad \text{unless } A = 0 \tag{11}$$

$$\| \alpha A \| = | \alpha | \cdot \| A \| \quad \text{for any } \alpha \text{ in the field} \tag{12}$$

$$\|A + B\| \leqslant \|A\| + \|B\| \tag{13}$$

$$\|A \cdot B\| \leqslant \|A\| \cdot \|B\| \tag{14}$$

The matrices are assumed to be square, which is no real restriction since one can always adjoin null rows and columns. A matrix norm is said to be consistent with a vector norm if for every A and for every $\underline{x}$

$$\|A\underline{x}\| \leqslant \|A\| \cdot \|\underline{x}\| \tag{15}$$

A matrix norm is said to be subordinate to a vector norm if it is consistent and if for every $A \neq 0$ there exists an $\underline{x} \neq 0$ such that

$$\|A\underline{x}\| = \|A\| \cdot \|\underline{x}\| \tag{16}$$

To every vector norm there corresponds a unique subordinate matrix norm defined by [14]

$$\|A\| = \max_{\underline{x} \neq 0} \frac{\|A\underline{x}\|}{\|\underline{x}\|} \tag{17}$$

The most commonly used vector norm is the Euclidean norm $\|\underline{x}\|_E$ defined by

$$\|\underline{x}\|_E = (\underline{x}^*\underline{x})^{1/2} \tag{18}$$

where * denotes complex conjugate transpose. The matrix norm subordinate to the vector Euclidean norm is the spectral norm $\|A\|_s$, defined as the largest singular value of A, i.e.,

$$\|A\|_s = \overline{\sigma}(A) = [\overline{\lambda}(A^*A)]^{1/2} = [\overline{\lambda}(AA^*)]^{1/2} \qquad (19)$$

where $\overline{\lambda}(\cdot)$ denotes the maximum eigenvalue of the given matrix. The weighted ℓ_p vector norm on the complex field C^n is given by

$$\|\underline{x}\|_{\underline{q}p} \triangleq \|Q^{-1}\underline{x}\|_p \triangleq \sum_{i=1}^{n}\left(\frac{|x_i|^p}{q_i^p}\right)^{1/p} \qquad (20)$$

where the q_i's are real and positive numbers

$$\underline{q} = \mathrm{col}\ [\ q_1\ q_2\ \cdot\ \cdot\ \cdot\ q_n\ ] \qquad (21)$$

and

$$Q = \mathrm{diag}\ [\underline{q}] = \mathrm{diag}\ [\ q_1\ q_2\ \cdot\ \cdot\ \cdot\ q_n\ ] \qquad (22)$$

The Euclidian vector norm is a special case of the weighted ℓ_p norm when $Q = I$ and $p = 2$. Of special interest here are the weighted ℓ_1 and ℓ_∞ norms. The weighted ℓ_1 norm is a special case of (20) when $p = 1$, and the weighted ℓ_∞ norm is

$$\|\underline{x}\|_{\underline{q}\infty} \triangleq \|Q^{-1}\underline{x}\|_\infty \triangleq \max_i\ (|x_i|/q_i) \qquad (23)$$

where $\|\cdot\|_\infty$ denotes the ℓ_∞ norm when the weight is evenly distributed (unweighted).

The matrix norm subordinate to the weighted ℓ_1 vector norm (called g´-norm by Householder [14]) is

$$\|A\|_{Q1} \triangleq \left\| \left\| A' \mid \underline{q} \right|\right\|_{\underline{q}\infty} \triangleq \left\| Q^{-1} |A*| \underline{q} \right\|_{\infty}$$

$$= \text{max row sum of } Q^{-1}|A*|Q \tag{24}$$

where $\underline{q}$ and Q are given by (21) and (22) respectively, A' is the transpose of A, and the absolute value sign $|\cdot|$, when applied to a complex vector or matrix as in (23), retains the magnitude of each element and drops the complex phase angles. The matrix norm subordinate to the weighted ℓ_∞ vector norm (called g-norm by Householder [14]) is

$$\|A\|_{Q\infty} \triangleq \left\| \left| A |\underline{q}| \right\|_{\underline{q}\infty} \triangleq \left\| Q^{-1}|A|\underline{q} \right\|_{\infty}$$

$$= \text{max row sum of } Q^{-1}|A|Q \tag{25}$$

The weighted ℓ_1 and ℓ_∞ norms are duals of one another in the sense that the ℓ_1 norm of a matrix is the ℓ_∞ norm of its complex conjugate transposition.

Expanding the $Q^{-1}|A|Q$ term on the right-hand side of (25) shows

$$\|A\|_{Q\infty} = \text{max row sum of } \begin{bmatrix} |a_{11}| & \dfrac{q_2}{q_1}|a_{12}| & \cdots & \dfrac{q_n}{q_1}|a_{1n}| \\[2mm] \dfrac{q_1}{q_2}|a_{21}| & |a_{22}| & \cdots & \dfrac{q_n}{q_2}|a_{2n}| \\[2mm] \vdots & \vdots & & \vdots \\[2mm] \dfrac{q_1}{q_n}|a_{n1}| & \dfrac{q_2}{q_n}|a_{n2}| & \cdots & |a_{nn}| \end{bmatrix} \tag{26}$$

Thus, the relationship between the norm and the structure of a matrix becomes explicit when a weighted ℓ_1 or ℓ_∞ norm is used. For example, if A is diagonal, the weighted ℓ_1 or ℓ_∞ norm is the maximum modulus of the diagonal elements of A regardless of the weighting vector $\underline{q}$. The extent to which the conservatism in robustness tests is reduced by using (5) or (7) instead of (1) or (2) depends upon the ability to simultaneously reduce the norms of $E(s)$ and $I + G(s)$ (or $I + G^{-1}(s)$). The use of weighted ℓ_1 or ℓ_∞ norms on these tests provides complete freedom in selecting $\underline{q}$ to minimize the norm of one matrix if the other is known to be diagonal. This freedom is totally lacking in the singular value inequalities of (1) and (2). If A is upper triangular, or skewed towards upper triangularity, and $\underline{q}$ is selected to be

$$\underline{q} = [\ 1 \ \ \delta \ \ \delta^2 \cdot \cdot \cdot \delta^{n-1}\ ] \tag{27}$$

then for δ sufficiently small, the above-diagonal elements have negligible effects on the weighted ℓ_1 norm of A. The advantage becomes especially notable if the off diagonal terms of a triangular matrix are dominant.

In selecting the weighting vector $\underline{q}$ to minimize the weighted ℓ_∞ norm (or ℓ_1 norm) of a matrix, the well established theory of nonnegative matrices [14], [15] can be used to great advantage. A matrix A is said to be reducible if there exists some permutation matrix P such that

$$P'AP = \begin{bmatrix} A_{11} & A_{12} \\ 0 & A_{22} \end{bmatrix} \tag{28}$$

where A_{11} and A_{22} are square submatrices. If no such permutation matrix exists, A is irreducible. A permutation matrix is a matrix whose elements

are only one's and zero's, with exactly one 1 in each row and in each column, and it has the property that $P^{-1} = P'$. The transformation described in (28) is equivalent to successively interchanging pairs of rows and corresponding pairs of columns. Physically, this is equivalent to relabeling the input-output pairs of the loop transfer matrix simultaneously. That means if x_i is renamed x_j then y_i is also renamed y_j, and so forth. Therefore, a system (assuming equal number of inputs and outputs) with a reducible transfer matrix means that there exists a subsystem (with an equal number of inputs and outputs) that does not receive crossfeed information from the rest of the system. It is well known, by a theorem attributed to Perron and Frobenius, that for an irreducible nonnegative matrix $|A|$ there exists 1) a positive eigenvalue $\bar{\lambda}$ (called the Perron eigenvalue of A) which is no less than the modulus of any other eigenvalue of $|A|$, 2) corresponding to $\bar{\lambda}$ there exists an eigenvector of all positive components (called the Perron eigenvector of A), and 3) $\bar{\lambda}$ is the only eigenvalue of $|A|$ that has a corresponding eigenvector of all positive components. Being a nonnegative matrix here does not mean being a positive semidefinite matrix, but refers to each matrix element being real and nonnegative. In the ensuing discussion, positive vectors and matrices are similarly defined. By virtue of the Perron-Frobenius theorem, if $\underline{q}$ is selected to be the Perron eigenvector of A, then the weighted ℓ_∞ norm of A is found to be the spectral radius (the magnitude of the largest eigenvalue) of $|A|$. Although there is no guarantee that $\bar{\lambda}(|A|)$ will always be smaller than $\bar{\sigma}(A)$, for most practical cases where the crossfeed structure is unsymmetrical this is found to be true and therefore a weighted ℓ_1 or ℓ_∞ norm may be used to reduce the conservatism in the robustness tests.

Moreover, it is obvious from (25) that if $|A| \geqslant |B|$, element for element, then $\|A\|_{Q\infty} \geqslant \|B\|_{Q\infty}$. Thus, the weighted ℓ_1 or ℓ_∞ norm can be used to find robustness bounds for the modulus of the elements of the perturbation matrix. This will be presented in the next section.

If A is a reducible matrix, then there is no loss of generality in considering A to be of the form of the right-hand side of (28) (or a general upper or lower triangular block matrix), since this can be achieved by relabeling the input and output variables. Suppose now that A_{11} and A_{22} are both irreducible. Let $\underline{q}_1$ and $\underline{q}_2$ be the Perron eigenvectors of A_{11} and A_{22} respectively. Then by substituting

$$\underline{q} = \text{col} \; [\; \underline{q}_1{}' \quad \epsilon \underline{q}_2{}' \;] \tag{29}$$

and the right-hand side of (28) for A into (25), the weighted ℓ_∞ norm of A is again found to be the spectral radius of $|A|$ (for sufficiently small ϵ), which is the larger of the Perron eigenvalues of A_{11} or A_{22}. If A_{11} or A_{22} is reducible, the same procedure of finding the minimum weighted ℓ_∞ norm can be imbedded. Thus, the off-diagonal block of a reducible matrix does not affect the value of the minimum weighted ℓ_∞ norm of the matrix. If the perturbation matrix, E(s), and the return difference matrix, I + G(s) or I + G^{-1}(s), are both upper or lower block triangular matrices of identical partitions then the off-diagonal block in E(s) does not affect the stability robustness of the closed-loop system. This property will be formally stated in the next section. The minimum weighted ℓ_∞ norm of a reducible matrix with nonnegligible off-diagonal blocks can be expected to be smaller than its maximum singular value.

If A is in block diagonal form with m blocks, then the weighting vector may be chosen as

$$\underline{q} = \text{col} [\underline{q}_1 \quad \underline{q}_2 \cdot \cdot \cdot \underline{q}_m] \tag{30}$$

where $\underline{q}_i$ is the Perron eigenvector of the ith block. (The term Perron eigenvector is slightly abused when the diagonal block is reducible.) The minimum weighted ℓ_∞ norm of A is again found to be the spectral radius of $|A|$, which is the maximum spectral radius of the diagonal blocks of $|A|$.

IV. Stability Robustness With Structured Uncertainty

In this section the main results are stated. For notational brevity, let

$$A(s) = [I + G^{\pm}(s)]^{-1} \tag{31}$$

Where $G^{\pm}(s)$ refers to $G(s)$ for the cases of Fig. 1 and Fig. 4, and to $G^{-1}(s)$ for the cases of Fig. 2 and Fig. 3. The notation max $[\cdot]$ denotes the maximum element of the nonnegative vector in the argument. An inequality of nonnegative matrices compares its two sides element for element. In all Lemmas and Theorems stated below, all the preliminary conditions on the nominal and perturbed systems are assumed satisfied, and all conditions derived are assumed to hold for all s on the Nyquist contour.

Lemma 1 : The perturbed systems of Fig. 1-4 are asympotically stable if there exists a positive vector $\underline{q}(s)$ such that

$$\max \ [Q^{-1}(s)|E(s)|\underline{q}(s)] < \cfrac{1}{\max \ [Q^{-1}(s)|A(s)|\underline{q}(s)]} \tag{32}$$

and in addition

$$\max \ [Q^{-1}(s)|E(s)|\underline{q}(s)] < 1 \tag{33}$$

for the case of Fig. 4, where $Q(s)$ and $\underline{q}(s)$ are a frequency dependent matrix and vector as in (22) and (21), respectively. This Lemma remains true if $E(s)$ and $A(s)$ are replaced by $E^*(s)$ and $A^*(s)$, respectively.

Proof : Using weighted ℓ_{∞} norms in inequalities (5)-(7) with weighting vector q gives the stated result of inequalities (32) and (33). If weighted ℓ_1 norms are used, $E(s)$ and $A(s)$ in this Lemma are replaced by $E^*(s)$ and $A^*(s)$.

Lemma 2 : The perturbed systems of Figs. 1-4 are asymptotically stable if $G(s)$ is irreducible and

$$\max \ [Q_a^{-1}(s)|E(s)|\underline{q}_a(s)] < \cfrac{1}{\overline{\lambda}[\,|A(s)|\,]} \tag{34}$$

and in addition

$$\max \ [Q_a^{-1}(s)|E(s)|\underline{q}_a(s)] < 1 \tag{35}$$

for the case of Fig. 4, where $\overline{\lambda}[\,|A(s)|\,]$ is the Perron eigenvalue of $A(s)$, and $\underline{q}_a(s)$ is the corresponding Perron eigenvector. This Lemma remains true if $E(s)$ and $A(s)$ are replaced by $E^*(s)$ and $A^*(s)$ respectively.

<u>Proof</u> : Since $G(s)$ is irreducible, $A^{-1}(s)$ and $A(s)$ are also irreducible and $\overline{\lambda}[\ |A(s)|\ ]$ and $q_a(s)$ are both positive. Since $\underline{q}_a(s)$ is the Perron eigenvector of $A(s)$,

$$\max\ [Q_a^{-1}|A(s)|\underline{q}_a(s)\ ]$$

$$= \max\ [Q_a^{-1}(s)\overline{\lambda}(|A(s)|)\underline{q}_a(s)] = \overline{\lambda}(|A(s)|) \tag{36}$$

Therefore, using $Q_a(s)$ and $\underline{q}_a(s)$ in (32) and (33) gives the stated result. If $E^*(s)$ and $A^*(s)$ are used in Lemma 1, then Lemma 2 is established with $E(s)$ and $A(s)$ replaced by $E^*(s)$ and $A^*(s)$, respectively.

<u>Theorem</u> <u>1</u> : The perturbed closed-loop systems of Figs. 1-4 are asymptotically stable if either $G(s)$ or $E(s)$ is diagonal and

$$\overline{\lambda}[\ |E(s)|\ ] < \frac{1}{\overline{\lambda}[\ |A(s)|\ ]} \tag{37}$$

and in addition

$$\overline{\lambda}[\ |E(s)|\ ] < 1 \tag{38}$$

for the case of Fig. 4.

<u>Proof</u> : Suppose $E(s)$ is diagonal. If $G(s)$ is irreducible, then (37) and (38) follow (34) and (35), respectively. If $G(s)$ is reducible, then relabeling the plant input and output variables (which is the same as performing a permutation transformation), transforms $A(s)$ into the form of the right-hand side of (28) while $E(s)$ remains diagonal. Choosing $\underline{q}_a(s)$ as in (29) for inequalities (34) and (35) gives the stated result. The case

where G(s) (and hence A(s)) is diagonal can be similarly proved by using the Perron eigenvector of E(s) as $\underset{\sim}{q}(s)$ in Lemma 1.

Note that for diagonal matrices, the Perron eigenvalue, the spectral radius, and the maximum singular value are identical. Hence, for the diagonally perturbed system (i.e., E(s) diagonal), (37) is a less conservative test if the Perron eigenvalue of A(s) is smaller than the spectral norm of A(s). This is true if G(s) is relatively skew, i.e., the crossfeeding is unsymmetrical.

Theorem 2 : The perturbed closed-loop systems of Figs. 1-4 are asymptotically stable if E(s) and G(s) are both upper or lower triangular and

$$\underset{i}{\max} \, [\, |e_{ii}(s)| \,] < \frac{1}{\underset{i}{\max} \, [\, |a_{ii}(s)| \,]} \tag{39}$$

and in addition

$$\underset{i}{\max} \, [\, |e_{ii}(s)| \,] < 1 \tag{40}$$

for the case of Fig. 4, where $e_{ii}(s)$ and $a_{ii}(s)$ denote the diagonal terms of E(s) and A(s), respectively. The off-diagonal terms of E(s) (the crossfeed perturbation) do not affect the stability robustness of the closed-loop system, and those of G(s) do not affect the robustness bound.

Proof : If G(s) is upper (lower) triangular, then so is A(s). If both E(s) and G(s) are upper triangular, using $\underset{\sim}{q}(s)$ of (27) in (32) and (33) gives the stated result. If both E(s) and G(s) are lower triangular, then letting δ be sufficiently large in (27) gives the stated result.

Theorem 2 offers a robustness criterion that is heavily structurally dependent and is significantly less conservative than the singular value tests when applicable. This will be demonstrated in an example in the next section. This theorem can also be generlized to the case where E(s) and G(s) are identically partitioned into upper or lower triangular block matrices.

Corollary 2.1 : The perturbed closed-loop systems of Figs. 1-4 are asymptotically stable if E(s) and G(s) are both upper or lower triangular block matrices with identical partitions, and if

$$\max_{i} \left\| E_{ii}(s) \right\|_{Q_i \infty} < \frac{1}{\max_{i} \left\| A_{ii}(s) \right\|_{Q_i \infty}} \tag{41}$$

and in addition

$$\max_{i} \left\| E_{ii}(s) \right\|_{Q_i \infty} < 1 \tag{42}$$

for the case of Fig. 4, where $E_{ii}(s)$ and $A_{ii}(s)$ are corresponding diagonal blocks of E(s) and A(s), respectively, and Q_i is an arbitrary diagonal weighting matrix with positive diagonal elements. The off-diagonal blocks of E(s) (the cross-feed perturbation between subsystems) do not affect the stability robustness of the closed-loop system, and those of G(s) do not affect the robustness bound. This corollary remains true if all weighted ℓ_∞ norms are replaced by weighted ℓ_1 norms.

Proof : If G(s) is upper (lower) block triangular, then so is A(s). If both E(s) and G(s) are upper block triangular with N diagonal blocks, then substituting

$$\underline{q} = \text{col } [\underline{q}_1{}' \quad \delta \underline{q}_2{}' \quad \delta^2 \underline{q}_3{}' \cdot \cdot \cdot \delta^{N-1} \underline{q}_N{}'] \qquad (43)$$

into (32) and (33) gives the stated result (for sufficiently small δ), where q_i is a vector composed of diagonal elements of Q_i. If both E(s) and G(s) are lower triangular block matrices, then letting δ be sufficiently large in (43) gives the stated result. The proof for weighted ℓ_1 norms may be analogously stated.

Theorem 2 gives robustness bounds on the magnitude of each diagonal element of E(s) if E(s) and G(s) are both upper or lower triangular. The off-diagonal elements may be left unbounded. Corollary 2.1 extends this result to the case where E(s) and G(s) are both upper or lower block triangular matrices, by measuring the weighted ℓ_∞ norms of the diagonal blocks instead of the magnitudes of the diagonal elements. The following theorems specify bounds on the magnitude of each element of A(s).

<u>Theorem 3</u> : The perturbed closed-loop systems of Figs. 1-4 are asymptotically stable if

$$\left|\left| E(s) \right|\right| < \frac{b}{\bar{\lambda}^2 [\left| A(s) \right|]} \left| A(s) \right| \qquad (44)$$

where

$$b = 1 \qquad (45)$$

for the systems of Figs. 1-3 and

$$b = \min \{ \bar{\lambda} \left| A(s) \right|, 1 \} \qquad (46)$$

for the system of Fig. 4.

Proof : Suppose $G(s)$ is irreducible. Then $A^{-1}(s)$ and $A(s)$ are also irreducible. Let $\underline{q}_a(s)$ be the Perron eigenvector $A(s)$. Then by definition

$$|A(s)|\underline{q}_a(s) = \overline{\lambda}[\,|A(s)|\,]\underline{q}_a(s) \tag{47}$$

Since an inequality of nonnegative matrices compares its two sides element for element, inequality (44) leads to

$$\max\,[Q_a^{-1}(s)|E(s)|\underline{q}_a(s)] < \frac{b}{\overline{\lambda}^2[\,|A(s)|\,]}\,\max\,[Q_a^{-1}(s)|A(s)|\underline{q}_a(s)]$$

$$= \frac{b}{\overline{\lambda}^2[\,|A(s)|\,]}\,\max\,[\,\overline{\lambda}\{|A(s)|\}Q_a^{-1}(s)\underline{q}_a(s)] = \frac{b}{\overline{\lambda}[\,|A(s)|\,]} \tag{48}$$

Comparing (48) with (34) shows that for the systems of Figs. 1-3, $b = 1$, but for the system of Fig. 4, it suffices to set $b = \overline{\lambda}[\,|A(s)|\,]$ if $\overline{\lambda}[\,|A(s)|\,] \leqslant 1$, and $b = 1$ if $\overline{\lambda}[\,|A(s)|\,] \geqslant 1$. This proves the theorem for irreducible $G(s)$.

If $G(s)$ is reducible, so are $A^{-1}(s)$ and $A(s)$. There is no loss of generality to consider $A(s)$ as an upper triangular block matrix. The Perron eigenvector of $A(s)$ is then given by (43) for arbitrarily small δ, with $\underline{q}_i$ chosen to be the Perron eigenvector of the ith block A_{ii} on the diagonal. Then the proof of the irreducible $G(s)$ case can be repeated to give the stated result.

It is worth noting here that for the reducible G(s) case, Theorem 2 and Corollary 2.1 give less conservative stability robustness criteria than Theorem 3, because the validity of (44)-(46) implies the validity of (39)-(42). Moreover, Theorem 2 or Corollary 2.1 permits the off-diagonal elements or off-diagonal blocks, respectively, of E(s) to be unrestricted in magnitude, but Theorem 3 imposes bounds on the magnitude of all elements in E(s). Nevertheless, Theorem 3 provides a way to structure E(s) when G(s) is irreducible, which cannot be covered by Theorem 2 and Corollary 2.1.

The following theorems specify, in different ways, uniform bounds for all elements of the perturbation matrix E(s).

<u>Lemma 3</u> : The perturbed systems of Figs. 1-4 are asymptotically stable if there exists a positive vector $\underline{q}(s)$ such that

$$\max_{i,j} \left| e_{ij}(s) \right| < \frac{\min_{i} \{q_i(s)\}}{\underline{d}'\underline{q}(s)\max \left[Q^{-1}(s) |A(s)| \underline{q}(s) \right]} \tag{49}$$

and, in addition, for the system of Fig. 4

$$\max_{i,j} \left| e_{ij}(s) \right| < \frac{\min_{i} \{q_i(s)\}}{\underline{d}'\underline{q}(s)} \tag{50}$$

where $e_{ij}(s)$ is the ij element of the perturbation matrix E(s), and $\underline{d}$ is the vector defined by

$$\underline{d} = \text{col} \left[1\ 1\ \cdots\ 1 \right] \tag{51}$$

This Lemma remains true if A(s) is replaced by A*(s).

<u>Proof</u> : Let U be the n x n matrix of which all elements are unity, i.e.,

$$U = \begin{bmatrix} 1 & 1 & \cdot & \cdot & \cdot & 1 \\ 1 & 1 & \cdot & \cdot & \cdot & 1 \\ \cdot & \cdot & & & & \cdot \\ \cdot & \cdot & & & & \cdot \\ \cdot & \cdot & & & & \cdot \\ 1 & 1 & \cdot & \cdot & \cdot & 1 \end{bmatrix} \tag{52}$$

It is obvious that for a nonnegative matrix $E(s)$,

$$|E(s)| \leqslant \left(\max_{i,j} |e_{ij}(s)| \right) U \tag{53}$$

and for any nonnegative vector $\underline{q}(s)$,

$$\max \left[Q^{-1}(s) |E(s)| \underline{q}(s) \right] \leqslant \max \left[Q^{-1}(s) \left(\max_{i,j} |e_{ij}(s)| \right) U \underline{q}(s) \right]$$

$$= \frac{\left(\max_{i,j} |e_{ij}(s)| \right) \underline{d}' \underline{q}(s)}{\min_{i} \{q_i(s)\}} \tag{54}$$

Substituting (54) into (49) yields (32), and substituting (54) into (50) yields (33). To prove the validity of this Lemma with $A(s)$ replaced by $A^*(s)$, simply use $E^*(s)$ and $A^*(s)$ in Lemma 1 and repeat the above argument with $E(s)$ replaced by $E^*(s)$ in (53) and (54).

Theorem $\underline{4}$: The perturbed systems of Figs. 1-4 are asymptotically stable if $G(s)$ is irreducible and

$$\max_{i,j} |e_{ij}(s)| < \frac{\min_{i} \{q_{ai}(s)\}}{\underline{d}' \underline{q}_a(s) \overline{\lambda} [|A(s)|]} \tag{55}$$

and, in addition, for the system of Fig. 4,

$$\max_{i,j} \left| e_{ij}(s) \right| < \frac{\min_{i} \{q_{ai}(s)\}}{\underline{d}' \underline{q}_a(s)} \qquad (56)$$

where $\underline{d}$ is given by (51), $\underline{q}_a(s)$ is the Perron eigenvector of $A(s)$, and $q_{ai}(s)$ is the ith element of $\underline{q}_a(s)$. This Theorem also remains valid if $\underline{q}_a(s)$ is chosen as the Perron eigenvector of $A^*(s)$ instead.

<u>Proof</u> : Since $G(s)$ is irreducible, the Perron eigenvector $\underline{q}_a(s)$ of $A(s)$ exists. Hence, $Q_a^{-1}(s)$ exists. Substituting $\underline{q}_a(s)$ for $\underline{q}(s)$, $Q_a(s)$ for $Q(s)$, and $q_{ai}(s)$ for $q_i(s)$ in Lemma 3 yields Theorem 4.

<u>Theorem 5</u> : The perturbed closed-loop systems of Figs. 1-4 are asymptotically stable if either

$$\max_{i,j} \left| e_{ij}(s) \right| < \frac{1}{n \cdot \max \text{ row sum of } \left| A(s) \right|} \qquad (57)$$

or

$$\max_{i,j} \left| e_{ij}(s) \right| < \frac{1}{n \cdot \max \text{ col sum of } \left| A(s) \right|} \qquad (58)$$

and, in addition, for the system of Fig. 4,

$$\max_{i,j} \left| e_{ij}(s) \right| < \frac{1}{n} \qquad (59)$$

<u>Proof</u> : Substituting $\underline{d}$ for $\underline{q}(s)$ and the identity matrix I for $Q(s)$ in (49) and (50) yields (57) and (59), respectively. If $A^*(s)$ is used in (49) instead of $A(s)$, then (58) and (59) follow.

Both Theorems 4 and 5 indicate that the bound on the magnitude of the elements of $E(s)$ is inversely proportional to the number of variables of

the multi-input multi-output system. This may be attributed to the fact that crossfeed perturbations of maximum magnitude are assumed for all elements in the perturbation matrix E(s). If this assumption is not imposed, a less conservative criterion will result, as given in the next Theorem.

Theorem 6 : The perturbed closed-loop system of Figs. 1-4 are asymptotically stable if

$$\text{max row sum of } \left| E(s) \right| < \frac{1}{\text{max row sum of } \left| A(s) \right|} \tag{60}$$

and, in addition, for the system of Fig. 4,

$$\text{max row sum of } \left| E(s) \right| < 1 \tag{61}$$

The Theorem remains valid if the operator "max row sum" is replaced by "max col sum".

Proof : Substituting $\underline{d}$ for $\underline{q}(s)$ and I for Q(s) in (32) and (33) gives (60) and (61). If $E^*(s)$ and $A^*(s)$ are used in Lemma 1, then "max col sum" replaces "max row sum" in (60) and (61).

It should be noted that (57) implies (60), and (59) implies (61). Therefore, Theorem 6 is a less conservative test than Theorem 5. However, more information about the structure of E(s) is needed to apply Theorem 6 than Theorem 5. Usually the A(s) matrix is completely known and there is no difficulty in obtaining the right-hand side of (57) and (58). However, it is possible to tighten (make it more conservative) the conditions (57) and (58) further so as to require less information about A(s) and make an even simpler test, as given in the next Theorem.

<u>Theorem</u> <u>7</u> : The perturbed closed-loop systems of Figs. 1-4 are asymptotically stable if

$$\max_{i,j} \left| e_{ij}(s) \right| < \frac{1}{n^2 \max_{i,j} \left| a_{ij}(s) \right|} \tag{62}$$

and in addition, for system of Fig. 4,

$$\max_{i,j} \left| e_{ij}(s) \right| < \frac{1}{n} \tag{6}$$

where $a_{ij}(s)$ is the ij element of $A(s)$.

<u>Proof</u> :

$$\max \text{ row sum of } \left| A(s) \right| \leq n \cdot \max_{i,j} \left| a_{ij}(s) \right| \tag{64}$$

Therefore, (62) implies (57). This establishes Theorem 7.

Alternatively, Theorem 7 can also be proved by using the absolute matrix norm in inequalities (5)-(7). The absolute matrix norm is defined by [16]

$$\left\| A \right\|_{abs} = n \cdot \max_{i,j} \left| a_{ij} \right| \tag{65}$$

which is consistent with, but not subordinate to, the absolute vector norm

$$\left\| \underline{x} \right\|_{abs} = n \cdot \max_{i} \left| x_i \right| \tag{66}$$

V. Illustrative Examples

Examples are used to demonstrate some of the abilities of the above theorems in exploiting the structural information of the plant uncertainties to determine the stability robustness of the feedback system. For the sake of comparison, the system used in the examples is taken from Lehtomaki, et al [2],[17]-[18].
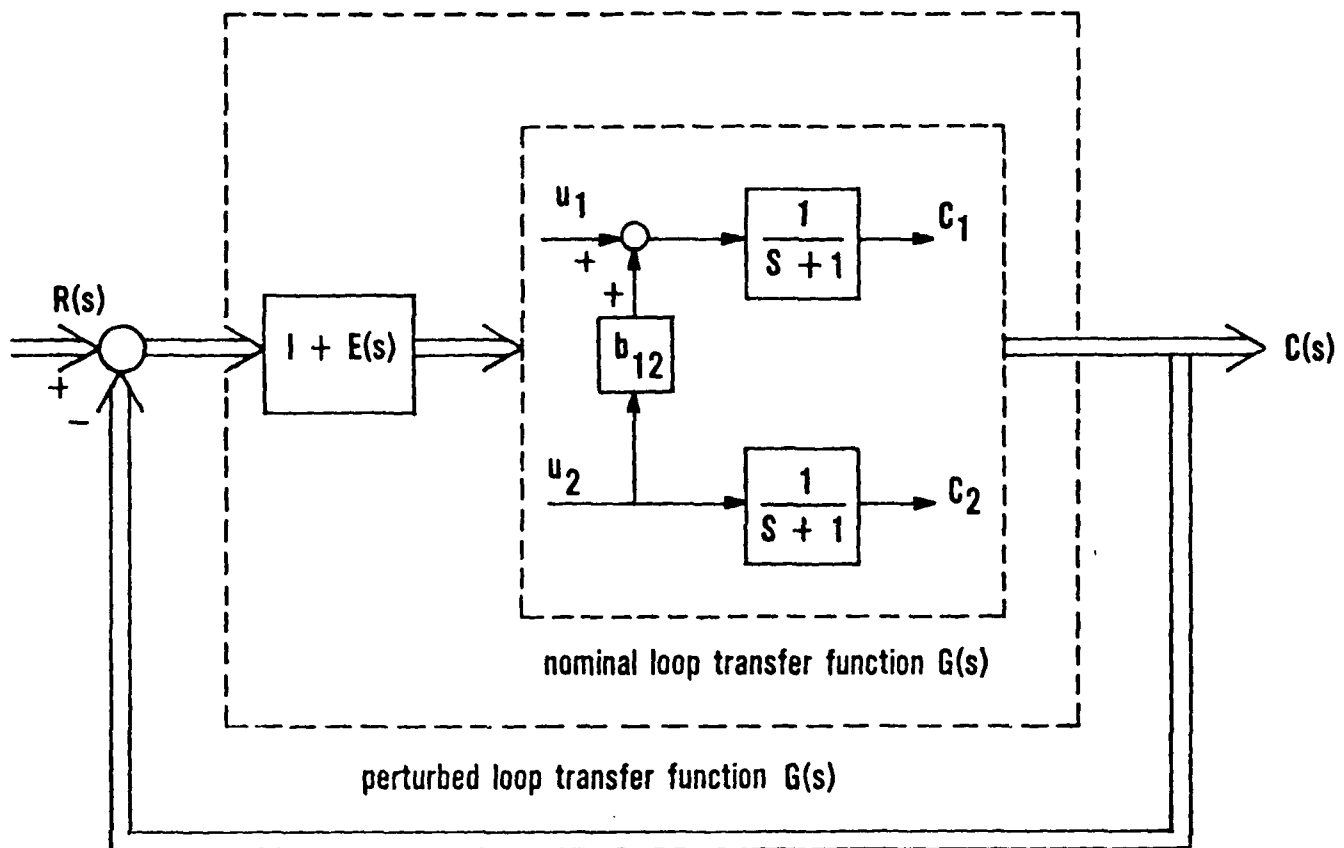

FIG. 5 FEEDBACK SYSTEM OF EXAMPLE 1

Consider the feedback system of Fig. 5 where the uncertainties in the open-loop transfer function are modeled as multiplicative perturbations. The theory developed in the above section can answer questions such as:

1) Suppose that the uncertainties of the open-loop transfer function lie only in the complex gains of the crossfeed and feedforward paths of the plant model, and there is no uncertainty about the existence or nonexistence of the signal paths. What are the sizes of the perturbations that the nominal closed-loop system can tolerate without becoming unstable?

2) If the only uncertainty in the model of the nominal transfer matrix is in the magnitude of the d.c. crossfeed gain b_{12}, what pertentage change in this gain can be tolerated before the closed-loop system becomes unstable?

3) Suppose that there are uncertainties in the existence or nonexistence of signal paths as well as the complex gains in the paths. What are the sizes of the perturbations that the nominal closed-loop system can tolerate without becoming unstable?

4) If the only uncertainty in the model of the nominal transfer matrix is the possible crossfeeding of signals from u_1 to u_2, which is not included in the model, what is the magnitude of the complex gain in this path, regardless of its phase, that the closed-loop system can tolerate without becoming unstable?

5) If the possible crossfeeding of signals from u_1 to u_2, as well as from u_2 to u_1, are the only uncertainties in the open-loop transfer function, what are the sizes of these crossfeed gains that the system can tolerate without becoming unstable?

6) If there are uncertainties only about some of the complex amplifier gains at the control variable inputs u_1 and u_2 (the so-called diagonal perturbation), what percentage changes in these gains can be tolerated before the system becomes unstable?

The nominal open-loop transfer matrix is given by

$$G(s) = \begin{bmatrix} \dfrac{1}{s+1} & \dfrac{b_{12}}{s+1} \\ 0 & \dfrac{1}{s+1} \end{bmatrix} \tag{67}$$

Therefore,

$$A(s) = [I + G^{-1}(s)]^{-1} = \begin{bmatrix} \dfrac{1}{s+2} & \dfrac{b_{12}(s+1)}{(s+2)^2} \\ 0 & \dfrac{1}{s+2} \end{bmatrix} \tag{68}$$

and

$$\max_i \left| a_{ii}(s) \right| = \left| \dfrac{1}{s+2} \right| \tag{69}$$

The assumption made in question 1) means that the perturbed open-loop transfer matrix $\widetilde{G}(s)$ must have the same crossfeed and feedforward structure as the nominal open-loop transfer matrix. This in turn means that the perturbation matrix $E(s)$ must also be upper triangular. By virtue of Theorem 2 and (69), $E(s)$ only has to satisfy

$$\max_i \left[\left| e_{ii}(s) \right| \right] < \left| s+2 \right| \tag{70}$$

or, since the off-diagonal terms of $E(s)$ and $A(s)$ do not play a role in the robustness measure in this case,

$$\left| E(s) \right| = \begin{bmatrix} \left| e_{11}(s) \right| & \left| e_{12}(s) \right| \\ \left| e_{21}(s) \right| & \left| e_{22}(s) \right| \end{bmatrix} < \begin{bmatrix} \left| s+2 \right| & \infty \\ 0 & \left| s+2 \right| \end{bmatrix} \tag{71}$$

Inequality (71) is the answer to question 1), provided the perturbed system satisfies the preliminary conditions of stability robustness stated in section II.

Under the conditions set in question 2), the perturbation matrix, E(s), is given by

$$E(s) = \begin{bmatrix} 0 & (k-1)b_{12} \\ 0 & 0 \end{bmatrix} \tag{72}$$

Then

$$\widetilde{G}(s) = G(s)[I + E(s)] = \begin{bmatrix} \dfrac{1}{s+1} & \dfrac{kb_{12}}{s+1} \\ 0 & \dfrac{1}{s+1} \end{bmatrix} \tag{73}$$

which means that the only perturbation in G(s) is the magnitude of b_{12}. In view of (71) and (72), it is seen that the closed-loop system can tolerate any perturbation in the real gain b_{12} without becoming unstable.

The concern raised in question 3) suggests that there may be a signal path going from u_2 to u_1 (Fig.5) that has been neglected in the nominal model G(s), and complex gains in all four signal paths are subject to perturbation. In this case, $e_{21}(s)$ of E(s) is no longer restricted to zero and Theorem 5 may be used if bounds on the elements of E(s) are to be found. Substituting A(s) of (68) into (57) or (58) gives

$$\max_{i,j} \left| e_{ij}(s) \right| < \frac{1/2}{\left| \dfrac{1}{s+2} \right| + \left| \dfrac{b_{12}(s+1)}{(s+2)^2} \right|} \tag{74}$$

One can also let

$$q_1 = \left| \frac{b_{12}(s+1)}{(s+2)^2} \right|^{1/2} \tag{75}$$

and

$$q_2 = \left| \frac{1}{s+2} \right|^{1/2} \tag{76}$$

in Lemma 3 and obtain

$$\max_{i,j} \left| e_{ij}(s) \right| < \frac{1}{\left| \dfrac{1}{s+2} \right| + \left| \dfrac{b_{12}(s+1)}{(s+2)^2} \right| + 2 \left| \dfrac{b_{12}(s+1)}{(s+2)^3} \right|^{1/2}} \tag{77}$$

which is a less conservative criterion than (74).

The concern raised in question 4) suggests that the perturbation matrix E(s) takes the form

$$E(s) = \begin{bmatrix} 0 & 0 \\ e_{21}(s) & 0 \end{bmatrix} \tag{78}$$

Then

$$\widetilde{G}(s) = G(s)[I + E(s)] = \begin{bmatrix} \dfrac{1}{s+1} + \dfrac{b_{12}e_{21}(s)}{s+1} & \dfrac{b_{12}}{s+1} \\[2ex] \dfrac{e_{21}(s)}{s+1} & \dfrac{1}{s+1} \end{bmatrix} \qquad (79)$$

which shows that a crossfeed from u_1 to c_1 through u_2 exists in the perturbed model. Application of Theorem 6 yields

$$\left| e_{21}(s) \right| < \dfrac{1}{\left| \dfrac{1}{s+2} \right| + \left| \dfrac{b_{12}(s+1)}{(s+2)^2} \right|} \qquad (80)$$

Alternatively, one can let $q_1 = 1$ and $q_2 \to \infty$ in (32) and apply Lemma 1 to yield

$$\left| e_{21}(s) \right| < \dfrac{1}{\left| \dfrac{b_{12}(s+1)}{(s+2)^2} \right|} \qquad (81)$$

Hence, the magnitude of the perturbation in the crossfeed path that is unmodeled shall be limited to the inverse of the magnitude of the gain in the "opposite" or "on-coming" path in the closed-loop system. This shows the seriousness of neglecting a signal path that is in the opposite direction of a high gain crossfeed path.

It is noted that the singular value method cannot be used to find answers to questions 1) and 3), and it fails to distinguish the structural difference between the perturbation matrices that represent the assumptions set in questions 2) and 4). (See Corollary 2.2 of [2].) More specifically, regardless of whether $E(s)$ takes the form of (78) or the form

$$E(s) = \begin{bmatrix} 0 & e_{12}(s) \\ 0 & 0 \end{bmatrix} \qquad (82)$$

the singular value method yields a small crossfeed tolerance given by [2]

$$\max \{ \left| e_{12}(s) \right| , \left| e_{21}(s) \right| \} < \underline{\sigma}[I + G(s)] \qquad (83)$$

and thus gives a misleading answer to question 2). Fig. 6 shows the graphs of the right-hand side of inequalities (80), (81), and (83) (designated by y_1, y_2, and y_3, respectively) on the same scale, for $b_{12} = 1$.
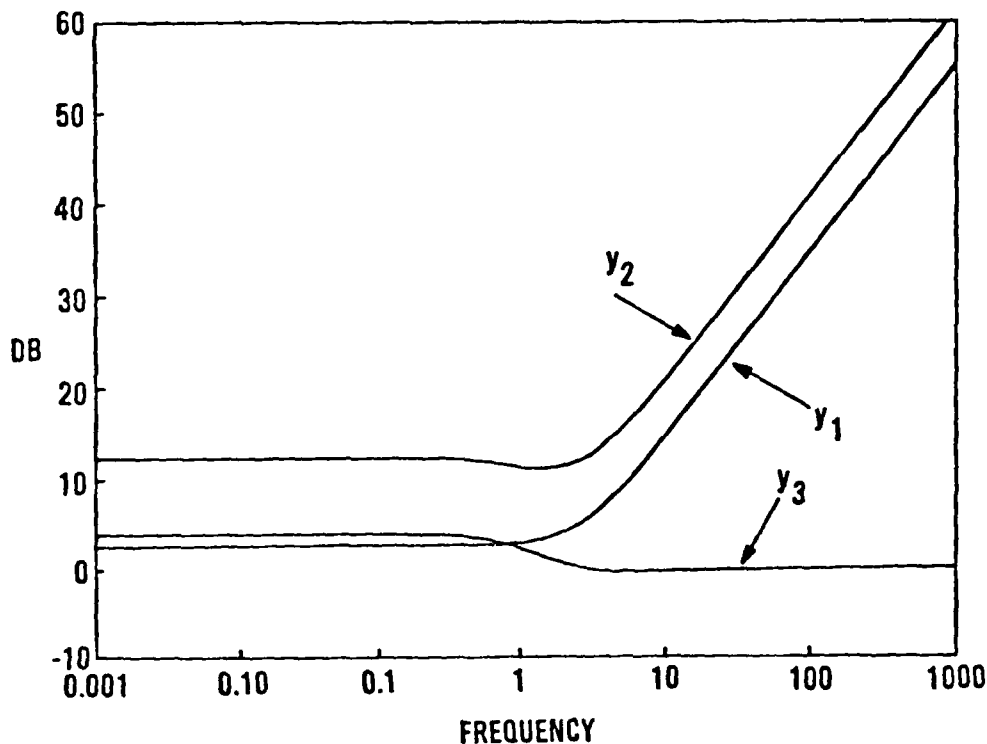

Fig. 6 Robustness bounds on the unmodeled crossfeed gain when $b_{12} = 1$

It is interesting to note that the bounds obtained by the optimally weighted ℓ_∞ norm method are significantly greater (less conservative) than the ones obtained by the singular value method at all frequencies. The

unweighted ℓ_∞ norm bounds (y_1 curve of Fig. 6) are only slightly lower than the singular value bounds at low frequencies but are exponentially higher at frequencies higher than 1 rad/sec. When $b_{12} = 0$, the robustness bounds are infinity (as indicated by the left-hand side of (81)), but the singular value method fails to reveal this. In fact, the singular value method would give a conservative bound of $\dfrac{|s+2|}{|s+1|}$. When the crossfeed gain b_{12} is large, the off-diagonal element in A(s) is dominant at low frequencies and the difference between the y_2 and y_3 curves diminishes, but as the frequency increases y_2 becomes significantly greater than y_3. Fig. 7 shows the graphs of y_2 and y_3 in dB versus frequency, for $b_{12} = 50$.
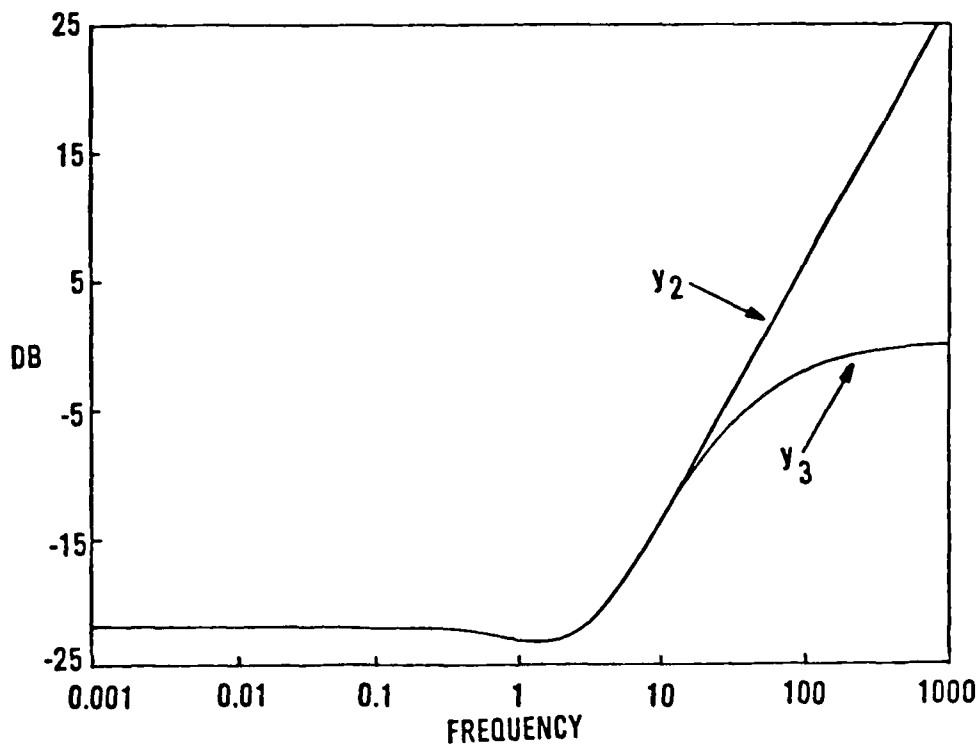

Fig. 7   Robustness bounds on the unmodeled crossfeed gain when $b_{12} = 50$

The curve y_1 is only a small fraction of a dB below y_2 throughout the entire frequency range and is omitted in Fig. 7 to maintain clarity.

The assumption set in question 5) implies the perturbation matrix

3-60

$$E(s) = \begin{bmatrix} 0 & e_{12}(s) \\ e_{21}(s) & 0 \end{bmatrix} \tag{84}$$

Note that this case is not covered by Corollary 2.2 of [2], in which I + E(s) must be a block triangular matrix. Application of Theorem 6 to this case yields an upper bound given by the right-hand side of (80) for both $\left|e_{12}(s)\right|$ and $\left|e_{21}(s)\right|$. However, a less conservative bound can be found (see Appendix) by selecting

$$\frac{q_1(s)}{q_2(s)} = \sqrt{\frac{\left|e_{12}(s)\right|}{\left|e_{21}(s)\right|}} \triangleq \beta \tag{85}$$

for the $\underline{q}(s)$ vector in (32), and then applying Lemma 1. This gives the upper bound of the greater of $\left|e_{12}(s)\right|$ or $\left|e_{21}(s)\right|$ as

$$\max \left\{ \left|e_{12}(s)\right|, \left|e_{21}(s)\right| \right\} < \frac{\max\left(\beta^2, 1\right)}{\beta\left|\dfrac{1}{s+2}\right| + \left|\dfrac{b_{12}(s+1)}{(s+2)^2}\right|} \tag{86}$$

This selection of $\underline{q}(s)$ vector is optimal in the sense that the bounds on $\left|e_{12}(s)\right|$ and $\left|e_{21}(s)\right|$ are maximized. Note that the ratio of $\left|e_{12}(s)\right|$ to $\left|e_{21}(s)\right|$ is given by β^2.

Finally, the conditions set in question 6) mean that the perturbation matrix E(s) is diagonal, i.e.,

$$E(s) = \begin{bmatrix} e_{11}(s) & 0 \\ 0 & e_{22}(s) \end{bmatrix} \tag{87}$$

The robustness bound on the magnitudes of $e_{11}(s)$ and $e_{22}(s)$ is readily found by application of Theorem 1. The result is the same as the answer to

3-61

question 1) (inequality (70)) since a diagonal $E(s)$ is a special case of an upper or lower triangular matrix. The result is clearly less conservative than that of the singular value method since b_{12} contributes significantly to the singular value of $A(s)$ but not to the Perron eigenvalue of $A(s)$.

The physical meaning of the reducibility of the open-loop transfer matrix $G(s)$ can also be demonstrated through the above system (Fig.5). It is seen that if $G(s)$ is reducible, $A(s)$ and $A^{-1}(s)$ are also reducible to block triangular matrices that are partitioned identically to $G(s)$. Hence the system can be said to be reducible. The reducibility of the system of Fig. 5 is characterized by the lack of crossfeed from u_1 or c_1 to u_2 or c_2. This constitutes the zero element below the diagonal in the $G(s)$ matrix of (67).

For control systems having a large number of inputs and outputs, the reducibility of the system can be similarly determined. Physically, this amounts to finding a subsystem (or subsystems) which does not receive crossfeeds from the signals of the rest of the systems. If such a subsystem exists (the determination of such subsystems may be facilitated by graph theory), the $G(s)$ matrix is reducible. For example, if $G(s)$ takes the form of the right-hand side of (28) after the input and output variables are relabeled, then the subsystem characterized by A_{22} does not receive any crossfeed from the subsystem characterized by A_{11}. If A_{11} or A_{22} is again reducible, then $G(s)$ can be further partitioned into an upper triangular block matrix having more than two diagonal blocks, after the input and output variables are appropriately relabeled. Note that a subsystem must have an equal number of inputs and outputs. Fictitious grounded (zero signal level) inputs or outputs can always be augmented to the system to

3-62

make the number of inputs and outputs virtually equal. Hence, if a system is reducible, Corollary 2.1 may be applied to characterize allowable perturbations of a similar structure. If the G(s) matrix is reducible to triangular form, Theorem 2 is applicable. If the system is irreducible, Lemma 2 and Theorem 4 may be applied. The rest of the Lemmas and Theorems apply to both reducible and irreducible systems.

VI. Conclusions

Techniques for using weighted ℓ_1 and ℓ_∞ norms to incorporate the structural information of a multivariable feedback control system in the measure of its stability robustness have been presented. The flexibility offered by these norms, along with the use of the theory of nonnegative matrices, enables one to assess individual bounds on elements of the open-loop perturbation matrix for stability robustness, under various assumptions on the structure of the plant uncertainty. Situations in which certain crossfeed perturbations in a given system may be unbounded without destabilizing the closed-loop system can be easily determined. Whether or not failure to include certain crossfeed signal paths in the system model can lead to serious miscalculations of the system stability can also be determined. Structure-dependent stability robustness criteria are derived via weighted ℓ_1 and ℓ_∞ norms. When the structure of plant uncertainty is known, these new criteria may be used to obtain less conservative uncertainty bounds than the singular-value based robustness tests.

Acknowledgement

APPENDIX

Derivation of Robustness Bounds for the Crossfeed
Perturbations for the Illustrative Example

Let

$$\left| A(s) \right| = \begin{bmatrix} a & b \\ 0 & a \end{bmatrix} \qquad (A-1)$$

and $E(s)$ be the one given in (84). Let

$$\frac{\left| e_{12}(s) \right|}{\left| e_{21}(s) \right|} \triangleq \beta^2 \qquad (A-2)$$

and

$$\frac{q_1(s)}{q_2(s)} \triangleq x \qquad (A-3)$$

Substituting these quantities into (32) gives the sufficient condition for

robustness as

$$\max \begin{bmatrix} \dfrac{1}{x} \left| e_{12}(s) \right| \\ \\ x \left| e_{21}(s) \right| \end{bmatrix} < \cfrac{1}{a + \dfrac{1}{x} b} \qquad (A-4)$$

where a and b are positive. In view of $(A-2)$, for $x \leqslant \beta$ it is seen that

$$\frac{1}{x} \left| e_{12}(s) \right| > x \left| e_{21}(s) \right| \qquad (A-5)$$

Hence, for all $x \leqslant \beta$, $(A-4)$ may be restated as

$$\frac{1}{x} \left| e_{12}(s) \right| < \frac{1}{a + \dfrac{1}{x} b} \tag{A-6}$$

which in turn gives

$$\left| e_{12}(s) \right| < \frac{1}{\dfrac{1}{x} \left(a + \dfrac{1}{x} b \right)} \tag{A-7}$$

Combining (A-2) and (A-7) gives

$$\left| e_{21}(s) \right| < \frac{1/\beta^2}{\dfrac{1}{x} \left(a + \dfrac{1}{x} b \right)} \tag{A-8}$$

Hence, it is desirable to have x as large as possible to give the least conservative bounds on the right-hand side of (A-7) and (A-8). Therefore, let $x = \beta$ in (A-7) and (A-8). This gives

$$\left| e_{12}(s) \right| < \frac{\beta^2}{\beta a + b} \tag{A-9}$$

and

$$\left| e_{21}(s) \right| < \frac{1}{\beta a + b} \tag{A-10}$$

For $x \geqslant \beta$ the inequality of (A-5) is reversed. Hence (A-4) implies

$$x \left| e_{21}(s) \right| < \frac{1}{a + \dfrac{1}{x} b} \tag{A-11}$$

or

$$\left| e_{21}(s) \right| < \frac{1}{xa + b} \qquad (A\text{-}12)$$

Combining (A-2) and (A-12) gives

$$\left| e_{12}(s) \right| < \frac{\beta^2}{xa + b} \qquad (A\text{-}13)$$

Hence, x should be selected to be as small as possible to give the least conservative robustness bounds. Therefore, in (A-12) and (A-13), x should again be set equal to β, again yielding (A-10) and (A-9), respectively.

Now (A-9) and (A-10) can be combined to read

$$\max \left\{ \left| e_{12}(s) \right|, \left| e_{21}(s) \right| \right\} < \frac{\max (\beta^2, 1)}{\beta a + b} \qquad (A\text{-}14)$$

Substituting appropriate numbers for a and b in (A-14) yields (86).

REFERENCES

[1] J.C. Doyle, and G. Stein, "Multivariable Feedback Design: Concepts for Classical/Modern Synthesis," IEEE Trans. Automat. Contr., Vol. AC-26, no 1, pp. 4-16, Feb. 1981.

[2] N.A. Lehtomaki, N.R. Sandell, Jr., and M. Athans, "Robustness Results in Linear-Quadratic Gaussian Based Multivariable Control Designs," IEEE Trans. Automat. Contr., Vol. AC-26, no. 1, pp 75-92, Feb 1981.

[3] V. Mukhopadhyay, and J.R. Newsom, "Application of Matrix Singular Value Properties for Evaluating Gain and Phase Margins of Multiloop Systems," AIAA Guidance and Control Conference, Aug. 9-11, 1982, San Diego, pp. 420-428.

[4] H.H. Rosenbrock, Computer-Aided Control System Design, Academic Press, 1974.

[5] A.G.J. McFarlane, and I. Postlethwaite, "The Generalized Nyquist Stability Criterion and Multivariable Root-Loci," Int. J. Control, vol. 23, no. 1, Jan. 1977, pp. 81-128.

[6] A.G.J. McFarlane, and B. Kouvaritakis, "A Design Technique for Linear Multivariable Feedback Systems", Int. J. Control, Vol. 23, no. 6, June 1977, pp. 837-874.

[7] J.C. Doyle, "Robustness of Multiloop Linear Feedback Systems," 17th IEEE Control and Decision Conference, Jan 1979, San Diego, pp. 12-18.

[8] N.A. Lehtomaki, D. Castanon, B. Levy, G. Stein, N.R. Sandell, and M. Athans, "Robustness Tests Utilizing the Structure of Modelling Error," 20th IEEE Control and Decision Conference, Dec. 1981, pp. 1173-1190.

[9] M.F. Barrett, "Conservatism with Robustness Tests for Linear Feedback Control Systems", 19th IEEE Control and Decision Conference, Dec 1980, pp. 885-890.

[10] M.G. Sofonov, "Stability Margins of Diagonally Perturbed Multivariable Feedback Systems," 20th IEEE Control and Decision Conference, Dec. 1981, pp. 1472-1478.

[11] W.H. Lee, S.W. Gully, J.S. Eterno, and N.R. Sandell, Jr., "Structural Information in Robustness Analysis," American Control Conference, Arlington, Virginia, June 1982.

[12] J.C. Kantor, and R.P. Andres, "Characterization of ´Allowable Perturbations´ for Robustness Stability," IEEE Trans. on Automat. Contr., Vol. AC-28, no. 1, pp. 107-109, Jan. 1983.

[13] S.S. Banda, D.B. Ridgely, and H.H. Yeh, "Robustness of Reduced Order Control," Proceedings of VPI & SU/AIAA Symposium on Dynamics and Control of Large Structures, Blacksburg, Va., June 1983.

[14] A.S. Householder, "The Approximate Solution of Matrix Problems," J. of the Assoc. for Computing Machinery, Vol. 5, pp. 205-243, 1958.

[15] A. Berman, and R.J. Plemmon, <u>Nonnegative</u> <u>Matrices</u> <u>in</u> <u>the</u> <u>Mathematical</u> <u>Sciences</u>, New York, Academic Press, 1979.

[16] M. Marcus, <u>Basic</u> <u>Theorems</u> <u>in</u> <u>Matrix</u> <u>Theory</u>, National Bureau of Standards, Applied Mathematics Series 57, Jan 22, 1960, For sale by Superint. of Documents, U.S. Gov. Printing Office, Washington D.C., 20402.

[17] N.A. Lehtomaki, "Practical Robustness Measures in Multivariable Control System Analysis", Ph.D. Thesis, Massachusetts Institute of Technology, May 1981.

[18] N.R. Sandell, Jr, S.W. Gully, W.H. Lee, and N.A. Lehtomaki, "Multivariable Stability Margins for Vehicle Flight Control Systems", TR-121, Sponsored by Office of Naval Research, Contract Number N00014-80-C-0509, December 1981.

[19] H.H. Yeh, S.S. Banda, and D.B. Ridgely, "Regions of Stability for Gain or Phase Variations in Multivariable Systems", 23rd IEEE Conference on Decision and Control, Las Vegas, December 1984.

APPENDIX 3B

(This Appendix contains two papers, the first paper was published in the Journal of Guidance, Control and Dynamics, Volume 8, Number 2, March-April 1985, pages 167-175. The second paper was published in the proceedings of 23rd Conference on Decision and Control, Las Vegas, Nevada, December 1984, pages 1409-1422.)

NONCONSERVATIVE EVALUATION OF UNIFORM

STABILITY MARGINS OF MULTIVARIABLE FEEDBACK SYSTEMS

Hsi-Han Yeh*, Capt D. Brett Ridgely+, and Siva S. Banda+
Flight Dynamics Laboratory   AFWAL/FIGC
Wright-Patterson Air Force Base OH 45433

Abstract

This paper discusses concepts of stability margins of multivariable feedback systems. Independent and uniform stability margins are defined. A previous conjecture that the uniform margins may be computed by using the eigenvalue magnitudes instead of the singular values in the robust stability criteria is theorized. The nonconservatism provided by this theory in the evaluation of uniform margins is discussed, along with limitations of the uniform margins. Also presented is a method of using the uniform margins to extend the region of stability beyond what can be specified by singular values. Results are demonstrated numerically in an example of a lateral attitude control system for a drone aircraft.

Introduction

Gain and phase margins have long been accepted as useful concepts in the specification of single-input single-output (SISO) feedback systems, because they give the user of a control system a feel of how safe the system is, so far as the stability is concerned. In extending these useful concepts to multiple-input multiple-output (MIMO) feedback systems,

---

* On leave from the University of Kentucky under AFOSR resident research program, 1982-1984
+ Aerospace Engineer, Member AIAA

diversity and ambiguity often arise. The one-loop-at-a-time stability margins fail to account for the simultaneous variations in a MIMO feedback system and hence may be unacceptable as relative stability measures[1]. The norm-bounded robustness criteria[1,2] guarantee closed-loop stability, but give the user no idea as to how the individual elements of the gain matrix may vary without destabilizing the closed-loop system. It is possible to obtain bounds on the magnitude of each element in the perturbation matrix of the loop transfer function for the stable operation of the feedback system[3,4]. In a general sense, these bounds are gain margins of the MIMO system. However, they are derived under the assumption that the phases and magnitudes of all elements in the perturbation matrix may vary simultaneously in the worst possible direction with unlimited phase variations. This is equivalent to having all the direct and crossfeed transfer functions varied independently and simultaneously. Since the worst possible variations are a mathematical extreme, these general gain margins are unduly conservative and, due to their uncorrelated multivariate nature, do not give a clear notion of how far the feedback system is from becoming unstable.

More meaningful stability margins may be defined[1] as limits within which the gains of all feedback loops may vary independently at the same time without destabilizing the system, while the phase angles remain at their nominal values, and vice versa. This amounts to setting the limits for independent gain or phase variations in a diagonal perturbation matrix for a multiplicative perturbation model. The zero off-diagonal elements in the perturbation matrix coordinate the variations of the crossfeed transfer functions and render the perturbation more tractable. However, these stability margins, as computed via the singular-value based robust

stability criterion[1], also tend to be very conservative. In an attempt to relax the conservatism in the evaluation of stability margins of a two-input two-output lateral attitude control system of a drone aircraft, Mukhopadhyay and Newsom[5] experimented with using the magnitudes of the eigenvalues instead of the singular values in the robustness criterion. By examining the Nyquist plot of the eigenvalues of the return difference matrix of the control system in their study, they conjectured that the "eigenvalue-based" gain (or phase) margins are limits within which the gains (or phases) of all feedback loops vary uniformly without destabilizing the feedback system while the phase angles (or gains) remain at their nominal values. In fact, since the spectral radius (maximum of the modulii of the eigenvalues) of a matrix is the greatest lower bound of all norms of that matrix, the conjecture of Ref. 5 is the least conservative for the evaluation of the uniform stability margins by means of norm-bounded robust stability criteria.

The uniform variations of multiloop gains and phases are also interesting in that the uniformity constraints give the multiloop variations a single-variable nature. Hence, the regions of stability in the gain and phase spaces degenerate into line segments. At each stable nominal operating point in the gain and phase spaces one such line segment may be constructed. In this fashion, the uniform gain and phase margins facilitate a nonconservative but discrete representation of the regions of stability in multidimensional gain and phase spaces.

In this paper, the conjecture given in Ref. 5 is proved. Uniformity in the gain and phase variations in feedback loops may be viewed as a special structure in the perturbation of an open-loop transfer matrix. Therefore,

3-72

weighted ℓ_1 and ℓ_∞ norms[3] are used in the norm-bounded stability robustness criteria to derive the formulas from which the uniform stability margins are computed. The concept and the one-dimensional characteristics of the uniform stability margins and their use in discretizing the regions of stability in multidimensional gain and phase spaces are demonstrated. The two-input two-output lateral attitude control system of a drone aircraft[5] is used again to demonstrate the extent of reduction of conservatism in determining the regions of stability and to demonstrate the feasibility of discretizing the regions of stability in multidimensional gain and phase spaces into line segments characterized by the uniform variation of loop gains and phases. The statement and proof of the conjecture are preceded by definitions of the commonly used[5,6] independent gain and phase margins and the proposed uniform gain and phase margins.

Stability Margins of Multivariable Feedback Systems

Definition 1: Independent gain margins are limits within which the gains of all feedback loops may vary independently at the same time without destabilizing the system, while the phase angles remain at their nominal values. Independent phase margins are limits within which the phase angles of all feedback loops may vary independently at the same time without destabilizing the system, while the gains remain at their nominal values.

The independent gain and phase margins vary with the point at which the complex loop gains are measured. For a general nonunity feedback system as shown in Fig. 1, if the loop is broken at $\underline{u}$ to measure the complex loop gains, then the simultaneous perturbation in each loop may be represented by a diagonal perturbation matrix $L(s)$ preceding the plant $G(s)$. If the

loop is to be broken at the output $\underline{y}$, then $L(s)$ should be inserted before the feedback block $H(s)$. For $s = j\omega$, let $L(s)$ be

$$L(j\omega) = \text{diag} \ [\quad \beta_1(\omega)e^{j\theta_1(\omega)} \quad \beta_2(\omega)e^{j\theta_2(\omega)} \quad . \quad . \quad . \quad \beta_n(\omega)e^{j\theta_n(\omega)} \quad] \quad (1)$$
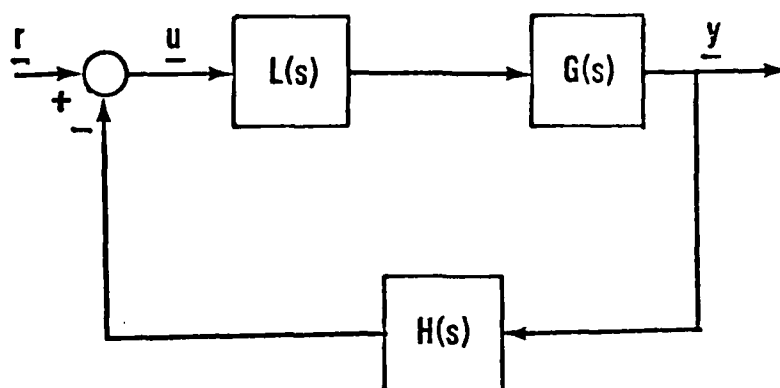

Fig. 1 Feedback system with input-multiplicative perturbations

Independent gain margins are limits within which $\beta_i(\omega)$ may vary independently for each i without destabilizing the system, while $\theta_i(\omega) = 0$ for all ω and all i. Independent phase margins are limits within which $\theta_i(\omega)$ may vary independently for each i without destabilizing the system, while $\beta_i(\omega) = 1$ for all ω and all i.

One can also let both $\beta_i(\omega)$ and $\theta_i(\omega)$ vary simultaneously and independently for each i. But then the limits within which $\beta_i(\omega)$ may vary depend upon $\theta_i(\omega)$ and vice versa, and hence are unwieldy for use as gain and phase margins.

<u>Definition</u> 2: Uniform gain margins are limits within which the gains of all feedback loops may vary uniformly at the same time without

destabilizing the system, while the phase angles remain at their nominal values. Uniform phase margins are limits within which the phase angles of all feedback loops may vary uniformly at the same time without destabilizing the system, while the gains remain at their nominal values.

For the system of Fig. 1, let $L(j\omega)$ be given by

$$L(j\omega) = \beta(\omega) e^{j\theta(\omega)} K(j\omega) \tag{2}$$

where $K(j\omega)$ is the nominal complex loop gain matrix given by

$$K(j\omega) = \text{diag}[\; k_1(j\omega) \quad k_2(j\omega) \cdots k_n(j\omega) \;] \tag{3}$$

Uniform gain margins with respect to the nominal loop gain $K(j\omega)$ are limits within which $\beta(\omega)$ may vary without destabilizing the feedback system while $\theta(\omega) = 0$ for all ω. Uniform phase margins with respect to the nominal loop gain $K(j\omega)$ are limits within which $\theta(j\omega)$ may vary without destabilizing the feedback system while $\beta(\omega) = 1$ for all ω.

The nominal gain $K(j\omega)$ also represents a nominal operating point in the gain and phase spaces, about which the system is uniformly perturbed. Since there is only one complex variable in (2), the regions of stability about each stable nominal operating point $K(j\omega)$ in the gain and phase spaces are straight-line segments. These one-dimensional regions facilitate a discrete representation of the regions of stability in multidimensional spaces. This will be demonstrated in an example after the formulas for nonconservative evaluation of the uniform stability margins are derived.

Nonconservative Evaluation of Uniform Stability Margins

For the system of Fig. 1, two robust stability criteria can be written; i.e., for all s on the Nyquist contour,

$$\overline{\sigma}[L(s) - I] < \underline{\sigma}[I + \{H(s)G(s)\}^{-1}] \tag{4}$$

and

$$\overline{\sigma}[L^{-1}(s) - I] < \alpha \leqslant \underline{\sigma}[I + H(s)G(s)] \tag{5}$$

where $\alpha \leqslant 1$, $\overline{\sigma}(\cdot)$ is the maximum singular value of the matrix in the argument, $\underline{\sigma}(\cdot)$ the minimum singular value, and I the identity matrix. Since these criteria are derived[1,2] on the basis of multivariable Nyquist theory, some preliminary conditions on the nominal and perturbed systems must hold. These conditions are[1,6]; (a) the open-loop characteristic polynomials of the nominal system and the perturbed system must have the same number of closed right-half plane roots, (b) all imaginary poles of the open-loop perturbed system must also be poles of the open-loop nominal system, and (c) the nominal system must be closed-loop stable. Since the right-hand sides of (4) and (5) are measures of the nearness of $\{H(s)G(s)\}^{-1}$ and $H(s)G(s)$ to the critical point of stability, (4) and (5) may be referred to as the inverse Nyquist formulation and the Nyquist formulation, respectively.

If these formulations are employed to determine the stability margins, the results obtained are always conservative. However, these criteria are special cases of inequalities involving general matrix norms[3,6,7], namely,

$$\left\| L(s) - I \right\| < \frac{1}{\left\| [I + \{H(s)G(s)\}^{-1}]^{-1} \right\|} \qquad (6)$$

and

$$\left\| L^{-1}(s) - I \right\| < \alpha \leqslant \frac{1}{\left\| [I + H(s)G(s)]^{-1} \right\|} \qquad (7)$$

where $\alpha \leqslant 1$ and the vertical double bars $\left\| \cdot \right\|$ denote general matrix norms which include the maximum singular value as a special case. Inequality (6) follows from a simple generalization of the derivation given in Ref. 2, and has been used in other papers[4,7]. Inequality (7) can be derived in the same fashion as the derivation of inequality (5) (see Ref. 1). Nevertheless, because the error matrix $L^{-1}(s)-I$ appears nonlinearly in the convex combination of nominal and perturbed loop transfer matrices, the generalization of the proof in Ref. 1 to the proof of inequality (7) is not trivial. The proof of (7) can be found in a recent paper[8]. It is evident that the conservatism of robust stability criteria may be reduced by using (6) or (7) instead of (4) or (5), respectively. This reduction will occur if for all s on the Nyquist contour the norms of $L(s)-I$ and $[I + \{H(s)G(s)\}^{-1}]^{-1}$, or $L^{-1}(s) - I$ and $[I+H(s)G(s)]^{-1}$ can be computed to be less than their respective maximum singular values (note that $\underline{\sigma}(A) = 1/\overline{\sigma}(A^{-1})$).

The conjecture of Mukhopadhyay and Newsom[5] states that, if $L(s)$ is characterized by (2) and if $K(j\omega) = I$, the maximum and minimum singular values in (5) may be replaced by the maximum and minimum magnitudes of the eigenvalues, respectively. More specifically, the conjecture states that under the above assumption, the stability of the system of Fig. 1, and hence the stability margins for $K(j\omega)=I$, may be determined by the inequality

$$\max_{i} \left| \lambda_i [L^{-1}(s) - I] \right| < \alpha \leqslant \min_{i} \left| \lambda_i [I + H(s)G(s)] \right| \qquad (8)$$

for $\alpha \leqslant 1$, and for all s on the Nyquist contour, where $\lambda_i(\cdot)$ denotes the ith eigenvalue of the matrix in the argument. Since any norm of a matrix is always greater than or equal to the spectral radius of the matrix, inequality (8) is the least conservative of all computations of (7), which includes (5) as a special case.

The subsequent development theorizes the above conjecture in a general framework and provides a proof, and then derives the nonconservative formulas of uniform stability margins. The same conjecture can also be applied to (4), and will also be proved here. In the formulation of uniform variations of complex multiloop gains, the nominal gain matrix $K(j\omega)$ of (2) is not an identity matrix in general and is given a priori. It may be treated as part of the plant. Therefore, the resulting norm-bounded robust stability criteria for the system of Fig. 1 with $L(s)$ characterized by (2) may be written as

$$\left\| [\beta(\omega)e^{j\theta(\omega)} - 1] I \right\| < \frac{1}{\left\| [I + \{H(j\omega)G(j\omega)K(j\omega)\}^{-1}]^{-1} \right\|} \qquad (9)$$

$$\left\| [\frac{1}{\beta(\omega)}e^{-j\theta(\omega)} - 1] I \right\| < \alpha \leqslant \frac{1}{\left\| [I + H(j\omega)G(j\omega)K(j\omega)]^{-1} \right\|} \qquad (10)$$

for $0 \leqslant \omega < \infty$. These inequalities are obtained by substituting $j\omega$ for s, $G(j\omega)K(j\omega)$ for $G(j\omega)$, and $\beta(\omega)\exp[j\theta(\omega)]$ for $L(j\omega)$ in (6) and (7). Practical systems with $H(s)G(s)K(s) \longrightarrow 0$ as $s \longrightarrow \infty$ are assumed.

<u>Lemma</u> <u>1</u>. Let A be an n x n matrix, $|A|$ be the nonnegative matrix formed by taking the absolute values of the elements of A, and $Q = \text{diag}[q_1 \quad q_2 \cdots q_n]$ be an n x n diagonal matrix with $q_i > 0$, for $i=1,2,\cdots,n$. The maximum row sum of the matrix product $Q^{-1}|A|Q$ is a norm of A, called the Q-weighted ℓ_∞ norm, denoted by

$$\|A\|_{Q^\infty} = \text{max row sum of } Q^{-1}|A|Q \tag{11}$$

The proof of Lemma 1 may be found in Ref. 9.

<u>Lemma</u> <u>2</u>. Given any nonsingular n x n matrix M, and any n x n matrix A, if $f(A)$ is a norm of A, then $f(M^{-1}AM)$ is also a norm of A.

This Lemma is also given in Ref. 9.

<u>Theorem</u> <u>1</u>. If the preliminary conditions following (4) and (5) hold, and L(s) is characterized by (2) ($K(j\omega)$ need not be diagonal), then the system of Fig. 1 is stable if either one of the following inequalities is satisfied:

$$\left| \beta(\omega) \, e^{j\theta(\omega)} - 1 \right| \quad < \quad \min_i \left| \lambda_i [I + \{H(j\omega)G(j\omega)K(j\omega)\}^{-1}] \right| \tag{12}$$

$$\left| [1/\beta(\omega)]e^{-j\theta(\omega)} - 1 \right| \quad < \quad \alpha \quad \leqslant \quad \min_i \left| \lambda_i [I + H(j\omega)G(j\omega)K(j\omega)] \right| \tag{13}$$

for $\alpha \leqslant 1$, and for all $0 \leqslant \omega < \infty$.

Proof: Let $M(s)$ be the modal matrix of $[I + \{H(j\omega)G(j\omega)K(j\omega)\}^{-1}]^{-1}$. Then $M^{-1}(j\omega)[I+\{H(j\omega)G(j\omega)K(j\omega)\}^{-1}]^{-1}M(j\omega)$ is in Jordan canonical form, and

all of its elements below the diagonal are zero. For notational brevity, let this Jordan canonical form be denoted by $J(j\omega)$, i.e.,

$$J(j\omega) = M^{-1}(j\omega)[I+\{H(j\omega)G(j\omega)K(j\omega)\}^{-1}]^{-1}M(j\omega) \qquad (14)$$

Let

$$Q = \text{diag} [\, 1 \;\; \varepsilon \;\; \varepsilon^2 \ldots \varepsilon^{n-1}\,] \qquad (15)$$

where ε is an arbitrarily small positive number. Then, by virtue of Lemmas 1 and 2, a special form of (9) may be written as

$$\left\| M^{-1}(j\omega)[\{\beta(\omega)e^{j\theta(\omega)} - 1\}I]M(j\omega) \right\|_{Q\infty} < \frac{1}{\left\| J(j\omega) \right\|_{Q\infty}} \qquad (16)$$

The left-hand side of the above inequality is readily computed to be $\left| \beta(\omega)e^{j\,\theta(\omega)} - 1 \right|$. With the aid of (11), (14), and (15), the Q-weighted ℓ_∞ norm of the Jordan canonical form of $J(j\omega)$ is found to be

$$\left\| J(j\omega) \right\|_{Q\infty} = \max_i \left| \lambda_i[(I + \{H(j\omega)G(j\omega)K(j\omega)\}^{-1})^{-1}] \right| + \delta\varepsilon \qquad (17)$$

The variable δ in (17) is either 1 or 0, depending on the superdiagonal elements in $J(j\omega)$. Thus, (16) is equivalent to

$$\left| \beta(\omega)e^{j\theta(\omega)} - 1 \right| < \frac{1}{\max_i \left| \lambda_i[(I + \{H(j\omega)G(j\omega)K(j\omega)\}^{-1})^{-1}] \right| + \delta\varepsilon} \qquad (18)$$

However, for any invertible A, any eigenvalue of the inverse of A is the inverse of an eigenvalue of A. Therefore, (18) is equivalent to

$$\left| \beta(\omega) e^{j\theta(\omega)} - 1 \right| < \frac{\min_i \left| \lambda_i[I + \{H(j\omega)G(j\omega)K(j\omega)\}^{-1}] \right|}{1 + \delta\epsilon \min_i \left| \lambda_i[I + \{H(j\omega)G(j\omega)K(j\omega)\}^{-1}] \right|} \quad (19)$$

which may be written as

$$\left| \beta(\omega) e^{j\theta(\omega)} - 1 \right| < \min_i \left| \lambda_i[I + \{H(j\omega)G(j\omega)K(j\omega)\}^{-1}] \right| - 0(\epsilon) \quad (20)$$

where $0(\epsilon)$ vanishes with ϵ in such a way that $0 \leqslant 0(\epsilon) < k\epsilon$ for some $k > 0$ and for sufficiently small ϵ. This proves inequality (12). Inequality (13) follows from (10) by the same reasoning. Q.E.D.

Corollary 1.1. If there exists $a_0 > 0$ such that for $0 \leqslant \omega < \infty$,

$$\min_i \left| \lambda_i[I + \{H(j\omega)G(j\omega)K(j\omega)\}^{-1}] \right| \geqslant a_0 \quad (21)$$

then the uniform gain margins of the MIMO system of Fig. 1 are given by

$$1 - a_0 < \beta(\omega) < 1 + a_0 \quad (22)$$

and the uniform phase margins are

$$-\pi \leqslant \theta(\omega) \leqslant \pi \qquad \text{if } 2 < a_0 \quad (23)$$

$$-2\sin^{-1}(a_0/2) < \theta(\omega) < 2\sin^{-1}(a_0/2) \qquad \text{if } a_0 \leqslant 2 \quad (24)$$

Proof: In view of (21) and (12), the system of Fig. 1 is stable if

$$\left| \beta(\omega) e^{j\theta(\omega)} - 1 \right| < a_0 \quad (25)$$

3-81

Letting $\theta(\omega) = 0$ in (25) gives (22). To obtain the uniform phase margins, let $\beta(\omega) = 1$ in (25) to yield

$$\left| e^{j\theta(\omega)} - 1 \right| < a_o \qquad (26)$$

Conditions (23) and (24) are a result of (26). Q.E.D.

Corollary 1.2. If there exists some $\alpha_o \leqslant 1$ such that for $0 \leqslant \omega < \infty$,

$$\min_i \left| \lambda_i[I + H(j\omega)G(j\omega)K(j\omega)] \right| \geqslant \alpha_o \qquad (27)$$

then the uniform gain and phase margins of the MIMO system of Fig. 1 are given by

$$\frac{1}{1 + \alpha_0} < \beta(\omega) < \frac{1}{1 - \alpha_0} \qquad (28)$$

and

$$-2\sin^{-1}(\alpha_0/2) < \theta(\omega) < 2\sin^{-1}(\alpha_0/2) \qquad (29)$$

respectively.

Proof: Letting $\vartheta(\omega) = 0$ and $\alpha = \alpha_0$ in (13) yields formula (28) for the uniform gain margins. Letting $\beta(\omega) = 1$ and $\alpha = \alpha_0$ in (13) yields formula (29) for the uniform phase margins. Q.E.D.

Theorem 1 and the Corollaries may be restated for independent gain and phase margins by substituting singular values for eigenvalues, $\beta_i(\omega)$ for $\beta(\omega)$, and $\theta_i(\omega)$ for $\theta(\omega)$, because the maximum singular value of a diagonal matrix is the magnitude of its largest element. However, in many cases less conservative results can be achieved by using norm measures other than singular values. For the sake of convenience, Corollaries 1.1 and 1.2 may be referred to as the inverse Nyquist formulation and the Nyquist formulation of uniform stability margins, respectively. Note that the inversion of the loop transfer function matrix in the inverse Nyquist formulation may be avoided by substituting $[I+H(s)G(s)]^{-1}H(s)G(s)$ for $[I+\{H(s)G(s)\}^{-1}]^{-1}$ in the right-hand side of (6) and then rewriting (12), (21), and (27) accordingly.

Since multivariable stability margins are based on sufficient conditions, the union of the stability regions given by different methods is also a valid region of stability. When computing uniform stability margins, the nominal system (when $L(s) = K(s)$) is required to be stable in order for the robust stability criteria to be valid. The selection of the nominal gain $K(s)$ may be aided by the formulas for independent gain margins. Thus, the combined use of independent and uniform stability margins enables one to extend beyond the conservative regions of stability established by the independent gain and phase margins along selected straight lines in the gain and phase spaces. This is demonstrated in the example in the next section.

Regions of Stability in the Gain and Phase Spaces

As in the SISO case, stability margins of a MIMO system guarantee the stability when either the gains or phases, but not both, of all the feedback loops may vary within the prescribed limits without destabilizing the closed-loop system. Therefore, if the uniform gain margin of a MIMO system at a nominal gain $K(j\omega)$ is $[g_{m1}, g_{m2}]$, then the system (Fig. 1) is stable when

$$L(j\omega) = \beta_o K(j\omega) \tag{30}$$

for all β_o satisfying $g_{m1} < \beta_o < g_{m2}$. To determine the region of stability in the gain space where phase angles of all feedback loops are assumed unperturbed, all elements in $K(j\omega)$ are selected to be real constants, i.e.,

$$K(j\omega) = \text{diag}[k_1 \quad k_2 \cdots k_n] \tag{31}$$

The coordinates of the gain space are loop gains (magnitudes of the elements of $L(j\omega)$ given by (30) and (31)) β_i, where $\beta_i = \beta_o k_i$, for $i = 1, 2, \cdots, n$. Thus, the region of stability specified by the uniform gain margin is a line segment between points $g_{m1}\underline{k}$ and $g_{m2}\underline{k}$ in the gain space, where $\underline{k}$ is the vector

$$\underline{k} = (k_1, k_2, \cdots, k_n) \tag{32}$$

In the phase space, the absolute gains of all feedback loops are assumed unperturbed. To determine the region of stability in the phase space, all elements in $K(j\omega)$ must be selected to be complex constants of unity magnitude, i.e.,

$$K(j\omega) = \text{diag}[\ e^{j\phi_1}\ \ e^{j\phi_2} \cdots e^{j\phi_n}\ ] \qquad (33)$$

Thus, if the uniform phase margin of a MIMO system at a nominal gain $K(j\omega)$ given by (33) is $[\ \phi_{m1}\ ,\ \phi_{m2}\ ]$ then the system is stable when

$$L(j\omega) = e^{j\theta_0}\ K(j\omega) \qquad (34)$$

for all θ_0 satisfying $\phi_{m1} < \theta_0 < \phi_{m2}$. The coordinates of the phase space are loop phases (phase angles of $L(j\omega)$ given by (33) and (34)) θ_i, where $\theta_i = \phi_i + \theta_0$, for $i = 1, 2, \cdots, n$. Thus, the region of stability specified by the uniform phase margin is a line segment between $\underline{\phi} + \phi_{m1}\underline{e}$ and $\underline{\phi} + \phi_{m2}\underline{e}$ in the phase space, where $\underline{e}$ and $\underline{\phi}$ are the n-vectors given by

$$\underline{e} = (\ 1\ \ 1\ \cdots\ 1\ ) \qquad (35)$$

$$\underline{\phi} = (\ \phi_1\ \ \phi_2 \cdots \phi_n\ ) \qquad (36)$$

In contrast with the uniform stability margins, the regions of stability prescribed by independent stability margins are hypercubes in the gain and phase spaces. It is easy to see from Definition 1 that if the independent gain margin of a MIMO system is $[g_a,\ g_b]$, the system is stable when

$$L(j\omega) = \text{diag}[\ \beta_1\ \ \beta_2\ \cdots\ \beta_n\ ] \qquad (37)$$

with $g_a < \beta_i < g_b$ for i=1,2,$\cdots$,n. If the independent phase margin of a MIMO system is [ϕ_a, ϕ_b], the system is stable when

$$L(j\omega) = \text{diag}[\ e^{j\theta_1}\ e^{j\theta_2}\cdots\ e^{j\theta_n}\ ] \tag{38}$$

with $\phi_a < \theta_i < \phi_b$ for i=1,2,$\cdots$,n.

Since the operating points inside the hypercube of the independent stability margins are guaranteed to be stable, they may be used as nominal gains $K(j\omega)$ in (30) and (34) to determine the one dimensional regions of stability in the n-dimensional gain and phase spaces.

Example: For the purpose of comparison, the 8th order lateral attitude control system of a drone aircraft used in Ref. 5 is used here.
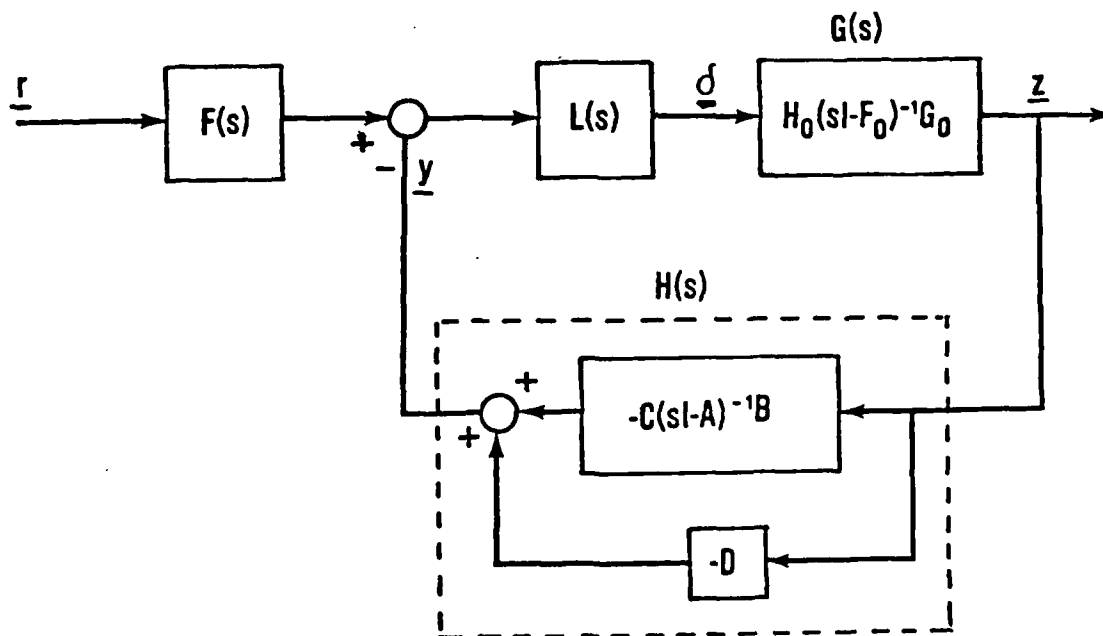
Fig. 2 Lateral attitude control system of a drone aircraft

The block diagram of the system is given in Fig. 2 and the numerical data of Fig. 2 are given in Table 1. The perturbation matrix $L(s)$ is characterized by

$$L(j\omega) = \begin{bmatrix} \beta_1 e^{j\theta_1} & 0 \\ \\ 0 & \beta_2 e^{j\theta_2} \end{bmatrix} \tag{39}$$

where β_1, β_2, θ_1, and θ_2 are constants in the gain and phase margin calculations.

The graphs of the minimum magnitudes of the eigenvalues and singular values of $I + H(j\omega)G(j\omega)$ and $I + \{H(j\omega)G(j\omega)\}^{-1}$ are plotted versus frequency in Fig. 3 and Fig. 4. The minimum values of these curves are found to be

$$\alpha_o = \min_{\omega} \min_{i} \left| \lambda_i [I + H(j\omega)G(j\omega)] \right| = 0.6494 \tag{40}$$

$$\alpha_o' = \min_{\omega} \underline{\sigma} [I + H(j\omega)G(j\omega)] = 0.2463 \tag{41}$$

$$a_o = \min_{\omega} \min_{i} \left| \lambda_i [I + \{H(j\omega)G(j\omega)\}^{-1}] \right| = 0.4417 \tag{42}$$

$$a_o' = \min_{\omega} \underline{\sigma} [I + \{H(j\omega)G(j\omega)\}^{-1}] = 0.2279 \tag{43}$$
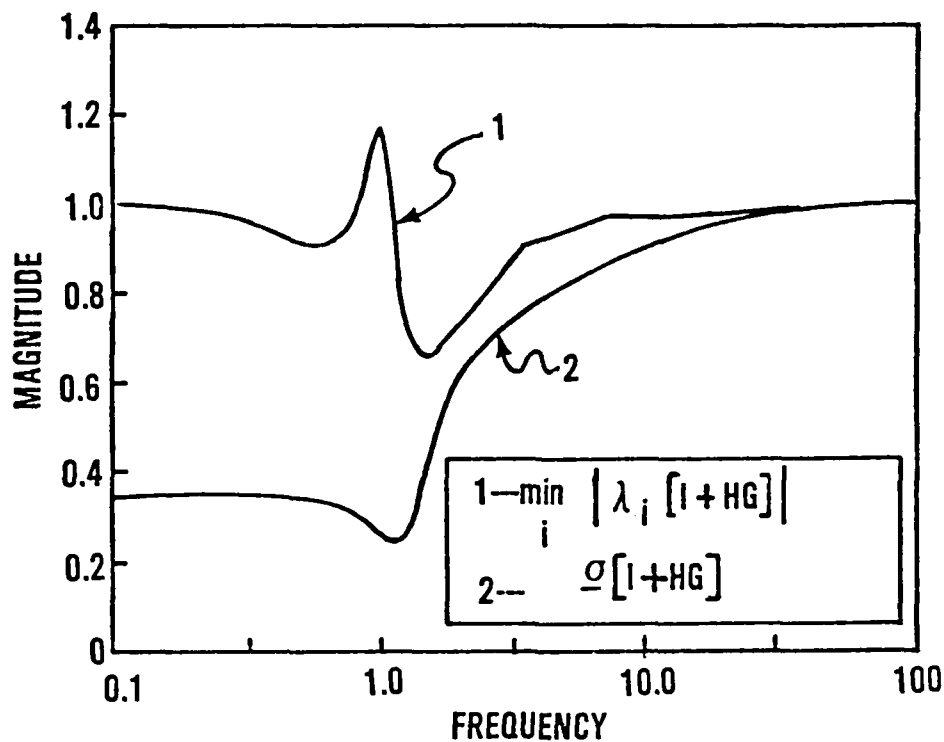
Fig. 3 Minimum eigenvalue and $\underline{\sigma}$ of return difference matrix of Fig. 2
when $L(j\omega) = I$
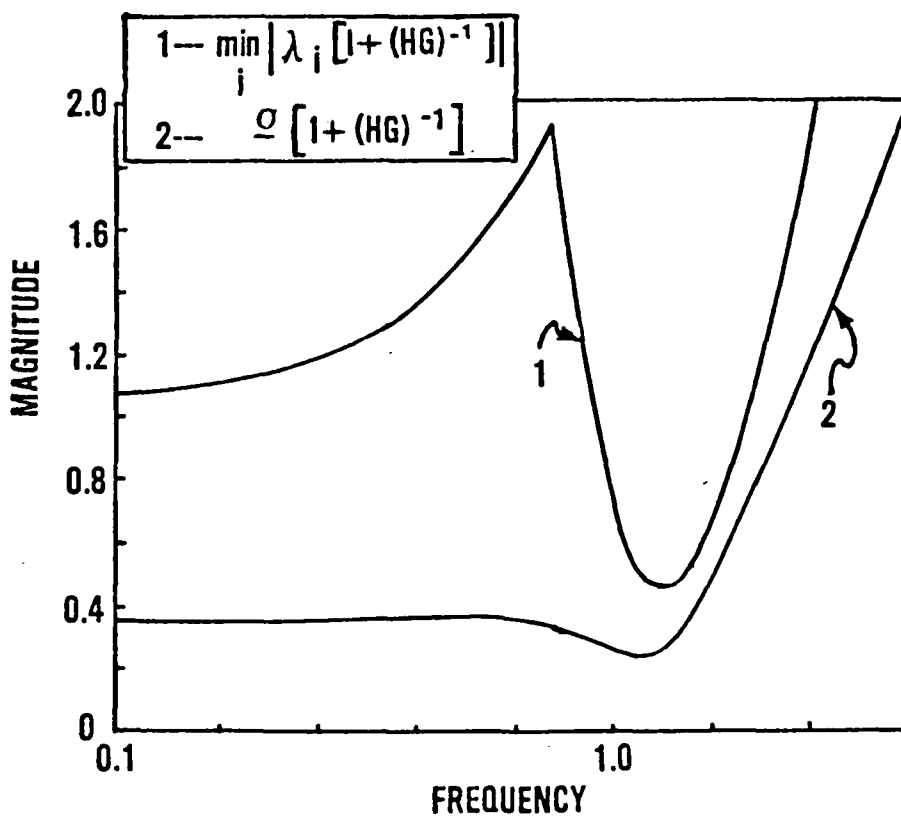
Fig. 4 Minimum eigenvalue and $\underline{\sigma}$ of inverse return difference matrix
of Fig. 2 when $L(j\omega) = I$

The independent gain and phase margins (IGM and IPM, respectively), may be calculated from α_o' and a_o' as

$$IGM = [\ 1/(1 + \alpha_o')\ ,\ 1/(1 - \alpha_o')\ ] = [\ 0.8024\ ,\ 1.3268\ ] \qquad (44)$$

$$IGM = [\ 1 - a_o'\ ,\ 1 + a_o'\ ] = [\ 0.7721\ ,\ 1.2279\ ] \qquad (45)$$

$$IPM = [\ -2\sin^{-1}(\alpha_o'/2)\ ,\ 2\sin^{-1}(\alpha_o'/2)\ ] = [\ -14.147^o\ ,\ 14.147^o\ ] \qquad (46)$$

$$IPM = [\ -2\sin^{-1}(a_o'/2)\ ,\ 2\sin^{-1}(a_o'/2)\ ] = [\ -13.09^o\ ,\ 13.09^o\ ] \qquad (47)$$

Note that the union of the regions of stability found by any sufficient stability criteria is contained in the actual region of stability. Hence, the gain margins of (44) and (45) may be combined. Similarly, the phase margins of (46) and (47) may also be combined, but the right-hand side of (47) is already contained in that of (46). Thus,

$$IGM = [\ 0.7721\ ,\ 1.3268\ ] \qquad (48)$$

$$IPM = [\ -14.147^o\ ,\ 14.147^o\ ] \qquad (49)$$

The regions of stability represented by (48) and (49) are shown as squares in the gain and phase planes in Fig. 5 and Fig. 6, respectively. These are the regions of stability specified by singular value robust stability criteria for independent loop gain variations when phase angles are kept at nominal values, and for independent loop phase variations when loop gains are kept at nominal values. Each point (β_1, β_2) in the gain plane of Fig. 5 represents an operating point of the system of Fig. 2, when

$L = \text{diag}[\beta_1, \beta_2]$. Similarly, each point (θ_1, θ_2) in the phase plane of Fig. 6 represents an operating point of the system of Fig. 2, when $L = \text{diag}[e^{j\theta_1}, e^{j\theta_2}]$. If the system operates anywhere inside the square ABCD in Fig. 5 or PQRS in Fig. 6, it is stable.
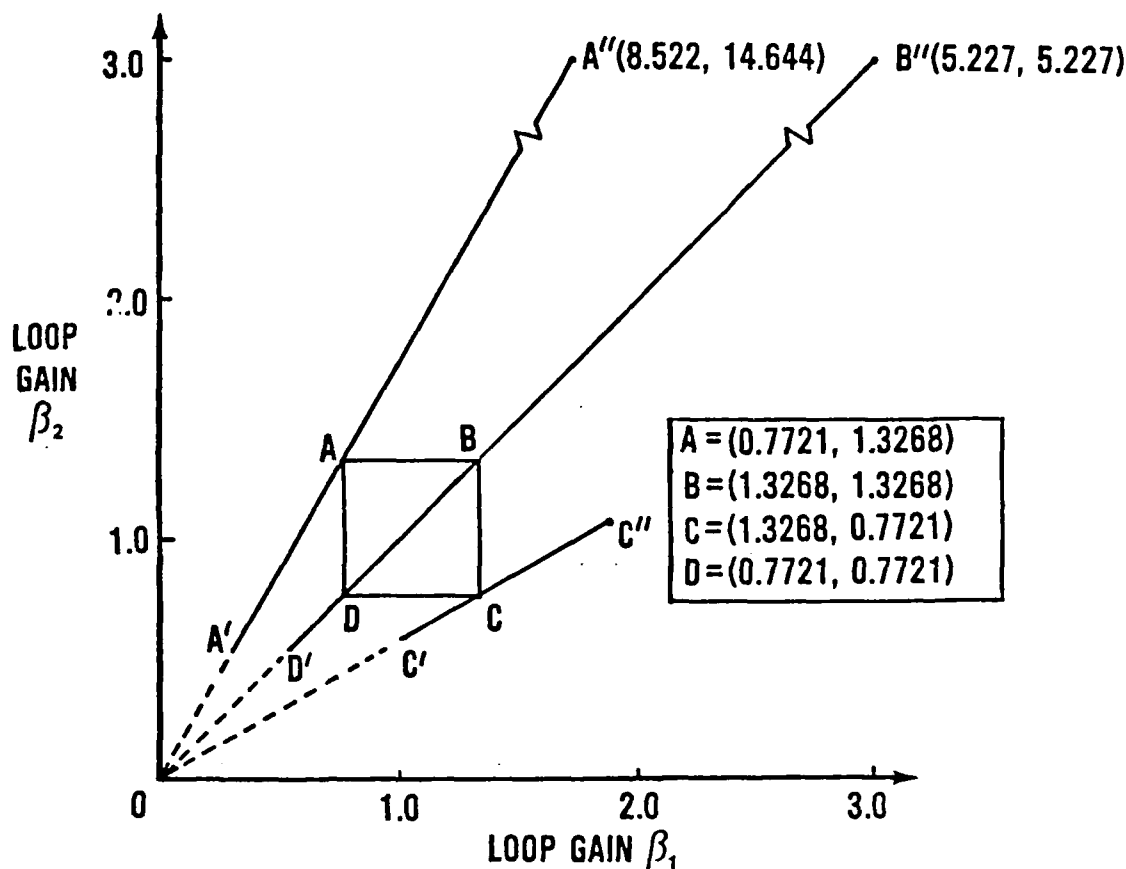

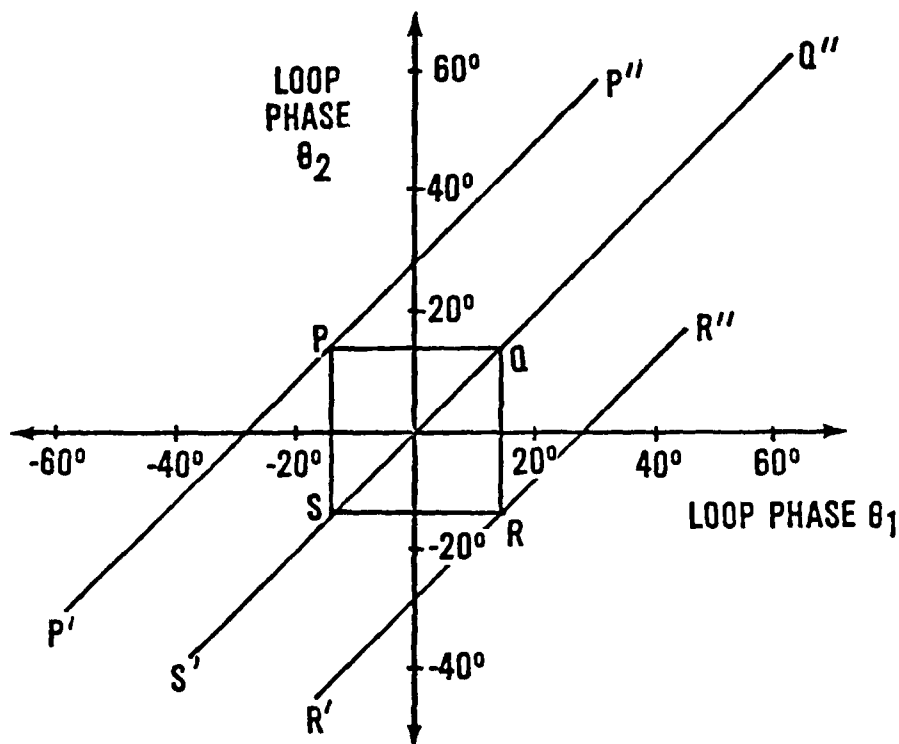Fig. 5 Gain-plane region of stability for the system of Fig. 2

Fig. 6   Phase-plane region of stability for the system of Fig. 2

The uniform gain and phase margins (where $\beta_1 = \beta_2 = \beta$, and $\theta_1 = \theta_2 = \theta$ in (39)) for which $K(j\omega) = I$ are calculated from α_o and a_o of (40) and (42). These are found to be $(0.5583, 2.8523)$ and $(-37.895^{\circ}, 37.895^{\circ})$, respectively. It is seen that these margins are much larger (less conservative) than those in (48) and (49), but yield only line segments in the gain and phase spaces versus the squares ABCD and PQRS in Figs. 5 and 6 obtained through independent margins. However, these line segments obtained by uniform margins can be used to extend the regions of stability in certain directions considerably beyond what can be established by independent margins.

To demonstrate this use of uniform gain and phase margins, let the nominal system be operating at point A (Fig. 5) and assume uniform perturbations. The uniform gain margins may be found by (22) and (28) using

$$K(j\omega) = K_a = \begin{bmatrix} 0.7721 & 0 \\ 0 & 1.3268 \end{bmatrix} \tag{50}$$

The graphs of the minimum magnitude of the eigenvalues of $I+H(j\omega)G(j\omega)K_a$ and $I+\{H(j\omega)G(j\omega)K_a\}^{-1}$ are plotted versus frequency in Fig. 7. The minimum values of these curves are found to be

$$\alpha_o = \min_{\omega} \min_{i} \left| \lambda_i[I + H(j\omega)G(j\omega)K_a] \right| = 0.9094 \tag{51}$$

$$a_o = \min_{\omega} \min_{i} \left| \lambda_i[I + \{H(j\omega)G(j\omega)K_a\}^{-1}] \right| = 0.6058 \tag{52}$$
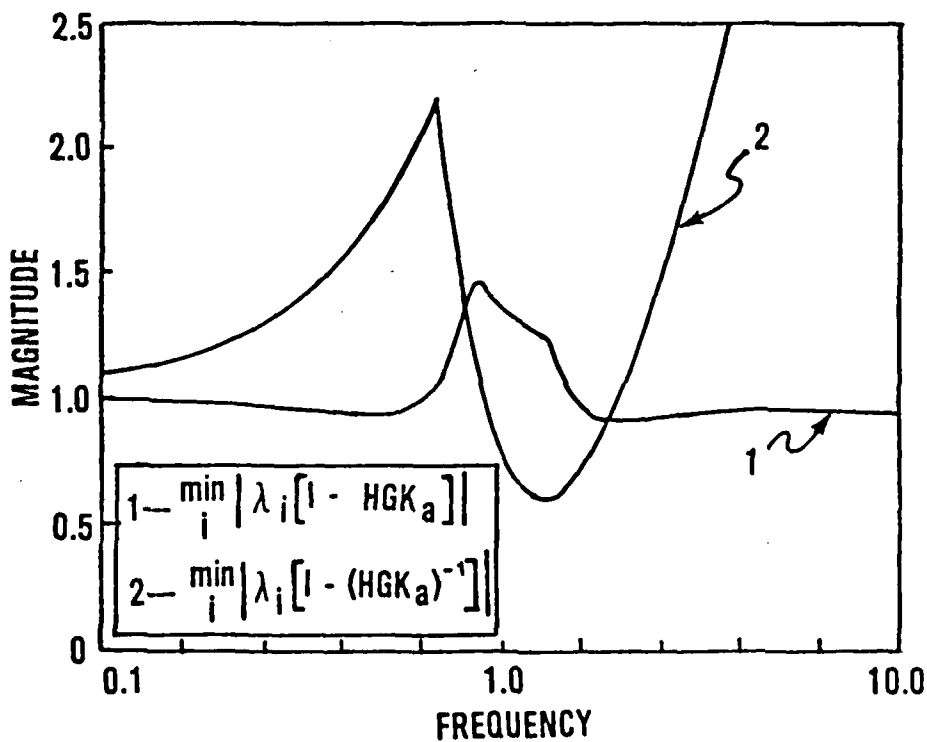
Fig. 7 Minimum eigenvalues when the system is operating at A in Fig. 5

The uniform gain margins based on the Nyquist and inverse Nyquist formulations are found to be

$$UGM = [\ 1/(1 + \alpha_o)\ ,\ 1/(1 - \alpha_o)\ ] = [\ 0.5237\ ,\ 11.0374\ ] \qquad (53)$$

$$UGM = [\ 1 - a_o\ ,\ 1 + a_o\ ] = [\ 0.3942\ ,\ 1.6058\ ] \qquad (54)$$

respectively. The combined UGM is

$$UGM = [\ 0.3942\ ,\ 11.0374\ ] \qquad (55)$$

The combined UGM of (55) specifies that the operating points on the line segment A′AA″ in the gain plane (Fig. 5) are stable, where

$$\overline{OA'}/\overline{OA} = 0.3942 \qquad (56)$$

$$\overline{OA''}/\overline{OA} = 11.0374 \qquad (57)$$

where the upper bar denotes the length of the line segment. Applying similar computations to points B, C, and D in Fig. 5 shows that the operating points on the line segments D′DBB″ and C′CC″ are stable operating points, where

$$\overline{OD'}/\overline{OD} = 0.7018 \qquad (58)$$

$$\overline{OB''}/\overline{OB} = 3.9397 \qquad (59)$$

$$\overline{OC'}/\overline{OC} = 0.7718 \qquad (60)$$

$$\overline{OC''}/\overline{OC} = 1.4146 \tag{61}$$

Table 2 shows the values of α_o and a_o at points B, C, and D. Note that the points B′ and D″ are not shown in Fig. 5 as they lie between the endpoints B″ and D′.

On the phase plane, let the system be operating at point P and assume uniform perturbations. The uniform phase margins may be found by formulas (23), (24), and (29), using

$$K(j\omega) = K_p = \begin{bmatrix} e^{-j14.147^{\circ}} & 0 \\ & \\ 0 & e^{j14.147^{\circ}} \end{bmatrix} \tag{62}$$

The graphs of the minimum magnitude of the eigenvalues of $I+H(j\omega)G(j\omega)K_p$ and $I+\{H(j\omega)G(j\omega)K_p\}^{-1}$ are plotted versus frequency in Fig. 8. The minimum values of these curves are found to be

$$\alpha_o'' = \min_{\omega} \min_{i} \left| \lambda_i[I + H(j\omega)G(j\omega)K_p] \right| = 0.7506 \tag{63}$$

$$a_o'' = \min_{\omega} \min_{i} \left| \lambda_i[I + \{H(j\omega)G(j\omega)K_p\}^{-1}] \right| = 0.4550 \tag{64}$$
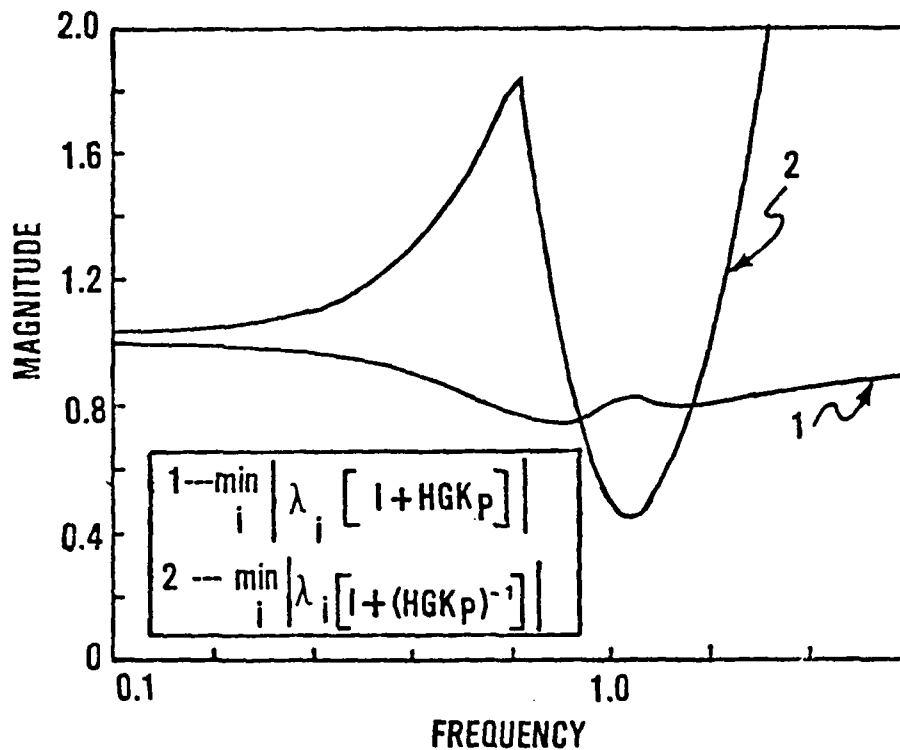
Fig. 8 Minimum eigenvalues when the system is operating at P in Fig. 6

The uniform phase margins (UPM) based on the Nyquist and inverse Nyquist formulations, respectively, are found to be

$$\text{UPM} = [\ -2\sin^{-1}(\alpha_o''/2)\ ,\ 2\sin^{-1}(\alpha_o''/2)\ ] = [\ -44.085^o\ ,\ 44.085^o\ ] \qquad (65)$$

$$\text{UPM} = [\ -2\sin^{-1}(a_o''/2)\ ,\ 2\sin^{-1}(a_o''/2)\ ] = [\ -26.301^o\ ,\ 26.301^o\ ] \qquad (66)$$

The region of stability specified by (66) is contained inside the one specified by (65). Hence, the uniform phase margin is given by (65). Thus, the operating points on the line segment P'PP" in the phase plane (Figure 6) are stable, with

$$\overline{P'P} = \overline{PP''} = \sqrt{2} \times 44.085^{\circ} \tag{67}$$

Similar computations on points Q, R, and S show that operating points on line segments S'SQQ" and R'R'R" are stable operating points, with

$$\overline{S'S} = \sqrt{2} \times 23.570^{\circ} \tag{68}$$

$$\overline{QQ''} = \sqrt{2} \times 48.634^{\circ} \tag{69}$$

$$\overline{R'R} = \overline{RR''} = \sqrt{2} \times 30.510^{\circ} \tag{70}$$

Table 2 shows the values of α_0 and a_0 at points Q, R, and S. Once again, Q' and S" are not shown in Fig. 6 as they lie between Q" and S'. The regions of stability in the gain and phase planes are thus extended considerably beyond the squares specified by the singular values along selected straight-line segments with the aid of uniform stability margins.

Note that near the actual boundary of stability, where the minimum singular value is small, ill-conditioning may be present and eigenvalue computations may be inaccurate. However, in that area, both the minimum singular value and the minimum eigenvalue are near zero, and there the singular value is preferable.

Conclusions

The concept of uniform stability margins is developed on the basis of uniform variations of multiloop gains and phases. It is proved that uniform stability margins may be computed by substituting modulii of eigenvalues

for singular values in the singular-value-bounded robust stability criteria. This is the least conservative computation that is possible when a norm-bound robust stability criterion is used.

Regions of stability in the gain and phase spaces as specified by uniform stability margins are line segments which pass through the given nominal operating points. The uniform stability margins may be used to extend the regions of stability beyond what can be specified by the singular values of the return difference matrix or the inverse return difference matrix along selected straight lines in the least conservative manner.

REFERENCES

[1] Lehtomaki,N.A., Sandell,N.R. Jr., and Athans,M., "Robustness Results in Linear- Quadratic-Gaussian Based Multivariable Control Designs," IEEE Trans Automat Contr, Vol AC-26, No. 1, Feb 1981, pp 75-92.

[2] Doyle,J.C., "Robustness of Multiloop Linear Feedback Systems," 17th IEEE Conference on Decision and Control, Jan 1979, San Diego CA, pp 12-18.

[3] Yeh,H.H., Banda,S.S., and Ridgely,D.B., "Stability Robustness Measures Utilizing Structural Information," American Control Conference, Jun 1984, San Diego CA. Also to appear in the International Journal of Control.

[4] Kantor,J.C., and Andres,R.P., "Characterization of 'Allowable Perturbations' for Robustness Stability," IEEE Trans on Automatic Contr, Vol AC-28, No. 1, Jan 1983, pp 107-109.

[5]Mukhopadhyay,V., and Newsom,J.R., "Application of Matrix Singular Value Properties for Evaluating Gain and Phase Margins of Multiloop Systems," AIAA Paper 82-1574, Aug. 1982.

[6]Lehtomaki,N.A., Castonon,D., Levy,B., Stein,G., Sandell,N.R., and Athans,M., "Robustness Tests Utilizing the Structure of Modelling Error," 20th IEEE Conference on Decision and Control, Dec 1981, pp 1173-1190.

[7]Barrett,M.F., "Conservatism with Robustness Tests for Linear Feedback Control Systems", 19th IEEE Conference on Decision and Control, Dec 1980, pp 885-890.

[8]Yeh,H.H., Banda,S.S., and Ridgely,D.B., "Regions of Stability for Gain or Phase Variations in Multivariable Systems", 23rd IEEE Conference on Decision and Control, Dec 1984, Las Vegas NV.

[9]Householder,A.S., "The Approximate Solution of Matrix Problems," J. of the Assoc for Computing Machinery, Vol 5, 1958, pp 205-243.

Table 1   Numerical data for the system of Fig. 2

$$A = \begin{bmatrix} 0 & 0 \\ 0 & -2 \end{bmatrix} \quad B = \begin{bmatrix} 1 & 0 \\ 0 & 1 \end{bmatrix} \quad C = \begin{bmatrix} 0.1491 & 0 \\ 0 & -4.116 \end{bmatrix} \quad D = \begin{bmatrix} 0 & 0 \\ 0 & 2.058 \end{bmatrix}$$

$$F(s) = \begin{bmatrix} 0.1491/s & 0 \\ 0 & 1 \end{bmatrix}$$

$$F_o = \begin{bmatrix} -0.0827 & -0.1423\times10^{-3} & -0.9994 & 0.0414 & 0 & 0.1862 \\ -46.86 & -2.757 & 0.3896 & 0 & -124.3 & 128.6 \\ -0.4248 & -0.06224 & -0.0671 & 0 & -8.792 & -20.46 \\ 0 & 1 & 0 & 0 & 0 & 0 \\ 0 & 0 & 0 & 0 & -20. & 0 \\ 0 & 0 & 0 & 0 & 0 & -20. \end{bmatrix}$$

$$\lambda(F_o) = \begin{bmatrix} -0.03701 & \text{spiral mode} \\ 0.1889 \pm j1.051 & \text{dutch roll} \\ -3.25 & \text{roll convergence} \\ -20.0 & \text{elevon actuator} \\ -20.0 & \text{rudder actuator} \end{bmatrix}$$

$$G_o = \begin{bmatrix} 0 & 0 \\ 0 & 0 \\ 0 & 0 \\ 0 & 0 \\ 1 & 0 \\ 0 & 1 \end{bmatrix} \quad H_o = \begin{bmatrix} 0 & 1 & 0 & 0 & 0 & 0 \\ 0 & 0.07 & 1 & 0 & 0 & 0 \end{bmatrix}$$

Table 2   Minimum eigenvalues for points in Figs. 5 and 6

	Point					
	B	C	D	Q	R	S
α_o	0.7462	0.2931	0.4003	0.8236	0.5262	0.4085
a_o	0.5648	0.2282	0.2982	0.4850	0.3974	0.3281

REGIONS OF STABILITY FOR GAIN OR PHASE VARIATIONS IN MULTIVARIABLE SYSTEMS

Hsi-Han Yeh*, Siva S Banda+ , and Lt D Brett Ridgely+

Flight Dynamics Laboratory (AFWAL/FIGC)

Wright-Patterson Air Force Base, OH 45433

Abstract

This paper extends the well-known norm-bounded robust stability criteria from strict inequalities that specify open sets to inequalities that specify closed sets. Both the Nyquist and inverse Nyquist type of norm-bounded criteria are considered. The extended criteria form the theoretical basis in the formulation of an iterative procedure for searching the regions of stability for simultaneous gain or phase variations in multivariable feedback systems. The basic idea of the iterative procedure lies in successively perturbing the feedback system from a set of nominal gains or phases that are on the boundary of a previously established region of stability. The iterative procedure is illustrated by a numerical example.

---

* On leave from the University of Kentucky under AFOSR resident research program, 1982-1984
+ Aerospace Engineer

I. Introduction

In extending the useful concept of single variable stability margins to multiple-input multiple-output (MIMO) feedback systems, diversity and ambiguity inevitably arise. The commonly used definitions of MIMO stability margins lead to what may be called independent gain and phase margins. They are defined as limits within which the gains of all feedback loops may vary independently at the same time without destablizing the system, while the phase angles remain at their nominal values and vice versa [1-3].

The MIMO independent gain and phase margins may be evaluated via norm-bounded robust stability criteria. The resulting stability margins specify two cubical regions of stability in the gain and phase spaces [2, 3]. As the norm-bounded robust stability criteria are sufficient conditions, the cubical regions of stability are often conservative (i.e., they yield only a portion of the actual stability region). If gain and phase margins are used in the specifications of a MIMO system, the actual regions of stability in the gain and phase spaces may be desired. However, there is no systematic or iterative method for computing the boundaries of the actual regions of stability at this time, to the authors' knowledge.

In a recent paper [2] where the desire to know the actual stability regions of a two-loop system arises, closed-loop poles are computed for many pairs of real loop gains. Pairs of real gains which yield purely imaginary closed-loop poles are points on the boundary of the actual region of stability in the gain plane. To compute the boundary of the stability region in the phase plane, fictitious complex loop gains of unit magnitude and variable phase angles are inserted into the loops. The complex determinant of the return difference matrix as a function of frequency is

plotted for many pairs of phase angles. Pairs of phase angles which yield a zero determinent at some frequency are points on the boundary of the actual region of stability in the phase plane. It is evident that this is a brute force method. There are no guidelines for finding points on the boundaries. The computation is formidable and is virtually impossible when the system has more than two loops.

This paper presents an iterative procedure for obtaining the actual regions of stability in the gain and phase spaces. This method is based upon the simple idea of perturbing the system further from a set of nominal gains that are on the boundary of a previously established region of stability. Thus instead of finding points which are on the boundaries of the actual regions of stability, the proposed method successively expands the regions of stability from the hypercubes that are originally established by the norm-bounded robustness stability criteria.

The theoretical basis of this iterative process is the fact that on the boundaries of the open sets of perturbation matrices specified by the norm-bounded stability criteria, the stability of the perturbed system can be conveniently determined by the invertibility of the return-difference matrix, which will then be used in the next iteration. This fact and its conditions may be regarded as extensions of the norm-bounded stability criteria. They are formulated into three theorems and two corollaries in the next section, and the proofs are given in the Appendices.

II. Norm-Bounded Robust Stability Criteria

Consider the MIMO feedback system of Fig 1, where G(s) is the nominal loop transfer function and L(s) is a transfer matrix representing the perturbation of the loop transfer matrix from its nominal value. For the

problem of finding a set of L(s) that does not destabilize the feedback system, two robust stability criteria can be written, i.e., for all s on the Nyquist contour,

$$\overline{\sigma}[L(s) - I] < \underline{\sigma}[I + G^{-1}(s)] \qquad (1)$$

or

$$\overline{\sigma}[L^{-1}(s) - I] < \alpha \leqslant \underline{\sigma}[I + G(s)] \qquad (2)$$

where $\alpha \leqslant 1$, $\overline{\sigma}(\cdot)$ is the maximum singular value of the matrix in the argument, $\underline{\sigma}(\cdot)$ the minimum singular value, and I is the identity matrix.
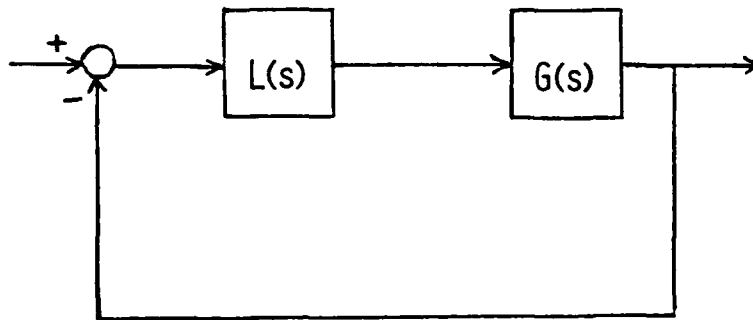
Fig. 1 A MIMO Feedback System

These criteria are sufficient conditions derived [1, 5] on the basis of multivariable Nyquist theory. The following preliminary conditions on the nominal (L(s)=I) and perturbed (L(s) $\neq$ I) systems must hold [1, 6] before criteria (1) and (2) can be applied:

(a) The open-loop characteristic polynomials (the common denominator of the elements of G(s) or the denominator of the determinant of the return difference matrix) of the nominal system and the perturbed system must have the same number of closed right-half plane roots.

(b) All imaginary poles of the open-loop perturbed system must also be poles of the open-loop nominal system. That is, $L(s)$ does not introduce imaginary poles into $G(s)L(s)$.

(c) The nominal system must be closed-loop stable.

Robustness criteria (1) and (2) are special cases of inequalities involving general matrix norms [6-8], namely,

$$\left\| L(s) - I \right\| < \frac{1}{\left\| [I + G^{-1}(s)]^{-1} \right\|} \quad ; \quad s \in D_R \tag{3}$$

and

$$\left\| L^{-1}(s) - I \right\| < \alpha \leqslant \frac{1}{\left\| [I + G(s)]^{-1} \right\|} \quad ; \quad s \in D_R \tag{4}$$

where D_R is the Nyquist contour, $\alpha \leqslant 1$, and the vertical double bars $\|\cdot\|$ denote general matrix norms which include the maximum singular value as a special case. Condition (3) follows from a simple generalization of the deriviation given in [5], and has been used in other papers [6-8]. Condition (4) can be derived in the same fashion as the derivation of condition (2), which is given in [1]. However, because $L^{-1}(s)-I$ does not appear as a linear term in the convex combination of $G(s)$ and $G(s)L(s)$, the generalization of the proof of (2) (as found in Ref [1]) to the proof of (4) is not trivial. The proof of (4) is given in Appendix A.

The right-hand sides of (1) - (4) are measures of the nearness of $G^{-1}(s)$ or $G(s)$ to some critical point of stability. In view of their similarity to the Nyquist and inverse Nyquist methods for single-input single-output (SISO) systems, conditions (1) and (3) may be referred to as the inverse Nyquist formulation, and conditions (2) and (4) the Nyquist formulation.

Conditions (3) and (4) specify open sets Σ and Σ' where

$$\Sigma \triangleq \left\{ L(s) \;\middle|\; \|L(s) - I\| < \frac{1}{\left\|[I + G^{-1}(s)]^{-1}\right\|} \;\; ; \;\; s \in D_R \right\} \quad (5)$$

$$\Sigma' \triangleq \left\{ L(s) \;\middle|\; \|L^{-1}(s) - I\| < \alpha \leqslant \frac{1}{\left\|[I + G(s)]^{-1}\right\|} \;\; ; \;\; s \in D_R, \alpha \leqslant 1 \right\} \quad (6)$$

If the perturbation matrix $L(s)$ of Fig. 1 belongs to Σ or Σ', then the feedback system is stable. However, since (3) and (4) are sufficient conditions, Σ and Σ' are only subsets of the set of all $L(s)$ that do not cause the feedback system to become unstable.

Let $\widetilde{\Sigma}$ and $\widetilde{\Sigma}'$ be boundaries of the sets Σ and Σ', respectively. The closed sets $\Sigma \cup \widetilde{\Sigma}$ and $\Sigma' \cup \widetilde{\Sigma}'$ are defined by

$$\Sigma \cup \widetilde{\Sigma} \triangleq \left\{ L(s) \;\middle|\; \|L(s) - I\| \leqslant \frac{1}{\left\|[I + G^{-1}(s)]^{-1}\right\|} \;\; ; \;\; s \in D_R \right\} \quad (7)$$

$$\widetilde{\Sigma} \cup \widetilde{\Sigma}' \triangleq \left\{ L(s) \;\middle|\; \|L^{-1}(s) - I\| \leqslant \alpha \leqslant \frac{1}{\left\|[I + G(s)]^{-1}\right\|} \;\; ; \;\; s \in D_R, \alpha \leqslant 1 \right\} \quad (8)$$

Note that if for some $s \in D_R$ the equalities hold for the norm relations in the bracketed terms in (7) or (8), then $L(s) \in \widetilde{\Sigma}$ or $L(s) \in \widetilde{\Sigma}'$, respectively. Criterion (3) can be readily extended to include points on $\widetilde{\Sigma}$, if $I+G(s)L(s)$ is nonsingular at these points. Criterion (4) can also be extended to include points on $\widetilde{\Sigma}'$ if $I+G(s)L(s)$ is nonsingular, provided that spectral norms are used, or that $L(s)$ is diagonal. These are formally stated in the following Theorems and their Corollaries.

Theorem 1: Under the preliminary conditions of the norm-bounded robust stability criteria, the feedback system of Fig. 1 is stable if $I+G(s)L(s)$ is nonsingular and

$$\| L(s) - I \| \leqslant \frac{1}{\left\| [I + G^{-1}(s)]^{-1} \right\|} \quad ; \quad s \in D_R \qquad (9)$$

Proof: See Appendix B.

It has been shown in a previous paper [3] that when complex loop gains of the system of Fig. 1 are uniformly perturbed ($L(s) = \ell(s)I$), a matrix norm $\| \cdot \|_m$ which is subordinate to some vector norm may be chosen such that

$$\left\| \ell(s)I - I \right\|_m = \left| \ell(s) - 1 \right| \qquad (10)$$

and

$$\frac{1}{\left\| [I + G^{-1}(s)]^{-1} \right\|_m} = \left| \underline{\lambda}[I + G^{-1}(s)] \right| \qquad (11)$$

where $\left| \cdot \right|$ signifies absolute value and $\underline{\lambda}(\cdot)$ signifies the eigenvalue that has the minimum magnitude. Therefore, if $L(s)$ is constrained to be $L(s) = \ell(s)I$, we have the following Corollary:

<u>Corollary 1.1</u>: Under the preliminary conditions of the norm-bounded robust stability criteria, the feedback system of Fig. 1 is stable if

(a) $L(s) = \ell(s)I$ \qquad (12)

(b) $\left| \ell(s) - 1 \right| \leqslant \left| \underline{\lambda}[I + G^{-1}(s)] \right|$; $s \in D_R$ \qquad (13)

(c) $\underline{\lambda}[I + G(s)L(s)] \neq 0$; $s \in D_R$ \qquad (14)

Proof: Condition (14) holds iff $I+G(s)L(s)$ is nonsingular. Substituting (12) into (9) and using $\| \cdot \|_m$ establishes (13) as a sufficient condition for stability. This completes the proof.

<u>Theorem 2</u>: Under the preliminary conditions of the norm-bounded robust stability criteria, the feedback system of Fig. 1 is stable if

$$\overline{\sigma}[L^{-1}(s) - I] \leqslant \alpha \leqslant \underline{\sigma}[I + G(s)] \quad ; \quad s \in D_R \ , \ \alpha \leqslant 1 \qquad (15)$$

and

$$\underline{\sigma}[I + G(s)L(s)] \neq 0 \quad ; \quad s \in D_R \qquad (16)$$

Proof: See   Appendix C.   Note that (16) holds iff I+G(s)L(s) is nonsingular.

Theorem 3:   Under the preliminary conditions of the norm-bounded robust stability criteria, the feedback system of Fig. 1 is stable if the following hold:

    (a) L(s) is diagonal,

    (b) I+G(s)L(s) is nonsingular for all $s \in D_R$,

    (c) The matrix norm is subordinate to some vector norm, and

$$(d) \quad \left\| L^{-1}(s) - I \right\| \leqslant \alpha \leqslant \frac{1}{\left\| [I + G(s)]^{-1} \right\|} \quad ; \quad s \in D_R \ , \ \alpha \leqslant 1 \qquad (17)$$

Proof: See Appendix D.

For the same reasons as in the establishment of Corollary 1.1, we also have the following corollary:

Corollary 3.1: Under the preliminary conditions of the norm-bounded robust stability criteria, the feedback system of Fig. 1 is stable if

    (a) $L(s) = \ell(s)I$ (18)

    (b) $\left| (1/\ell(s)) - 1 \right| \leqslant \alpha \leqslant \left| \underline{\lambda}[I+G(s)] \right| \quad ; \quad s \in D_R \ , \ \alpha \leqslant 1$ (19)

and

    (c) $\underline{\lambda}[I+G(s)L(s)] \neq 0 \quad ; \quad s \in D_R$ (20)

Proof: Analogous to the proof of Corollary 1.1.

Theorems 1, 2 and 3 essentially argue that the robustness of a system that is already perturbed by an $L(s)$ on $\tilde{\Sigma}$ or $\tilde{\Sigma}'$ can be determined by $\left\|[I+\{G(s)L(s)\}^{-1}]^{-1}\right\|$ or $\left\|[I+G(s)L(s)]^{-1}\right\|$, since the nonsingularity of $I+G(s)L(s)$ guarantees the applicability of the robust stability criteria to the perturbed system. This justifies the idea of successively expanding the region of stability by successively perturbing the system using a perturbation matrix that is on the boundary of a previously established region of stability. When the inverse Nyquist formulation is used in this successive perturbation, $L(s)$ may be non-diagonal and any matrix norm can be used, as ruled by Theorem 1. For the Nyquist formulation, it has only been established here that the spectral norm (maximum singular value) should be used when $L(s)$ is nondiagonal (Theorem 2), but any subordinate matrix norm can be used when $L(s)$ is diagonal. Fortunately, this poses no real problem because in stability margin computations, $L(s)$ is usually chosen to be diagonal, and to every vector norm there is unique subordinate matrix norm. Furthermore, when there is no crossfeed perturbation ($L(s)$ is diagonal) and all loops are uniformly perturbed (diagonal elements of $L(s)$ are identical), the robustness, and therefore the stability margins, may be measured using the magnitude of the minimum eigenvalue of the return-difference or the inverse-return-difference matrix (Corollaries 1.1 and 3.1). This enables the iterative expansions to make larger strides than using any norm measure, but restricts the expansion to certain directions. Further development of this idea of expanding the region of stability by an iterative procedure is presented in the next section, which is followed by a numerical example.

III. Regions of Stability in Gain and Phase Spaces

In this section, the development will be based on the Nyquist formulation. Results based on the inverse Nyquist formulation can be similarly stated.

For the system of Fig. 1, let L(s) be diagonal with complex constant elements ℓ_i, i.e.,

$$\ell_i(s) = \ell_i = \rho_i e^{j\theta_i} \qquad i = 1, 2, \cdots, n \qquad (21)$$

Where ρ_i and θ_i are real numbers. For notational convenience, let

$$\underline{\ell} = (\ell_1, \ell_2, \cdots, \ell_n) \qquad (22)$$

$$L = \text{diag}[\underline{\ell}] \qquad (23)$$

The variable s is dropped from L(s) because L(s) is constant for computing gain and phase margins.

The gain region of stability is the region in the space of $(\rho_1, \rho_2, \cdots, \rho_n)$ in which the MIMO system of Fig. 1 is stable if $\theta_i = 0$ for all i. The phase region of stability is the region in the space of $(\theta_1, \theta_2, \cdots, \theta_n)$ in which the MIMO system of Fig. 1 is stable if $\rho_i = 1$ for all i. This concept of regions of stability in gain and phase spaces of MIMO systems is a natural extension of the stability margin concept of SISO systems, where gain margins are computed when the phase angle of the loop is held constant at the nominal value, and phase margins are computed when the loop gain is held at the nominal value.

When L(s) is given by (23), a subset of the region of stability in the gain or phase space is easily established via formula (6). The problem now is to derive an iterative procedure to extend this subset into the entire region of stability. The basic idea of this iterative procedure is to alter the perturbation matrix successively until the boundary of the region of stability is reached, as illustrated in the block diagram of Fig. 2.
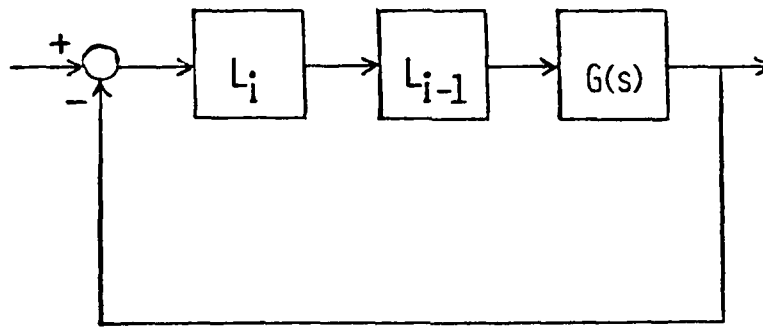
Fig. 2   A MIMO Feedback System With Successive Gain Perturbations

Region of Stability in the Gain Space

In the MIMO system of Fig. 2, let

$$\underline{\rho}_i \triangleq (\rho_{i1}, \rho_{i2}, \cdots, \rho_{in}) \tag{24}$$

$$\log \underline{\rho}_i \triangleq (\log \rho_{i1}, \log \rho_{i2}, \cdots, \log \rho_{in}) \tag{25}$$

$$L_i \triangleq \text{diag}[\underline{\rho}_i] \tag{26}$$

$$\hat{L}_i \triangleq L_{i-1}L_i = \text{diag}[\underline{\rho}_{i-1}]\text{diag}[\underline{\rho}_i] \qquad \text{for} \quad i \geqslant 0 \tag{27}$$

$$\hat{L}_i \triangleq L_i \triangleq I \qquad \text{for} \quad i < 0 \tag{28}$$

To each set of L_i (or $\hat{L}_i$) given by (26) – (28) there corresponds a set R_i (or $\hat{R}_i$) in the space of (ρ_1, ρ_2,···, ρ_n) such that if $\underline{\rho} \in R_i$ (or $\hat{R}_i$) then diag[$\underline{\rho}$] belongs to the set of L_i (or $\hat{L}_i$). The converse is also true.

Let R_o denote the set of $\underline{\rho}$ { = (ρ_1, ρ_2, ···, ρ_n) } such that L (= diag[$\underline{\rho}$]) satisfies inequality (4). Thus, if $\underline{\rho}_o \in R_o$ and L_o = diag[$\underline{\rho}_o$], then the system of Fig. 2 for i = 0 is stable. It is easily shown that if spectral norms (maximum singular values) are used in (4), R_o is an open hypercube (not including the boundary) in the gain space characterized by [1, 2, 3]

$$\frac{1}{1 + \alpha_o} < \rho_j < \frac{1}{1 - \alpha_o} \tag{29}$$

for j = 1, 2 ,···, n , where α_o is either $\min\limits_{s \in D_R} \underline{\sigma}[I+G(s)]$ or 1, whichever is smaller. In logarithmic units (29) may be rewritten as

$$-\log(1 + \alpha_o) < \log \rho_j < \log[1/(1 - \alpha_o)] \tag{30}$$

Here R_o is a hypercube whose edges are parallel to the coordinates of the gain space and whose diagonal extends from { $-\underline{e} \cdot \log(1 + \alpha_o)$ } to { $\underline{e} \cdot \log[1/(1 - \alpha_o)]$ }, for $\underline{e}$ = (1, 1,···, 1) (see Fig. 3).
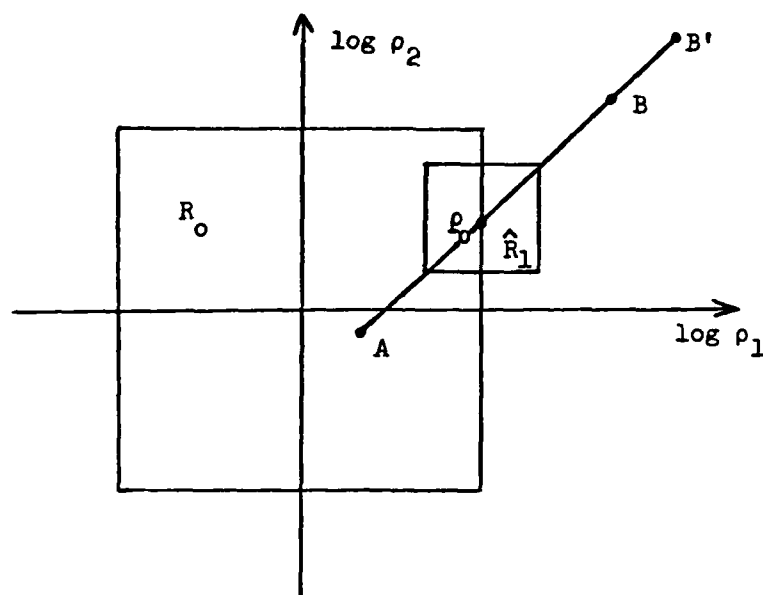
Fig. 3   Establishing the Region of Stability in the Gain Space

Let $\widetilde{R}_o$ denote the boundary of the hypercube R_o. Let $\underline{\rho}_o$ be a point arbitrarily chosen from $\widetilde{R}_o$, and L_o = diag$[\underline{\rho}_o]$. If $I+G(s)L_o$ is singular at some $s \in D_R$ then det$[I + G(s)L_o]$ has a root on D_R. This means that the closed-loop transfer matrix $G(s)L_o(I + G(s)L_o)^{-1}$ has a pole on D_R. Thus, the system of Fig. 2 for $i = 0$ is unstable and $\underline{\rho}_o$ is a point on the boundary of the region of stability in the gain space. On the other hand, if $I+G(s)L_o$ is nonsingular for all $s \in D_R$, then in view of Theorem 2, the system of Fig. 2 for $i = 0$ is stable. Therefore, the norm-bounded robust stability criteria may be applied to Fig. 2 for $i = 1$. As a result, the system of Fig. 2 for $i = 1$ is stable if $I+G(s)L_o$ is nonsingular for all $s \in D_R$ and

$$\left\| L_1 - I \right\| < \alpha_1 \leqslant \frac{1}{\left\| [I + G(s)L_o]^{-1} \right\|} \quad ; \quad s \in D_R , \quad \alpha_1 \leqslant 1 \qquad (31)$$

Let R_1 be the set in the gain space corresponding to the set of L_1's that satisfy (31). Let $\hat{R}_1$ be the set in the gain space corresponding to

the set of $\hat{L}_1$'s such that $\hat{L}_1 = L_0 L_1 = \text{diag}[\underline{\rho}_o]\text{diag}[\underline{\rho}_1]$, with $\underline{\rho}_1 \in R_1$ for a given $\underline{\rho}_o$. Again, if spectral norms are used, R_1 is found to be an open hypercube in the gain space (not shown in Fig. 3), characterized by

$$-\log(1 + \alpha_1) < \log \rho_j < \log[1/(1 - \alpha_1)] \qquad (32)$$

for $j = 1, 2, \cdots, n$, and α_1 is either $\min\limits_{s \in D_R} \underline{\sigma}[I + G(s)L_o]$ or 1, whichever is smaller. For a given $\underline{\rho}_o$, $\hat{R}_1$ is readily seen to be characterized by

$$-\log(1 + \alpha_1) + \log \rho_{oj} < \log \rho_j < \log[1/(1 - \alpha_1)] + \log \rho_{oj} \qquad (33)$$

The set $\hat{R}_1$ is the hypercube (Fig. 3) whose main diagonal extends from $\{ \log \underline{\rho}_o - \underline{e} \cdot \log(1 + \alpha_1) \}$ to $\{ \log \underline{\rho}_o + \underline{e} \cdot \log[1/(1 - \alpha_1)] \}$ where $\underline{e} = (1, 1, \cdots, 1)$.

The procedure of generating $\hat{R}_1$ from a point on $\tilde{R}_o$ may be iterated again by arbitrarily selecting a point $\underline{\rho}_1$ on the boundary of $R_o \cup \hat{R}_1$. For this $\underline{\rho}_1$, if $I+G(s)L_1$ is singular at some $s \in D_R$ then $\underline{\rho}_1$ is a point on the boundary of the region of stability in the gain space. Therefore, another $\underline{\rho}_1$ should be selected instead. Otherwise, $\hat{R}_2$ is found to be a hypercube whose edges are parallel to the coordinates of the gain space and whose diagonal extends from $\{ \log \underline{\rho}_1 - \underline{e} \cdot \log(1 + \alpha_2) \}$ to $\{ \log \underline{\rho}_1 + \underline{e} \cdot \log[1/(1 - \alpha_2)] \}$ where α_2 may be chosen as

$$\alpha_2 = \min \{ 1 , \min\limits_{s \in D_R} \underline{\sigma}[I + G(s)L_1] \} \qquad (34)$$

For the ith iteration, a point $\underline{\rho}_{i-1}$ is arbitrarily selected on the boundary of $\bigcup\limits_{j=0}^{i-1} \hat{R}_j$ (where $\hat{R}_o = R_o$). If $I+G(s)L_{i-1}$ is singular for some $s \in D_R$, then $\underline{\rho}_{i-1}$ is already a point on the boundary of the region of

3-114

stability in the gain space and another $\underline{\rho}_{i-1}$ should be tried. If $I+G(s)L_{i-1}$ is nonsingular for all $s \in D_R$ then $\hat{R}_i$ *is established as a* hypercube with edges parallel to the coordinates of the gain space and with a diagonal extending from $\{ \log \underline{\rho}_{i-1} - \underline{e} \cdot \log(1 + \alpha_i) \}$ to $\{ \log \underline{\rho}_{i-1} + \underline{e} \cdot \log[1/(1 - \alpha_i)] \}$ where α_i may be chosen as

$$\alpha_i = \min \{ 1 , \min_{s \in D_R} \underline{\sigma}[I + G(s)L_{i-1}] \} \tag{35}$$

If the iteration process goes on until $\bigcup_{j=0}^{i} \hat{R}_j$ is so large that $\min_{s \in D_R} \underline{\sigma}[I + G(s)L_i]$ is negligible for all $\underline{\rho}_i$ on the boundary of $\bigcup_{j=0}^{i} \hat{R}_j$, then $\bigcup_{j=0}^{i} \hat{R}_j$ is approximately the region of stability in the gain space.

It has been shown that [3] if the loop gains of the systems of Fig. 2 vary uniformly, (that is, $L(s) = \ell(s)I$ for some scalar function $\ell(s)$) then the robust stability condition (4) is implied by

$$\left| (1/\ell(s)) - 1 \right| < a_0 \leqslant \left| \underline{\lambda}[I+G(s)] \right| \quad ; \quad s \in D_R , a_0 \leqslant 1 \tag{36}$$

where $\underline{\lambda}(\cdot)$ is the eigenvalue with the smallest absolute value. When $\ell(s) = \rho = $ real constant, condition (36) requires that

$$-\log(1 + a_0) < \log \rho < \log(1/(1 - a_0)) \tag{37}$$

where a_0 is the smaller of $\min_{s \in D_R} \left| \underline{\lambda}[I + G(s)] \right|$ or 1. However, the region of stability for $L(s)$ as determined by (36) is not a hypercube, but a line segment between $\{ -\underline{e} \log(1 + a_0) \}$ and $\{ \underline{e} \log[1/(1 - a_0)] \}$, for $\underline{e} = (1, 1, \cdots, 1)$.

Based upon inequality (36) and Corollary 3.1 an iterative procedure for searching the region of stability using the minimum eigenvalue of the

return difference matrix can be formulated. The procedure still starts on the boundary of the set R_o of Fig. 3 because the nominal system is required to be stable. First, chose $L_o = \text{diag}[\ \underline{\rho}_o\ ]$ for some $\underline{\rho}_o \ \epsilon \widetilde{R}_o$. For i = 1 in the system of Fig. 2, the diagonal elements of L_1 are required to be identical, i.e., $\rho_{11} = \rho_{12} = \cdots = \rho_{1n}$. The set $\hat{R}_1$ (in the space of $(\rho_1, \rho_2, \cdots, \rho_n)$) corresponding to $\hat{L}_1$ ($= L_o L_1$) is characterized by

$$\log\ \rho_j = \log\ \rho_{oj} + \log\rho \tag{38}$$

$$-\log(\ 1 + a_1\ ) \ < \ \log\rho \ < \ \log[\ 1/(\ 1 - a_1\ )\ ] \tag{39}$$

for j = 1, 2,$\cdots$, n, where

$$a_1 = \min\ \{\ 1\ ,\ \min_{s\epsilon D_R}\ \left|\ \underline{\lambda}[\ I + G(s)L_o\ ]\ \right|\ \} \tag{40}$$

In other words, the set $\hat{R}_1$ is a line segment of unity slope extending from $\{\ \log\ \underline{\rho}_o - \underline{e}\cdot\log(1+a_1)\ \}$ to $\{\ \log\ \underline{\rho}_o + \underline{e}\cdot\log[1/(1-a_1)]\ \}$ (point A to point B in Fig. 3). In the next iteration, $\underline{\rho}_1$ is chosen at point B and $\hat{R}_2$ is the line segment of unity slope, extending from $\{\ \log\ \underline{\rho}_1 - \underline{e}\cdot\log(1+a_2)\ \}$ (between points A and B on the line segment AB) to $\{\ \log\ \underline{\rho}_1 + \underline{e}\cdot\log[1/(1-a_2)]\ \}$ (at point B′), where

$$a_2 = \min\ \{\ 1\ ,\ \min_{s\epsilon D_R}\ \left|\ \underline{\lambda}[\ I + G(s)L_1\ ]\ \right|\ \} \tag{41}$$

In this fashion, the iteration will eventually extend the line segment AB in the upward direction sufficiently close to the boundary of the region of stability. Iteration can also be initiated at point A and extend the line segment BA in the downward direction towards the boundary of the region of

stability. Note that since the absolute value of an eigenvalue is greater than or equal to the minimum singular value of a given matrix, the eigenvalue method generally makes larger strides than the singular value method in claiming the region of stability. But each iteration of the singular value method claims a region inside an n-dimensional hypercube, whereas each iteration of the eigenvalue method claims a line segment along the diagonal of the hypercube obtained by the singular value method.

The eigenvalue method also needs to be initiated from points that are outside of the set $R_o \cup \widetilde{R}_o$ obtained by the singular value criterion but are still inside the regions of stability. This can be done with the aid of singular value iterations. Thus, the combined use of the two methods is most advantageous in establishing the region of stability.

Region of Stability in the Phase Space

In the MIMO system of Fig. 2, let

$$\underline{\theta}_i \triangleq (\theta_{i1}, \theta_{i2}, \cdots, \theta_{in}) \tag{42}$$

$$e^{j\underline{\theta}_i} \triangleq (e^{j\theta_{i1}}, e^{j\theta_{i2}}, \cdots, e^{j\theta_{in}}) \tag{43}$$

$$L_i \triangleq \text{diag}[e^{j\underline{\theta}_i}] \tag{44}$$

$$\hat{L}_i \triangleq L_{i-1}L_i = \text{diag}[e^{j\underline{\theta}_{i-1}}]\text{diag}[e^{-\theta_i}] \qquad \text{for } i \geqslant 0 \tag{45}$$

For $i < 0$, $\hat{L}_i$ and L_i are again set equal to I. Let S_o denote the set of $\underline{\theta}\{ = (\theta_1, \theta_2, \cdots, \theta_n) \}$ such that L ($= \text{diag}[e^{j\underline{\theta}}]$) satisfies (4). Thus, if $\underline{\theta}_o \in S_o$ and $L_o = \text{diag}[e^{j\underline{\theta}_o}]$), then the system of Fig. 2 for $i = 0$ is stable. It has been shown that if spectral norms are used in (4),

S_o is an open hypercube (excluding the boundary) in the phase space (Fig. 4), characterized by [1, 2, 3]

$$-2\sin^{-1}(\alpha_o/2) < \theta_j < 2\sin^{-1}(\alpha_o/2) \qquad (46)$$

for $j = 1, 2, \cdots, n$, where α_o is either $\min\limits_{s \in D_R} \underline{g}[I+G(s)]$ or 1, whichever is smaller.
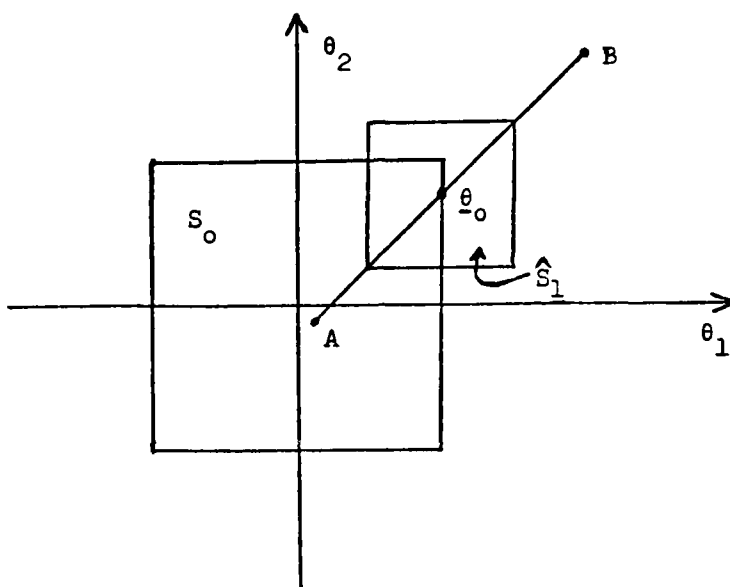
Fig. 4   Establishing the Region of Stability in the Phase Space

Now, following the same reasoning as in the derivation of the iterative procedure used in the gain space, select a point θ_o (arbitrarily) from the boundary of S_o. An open set $\hat{S}_1$ which is guaranteed by the robust stability criterion (4) to be within the region of stability can be constructed around θ_o. If spectral norms are used in (4), then $\hat{S}_1$ is characterized by

$$\theta_{oj} - 2\sin^{-1}(\alpha_1/2) < \theta_j < \theta_{oj} + 2\sin^{-1}(\alpha_1/2) \qquad (47)$$

for $j = 1, 2, \cdots, n$, where α_1 is either $\min_{s \in D_R} \underline{\sigma}[I+G(s)L_o]$ or 1, whichever

is smaller. For the ith iteration, a point $\underline{\theta}_{i-1}$ is arbitratily selected on

the boundary of $\bigcup_{j=0}^{i-1} \hat{S}_j$ (where $\hat{S}_o = S_o$). If $I+G(s)L_{i-1}$ is singular for some

$s \in D_R$, then $\underline{\theta}_{i-1}$ is a point on the boundary of the region of stability in

the phase space. Another $\underline{\theta}_{i-1}$ should be tried. Otherwise, $\hat{S}_i$ is

established as a hypercube with edges parallel to the coordinates of the

phase space, centered at $\underline{\theta}_{i-1}$, and length of each edge equal to

$4\sin^{-1}(\alpha_i/2)$, i.e.,

$$\theta_{i-1,j} - 2\sin^{-1}(\alpha_i/2) < \theta_j < \theta_{i-1,j} + 2\sin^{-1}(\alpha_i/2) \qquad (48)$$

for $j = 1, 2, \cdots, n$, where α_i is computed by (35) with (42) – (44) used

for L_{i-1}. In other words, $\hat{S}_i$ is a hypercube, whose diagonal has unity

slope, and extends from $\underline{\theta}_{i-1} - \{2\sin^{-1}(\alpha_i/2)\}\underline{e}$ to $\underline{\theta}_{i-1} + \{2\sin^{-1}(\alpha_i/2)\}\underline{e}$,

where $\underline{e} = (1, 1, \cdots, 1)$.

If the loop gains are uniformly perturbed i.e., $L(s) = \ell(s)I$ for some

scalar function $\ell(s)$ (Fig. 1), the above procedure can also be formulated

with eigenvalues. The procedure again starts on the boundary of S_o,

because for θ_o on $\tilde{S}_o$, the stability of the system of Fig. 2 for $i = 0$ is

determined by the singularity of its return-difference matrix, $I+G(s)L_o$.

The iteration procedure, warranted by Theorem 3 and Corollary 3.1, is the

same as the one described for singular values, except that α_i is replaced

by a_i, where

$$a_i = \min \left\{ 1 , \min_{s \in D_R} \left| \underline{\lambda}[I + G(s)L_{i-1}] \right| \right\} \qquad (49)$$

and $\hat{S}_i$ is no longer a hypercube, but a line segment of unity slope along a

diagonal of the hypercube obtained by the singular-value method, extending

3-119

from $\{ \underline{\theta}_{i-1} - [2\sin^{-1}(a_i/2)]\underline{e} \}$ to $\{ \underline{\theta}_{i-1} + [2\sin^{-1}(a_i/2)]\underline{e} \}$ (point A to point B in Fig. 4, for i = 1), where $\underline{e} = (1, 1, \cdots, 1)$. In other words, $\hat{S}_i$ is the set of $\underline{\theta}$ characterized by

$$\theta_j = \theta_{i-1,j} + \phi_i \qquad ; \; j = 1, 2, \cdots, n \qquad (50)$$

$$-2\sin^{-1}(a_i/2) < \phi_i < 2\sin^{-1}(a_i/2) \qquad (51)$$

In both the gain space (in decibel units) and the phase space, the eigenvalue method establishes regions of stability as line segments of unity slope. Hence they give discrete representations of the regions of stability. The eigenvalue method enables the iterative procedure to make larger strides toward the boundary. The singular-value method assures that the immediate neighborhood along the line segment claimed by the eigenvalue method belongs to the region of stability. Numerically, singular value computations are considered to be more accurate than eigenvalue computations. The next section demonstrates the combined use of the two methods in establishing the regions of stability through a lateral attitude control system of a drone aircraft [2, 3] and compares the results with what has been previously obtained via brute force computations.

The same iterative procedure based on the inverse Nyquist formulation can be analogously stated. Since both the Nyquist and inverse Nyquist formulations of the robust stability criteria are sufficient conditions, the union of the stability regions established by both formulations in each step is again a valid region of stability. Thus, the two formulations complement one another and their combined use facilitates the establishment of the actual region of stability. The numerical example in the next section also demonstrated the combined use of these two formulations.

IV. Numerical Example

Consider the 8th order lateral attitude control system of a drone aircraft used in References [2] and [3]. The block diagram of the system is given in Fig. 5 and the numerical data of Fig. 5 are given in Table 1. When computing the regions of stability in gain and phase spaces, the perturbation matrix L is first expressed as

$$L = \text{diag}(\rho_1 e^{j\theta_1}, \rho_2 e^{j\theta_2}) \tag{52}$$
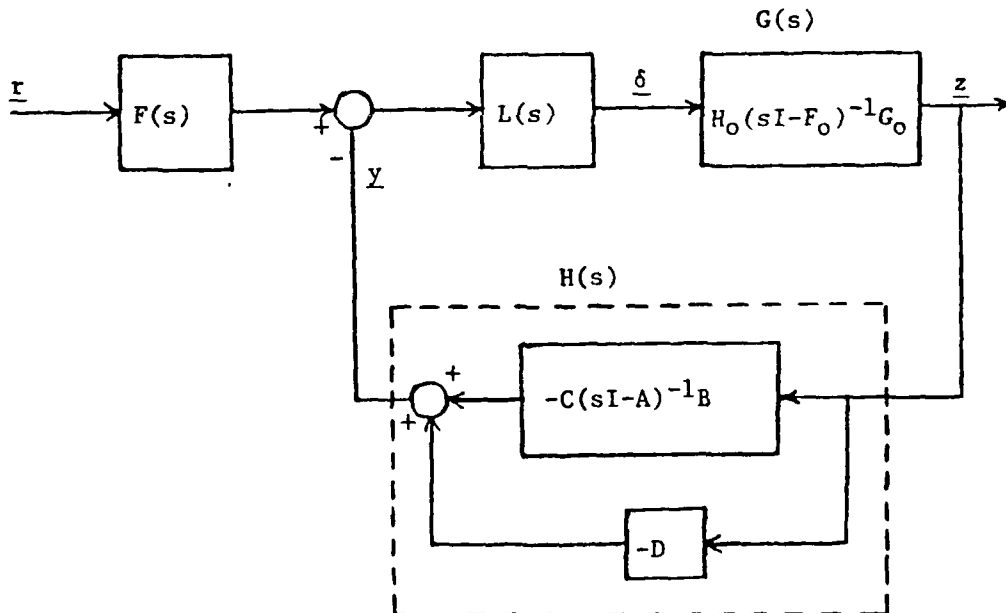
Fig. 5 Lateral Attitude Control System of a Drone Aircraft

Region of Stability in the Gain Space

Computation of the region of stability in the gain space is started by setting $\theta_1 = \theta_2 = 0$. Independent gain margins for the perturbed system may be calculated using

$$-20\log(1 + \alpha_o) < \rho_j \text{ (dB)} < 20\log[1/(1 - \alpha_o)] \quad ; \quad j = 1,2 \quad (53)$$

and

$$-20\log(1 + \alpha_o{}') < \rho_j \text{ (dB)} < 20\log[1/(1 - \alpha_o{}')] \quad ; \quad j = 1,2 \quad (54)$$

where

$$\alpha_o = \min_\omega \underline{\sigma}[I + H(j\omega)G(j\omega)L] \quad (55)$$

$$\alpha_o{}' = \min_\omega \underline{\sigma}\{ I + [H(j\omega)G(j\omega)L]^{-1} \} \quad (56)$$

Since (53) and (54) are sufficient conditions for stability, the union of the two inequalities is also a valid region of stability. This property will be used throughout this example.
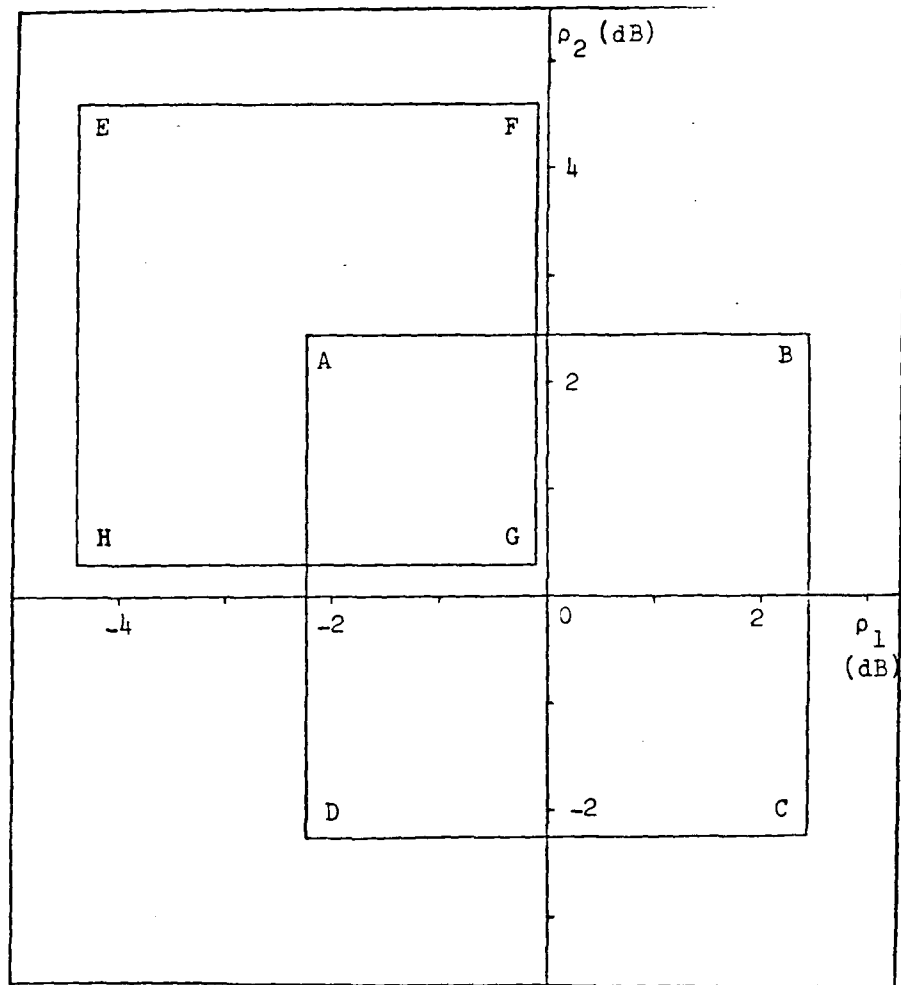
Fig. 6 Gain-Plane Region of Stability -- Initial Stage 1 Calculations

The union of (53) and (54) form a square in the gain space, which is a part of the actual region of stability. The initial region of stability with L = I is shown as ABCD in Fig. 6. For the next iteration, chose L to have the loop gains of point A in Fig. 6, and calculate (55) and (56) again for this L. If $\alpha_o \neq 0$ or $\alpha_o' \neq 0$, the system perturbed by this L is stable (otherwise A is already on the boundary of the actual region of stability). Point A may now be used as a new nominal operating point and (53) - (54) are computed again using the new α_o and α_o' to obtain square EFGH. Successively using the upper-left corner of each square as a new nominal operating point, as well as starting at point C and continuing with the lower-right corners, forms the progression of squares shown in Fig. 7.

These calculations are refered to as stage 1. As the squares approach the actual boundary of the region of stability, the right-hand sides of (55) and (56) become smaller and smaller, and so do the squares. It is not practical to expect $\underline{\sigma}$ to equal exactly zero (due to computational difficulties to be mentioned later), therefore the iterations are stopped either when $\underline{\sigma}$ becomes extremely small or when $\underline{\sigma}$ starts to increase from one iteration to the next. The latter indicates that the boundary has been crossed due to numerical errors in computing α_o and α_o'. This will also be explained later in this section.
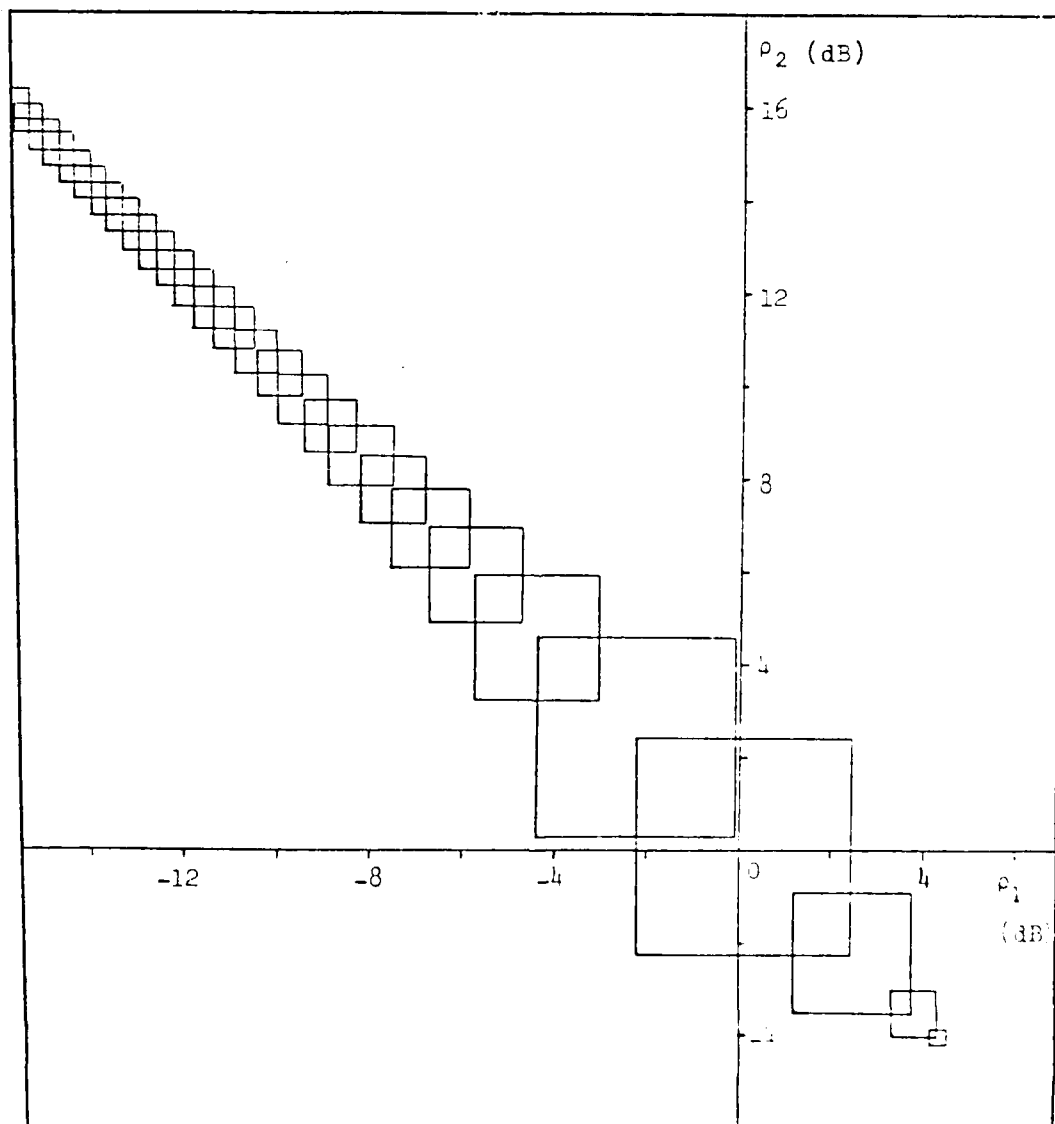
Fig. 7 Gain-Plane Region of Stability -- Stage 1 Calculations Completed

The union of all the squares in Fig. 7 is further expanded in the next stage of the gain space computations, where uniform gain margins are used. The uniform gain margin is obtained by combining (53) and (54), with α_o and $\alpha_o{'}$ replaced by a_o and $a_o{'}$, respectively, where

$$a_o = \min_{\omega} \left| \underline{\lambda}[\ I + H(j\omega)G(j\omega)L \ ] \right| \tag{57}$$

$$a_o{'} = \min_{\omega} \left| \underline{\lambda}\{ \ I + [\ H(j\omega)G(j\omega)L \ ]^{-1} \ \} \right| \tag{58}$$

For a system at the nominal operating point B (Fig. 8), L is chosen to have the gains at B. The upper limit of the uniform gain margin gives the line segment BJ of Fig. 8 as part of the region of stability. In the next iteration, the elements of L are taken from point J and the line segment JK is established as part of the region of stability. This procedure is repeated until the boundary is reached, which is determined the same way as in the singular value computations.
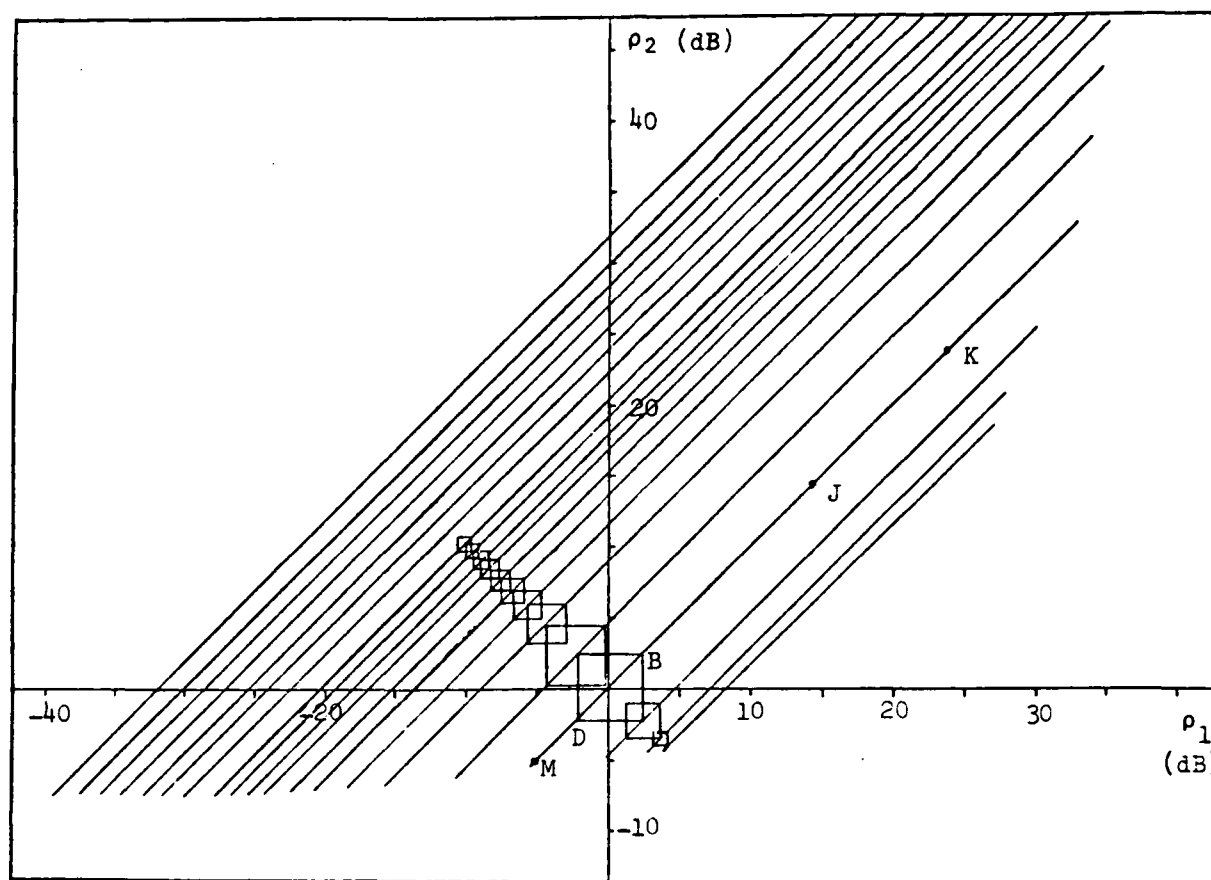
Fig. 8   Gain-Plane Region of Stability -- Combined Stage 1 & 2 Calculations

Next, point D is used as the nominal operating point, and the lower limit of the uniform gain margin is used to produce line segment DM. The upper limit of the margin does not extend the linear region beyond point J, and therefore is unnecessary. The same is true for the lower limit of the margin at point J (i.e., it does not extend beyond point M). The segment DM is then successively extended to the stability boundary. This "up" and "down" procedure is then used on each of the upper-right and lower-left corners of the remaining singular value squares. This completes stage two.

Realize that the union of the squares and 45° lines at the end of stage two is a valid subset of the region of stability. If this union yields a

complete picture of the entire region, the computations are complete. If, however, the range of the 45° lines is too small to yield a continuous boundary of the region of stability, this range may be extended by choosing stable points on the outermost lines and using stages one and two to probe further into the region. This is referred to as stage three. Stage four obtains finer detail at the boundary in a chosen area, if desired. Here, points on the singular value squares (other than the corners) may be used to generate more 45° lines, and stage two used to find the boundary points along these lines.

All of the points on the boundary found through stage two calculations (including those in stages three and four) may then be connected to form a smooth curve. This curve should be drawn conservatively, that is, do not allow the curve to exceed any of the boundary points. This curve then represents the actual region of stability, and is shown in Fig. 9 for this example. The squares and line segments are omitted from the figure for clarity.
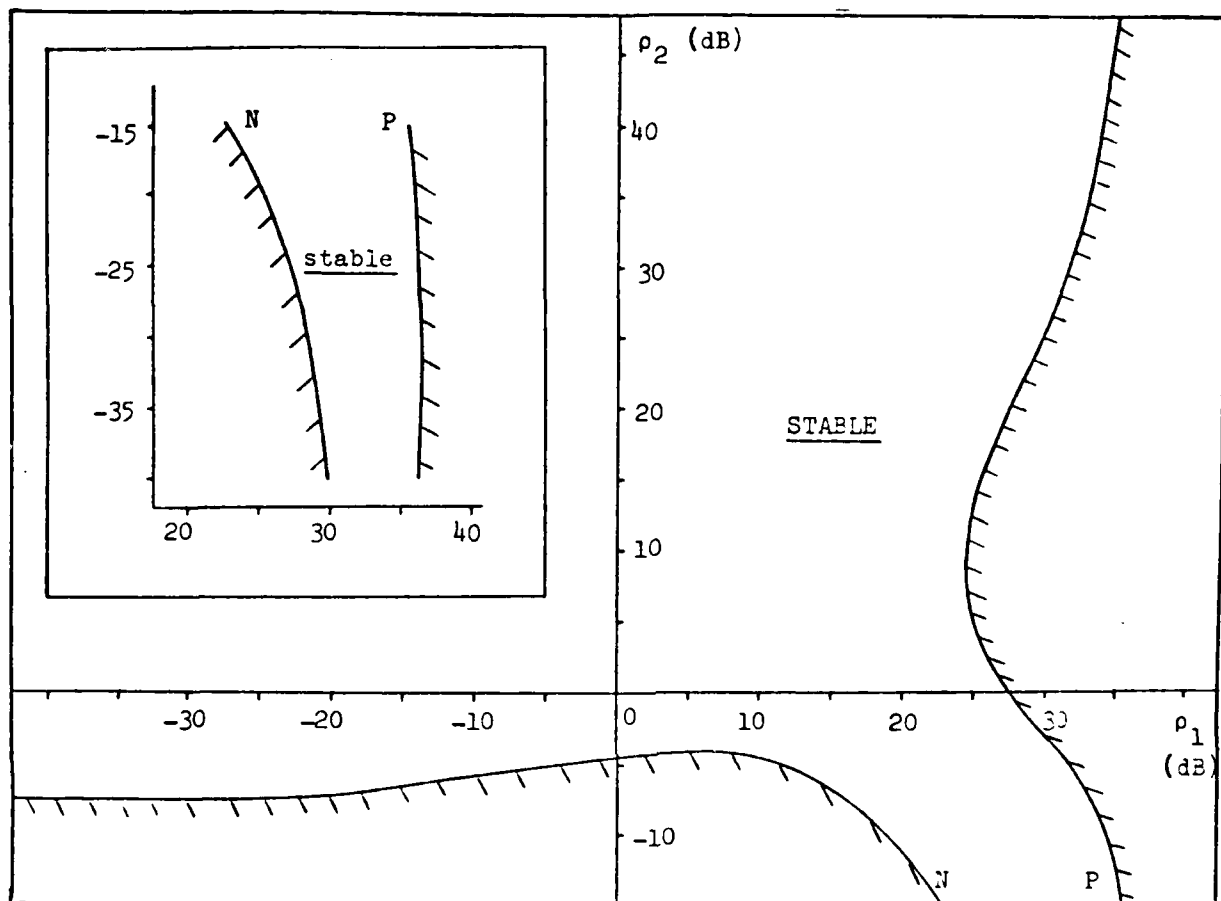
Fig. 9 Gain-Plane Region of Stability -- Completed

Region of Stability in the Phase Space

Calculation of the actual region of stability in the phase space is carried out through the same four-stage procedure as in the gain space. There are, however, some subtle differences which will be elaborated upon. The perturbation matrix L is characterized first by equation (52), except that here $\rho_1 = \rho_2 = 1$ and θ_1 and θ_2 vary. Equations (53) and (54) are replaced by

$$-2\sin^{-1}(\alpha_o/2) < \theta_j \text{ (deg)} < 2\sin^{-1}(\alpha_o/2) \quad ; \quad j = 1,2 \qquad (59)$$

3-128

$$-2\sin^{-1}(\alpha_o{}'/2) \quad < \quad \theta_j \text{ (deg)} \quad < 2\sin^{-1}(\alpha_o{}'/2) \quad ; \quad j = 1,2 \qquad (60)$$

where α_o and $\alpha_o{}'$ are still given by (55) and (56), and $L = I$ when the nominal operating point is at the origin of the phase plane. The union of these inequalities is again used, but since the margins are symmetrical, one will be completely contained within the other. Also, due to the symmetry, the squares produced by singular values will be centered about the chosen nominal operating point. In Stage 2 calculations, α_o and $\alpha_o{}'$ in (59) and (60) are replaced by a_o and $a_o{}'$, respectively, which are still given by (57) and (58). Fig. 10 shows the squares and 45° lines produced by stages one and two. Fig. 11 shows the completed region. Note that points were added through stage three and stage four calculations. The boundary here is more "uncertain" than in the gain space calculations due to the lack of a back-up test -- this will be explained in the next subsection.
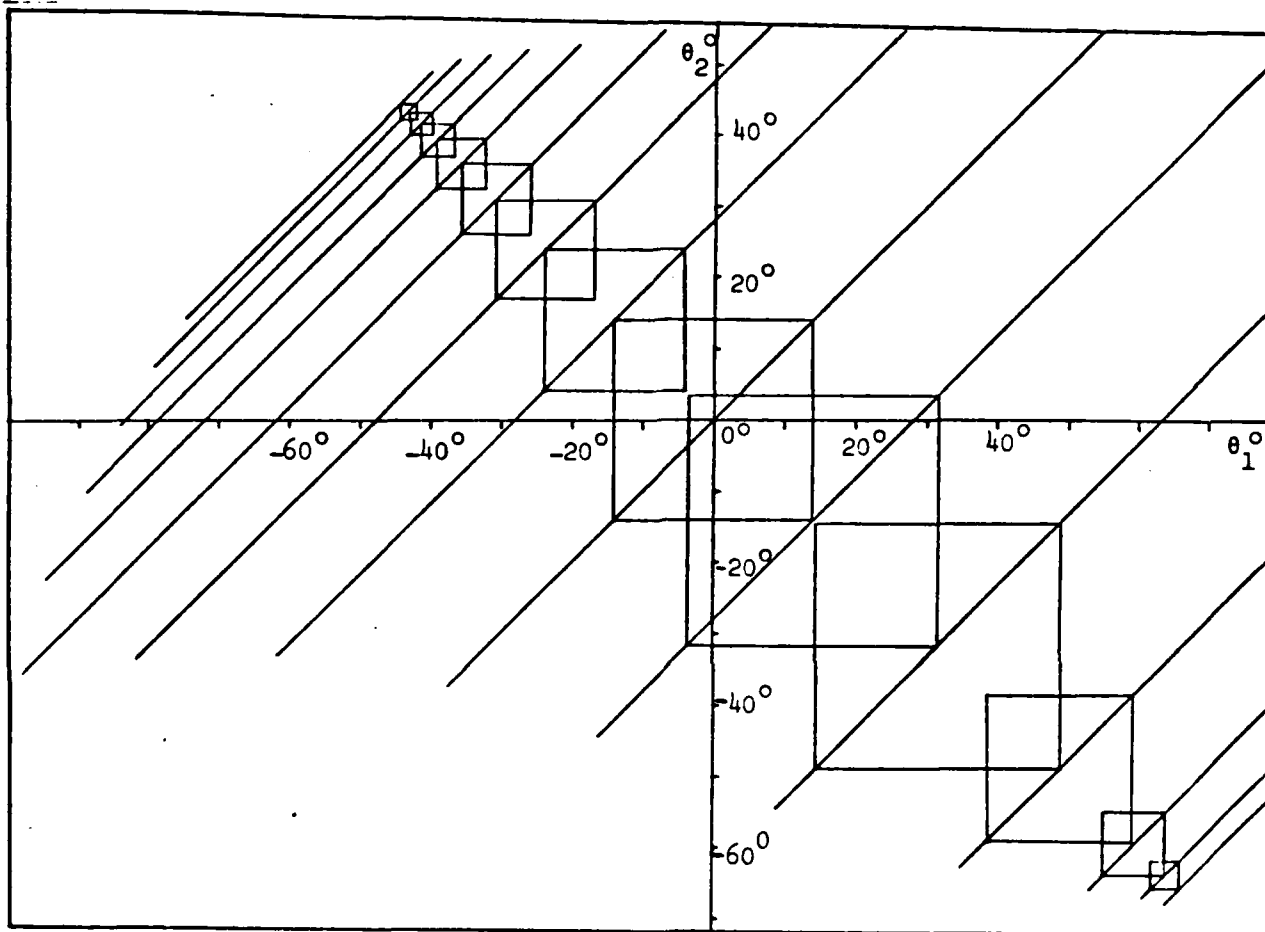
Fig. 10 Phase-Plane Region of Stability — Combined Stage 1 & 2 Calculations
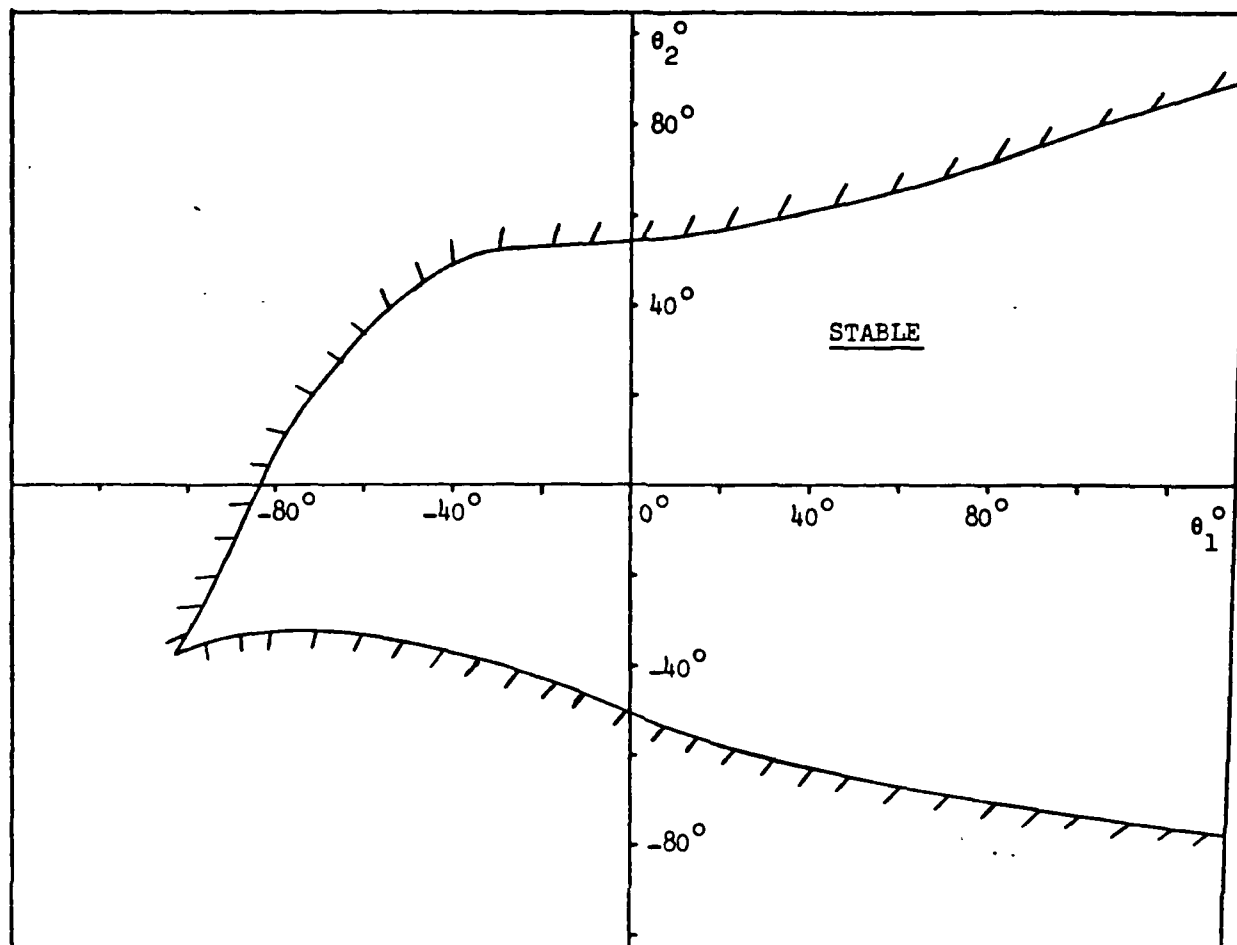
Fig. 11   Phase-Plane Region of Stability — Completed

Computational Comments

There are several computational aspects of the iterative procedure that require further discussion. First, finding the precise location of the boundaries is over-ambitious. Practically speaking, only a good approximation would ever be desired. Computationally speaking, finding the exact minimum of the singular value or eigenvalue is nearly impossible due to the fact that the minimum is found by evaluating the return and inverse return difference matrices at a finite number of frequencies. Therefore, it is probable that the calculated minimum will only be close to the actual. Unfortunately, this error will yield a value slightly larger than

the true minimum, yielding a larger than true margin. This is critical near the boundary, since once the boundary is crossed, the minimum will begin to increase and move the following iterations further into the unstable region.

This is not a disasterous result, however. If enough frequency samples are taken (fifty points-per-decade seems to work well), the calculated minimum will be very close to the actual. Also, there are ways to determine when the boundary has been crossed. In the phase space, if the minimum singular value becomes smaller and smaller in progressive iterations, then begins to increase, the first-increase results and the one previous to it should be discarded to insure stability. In the gain space, there is an even better solution, although the previous one will also work. This solution is simply to check the closed-loop eigenvalues (to see if they are all in the open left-half plane) at the loop gains in question. This will not work in the phase space, since the transfer function of the perturbation matrix in the s-domain is not known, and therefore closed-loop eigenvalues cannot be computed.

The fact that closed-loop eigenvalues may be checked allows higher accuracy in determining the actual region of stability in the gain space. The "kink" in the phase space region (Fig. 11) may actually be a "tube" as found in the gain space (Fig. 9). This is of little consequence from a practical point of view, however, since the knowledge of the region to that precision would not alter the analyst's conclusions as to the merits or deficiencies of the designed system.

It may be worth noting that singular values alone may be used to determine the entire region, while eigenvalues alone are insufficient. Singular values could be used in the stage two (and four) computations, but in many cases this would require a great many more

iterations to reach the boundary. This is due to the fact that the singular value computations are more conservative than eigenvalues, as shown in [3]. Eigenvalues cannot be used in stage one (or three), however, as they produce only lines with a positive unity slope. They do not allow movement along lines with negative slope, and therefore eigenvalue computations alone would only yield the boundary points along a line of unity slope passing through the origin (nominal system operating point).

V. Conclusions

The extension of the norm-bounded robust stability criteria from strict inequalities specifying open sets to inequalities specifying closed sets forms the theoretical basis of an iterative procedure for searching the regions of stability for *simultaneous gain or phase variations* in multivariable feedback systems. The iterative procedure is initiated in the interior of the region of stability and terminates when the boundary is reached. Algorithms can be written so that complete regions of stability in the gain and phase spaces of a multi-input multi-output feedback system can be determined. These algorithms are useful where information about the boundaries of the regions of stability in the gain and phase spaces is desired.

Appendix A

Proof of (4) as a sufficient condition for stability
of the system of Fig. 1

This proof is facilitated by the following lemma:

Lemma 1. Let $L(s)$ be a square matrix, and

$$P_\delta(s) = (1 - \delta)I + \delta L(s) \tag{A-1}$$

If

$$\left\| L^{-1}(s) - I \right\| < 1 \tag{A-2}$$

then, for all $\delta \in [0, 1]$,

$$\left\| P_\delta^{-1}(s) - I \right\| \leqslant \left\| L^{-1}(s) - I \right\| \tag{A-3}$$

Proof: (For notational brevity, the variable s will be suppressed from here on). Let E be defined as

$$E \triangleq L^{-1} - I \tag{A-4}$$

It is seen from (A-1) and (A-4) that

$$P_\delta L^{-1} = L^{-1} P_\delta = I + (1 - \delta)E \tag{A-5}$$

Since $\|E\| < 1$, $\|(1-\delta)E\| < 1$. Therefore $[I + (1-\delta)E]^{-1}$ exists as a bounded linear operator and [9]

3-134

$$[\; I + (\; 1 - \delta \;)E \;]^{-1} = \sum_{n=0}^{\infty} \; (\delta - 1)^{n} E^{n} \tag{A-6}$$

where the series on the right is convergent in the norm. Hence, by virtue of (A-5), for all $\delta \in (0, 1]$,

$$\left\| P_{\delta}^{-1} L \right\| = \left\| [\; I + (\; 1 - \delta \;)E \;]^{-1} \right\| \leqslant \sum_{n=0}^{\infty} \; (\; 1 - \delta \;)^{n} \left\| E \right\|^{n}$$

$$= \frac{1}{1 - (\; 1 - \delta \;) \left\| E \right\|} \leqslant \frac{1}{1 - (\; 1 - \delta \;)} \leqslant \frac{1}{\delta} \tag{A-7}$$

where it is assumed that the matrix norm is subordinate to some vector norm so that $\left\| I \right\| = 1$. Now, by virtue of (A-1),

$$P_{\delta}^{-1}[\; I + \delta \; (\; L - I \;) \;] = I \tag{A-8}$$

Hence

$$P_{\delta}^{-1} - I = \delta P_{\delta}^{-1}(\; I - L \;) = \delta P_{\delta}^{-1} LE \tag{A-9}$$

Therefore, by virtue of (A-7) and (A-9),

$$\left\| P_{\delta}^{-1} - I \right\| \leqslant \delta \left\| P_{\delta}^{-1} L \right\| \cdot \left\| E \right\| \leqslant \left\| E \right\| \tag{A-10}$$

The fact that (A-3) holds for $\delta = 0$ is obvious. This completes the proof of Lemma 1.

Proof of (4) as a sufficient condition for stability:

It has been shown in [1] that under the preliminary conditions stated for (4), the system of Fig. 1 is stable if

$$\det(\, I + GP_\delta \,) \neq 0 \; ; \quad s \in D_R \;, \delta \in [0, 1] \tag{A-11}$$

where P_δ is defined in (A-1). Now, for square matrices G and L,

$$I + GP_\delta = [\, (P_\delta^{-1} - I)(I + G)^{-1} + I \,](I + G)P_\delta \tag{A-12}$$

In view of Lemma 1, if condition (4) holds for $\alpha \leqslant 1$, then, for all $\delta \in [0, 1]$ and $s \in D_R$,

$$\left\| (P_\delta^{-1} - I)(I + G)^{-1} \right\| \leqslant \left\| P_\delta^{-1} - I \right\| \cdot \left\| (I + G)^{-1} \right\|$$

$$\leqslant \left\| L^{-1} - I \right\| \cdot \left\| (I + G)^{-1} \right\| < 1 \tag{A-13}$$

Since $(I + G)$ and L are already assumed to be nonsingular, (A-13) guarantees (A-11). This proves condition (4).

Appendix B

Proof of Theorem 1:

For square matrices G and L,

$$I + GP_\delta = I + (1 - \delta)G + \delta GL = (I + G)[\, I + \delta (I + G^{-1})^{-1}(L - I) \,] \tag{B-1}$$

The invertibility of $I + GP_\delta$ for all $\delta \in [0, 1]$ and $s \in D_R$ is guaranteed by

$$\left\| (\, I + G^{-1} \,)^{-1} \right\| \cdot \left\| L - I \right\| < 1 \quad ; \quad s \in D_R \tag{B-2}$$

This proves (3) as a sufficient condition for robust stability. This proof is a trivial generalization of the proof of (1) (see [5]). Now for $\delta \in [0, 1)$ and $s \in D_R$, the invertibility of $I+GP_\delta$ is guaranteed by

$$\left\| (I + G^{-1})^{-1} \right\| \cdot \left\| L - I \right\| \leqslant 1 \quad ; \quad s \in D_R \qquad \text{(B-3)}$$

due to the δ in the right-hand side of (B-1). At $\delta = 1$, $(I + GP_\delta) = (I + GL)$, whose invertibility is given in the assumption. This proves Theorem 1.

Appendix C

Proof of Theorem 2:

Theorem 2 can be proved by modifying a proof shown in Lehtomaki, et al [1]. First, it can be shown by using the norm definition that $\overline{\sigma}(P_\delta^{-1} - I) < \alpha$ if and only if

$$\alpha^2 P_\delta^H P_\delta - (P_\delta - I)^H (P_\delta - I) > 0 \qquad \text{(C-1)}$$

where the superscript H denotes Hermitian transpose, "> 0" denotes positive definiteness, and P_δ is given in (A-1). The variable s has been suppressed again for brevity. Expanding the left-hand side of (C-1) gives

$$\alpha^2 P_\delta^H P_\delta - (P_\delta - I)^H (P_\delta - I)$$

$$= \delta^2 [\alpha^2 L^H L - (L - I)^H (L - I)] + \alpha^2 (1 - \delta)[(1 - \delta)I + \delta (L + L^H)] \quad \text{(C-2)}$$

Now, $\overline{\sigma}(L^{-1} - I) \leqslant \alpha \leqslant 1$ is equivalent to

$$L^H + L \geqslant I + (1 - \alpha^2)L^H L \qquad (C-3)$$

The right-hand side of (C-3) is positive definite, therefore $(L^H + L)$ is positive definite, which makes the second term on the right-hand side of (C-2) positive definite for all $\delta \in [0, 1)$. Therefore, $\overline{\sigma}(L^{-1}-I) \leqslant \alpha$ guarantees that $\overline{\sigma}(P_\delta^{-1} - I) < \alpha$ for all $\delta \in [0, 1)$. This fact and condition (10) lead to

$$\overline{\sigma}[(P_\delta^{-1} - I)(I + G)^{-1}] \leqslant \frac{\overline{\sigma}(P_\delta^{-1} - I)}{\underline{\sigma}(I + G)} < \frac{\alpha}{\underline{\sigma}(I + G)} \leqslant 1 \qquad (C-4)$$

(A-12) and (C-4) guarantee that

$$\det(I + GP_\delta) \neq 0 \quad ; \quad s \in D_R \quad , \quad \delta \in [0, 1) \qquad (C-5)$$

Note that (C-5) is different from (A-11) in the interval of δ. However, for $\delta = 1$, $P_\delta = L(s)$. The nonsingularity of $I+G(s)P_\delta(s)$ is guaranteed by (16). This proves Theorem 2.

Appendix D

Proof of Theorem 3:

We shall show that if the matrix norm is subordinate to some vector norm, then for $L = \text{diag}[\ell_1, \ell_2, \cdots, \ell_n]$,

$$\|L\| = \max_i | \ell_i | \qquad (D-1)$$

There is no loss of generality in assuming that $\left|\ell_i\right| \geqslant \left|\ell_{i+1}\right|$, for $i = 1, 2, \cdots, n-1$. Let $\underline{x} = (1, 0, 0, \cdots, 0)$. Then

$$\left\|L\underline{x}\right\| = \left\|\left|\ell_1\right|\underline{x}\right\| = \left|\ell_1\right| \cdot \left\|\underline{x}\right\| \leqslant \left\|L\right\| \cdot \left\|\underline{x}\right\| \tag{D-2}$$

Therefore

$$\left|\ell_1\right| \leqslant \left\|L\right\| \tag{D-3}$$

Since the matrix norm is subordinate to some vector norm there exists a vector $\underline{y}$ satisfying

$$\left\|L\underline{y}\right\| = \left\|L\right\| \cdot \left\|\underline{y}\right\| \tag{D-4}$$

But

$$\left\|L\underline{y}\right\| = \left\|(\ell_1 y_1, \ell_2 y_2, \cdots, \ell_n y_n)\right\|$$

$$= \left|\ell_1\right| \cdot \left\|(y_1, \ell_2 y_2/\ell_1, \cdots, \ell_n y_n/\ell_1)\right\| \tag{D-5}$$

Let K signify a convex body that is symmetrical with respect to all axes and centered at the origin of the complex space C^n. Since $\left|\ell_i/\ell_1\right| \leqslant 1$ for $i = 2, 3, \cdots, n$, if such a convex body K contains $\underline{y}$, it must also contain $(y_1, \ell_2 y_2/\ell_1, \cdots, \ell_n y_n/\ell_1)$. Therefore [10]

$$\left\|\underline{y}\right\| \geqslant \left\|(y_1, \ell_2 y_2/\ell_1, \cdots, \ell_n y_n/\ell_1)\right\| \tag{D-6}$$

3-139

In view of (D-4), (D-5) and (D-6) we see

$$\left\| L \right\| \leqslant \left| \ell_1 \right| \tag{D-7}$$

Combining (D-3) and (D-7) establishes (D-1). Now let E be defined by (A-4), and P_δ by (A-1). Since L(s) is diagonal, E(s) is also diagonal. Let the iith element of E(s) be $e_i(s)$. Invoking (A-5), (A-9) and (D-1) gives, for $\delta \epsilon(0, 1)$

$$\left\| P_\delta^{-1} - I \right\| = \left\| \delta P_\delta^{-1} L E \right\| = \left\| \delta [I + (1 - \delta)E]^{-1} E \right\|$$

$$= \max_i \left| \frac{\delta e_i}{1 + (1 - \delta)e_i} \right| = \max_i \left| \frac{e_i}{\beta + (\beta - 1)e_i} \right| \tag{D-8}$$

where $\beta = 1/\delta$. However, since $\left| e_i \right| = \left| \{1/\ell_i(s)\}-1 \right| \leqslant 1$ and $1/\ell_i(s) \neq 0$ for all i, we have $e_i(s) \neq -1$, and therefore

$$\left| \beta + (\beta - 1)e_i \right| > 1 \tag{D-9}$$

for all i. Therefore, for all $\delta \epsilon(0, 1)$

$$\left\| P_\delta^{-1} - I \right\| < \max \left| e_i \right| = \left\| E \right\| \leqslant \alpha \leqslant 1 \tag{D-10}$$

It is obvious that (D-10) holds for $\delta = 0$. Therefore,

$$\left\| (P_\delta^{-1} - I)(I + G)^{-1} \right\| \leqslant \left\| P_\delta^{-1} - I \right\| \cdot \left\| (I + G)^{-1} \right\|$$

$$< \left\| L^{-1} - I \right\| \cdot \left\| (I + G)^{-1} \right\| \leqslant 1 \tag{D-11}$$

for $\delta \in [0, 1)$. Note that the last two inequalities in (D-11) are different from those of (A-13), and the intervals of δ are also different. Now (D-11) again guarantees (C-5). Since at $\delta = 1$, $(I + GP_\delta) = (I + GL)$, whose nonsingularity is given in the assumption, the system of Fig. 1 is stable. This proves Theorem 3.

References

[1] N. A. Lehtomaki, N. R. Sandall, Jr., and M. Athans, "Robustness Results in Linear-Quadratic-Gaussian Based Multivariable Control Designs", IEEE Trans Automat Contr, Vol AC-26, No. 1, pp 75-92, Feb 1981.

[2] V. Mukhopadyay, and J. R. Newsom, "Application of Matrix Singular Value Properties for Evaluating Gain and Phase Margins of Multiloop Systems", AIAA Guidance and Control Conference, 9-11 Aug 1982, San Diego CA, pp 420-428.

[3] H. H. Yeh, D. B. Ridgely, and S. S. Banda, "Nonconservative Evaluation of Uniform Stability Margins of Multivariable Feedback Systems", 1984 AIAA Guidance and Conference, Aug 20-22, Seattle WA.

[4] A. G. J. MacFarlane and I. Postlewaite, "The Generalized Nyquist Stability Criterion and Multivariable Root Loci", Int. J. Control, 1977, Vol 25, No. 1, pp 81-127.

[5] J. C. Doyle, "Robustness of Multiloop Linear Feedback Systems", 17th IEEE Control and Decision Conference, Jan 1979, San Diego CA, pp 12-18.

[6] N. A. Lehtomaki, D. Castonon, B. Levy, G. Stein, N. R. Sandell, and M. Athans, "Robustness Tests Utilizing the Structure of Modelling Error", 20th IEEE Control and Decision Conference, Dec 1981, pp 1173-1190.

[7] M. F. Barrett, "Conservatism with Robustness Tests for Linear Feedback Control Systems", 19th IEEE Control and Decision Conference, Dec 1980, pp 885-890.

[8] H. H. Yeh, S. S. Banda, and D. B. Ridgely, "Stability Robustness Measures Utilizing Structural Information", American Control Conference, 6-8 Jun 1984, San Diego CA.

[9] E. Kreyzig, "Introductory Functional Analysis with Applications", (7.3) John Wiley & Sons, 1978.

[10] A. S. Householder, "The Approximate Solution of Matrix Problems", J. of the Assoc for Computing Machinery, Vol 5, pp 205-243, 1958.

$$A = \begin{bmatrix} 0 & 0 \\ 0 & -2 \end{bmatrix} \quad B = \begin{bmatrix} 1 & 0 \\ 0 & 1 \end{bmatrix} \quad C = \begin{bmatrix} 0.1491 & 0 \\ 0 & -4.116 \end{bmatrix} \quad D = \begin{bmatrix} 0 & 0 \\ 0 & 2.058 \end{bmatrix}$$

$$F(s) = \begin{bmatrix} 1 & 0 \\ 0 & 0.1491/s \end{bmatrix}$$

$$F_o = \begin{bmatrix} -0.0827 & -0.1423 \times 10^{-3} & -0.9994 & 0.0414 & 0 & 0.1862 \\ -46.86 & -2.757 & 0.3896 & 0 & -124.3 & 128.6 \\ -0.4248 & -0.06224 & -0.0671 & 0 & -8.792 & -20.46 \\ 0 & 1 & 0 & 0 & 0 & 0 \\ 0 & 0 & 0 & 0 & -20. & 0 \\ 0 & 0 & 0 & 0 & 0 & -20. \end{bmatrix}$$

$$\lambda(F_o) = \begin{bmatrix} -0.03701 & \text{spiral mode} \\ 0.1889 \pm j1.051 & \text{dutch roll} \\ -3.25 & \text{roll convergence} \\ -20.0 & \text{elevon actuator} \\ -20.0 & \text{rudder actuator} \end{bmatrix}$$

$$G_o = \begin{bmatrix} 0 & 0 \\ 0 & 0 \\ 0 & 0 \\ 0 & 0 \\ 1 & 0 \\ 0 & 1 \end{bmatrix} \quad H_o = \begin{bmatrix} 0 & 1 & 0 & 0 & 0 & 0 \\ 0 & 0.07 & 1 & 0 & 0 & 0 \end{bmatrix}$$

Table 1   Numerical Data for the System of Fig. 5

APPENDIX 3C

(This paper was published in the Journal of Guidance, Control and Dynamics,
Volume 8, Number 4, July-August 1985, pages 520-525.)

Time Domain Stability Robustness Measures for Linear Regulators

Rama Krishna Yedavalli*

Asst. Professor

Dept. of Mechanical Engg.

Stevens Inst. of Technology

Hoboken, N.J. 07030

Siva S. Banda and Lt. D. Brett Ridgely

Flight Dynamics Laboratory

Wright Patterson Air Force Base

Ohio, 45433

Abstract

In this paper, the aspect of 'Stability Robustness' of linear systems is analyzed in the time domain. A bound on the perturbation of an asymptotically stable linear system is obtained to maintain stability using Liapunov matrix equation solution. The resulting bound is shown to be an improved upper bound over the ones recently reported in the literature. The proposed methodology is then extended to Linear Quadratic (LQ) and Linear Quadratic Gaussian (LQG) Regulators. Examples given include comparison with an aircraft control problem previously analyzed.

*Member AIAA

Nomenclature

R^{α} = Real vector space of dimension α

δ = Dirac delta

ϵ = Belongs to

$\rho[\cdot]$ = Spectral radius of the matrix [ ] =

The largest of the modulus of the eigenvalues of [ ]

$\sigma[\cdot]$ = Singular values of the matrix [ ]

$\lambda[\cdot]$ = Eigenvalues of the matrix [ ]

$[\cdot]_s$ = Symmetric part of a matrix [ ]

$|[\cdot]|$ = Modulus matrix = Matrix with modulus entries

$\forall i$ = For all i

$||[\cdot]||$ = Euclidean norm of a matrix $[\cdot]$

$||[\cdot]||_s$ = Spectral norm of a matrix $[\cdot] = \sigma_{max}[\cdot]$

3-145

Introduction

In the present day applications of control systems theory and practice, one of the fundamental challenges a control designer is faced with is to account for and accommodate the inaccuracies in the mathematical models of physical systems used for control design. It is the inevitable presence of these errors in the model used for design that eventually limits the attainable performance of the control system designs produced by either classical (frequency domain) or modern (time domain) control theory. Thus, it is clear that 'robustness is an extremely desirable (sometimes, necessary) feature of any proposed feedback control design, especially for large scale linear regulators.

For our present purposes, a 'robust' control design is that design which behaves in an 'acceptable' fashion (i.e. satisfactorily meets the system specifications) even in the presence of modeling errors. Since the system specifications could be either in terms of stability and/or performance (regulation, time response, etc.), we can conceive two types of robustness, namely 'Stability Robustness' and 'Performance Robustness'. Limiting our attention in this research to 'parameter errors' as the type of modeling errors that may cause instability or performance degradation in the system, we formally define 'stability robustness' and 'performance robustness' as follows:

'Stability Robustness': Maintaining closed-loop system stability in the presence of modeling errors, mainly parameter variations.

'Performance Robustness': Maintaining a satisfactory level of performance in the presence of modeling errors, mainly parameter variations.

This paper addresses the aspect of 'Stability-Robustness' in multivariable LQG regulators. Even though the aspect of 'Performance Robustness' (or 'regulation robustness', to be more precise for the case of regulators) is equally important, it is known that 'Performance Robustness' studies assume or require stability to start with. This paper, therefore, concentrates on

the stability robustness aspect. The recent published literature on this 'Stability Robustness' analysis can be viewed from two perspectives, namely i) frequency domain analysis and ii) time domain analysis. The analysis in _frequency domain_ is carried out using the singular value decomposition [1-4], where the nonsingularity of a matrix is the criterion in developing the robustness conditions. Barrett [4] presents a useful summary and compariosn of the different robustness tests are available with respect to their conservatism. Bounds are obtained by Kantor and Andres [5] in frequency domain using eigenvalue and M matrix analysis. On the other hand, the _time domain_ stability robustness analysis is presented using Liapunov Stability Analysis starting from Barnett and Storey [6], Bellman [7], Desoer et al. [8] Davison [9], Ackermann [10], Franklin & Ackermann [11], Barmish et al [12], Eslami et al. [13] (in the context of robust controller design). Despite the availability of considerable anaylsys in the time domain stability conditions in the above references, _explicit_ bounds on the perturbation of a linear system to maintain stability have been reported only recently by Patel, Toda, Sridhar [14] Patel and Toda [15] and Lee [16]. In [15], bounds are given for 'highly structured perturbations' as well as for 'weakly structured perturbations' (according to the classification given by Barrett [4]), while Lee's condition [15] treats 'weakly structured perturbations'. Highly structured perturbations are those for which only a magnitude bound on individual elements of the perturbation matrix is known for given model structure. Weakly structured perturbations are those for which only a spectral norm bound for the error is known.

In this paper, the analysis is carried out in the time domain (in the lines of Patel & Toda [15]). A new mathematical result is presented [17] for the case of highly structured perturbations provides an improved upper

bound over [15]. An aircraft control example is presented which illustrates the 'optimism' of the proposed bound compared with the one provided by [15]. The analysis is then extended to the case of LQ (Linear Quadratic) and LQG (Linear Quadratic Gaussian) Regulators. The usefulness of the proposed analysis in designing 'robust' controllers is discussed.

Stability Robustness Measures in Time Domain for Linear State Space Models

In this section, we first present the recently available robustness measures of Patel et al. [15]. Then a new robustness measures is presented for structured perturbation and this measure is shown to be an improved measure in the sense that it is less conservative than the result of [15

Robustness Measures Due to Patel and Toda:

In ref. [15], Patel and Toda consider the following state space description of a dynamic system,

$$\dot{x}(t) = A \, x(t) + E \, x(t) = (A + E) \, x(t) \tag{1}$$

where x is the n dimensional state vector (R^n), A is an nxn time invariant asymptotically stable matrix and E is an nxn 'error' matrix. However, in a practical situation, one doesn't exactly know the matrix E. One may only have knowledge of the magnitude of the maximum deviation that can be expected in the entries of A. In this case (highly structured perturbation), the entries of E are such that

$$|E_{ij}| \leq \epsilon \tag{2}$$

where ϵ is the magnitude of the maximum deviation.

For this situation, it is shown in [15], that the system of (1) is stable if

$$\varepsilon < \mu_{\varepsilon P} \equiv \frac{1}{n} \frac{1}{\sigma_{max}[P]} \qquad (3a)$$

$$\text{or} \qquad || E || < \mu_P \equiv \frac{1}{\sigma_{max}[P]} \qquad (3b)$$

where P is the solution of the Lyapunov matrix equation

$$A^T P + PA + 2I_n = 0 \qquad (I_n \text{ is an nxn identity matrix}). \qquad (4)$$

Now, in what follows, we present the main mathematical result (as a new theorem [17]) which forms the basis for developing a condition for the stability of a perturbed matrix.

Main Result: Let F and E be two real matrices.

Lemma 1: If F is negative definite, then the matrix F + E is negative definite if

$$\rho\{[E_s(F_s)^{-1}]_s\} \equiv \sigma_{max}\{[E_s(F_s)^{-1}]_s\} < 1 \qquad (5)$$

Proof: Given in Appendix A.

We now apply the above result to get an upperbound for the perturbation matrix E of system (1), assuming highly structured perturbation.

Theorem 1: The system matrix A + E of (1) is stable if

$$a) \quad |E_{ij}|_{max} = \varepsilon < \frac{1}{\sigma_{max}[|P|U_n]_s} \equiv \mu_{\varepsilon\gamma} \qquad (6a)$$

where U_n is an nxn matrix whose entries are unity i.e., $U_{nij} = 1$ for all i, j=1,...n and P satisfies the Liapunov equation given by (4).

Proof: Given in Appendix B.

Example 1: We consider the same example as the one considered in Ref [15]. The nominal stable matrix is

$$A = \begin{bmatrix} -3 & -2 \\ 1 & 0 \end{bmatrix} \qquad (7)$$

Applying the analysis of [15], and this paper, the following bounds are obtained

Patel & Toda	Yedavalli	
$\mu_{\varepsilon P}$	$\mu_{\varepsilon Y}$	(8)
0.191	0.236	

Thus, the proposed robustness measure gives an improved upper bound. For many other examples considered, it was seen that in general

$$\mu_{\varepsilon Y} \geq \mu_{\varepsilon P}$$

In fact, the following theorem guarantees the same for a class of systems.

Theorem 2: The bound $\mu_{\varepsilon Y} \geq \mu_{\varepsilon P}$ if $|P| = P$ (9)

Proof: It can be seen that, for $|P| = P$

$$\sigma_{max}(|P|U_n)_s \leq \sigma_{max}(PU_n) \leq \sigma_{max}(P)\,\sigma_{max}(U_n) \leq \sigma_{max}(P)\,n \qquad (10)$$

Thus, $\dfrac{1}{\sigma_{max}(|P|U_n)_s} \geq \dfrac{1}{\sigma_{max}(P)n}$ (11)

$$\rightarrow \frac{n}{\sigma_{max}[(|P|U_n)_s]} \geq \frac{1}{\sigma_{max}[P]} \qquad (12)$$

Incidentally, in example 1, it happens that $|P| = P$. From the experience with many other examples, it is conjectured that $\mu_{\varepsilon Y}$ is always greater than or equal to $\mu_{\varepsilon P}$ with no restrictions on P, and efforts are underway to investigate the same.

3-150

Extension to Linear Regulators

We now extend the above analysis to the case of large scale linear regulators having parameter variations as the modeling error.

Let us consider a continuous linear time invariant system described by

$$\dot{x}(t) = A x(t) + B u(t) + D w(t) \quad , \quad x(0) = x_0 \tag{13a}$$

$$y(t) = C x(t) \tag{13b}$$

$$z(t) = M x(t) + v(t) \tag{13c}$$

where the state vector x is nx1, the control u is mx1, the external disturbance w is qx1, the output y (the variables we wish to control) is kx1 and the measurement vector z is ℓx1. Accordingly, the matrix A is of dimension nxn, B is nxm, D is nxq, C is kxn and M is ℓxn. The initial condition x(0) is assumed to be a zero-mean, gaussian random vector with variance X_o, i.e.

$$E[x(0)] = 0, \qquad E[x(0) \, x^T(0)] = X_o \tag{14}$$

Similarily, the process noise w(t) and the measurement noise v(t) ..re assumed to be zero-mean white noise processes with gaussian distributions having constant convariances W and V respectively, i.e.

$$E[w(t)] = E[v(t)] = 0 \tag{15}$$

$$E\begin{bmatrix} w(t) \\ \\ v(t) \end{bmatrix} [w^T(\tau) \quad v^T(\tau)] = \begin{bmatrix} W & 0 \\ & \\ 0 & \rho_e V_o \end{bmatrix} \delta(t-\tau) \tag{16}$$

where ρ_e is a scalar greater than zero and $V = \rho_e V_o$.

Let the above system be evaluated for any control u by the quadratic performance index

$$J = \lim_{t \to \infty} \frac{1}{t} E \int_0^t [(y^T(\tau) Q y (\tau) + u^T(\tau)\rho_c R_0 u(\tau)] d\tau \qquad (17)$$

where scalar $\rho_c > 0$ and Q, R_0 are (kxk) and (mxm) symmetric, positive definitive matrices, respectively.

For the case of a deterministic system, the following modifications in the system description are in order:

i) Dw = 0, v = 0

ii) the initial condition, $x(0) = x_0, x_0 x_0^T = X_0$

and the index J of (20) reads

$$J = \int_0^\infty [y^T(t) Q y (t) + u^T (t) \rho_c R_0 u(t)]dt \qquad (18)$$

If the state x(t) of the stochastic system is estimated as a function of the measurements we assume the state estimator to be of the following structure

$$\dot{\hat{x}}(t) = A \hat{x} (t) + \hat{G} \hat{z} (t) \qquad (19)$$

where

$$\hat{z}(t) = z(t) - M \hat{x}(t)$$

is called the 'measurement residual'. For a 'manimum variance' requirement, the estimator of (19) is the standard Kalman filter [18]. We refer to the system presented in this section as the 'Basic System'.

Also, the following assumptions are made with respect to the model described by equations (13).

3-152

Assumption 1: The matrix pairs $[A, B]$ and $[A, D]$ are completely controllable and the pairs $[A, C]$ and $[A, M]$ are completely observable.

Case 1: LQ Regulators:

For this case, the nominal closed loop system matrix is given by

$$A_{CL} = A + BG \tag{20a}$$

where

$$G = \frac{-1}{\rho_c} R_o^{-1} B^T K \tag{20b}$$

and

$$KA + A^T K - KB \frac{R_o^{-1}}{\rho_c} B^T K + C^T Q C = 0 \tag{20c}$$

Let ΔA, ΔB be the maximum modulus perturbations in the system matrices A&B respectively. Then the perturbed system matrix is

$$A_{CLP} = (A + \Delta A) + (B + \Delta B)G \tag{21}$$

Design Observation 1: The perturbed LQ Regulator system is stable for all perturbations in A&B (in the sense of (2)) if

$$\varepsilon \equiv \left| \Delta A + \Delta B |G| + |B + \Delta B| \cdot |\Delta G| \right|_{\tilde{v}_{max}} < \mu_{\varepsilon \gamma} \equiv \frac{1}{\sigma_{max}[(|P|U_n)_s]} \tag{22a}$$

where P satisfies

$$A_{CL}^T P + P A_{CL} = -2 I_n \tag{22b}$$

Note that $||E||$ and μ_γ are functions of the control gain G.

Case 2: LQG Regulators:

For this case the optimal control for nominal values of the parameters is given by

$$u = G \hat{x} = -\frac{1}{\rho_c} R_o^{-1} B^T K \hat{x} \tag{23a}$$

3-153

where

$$\dot{\hat{x}} = A \hat{x} + B u + \hat{G}(z - M \hat{x}), \quad \hat{x}(0) = 0 \tag{23b}$$

$$= (A + B G - \hat{G} M) \hat{x} + \hat{G} z \tag{23c}$$

$$\hat{G} = \frac{1}{\rho_e} \bar{P} M^T V_o^{-1} \tag{23d}$$

and P and K satisfy the algebraic matrix Riccati equations

$$KA + A^T K - KB \frac{R_o^{-1}}{\rho_c} B^T K + C^T Q C = 0 \tag{23e}$$

$$\bar{P} A^T + A \bar{P} - \bar{P} M^T \frac{V_o^{-1}}{\rho_e} M \bar{P} + D W D^T = 0 \tag{23f}$$

The nominal closed loop system is given by

$$\begin{bmatrix} \dot{x} \\ \dot{\hat{x}} \end{bmatrix} = \begin{bmatrix} A & BG \\ \hat{G} M & \hat{A}_c \end{bmatrix} \begin{bmatrix} x \\ \hat{x} \end{bmatrix} + \begin{bmatrix} D & 0 \\ 0 & \hat{G} \end{bmatrix} \begin{bmatrix} w \\ v \end{bmatrix} \tag{24a}$$

$$\begin{bmatrix} y \\ u \end{bmatrix} = \begin{bmatrix} C & 0 \\ 0 & G \end{bmatrix} \begin{bmatrix} x \\ \hat{x} \end{bmatrix} \tag{24b}$$

where $\hat{A}_c = A + BG - \hat{G} M$ and the closed - loop system is asymptotically

stable.

We are now interested in examining the stability robustness of the
closed-loop system in the presence of parameter variations alone.
Let ΔA, ΔB, ΔC, ΔM and ΔD be the maximum modulus perturbations in the
system matrices, A, B, C, M and D respectively. Then the perturbed system

3-154

matrix can be written as

$$A_{CLP} = \begin{bmatrix} A+\Delta A & (B+\Delta B)(G+\Delta G) \\ (\hat{G}+\Delta\hat{G})(M+\Delta M) & \hat{A}_c+\Delta\hat{A}_c \end{bmatrix}$$ (25)

<u>Design Observation 2</u>: The perturbed LQG regulator system is stable for all perturbations in $A,B,C,M,D,G\&\hat{G}$ (in the sense of (2))if

$$\varepsilon = E_{ij_{\kappa_i}} < \mu_{\varepsilon Y} \equiv \frac{1}{\sigma_{max} [(|P|U_n)_s]}$$ (26)

where

$$A_{CL} = \begin{bmatrix} A & BG \\ \hat{G}M & \hat{A}_c \end{bmatrix}$$

$$E = \begin{bmatrix} \Delta A & \Delta B|G| + |B+\Delta B)||\Delta G| \\ |\hat{G}|\Delta M + |M+\Delta M)||\Delta\hat{G}| & \Delta\hat{A}_c \end{bmatrix}$$ (27)

and P satisfies equation (22b) with I_{2n} as a forcing function.

Discussion of the Design Observations:

Some discussion about the implications of these design observations is now in order. First, it may be noted that the proposed stability conditions are similar, conceptually, to the frequency domain results reported in Ref. [1]. However, there are also some interesting differences between these two (frequency domain and time domain) versions. Some preliminary observations are presented in the following sections. Secondly, these design observations are useful in many ways in both the analysis and synthesis of robust controllers. These are discussed in later sections.

a) Comparison and Contrast Between Frequency Domain Analysis and the

Time Domain Analysis

The main differences between the frequency domain treatment and the time domain treatment are as follows:

i) In the frequency domain treatment the stability robustness condition involves the calculation of singular values of a complex matrix at various frequencies. In the stability conditions of time domain, no time dependence is present. Only the   Singular   values of a real symmetric matrix are to be computed.

ii) In the case of frequency domain results, the perturbations are mainly viewed in terms of 'gain' and 'phase' changes [19]. In the proposed time domain analysis the perturbations are viewed as 'system parameter variations' with constant, fixed gains. It may be noted that in the time domain treatment the nominally stable closed-loop matrix and the perturbed closed-loop matrix are both functions of the constant controller gains.

iii) In the frequency domain treatment, considering an uncertainity, for example, as an additive perturbation,several stability robustness conditions can be written which do not imply each other for practical systems [20]. In the present time domain approach such difficulty is not present as the perturbations are modelled as additive perturbations and yield only one robustness test.

These are some of the preliminary observations made with respect to the frequency domain and time domain approaches for 'stability robustness'. Evidently further in-roads have to be made in the investigation of this relationship and this is suggested as a future-research topic. In the following section, the usefulness of the proposed design observations is briefly discussed.

b) Usefulness of the Design Observations

The proposed design observations are helpful in many ways.

· Given the perturbations ΔA, ΔB, and ΔM one may determine the controller gains to achieve stability robustness.

· This type of 'Perturbation Bound Analysis' can be used to compare different models and control design schemes from a stability robustness point of view, as well as in 'Robust Controller Design'.

·Finally these tests can find applications in spillover reduction paoblems and sensor/actuator location problems.

Application to an Aircraft Control Problem

We now consider two same application example as the one considered by Patel , Toda & Sridhar in [14]. For completeness sake, we briefly reproduce here the mathematical model of [14].

In [14], the system chosen is the flare control of the Augmentor Wing
Jet STOL Research Aircraft (AWJSRA). The purpose of the flare control is
to make a smooth transition from an initial steep flight path angle of $-7.5°$
on the glide slope at an altitude of approximately 65 ft to a final smaller
flight path angle ($-1°$) more appropriate for touchdown.

The equations for the longitudinal dynamics of the AWJSRA at an
airspeed of 110 ft/s and flight path angle of $-1°$ are given by

$$\dot{x} = A x + B u \qquad (28a)$$

where

$x = [\delta v \quad \delta \gamma \quad \delta \theta \quad \delta q \quad \delta h]^T$

$u = [\delta e \quad \delta n]^T$

δv = change in airspeed, ft/s

$\delta \gamma$ = change in flight path angle, deg

$\delta \theta$ = change in pitch angle, deg

δq = change in pitch rate, deg/s

δh = deviation from nominal altitude, ft

δe = change in elevator deflection, deg

δn = change in nozzle angle, deg

$$A = \begin{bmatrix} -0.0547 & -0.298 & -0.2639 & -0.0031 & 0.0 \\ 0.16 & -0.4712 & 0.4661 & 0.0437 & 0.0 \\ 0.0 & 0.0 & 0.0 & 1.0 & 0.0 \\ 0.1752 & 0.1236 & -0.1236 & -1.3 & 0.0 \\ -0.0174 & 1.92 & 0.0 & 0.0 & 0.0 \end{bmatrix} \qquad (28b)$$

$$B = \begin{bmatrix} -0.00315 & -0.0943 \\ 0.0408 & 0.0224 \\ 0.0 & 0.0 \\ -1.1200 & -0.08 \\ 0.0 & 0.0 \end{bmatrix} \qquad (28c)$$

The open loop poles of the system are at 0.0, $-0.0105 \pm j0.2737$,
-0.6757 and -1.129.

The Performance index considered is

$$J = \int_{0}^{\infty} (x^T Q x + u^T R u) \, dt \tag{29a}$$

with $R = \text{Diag } [16, 0.5]$ and $Q = q I_5$. $\qquad$ (29b)

Applying the analysis of [15] and this paper, the bounds μ_Y and μ_P

and their variation with q are summarized in Table 1 and Fig. 1.   Here

$$\mu_Y = n \mu_{\varepsilon Y}$$

and

$$\mu_P = n \mu_{\varepsilon P}$$

Clearly it is seen that μ_Y is greater than μ_P for the values of q

considered and the 'optimism' of μ_Y over μ_P increases as q is increased.

Conclusions

In this paper, stability robustness analysis is carried out in the time

domain, which promises to be a viable supplement and/or alternative to the

frequency domain approach, particularly for Linear State Space models.

An improved upper bound on the perturbation of an asymptotically stable

linear system is obtained which is easy to determine numerically.   Extension

to LQG regulators is discussed which offers extensive scope for further

research.   Some advantages of this time domain approach are i) tractability

of problem formulation ii) explicit consideration of model error information

and iii) computational simplicity, among others.   Further research is being

carried out on obtaining similar improved robustness measures for 'weakly

structured perturbations' and for different types of modeling errors such

as 'truncated modes' and 'nonlinearities' as well as the application of this

kind of "perturbation Bound Analysis" in designing 'robust' control systems.

q	μ_P	μ_Y
0.1	0.0055	0.0061
0.25	0.0082	0.0093
0.5	0.0107	0.0125
1.0	0.0137	0.0164
5	0.0213	0.0272
10	0.0240	0.0322
50	0.0305	0.0420
10^2	0.0323	0.0451
10^4	0.0364	0.0530

Table 1

Variation of μ_Y and μ_P with q
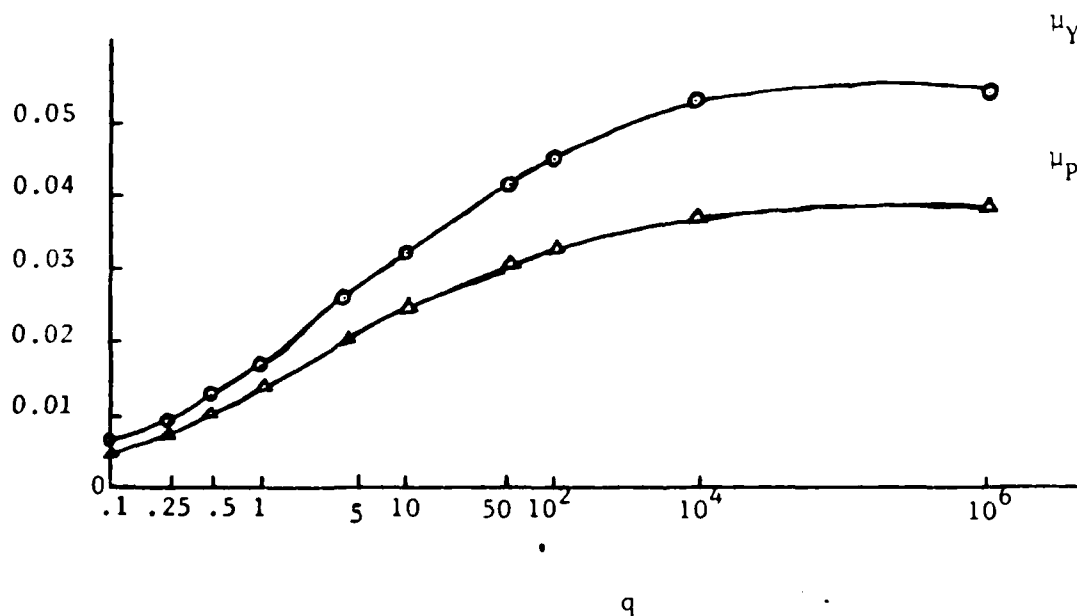
Fig. 1

Plot of μ vs q

Acknowledgement

References

1. Lehtomaki et. al. "Robustness Tests Utilizing the Structure of Modeling Error". Proceedings of Conference on Decision and Control (CDC) 1981, pp. 1173-1190.

2. Lehtomaki, N.A., Sandell, N.R. and Athans, M., "Robustness Results in Linear Quadratic Guassian Based Multivariable Control Designs", IEEE Trans. on Automatic Control, Vol. AC-26, pp. 75-92, 1981.

3. IEEE Trans. on Autom. Control, Special issue on "Linear Multivariable Control Systems", Vol. A C-26, No. 1, Feb. 1981.

4. Barrett, M.F., "Conservation with Robustness Tests for Linear Feedback Control Systems", Proc. of American Control Conference, 1982. pp. 885-890.

5. Kantor, J.C. and Andres, R.P. "Characterization of Allowable Perturbations for Robust Stability", IEEE Trans. on Autom. Control, Vol. A C-28, No 1, Jan. 1983, pp. 107-109.

6. Barnett, S. and Storey, C., "Matrix Methods in Stability Theory", Barnes & Noble, New York, 1970.

7. Bellman, R., "Stability Theory of Differential Equations", New York, Dover, 1969.

8. Desoer, C.A., Callier, F.M. and Chan, W.S., "Robustness of Stability Conditions for Linear Time Invariant Feedback Systems", IEEE Trans. on Autom. Control, Vol. A C-22, pp. 945-949, Dec. 77.

9. Davison, E.J., The Robust Control of a Servomechanism Problem for Linear Time Invariant Multivariable Systems", IEEE Trans. on Autom. Control, Vol. A C-21, pp. 25-34, 1976.

10. Ackermann, J., "Parameter Space Design of Robust Control Systems"., IEEE Trans. on Automatic Control, Vol A C-25, No 6, Dec. 1980, pp. 1058-1071.

11. Franklin, S.N. and Ackermann, J., "Robust Flight Control: A design example", Journal of Guidance, Control & Dynamics., Nov.-Dec. 1981.

12. Barmish, B.R., Petersen, I.R. and Feuer, A: "Linear Ultimate Boundedness Control of Uncertain dynamical systems", Automatica, Vol 19, No. 5, Sept. 1983, pp. 523-532.

13. Eslami, M. and Russell, D.L. "On Stability with Large Parameter Variations Stemming from the Direct Method of Lyapunov", IEEE Trans. on Automatic Control, Vol. A C-25, No. 6, Dec. 1980, pp. 1231-1234.

14. Patel, R.V.,Toda, M. and Sridhar, B., "Robustness of Linear Quadratic State Feedback Designs in the Presence of System Uncertainity", IEEE Trans. on Autom. Control, Vol. A C-22, pp. 945-949, Dec. 77.

15. Patel, R.V. and Toda, M., "Quantitative Measures of Robustness for Milti-variable Systems", Proc. of Joint Automatic Control Conference, San Francisco, 1980, TDS-A.

16. Lee, W.H., "Robustness Analysis for State Space Models", Alphatech Inc. TP-151, Sept. 1982.

17. Yedavalli, R.K., "Time Domain Robustness Analysis for Linear Regulators", Proceedings of American Control Conference, SanDiego, June 1984, pp. 975-980.

18. Kwakernaak H., and Sivan, R., "Linear Optimal Control Systems", Wiley Interscience, 1972.

19. Mukhopadhyay, V., and Newsom, J.R. "Application of Matrix Singular Value Properties for Evaluating Gain and Phase Margins of Multiloop Systems", Proceedings of the AIAA Guidance and Control Conference, 1982, pp. 420-428.

20. Banda S.S., Ridgely, D.B., and Hsi-Han Yeh., "Robustness of Reduced order Control"., Proceedings of the VPIGSU/AIAA Symposium on Dynamics of Control of Large Structures., Blacksburg., VA., June 6-8, 1983.

21. Lancaster, P., "Theory of Matrices", Academic Press, 1969.

Appendix A

<u>Proof of Lemma 1</u>:

Let $\rho[(E_s(F_s)^{-1})_s] < 1$

$\rightarrow \quad |\lambda(E_s(F_s)^{-1})_{s_{max}}| < 1$

$\rightarrow \quad |\lambda_i(E_s(F_s)^{-1})_s| < 1$

$\rightarrow \quad 1 + \lambda_i\{[E_s(F_s)^{-1}]_s\} > 0$

$\rightarrow \quad \lambda_i\{I + (E_s(F_s)^{-1})_s\} > 0$

$\rightarrow \quad \lambda_i\{[I + E_s(F_s)^{-1}]_s\} > 0$

$\rightarrow \quad [I + E_s(F_s)^{-1}]$ is positive definite

$\rightarrow \quad [I + E_s(F_s)^{-1}] [-F_s]$ has positive, real eigenvalues because 1) if

A_s and B_s are positive definite, AB_s has positive

real eigenvalues. (Ref. [21, 6])

and

2) If A_s is negative definite, $-A_s$ is positive

definite and hence $-F_s$ is positive definite

(Ref. [6]).

$\rightarrow \quad -(F_s + E_s)$ has positive, real eigenvalues
[because $[I + E_s(F_s)^{-1}] [-F_s] = -(F_s + E_s)$]

$\rightarrow \quad -(F_s + E_s)$ is positive definite (because $-(F_s + E_s)$ is symmetric too)

$\rightarrow \quad (F_s + E_s)$ is negative definite

$\rightarrow \quad (F+E)_s$ is negative definite

$\rightarrow \quad (F+E)$ is negative definite

$\rightarrow \quad (F+E)$ has negative real part eigenvalues

$\rightarrow \quad (F+E)$ is stable.

Appendix B

Proof of Theorem 1: Consider $\quad \dot{x} = (A+E) \, x(t)$ $\qquad\qquad$ (B1)

where

$|E_{ij}|_{max} = \varepsilon$ (scalar) and $\Delta \equiv \varepsilon U_n$

where U_n is an nxn matrix with

$U_{n_{ij}} = 1$ for all i, j=1,2,...n.

$\qquad$ Let $V(x) = x^T P \, x > 0$ be the Liapunov function for the system in (B1)

where P is the symmetric positive definite solution of

$\qquad A^T P + PA = -2I_n$ $\qquad\qquad$ (B2)

Then

$\qquad \dot{V}(x) = -x^T 2I_n x + x^T(E^T P + PE)x$ $\qquad\qquad$ (B3)

Now

Let $\varepsilon < \dfrac{1}{\sigma_{max}(|P| \; U_n)_s}$

$\quad \rightarrow \quad \sigma_{max}(|P|\Delta)_s < 1$

$\quad \rightarrow \quad \sigma_{max}(PE)_s < 1$

$\quad \rightarrow \quad \sigma_{max}\{-(PE)_s\} < 1$

$\quad \rightarrow \quad \sigma_{max}\{(PE)_s(-I_n)^{-1}\}_s < 1$

$\quad \rightarrow \quad \{-I_n + (PE)_s\}$ is negative definite (by virtue of Lemma 1)

$\quad \rightarrow \quad \{-2I_n + E^T P + PE\}$ is negative definite

$\quad \rightarrow \quad \dot{V}(x)$ of (B3) is < 0 for all x

$\quad \rightarrow \quad$ (A+E) of (B1) is stable.

Chapter 3 References

[3-1] M.G. Safonov, <u>Stability and Robustness of Multivariable Feedback Systems</u>, MIT Press, 1980.

[3-2] M.G. Safonov, "Tight Bounds on the Response of Multivariable Systems with Component Uncertainties", Proceedings of the Allerton Conference on Communication and Computing, Monticello, IL, Oct 4-6, 1978.

[3-3] G. Zames, "On the Input-Output Stability of Time-Varying Nonlinear Feedback Systems - Part I: Conditions Using Concepts of Loop Gain Conicity and Positivity," IEEE Trans. Autom. Contr., Vol. AC-11, pp 228-238, Apr 1966.

[3-4] G. Zames, "On the Input-Output Stability of Time Varying Nonlinear Feedback Systems - Part II: Conditions Involving Circles in the Frequency Plane and Sector Nonlinearities", IEEE Trans. Autom. Contr., Vol AC-11, pp 465-476, July 1966.

[3-5] J.C. Doyle, "Robustness of Multiloop Linear Feedback Systems," Proceedings of 1978 IEEE conference on Decision and Control, San Diego, CA, Jan 10-12, 1979.

[3-6] J.C. Doyle, "Analysis of Feedback Systems with Structured Uncertainties," IEE Proceedings, Vol 129, Pt, D, No 6, pp 242-250, 1982.

[3-7] J.C. Doyle, "Matrix Interpolation Theory and Optimal Control," Ph.D. Dissertation, University of California, Berkeley, Dec 1984.

[3-8] J.J. D'Azzo and C.H. Houpis, <u>Linear Control System Analysis and Design</u>, McGraw-Hill, 1981.

[3-9] R.K. Yedavalli, "Perturbation Bounds for Robust Stability in Linear State-Space Models", to appear in Int. J. of Control in 1985.

[3-10] R.K. Yedavalli, "Improved Measures of Stability Robustness for Linear State-Space Models", to appear in IEEE Trans Auto Control in May, 1985.

4. USING SINGULAR VALUES TO DESIGN A GOOD MULTIVARIABLE CONTROL LOOP

Now that we have seen some of the tools available to analyze a
multivariable control system, it is time to turn our attention to
synthesis. Before we can attempt to design a good controller, we must
define what constitutes a good multivariable control loop. First, since
it should be more comfortable, we will discuss the SISO control loop.
Most of this section is taken directly from Reference [4-1]. Then, with
the help of singular values and matrix theory, we will extend these
ideas to the multivariable case.

4.1 Single-Input Single-Output Control Loops

First, let's look at a generic feedback system, as shown in Fig
4.1.
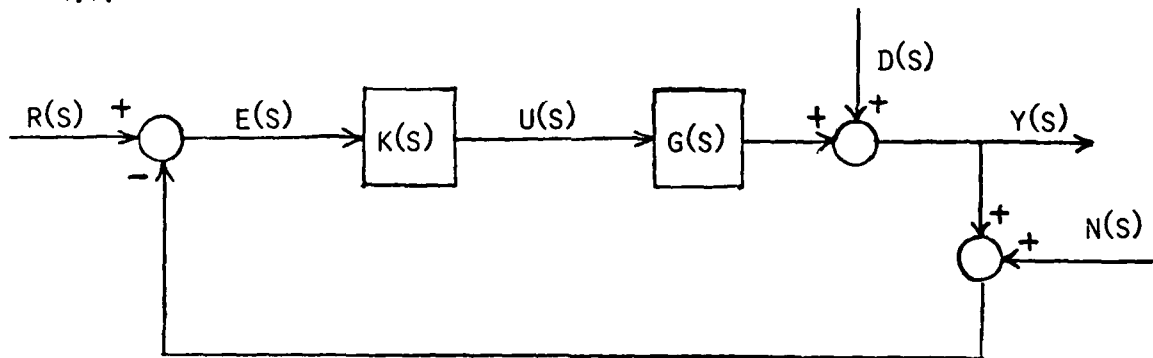
Fig 4.1 A Generic SISO Control System

where

$r(s)$ - input command reference signal

$e(s)$ - error signal

$u(s)$ - control input signal

$d(s)$ - (output) disturbance signal

$y(s)$ - output signal

$n(s)$ - sensor noise signal

g(s) - plant transfer function (given)

k(s) - compensator transfer function (to be designed)

Now we can derive some relationships between the different variables

$$y(s) = d(s) + g(s)k(s)e(s) \tag{4.1}$$

$$e(s) = r(s) - [n(s) + v(s)] \tag{4.2}$$

Plugging (4.2) into (4.1) and rearranging yields

$$y(s) = d(s) + g(s)k(s)[r(s) - n(s) - y(s)]$$

$$= d(s) + g(s)k(s)r(s) - g(s)k(s)n(s) - g(s)k(s)y(s) \tag{4.3}$$

or

$$[1 + g(s)k(s)] \, y(s) = g(s)k(s)r(s) + d(s) - g(s)k(s)n(s) \tag{4.4}$$

Dividing both sides of (4.4) by $[1 + g(s)k(s)]$ yields

$$y(s) = \frac{g(s)k(s)}{1 + g(s)k(s)} \, [r(s) - n(s)] + \frac{1}{1 + g(s)k(s)} \, d(s) \tag{4.5}$$

Equation (4.5) relates how the commands, disturbances, and sensor noise
each affect the output. To provide more common terminology,

$g(s)k(s)$ - open-loop (loop) transfer function

$1 + g(s)k(s)$ - return difference transfer function

$\dfrac{g(s)k(s)}{1 + g(s)k(s)}$ - closed-loop transfer function

$\dfrac{1}{1 + g(s)k(s)}$ - sensitivity transfer function

We will now procede to give a qualitative description of what consti-
tutes a "good" loop transfer function.

4.1.1 Closed-Loop Stability

First, the closed-loop transfer function must be stable - that
is, the roots of $1 + g(s)k(s) = 0$ must all lie in the left-half s-plane.
Without closed-loop stability, a discussion of performance is

4-2

meaningless. It is critically important to realize that the compensator k*(s) is actually designed to stabilize a nominal open-loop plant, g*(s). Thus, the <u>nominal</u> closed-loop transfer function is

$$g^*_{CL} = \frac{g^*(s)k^*(s)}{1 + g^*(s)k^*(s)} \qquad (4.6)$$

This is what we design to be stable, and will learn techniques to do so later. Unfortunately, the true plant is different from the nominal plant due to unavoidable modelling errors, denoted by $\delta g(s)$. Thus, the true plant may be represented by

$$g(s) = g^*(s) + \delta g(s) \qquad (4.7)$$

and the <u>true</u> closed-loop transfer function is

$$g_{CL}(s) = \frac{[g^*(s) + \delta g(s)]k^*(s)}{1 + [g^*(s) + \delta g(s)]k^*(s)} \qquad (4.8)$$

This transfer function must also be stable, and knowledge of $\delta g(s)$ should influence the design of k*(s). In the following discussion, we will assume the actual closed-loop system of (4.8) is stable.

4.1.2 Command Following Performance

Typically, we desire the output y(t) to follow the reference input r(t) closely. This may be represented in the frequency domain by

$$y(s) \approx r(s) \qquad \text{for } s\epsilon\ S_r \qquad (4.9)$$

where S_r denotes the set of frequencies where r(s) has most of its frequency content. For common inputs, such as steps, ramps, and sinusoids, most of their energy lies in the low frequency region.

To look at command following performance, we let n(s) = d(s) = 0. Then, equation (4.5) becomes

$$y(s) = \frac{g(s)k(s)}{1 + g(s)k(s)}\ r(s) \qquad (4.10)$$

It is obvious that if we require

$$1 + g(s)k(s) \quad \text{"large"} \qquad \text{for } s \varepsilon \ S_r \qquad (4.11)$$

which in turn implies

$$g(s)k(s) \quad \text{"large"} \qquad \text{for } s \varepsilon \ S_r \qquad (4.12)$$

then (4.9) will be satisfied. Thus, for good command following, the return difference and hence the loop transfer function should be large for the range of reference input signal frequencies.

4.1.3 Disturbance Rejection

It is typically desired to have the closed-loop system reject disturbances. To see what is required for this, it is easier if we examine the error signal, e(s). To simplify the algebra, let $n(s) = 0$, and examine

$$e(s) = r(s) - y(s) \qquad (4.13)$$

Substituting (4.1) into (4.13) yields

$$e(s) = r(s) - [d(s) + g(s)k(s)e(s)]$$

$$= r(s) - d(s) - g(s)k(s)e(s) \qquad (4.14)$$

or

$$[1 + g(s)k(s)]e(s) = r(s) - d(s) \qquad (4.15)$$

Now, assuming that the reference command signal $r(s) = 0$ so that the desired output y(s) also equals zero, dividing both sides of (4.15) by $1 + g(s)k(s)$ yields

$$e(s) = - \frac{1}{1 + g(s)k(s)} \ d(s) \qquad (4.16)$$

It is immediately obvious from the above that disturbance rejection is accomplished if

$$1 + g(s)k(s) \quad \text{"large"} \qquad \text{for } s \varepsilon \ S_d \qquad (4.17)$$

which implies

$$g(s)k(s) \quad \text{"large"} \qquad \text{for } s \epsilon S_d \qquad (4.18)$$

Therefore, for good disturbance rejection, the loop transfer function must be large at the frequencies (denoted by S_d) where the disturbances have their major energy content.

4.1.4 Sensitivity of Command Following to Modelling Errors

First, let's look at how modelling errors affect open-loop command following. Let $g*(s)$ denote the nominal plant, and $y*(s)$ the nominal output. Then

$$y*(s) = g*(s)r(s) \qquad (4.19)$$

Now, suppose the actual plant is related to the nominal by

$$g(s) = g*(s) + \delta g(s) \qquad (4.20)$$

Then the actual output is

$$
\begin{aligned}
y(s) &= g(s)r(s) \\
&= [g*(s) + \delta g(s)]r(s) \\
&= g*(s)r(s) + \delta g(s)r(s) \\
&= y*(s) + \delta g(s)r(s) \qquad (4.21)
\end{aligned}
$$

If we define $\delta y(s)$, the deviation of the actual output from the nominal due to modelling errors, by

$$\delta y(s) = \delta g(s)r(s) \qquad (4.22)$$

and divide (4.22) by (4.19) we get

$$\frac{\delta y(s)}{y*(s)} = \frac{\delta g(s)}{g*(s)} \qquad (4.23)$$

Equation (4.23) shows that in open-loop command following the deviation $\delta y(s)$ of the output is proportional to the modelling error $\delta g(s)$. This may be unacceptable if the modelling error is appreciable.

Now let's examine closed-loop sensitivity. Using the previous notation

$$y^*(s) = \frac{g^*(s)k(s)}{1 + g^*(s)k(s)} \; r(s) \qquad (4.24)$$

Note that the asterisk is dropped from k(s) since the designed is the actual. Using (4.20) - (4.22),

$$y(s) = y^*(s) + \delta y(s) = \frac{[g^*(s) + \delta g(s)]k(s)}{1 + [g^*(s) + \delta g(s)]k(s)} \; r(s) \qquad (4.25)$$

We now wish to find the ratio $\frac{\delta y(s)}{y^*(s)}$ to compare with (4.23). From Appendix 4A, this is given by

$$\frac{\delta y(s)}{y^*(s)} = \frac{1}{1 + g(s)k(s)} \; \frac{\delta g(s)}{g^*(s)} \qquad (4.26)$$

It is clear to see that if the loop transfer function, and hence the return difference, is large, then a significant percentage error in modelling the plant would result in a small percentage error in the output. Thus, in any frequency region where loop gains are high, command following is insensitive to modelling errors under feedback.

All of the above properties of feedback systems have shown that high loop gains are desirable. First, since physical systems must have more poles than zeros, g(s) eventually approaches zero and thus high loop gains are not achievable at high frequencies (unless k(s) is very large there). More importantly, there are limitations on performance from several factors which make high loop gains at high frequencies undesirable. These factors will now be discussed.

4.1.5 Stability Robustness with Unmodelled Dynamics

In almost all real systems, dynamics at high frequencies are not well known. Furthermore, to limit the size of the plant to a tractable level, many times these dynamics are purposely ignored. Unfortunately, injecting high amounts of control energy into these frequencies may

4-6

drive the poorly modelled or neglected dynamics unstable. Therefore,
high loop gains at high frequencies may destroy the stability assumption
we made in our previous development, and thus the loop transfer function
and return difference must be "small" at high frequencies.

4.1.6 Sensor Noise Response

Let's look at our equation for the output again.

$$y(s) = \frac{g(s)k(s)}{1 + g(s)k(s)} [r(s) - n(s)] + \frac{1}{1 + g(s)k(s)} d(s) \qquad (4.5)$$

We have already concluded that $g(s)k(s)$ should be large at frequencies
where $r(s)$ has its energy, typically low frequencies. If $n(s)$ also has
significant energy content at low frequencies, it is obvious that these
noises will be passed to the output, thus creating a serious conflict in
objectives. Fortunately, sensor noise is typically a high frequency
phenomenon, and thus it is desirable to make $g(s)k(s)$ small (see
equation (4.5) above) to attenuate its affect. Thus, the sensor noise
rejection requirement is

$$g(s)k(s) \quad \text{"small"} \qquad \text{for } s\epsilon\ S_n \qquad (4.27)$$

where S_n denotes the frequencies where the noise has its major energy
content.

4.1.7 Bode Diagram Interpretation

All of the above requirements may be represented graphically
through the use of a Bode magnitude diagram. Here we assume that
command following and disturbance rejection are to be accomplished at
low frequencies while sensor noise and unmodelled dynamics dominate at
high frequencies. These requirements impose restrictions on the size of
$g(s)k(s)$, and are shown as "barriers" on Fig 4.2. The design problem
then becomes:

Given a plant transfer function g(s), find a compensator k(s) which yields a stable closed-loop system and whose loop transfer function has the properties shown in Fig 4.2.
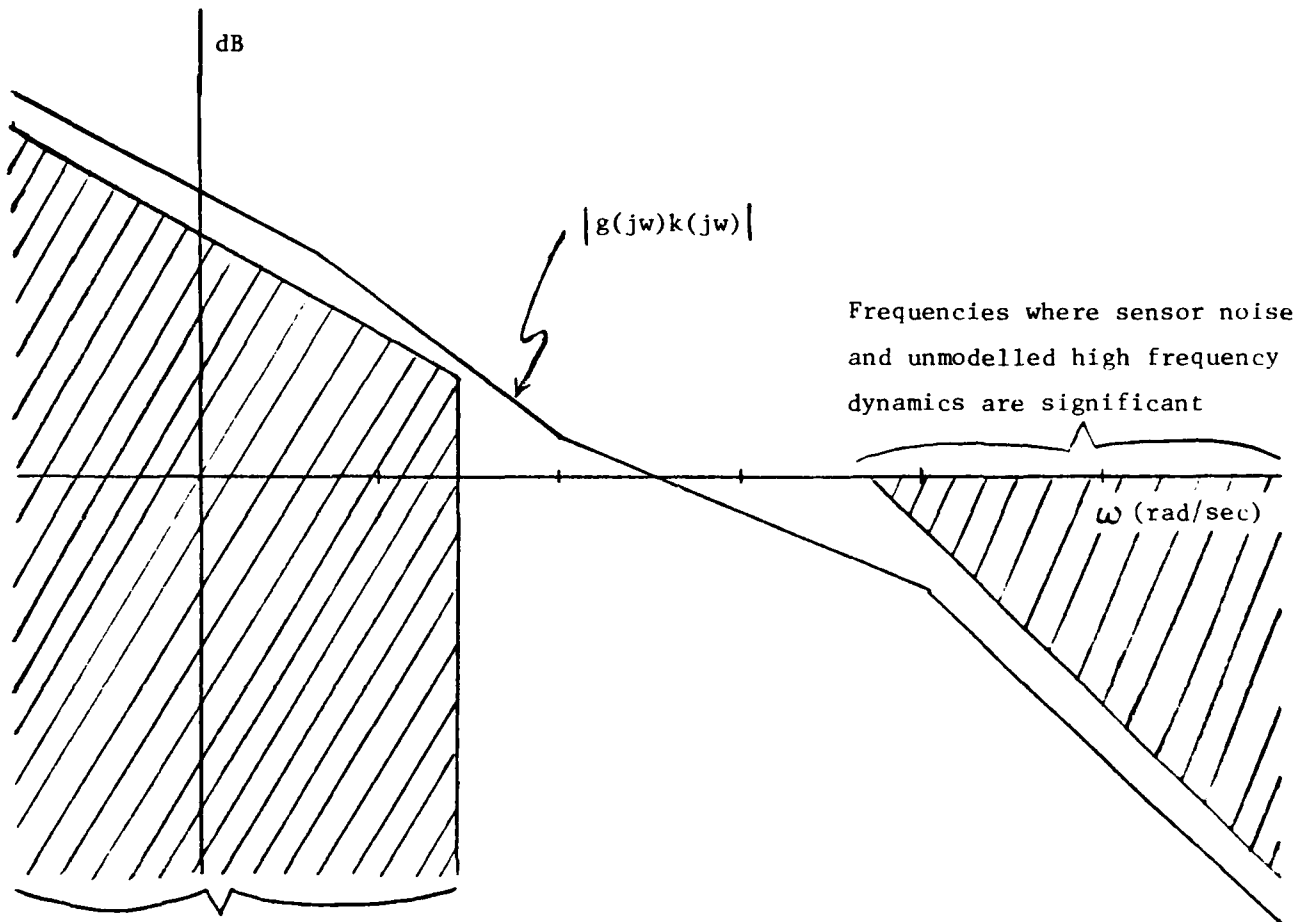
Fig 4.2 Bode Magnitude Plot of a "Good" Loop Transfer Function

4.2 Multivariable Control Loops

Now we need to extend the SISO ideas just presented to multivariable systems, and try to quantify them as well. Once again, let's look at a generic multivariable feedback system, as shown in Fig 4.3.
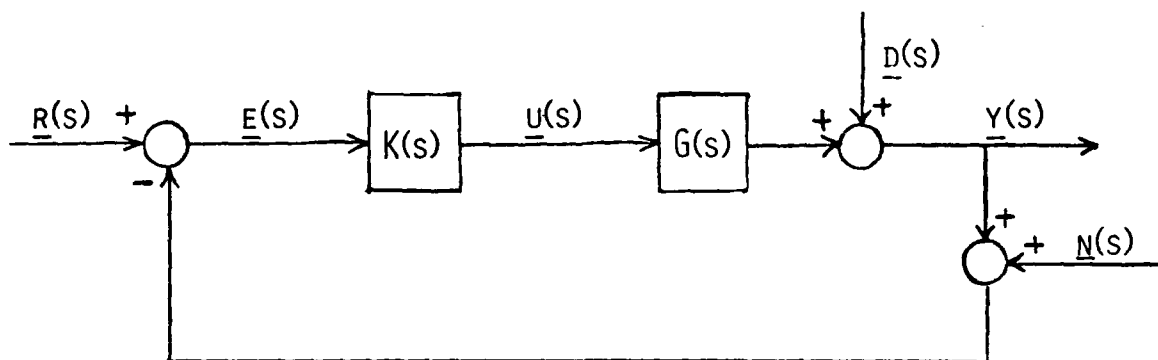
Fig 4.3 A Generic MIMO Control System

All of the variables have the same definitions as before, except here the signals are vectors of signals and the transfer functions are transfer function matrices. Henceforth, the underbars will be dropped. The input and output vectors may not be the same dimension, in which case $K(s)$ and $G(s)$ are not square matrices. We will define their sizes more specifically later.

Again, we derive some of the relationships between the variables

$$e(s) = r(s) - n(s) - y(s) \tag{4.28}$$

$$y(s) = d(s) + G(s)K(s)e(s) \tag{4.29}$$

I) Output equation: Substituting (4.28) into (4.29) we get

$$y(s) = d(s) + G(s)K(s)r(s) - G(s)K(s)n(s) - G(s)K(s)y(s) \tag{4.30}$$

or

$$[I + G(s)K(s)]y(s) = d(s) + G(s)K(s)[r(s) - n(s)] \tag{4.31}$$

Premultiplying both sides of (4.31) by $[I + G(s)K(s)]^{-1}$ we get an expression for the output, given by

$$y(s) = [I + G(s)K(s)]^{-1}G(s)K(s)[r(s) - n(s)] + [I + G(s)K(s)]^{-1}d(s) \tag{4.32}$$

II) Error equation: To examine the effect of noise on the error signal, we need to eliminate $n(s)$ from (4.28). What we want to do is to minimize the effect of $n(s)$ upon the difference

$$e_1(s) = r(s) - y(s) \tag{4.33}$$

Representing $r(s)$ in (4.33) by $[I + G(s)K(s)]^{-1}[I + G(s)K(s)]r(s)$ and substituting (4.32) into (4.33), we get [suppressing the functional dependence on s in the intermediate steps]

$$e_1(s) = [I + GK]^{-1}[I + GK]r - [I + GK]^{-1}GKr + [I + GK]^{-1}GKn - [I + GK]^{-1}d$$

$$= [I + GK]^{-1}r + [I + GK]^{-1}GKr - [I + GK]^{-1}GKr$$

$$+ [I + GK]^{-1}GKn - [I + GK]^{-1}d$$

$$= [I + G(s)K(s)]^{-1}[r(s) - d(s)] + [I + G(s)K(s)]^{-1}G(s)K(s)n(s) \qquad (4.34)$$

III) Sensitivity equation: In order to examine the effects of open-loop plant variations on the closed-loop output, we need to derive an equation for closed-loop sensitivity. First we let $d(s) = n(s) = 0$, and let $G^*(s)$ denote the nominal plant and $y^*(s)$ denote the nominal output to a command $r(s)$. Then

$$y^*(s) = [I + G^*(s)K(s)]^{-1}G^*(s)K(s)r(s) \qquad (4.35)$$

Suppose the actual plant is given by

$$G(s) = G^*(s) + \delta G(s) \qquad (4.36)$$

which results in a change of the output

$$y(s) = y^*(s) + \delta y(s)$$

$$= [I + \{G^*(s) + \delta G(s)\}K(s)]^{-1}\{G^*(s) + G(s)\}K(s)r(s) \qquad (4.37)$$

After some fancy linear algebra, similar to that in Appendix 4A, we get the following result

$$\delta y(s) = [I + G(s)K(s)]^{-1}\delta G(s)[G^*(s)]^{-1}y^*(s) \qquad (4.38)$$

Finally, defining some terminology

$G(s)K(s)$ - loop transfer matrix

$I + G(s)K(s)$ - return difference matrix

$[I + G(s)K(s)]^{-1}$ - inverse return difference matrix

$[I + G(s)K(s)]^{-1}G(s)K(s)$ - closed-loop transfer matrix

4.2.1 Singular Values as a Measure of Size of a Matrix

Next we will use the relationships derived above to examine what is required of the loop transfer matrix in order to meet our performance requirements. To quantify these requirements, we first need a measure of the "size" of a matrix. In the SISO case, this is not a problem - size is simply the magnitude of the complex number you're interested in. For a matrix, there is no such clear-cut measure of size. Eigenvalues can be shown to be poor measures of size. A much better measure of size is the spectral norm, also known as a singular value. These are defined in detail in Chapter 2, and are given by

$$\sigma_i(A) = [\lambda_i(A^*A)]^{1/2} \tag{4.39}$$

A*A is positive semidefinite and Hermitian, and therefore its eigenvalues are real and non-negative. Therefore, singular values are all real and non-negative. The smallest singular value, called the minimum singular value, is denoted by $\underline{\sigma}(\cdot)$. The largest, called the maximum singular value, is denoted by $\bar{\sigma}(\cdot)$. $\underline{\sigma}(A)$ gives a measure of how much attenuation the function A produces on a given signal; $\bar{\sigma}(A)$ a measure of how much amplification. If $\underline{\sigma}(A) = 0$, the matrix is singular (does not have full rank). Therefore, if $\underline{\sigma}(A)$ is "large", then the matrix is said to be large. Conversely, if $\bar{\sigma}(A)$ is "small", then A is said to be small. Of course, "small" and "large" are relative terms (the same problem exists in the scalar case also).

Realize that A above is not necessarily a constant matrix. For our applications, A is a transfer function matrix of some type, which is a function of frequency. This should not be confusing - in the SISO case, magnitude is also a function of frequency. The singular values may be plotted against frequency, thus creating the multivariable extension of a Bode plot. These will be called singular value plots.

4.2.2 Multivariable Performance Properties

Now we will use singular values to extend the performance requirements in Section 4.1 to the multivariable case. In order to quantify the relationships, we will replace s by jw so that we are working in the frequency domain explicitly.

For good command following (let $d(jw) = n(jw) = 0$), we want

$$y(jw) \simeq r(jw) \qquad \forall \ w < w_0 \qquad (4.40)$$

where w_0 is the active frequency range of the system. From equation (4.30), this means we want

$$[I + G(jw)K(jw)]^{-1}G(jw)K(jw) \simeq I \qquad \forall \ w < w_0 \qquad (4.41)$$

Looking at (4.33), we also need

$$e_1(jw) \simeq 0 \qquad \forall \ w < w_0 \qquad (4.42)$$

so that, from (4.34),

$$[I + G(jw)K(jw)]^{-1} \simeq 0 \qquad \forall \ w < w_0 \qquad (4.43)$$

The above equation says that we want the inverse return difference to be small, which may be stated as

$$\overline{\sigma}[\{I + G(jw)K(jw)\}^{-1}] \quad \text{"small"} \qquad \forall \ w < w_0 \qquad (4.44)$$

Using the singular value identity

$$\overline{\sigma}(A) = 1/\underline{\sigma}(A^{-1}) \qquad (4.45)$$

this may be rewritten as

$$\underline{\sigma}[I + G(jw)K(jw)] \quad \text{"large"} \qquad \forall \ w < w_0 \qquad (4.46)$$

Rather than use "large", let's define p(w) as a large, positive function of frequency, so that (4.46) becomes

$$\underline{\sigma}[I + G(jw)K(jw)] \geqslant p(w) \qquad \forall \ w < w_0 \qquad (4.47)$$

Using the singular value inequality

$$\underline{\sigma}[G(jw)K(jw)] - 1 \leqslant \underline{\sigma}[I + G(jw)K(jw)] \leqslant \underline{\sigma}[G(jw)K(jw)] + 1 \qquad (4.48)$$

we may conclude that (4.47) is satisfied if

$$\underline{\sigma}[G(jw)K(jw)] \quad \text{"large"} \qquad \qquad \forall \; w < w_0 \qquad\qquad (4.49)$$

and therefore $\underline{\sigma}[G(jw)K(jw)]$ approximates $\underline{\sigma}[I + G(jw)K(jw)]$. This last
fact also guarantees that (4.41) is satisfied. This all becomes a
restatement of the fact that high loop gains yield good command following.

From (4.32) or (4.34) we can see that for good disturbance rejection,

$$[I + G(jw)K(jw)]^{-1} \simeq 0 \qquad\qquad \forall \; w < w_0 \qquad\qquad (4.50)$$

which again leads to equation (4.47). Looking at (4.38), it is clear that
large loop gains will also reduce sensitivity to low frequency modelling
errors. Therefore, high loop gains also reject disturbances and minimize
sensitivity.

High loop gain at all frequencies is not a good design objective,
however (good thing – for real systems, it's impossible anyway). Assuming
no disturbances and a zero reference command, (4.34) gives the system error
response as

$$e_1(jw) = [I + G(jw)K(jw)]^{-1}G(jw)K(jw)n(jw) \qquad\qquad (4.51)$$

If $G(jw)K(jw)$ is large, by (4.48) it roughly equals $[I + G(jw)K(jw)]$, and
(4.51) becomes

$$e_1(jw) \simeq [I]n(jw) \qquad\qquad (4.52)$$

Thus, if $G(jw)K(jw)$ is large where the noise has most of its energy, the
noise will pass through into the error and thus into the output. Therefore,
to minimize the effect of sensor noise, $[I + G(jw)K(jw)]^{-1}G(jw)K(jw)$ should
be small at the noise frequencies, or

$$\bar{\sigma}[\{I + G(jw)K(jw)\}^{-1}G(jw)K(jw)] << 1 \qquad\qquad (4.53)$$

Using the singular value inequality

$$\bar{\sigma}[AB] \leq \bar{\sigma}[A]\bar{\sigma}[B] \qquad\qquad (4.54)$$

(4.53) will be satisfied if

4-13

$$\overline{\sigma}[\{I + G(jw)K(jw)\}^{-1}] \overline{\sigma}[G(jw)K(jw)] << 1 \tag{4.55}$$

and by (4.45), this may be rewritten

$$\frac{\overline{\sigma}[G(jw)K(jw)]}{\underline{\sigma}[I + G(jw)K(jw)]} << 1 \tag{4.56}$$

This inequality will be satisfied if $\overline{\sigma}[G(jw)K(jw)] << 1$, so that small loop gain will tend to minimize the effects of sensor noise.

Another argument against high loop gains at high frequency may be made by examining the expression for control activity,

$$u(jw) = K(jw)e(jw) \tag{4.57}$$

where $e(jw)$ may be found from (4.28) and (4.29) to be

$$e(jw) = r(jw) - n(jw) - y(jw)$$
$$= r(jw) - n(jw) - d(jw) - G(jw)K(jw)e(jw) \tag{4.58}$$

or

$$[I + G(jw)K(jw)]e(jw) = r(jw) - n(jw) - d(jw) \tag{4.59}$$

so that

$$e(jw) = [I + G(jw)K(jw)]^{-1}[r(jw) - n(jw) - d(jw)] \tag{4.60}$$

Substituting (4.60) into (4.57) yields

$$u(jw) = K(jw)[I + G(jw)K(jw)]^{-1}[r(jw) - n(jw) - d(jw)] \tag{4.61}$$

For $G(jw)K(jw)$ large, $I + G(jw)K(jw)$ is approximately equal to $G(jw)K(jw)$, and (4.61) becomes

$$u(jw) \simeq K(jw)[G(jw)K(jw)]^{-1}[r(jw) - n(jw) - d(jw)]$$
$$= K(jw)K^{-1}(jw)G^{-1}(jw)[r(jw) - n(jw) - d(jw)]$$
$$= G^{-1}(jw)[r(jw) - n(jw) - d(jw)] \tag{4.62}$$

where we have assumed $G(jw)$ and $K(jw)$ to be square and invertible for convenience. Beyond the bandwidth of $G(jw)$ (where it rolls off), $G^{-1}(jw)$ grows large and therefore the control activity $u(jw)$ does also. This is

uracceptable, and provides another reason why high loop gains at high frequency must be avoided.

The trade-offs discussed above, high loop gain at low frequency but not at high frequency, are not difficult by themselves. What compounds the problem is:

1) designing the transition between the regions

2) accounting for the destabilizing effects of (high-frequency) uncertainties.

These will be discussed next.

4.2.3 Modelling Uncertainty

The models we use for designing control systems are just that — models of reality. Inherent in all models are errors due to our inability to accurately represent the real world, such as nonlinearities, truncated modes, neglected dynamics, parameter variations, etc. The best we can do is try to estimate these errors and design systems that will remain stable in spite of them. One possible representation of the modelling error is called additive unstructured uncertainty, given by

$$G'(jw) = G(jw) + \Delta G(jw) \tag{4.63}$$

where

$$\overline{\sigma}[\Delta G(jw)] < \ell_a(w) \qquad \forall \ w \geqslant 0 \tag{4.64}$$

Here, $G'(jw)$ is the true plant, $G(jw)$ the model of the plant, $\Delta G(jw)$ the error, and $\ell_a(w)$ is a positive scalar function. The error is called unstructured because all we claim to know about it is that it is bounded by the function $\ell_a(w)$. Therefore, this representation confines $G'(jw)$ to a neighborhood of $G(jw)$ with magnitude $\ell_a(w)$.

Another representation for uncertainty is called (output) multiplicative unstructured uncertainty, given by

$$G'(jw) = [I + L(jw)]G(jw) \qquad\qquad (4.65)$$

where

$$\overline{\sigma}[L(jw)] < \ell_m(w) \qquad\qquad \forall\ w \geqslant 0 \qquad\qquad (4.66)$$

Here, $L(jw)$ is the uncertainty and $\ell_m(w)$ is a positive scalar function that bounds the maximum singular value of $L(jw)$. This representation confines $G'(jw)$ to a normalized neighborhood of $G(jw)$, and has an advantage over the additive form in that it applies to $G(jw)K(jw)$ as well as $G(jw)$. For this reason, we will look primarily at the multiplicative form.

The better we represent uncertainty, the better our overall design will be. Therefore, it is important to use the best model available for different types of uncertainty. Usually, low frequency errors (such as parameter variations) are best modelled by highly structured forms of uncertainty. There are always high frequency errors remaining, however, which cannot be covered this way. These are typically the critical destabilizing errors, and the unstructured uncertainties model these well. Therefore, we will focus our attention on uncertainties represented by (4.65) and (4.66).

One further assumption we will make is that the number of unstable modes of $G'(jw)$ is the same as in $G(jw)$. These modes need not be identical, which does allow $L(jw)$ to be an unstable operator. Also, we assume $G'(jw)$ remains a strictly proper, finite-dimensional linear time-invariant transfer function. These requirements make the development easier - in References [4.2] and [4.3] more general perturbations are covered, but will not be discussed here. Given all of these assumptions, the bounding functions $\ell_m(w)$ commonly are small at low frequencies and grow to unity and above at high frequencies. This is shown in Fig 4.4.

4-16
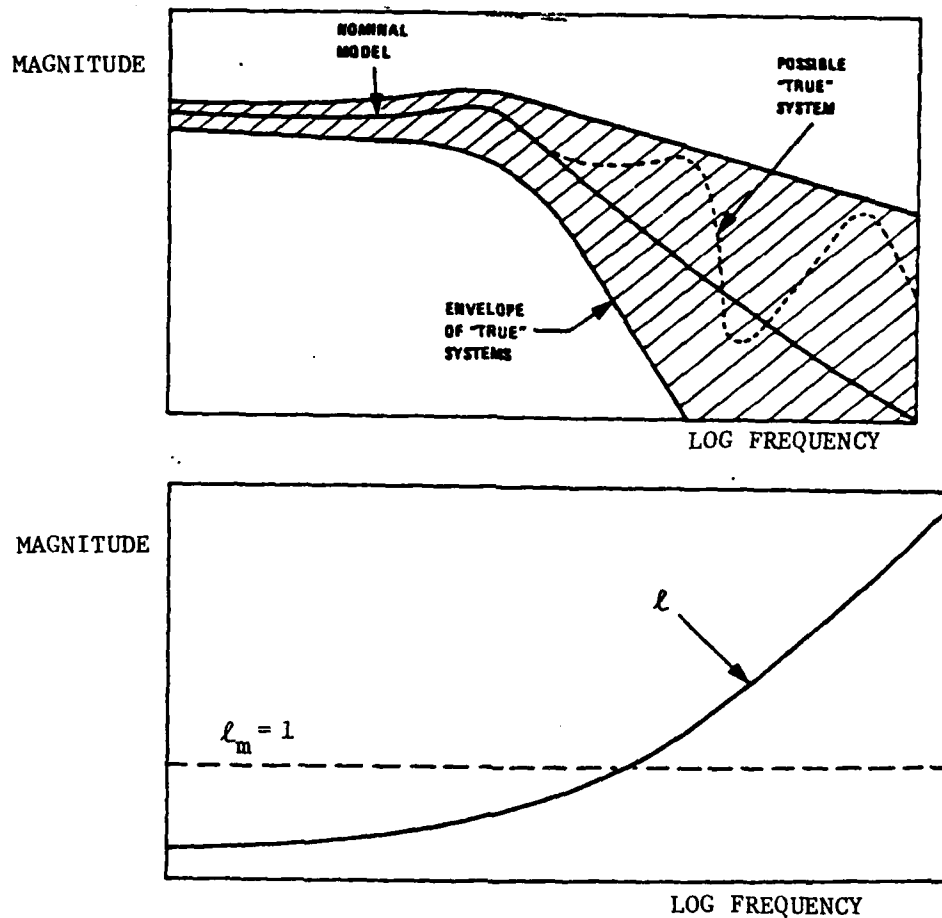
Fig 4.4 Typical Behavior of Multiplicative Perturbations

It is important to note that constructing these uncertainty bounds is not
trivial. At present, it is an ad hoc procedure based on reasonable estimates.
The bound assumes a worst case uncertainty magnitude applicable to all
channels. If more is known about the levels in various channels, it may be
necessary to scale the input-output variables or apply frequency-dependent
transformations to $G(jw)$ so that $\ell_m(w)$ becomes more uniformly tight. More on
this may be found in Ref [4-3] and Chapter 5. Here, these scale factors and/or
transformations are assumed to be part of the nominal model $G(jw)$.

4.3.4 Design in the Face of Uncertainties

Now we need to put our stability and performance requirements together and
make sure we satisfy them in the face of the uncertainties we have assumed.

4-17

Once we have a design model $G(jw)$ and accept uncertainties in the form of (4.65) and (4.66), we must find a compensator $K(jw)$ such that

1) The nominal feedback system, $G(jw)K(jw)[I + G(jw)K(jw)]^{-1}$, is stable (note that $[I + GK]^{-1}GK = GK[I + GK]^{-1}$

2) The perturbed system, $G'(jw)K(jw)[I + G'(jw)K(jw)]^{-1}$, is stable for __all__ $G'(jw)$ given by (4.65) and (4.66)

3) Performance objectives for __all__ $G'(jw)$ are satisfied

Requirement 1) is just the standard closed-loop stability requirement, which is completely solved by using the Nyquist stability criteria, or in the MIMO case, its multivariable generalization [encirclement count of the map $\det[I + G(jw)K(jw)]$, evaluated on the Nyquist D-contour, be equal to the negative number of unstable open-loop modes of $G(jw)K(jw)$]. More details on this criteria may be found in Chapter 2 of these notes.

Requirement 2) is a bit more complicated. It may be satisfied by a similar requirement on $[I + G'(jw)K(jw)]$. Since we assumed $G'(jw)$ has the same number of unstable modes as $G(jw)$, the Nyquist criteria requires that the number of encirclements of $\det[I + G'(jw)K(jw)]$ remains unchanged for all $G'(jw)$. Checking this would be ridiculous, as there are an infinite number of $G'(jw)$, and we therefore need a better way. The above requirement is assured if $\det[I + G'(jw)K(jw)]$ remains nonzero as $G(jw)$ is warped continuously toward $G'(jw)$. Requiring the minimum singular value of a function to be greater than zero assures a nonzero determinant, so that this requirement translates into

$$0 < \underline{\sigma}\{ I + [I + \varepsilon L(jw)]G(jw)K(jw) \} \quad \forall \quad 0 \le \varepsilon \le 1 \ , \quad w \ge 0 \qquad (4.67)$$

and for all $L(jw)$ satisfying (4.66). The ε varying from zero to one gives us the warping from $G(jw)$ to $G'(jw)$. Expanding (4.67) gives

$$0 < \underline{\sigma}[I + G(jw)K(jw) + \varepsilon L(jw)G(jw)K(jw)] \qquad \forall \begin{cases} 0 \le \varepsilon \le 1 \\ \omega \ge 0 \\ L(jw) \end{cases} \qquad (4.68)$$

Now, factoring $G(jw)K(jw)$ out to the right yields

$$0 < \underline{\sigma}[\{[I + [G(jw)K(jw)]^{-1} + \epsilon L(jw)\}G(jw)K(jw)] \qquad \forall \begin{cases} 0 \leqslant \epsilon \leqslant 1 \\ \omega \geqslant 0 \\ L(j\omega) \end{cases} \quad (4.69)$$

where we assume $[G(jw)K(jw)]^{-1}$ exists. Using the relation $\underline{\sigma}[AB] \geqslant \underline{\sigma}[A]\underline{\sigma}[B]$, (4.69) is satisfied if

$$0 < \underline{\sigma}[I + \{G(jw)K(jw)\}^{-1} + \epsilon L(jw)] \, \underline{\sigma}[G(jw)K(jw)] \qquad \forall \begin{cases} 0 \leqslant \epsilon \leqslant 1 \\ \omega \geqslant 0 \\ L(j\omega) \end{cases} \quad (4.70)$$

is satisfied. Since $[G(jw)K(jw)]^{-1}$ exists, $\underline{\sigma}[G(jw)K(jw)] \neq 0$, and we divide it out of (4.70) to get

$$0 < \underline{\sigma}[I + \{G(jw)K(jw)\}^{-1} + \epsilon L(jw)] \qquad \forall \begin{cases} 0 \leqslant \epsilon \leqslant 1 \\ \omega \geqslant 0 \\ L(j\omega) \end{cases} \quad (4.71)$$

Using the fact that

$$\underline{\sigma}(A) > \overline{\sigma}(E) \implies \underline{\sigma}(A + E) > 0 \qquad (4.72)$$

from Chapter 2 of these notes, and letting $A = I + [G(jw)K(jw)]^{-1}$ and $E = \epsilon L(jw)$, we can see that

$$\underline{\sigma}[I + \{G(jw)K(jw)\}^{-1}] > \overline{\sigma}[\epsilon L(jw)] \qquad \forall \begin{cases} 0 \leqslant \epsilon \leqslant 1 \\ \omega \geqslant 0 \\ L(j\omega) \end{cases} \quad (4.73)$$

implies what we want. That is, if we satisfy (4.73), we are guaranteed to satisfy (4.71), which is guaranteed to satisfy (4.67). This form is still inconvenient. First, realize that $\overline{\sigma}[\epsilon L(jw)] = \epsilon \overline{\sigma}[L(jw)]$, because ϵ is a constant positive scalar. Next, recall that $\underline{\sigma}[A] = 1/\overline{\sigma}[A^{-1}]$. Therefore, (4.73) becomes

$$\frac{1}{\overline{\sigma}\{[I + \{G(jw)K(jw)\}^{-1}]^{-1}\}} > \frac{\epsilon}{\underline{\sigma}[L^{-1}(jw)]} \qquad \forall \begin{cases} 0 \leqslant \epsilon \leqslant 1 \\ \omega \geqslant 0 \\ L(j\omega) \end{cases} \quad (4.74)$$

Using the identity

$$[I + (GK)^{-1}]^{-1} = [\{I + GK\}(GK)^{-1}]^{-1} = GK[I + GK]^{-1} \qquad (4.75)$$

(4.74) may be rewritten as (after cross-multiplying)

4-19

$$\frac{1}{\epsilon} \, \underline{\sigma}[L^{-1}(jw)] > \overline{\sigma}[G(jw)K(jw)\{I + G(jw)K(jw)\}^{-1}] \qquad \forall \begin{cases} 0 \leqslant \epsilon \leqslant 1 & (4.76) \\ \omega \geqslant 0 \\ L(j\omega) \end{cases}$$

Now, if we rewrite (4.66) as

$$\frac{1}{\underline{\sigma}[L^{-1}(jw)]} < \ell_m(w) \qquad \forall \ w \geqslant 0 \qquad (4.77)$$

or

$$\frac{1}{\ell_m} < \underline{\sigma}[L^{-1}(jw)] \qquad \forall \ w \geqslant 0 \qquad (4.78)$$

we can easily see that by satisfying

$$\frac{1}{\epsilon} \cdot \frac{1}{\ell_m(w)} > \overline{\sigma}[G(jw)K(jw)\{I + G(jw)K(jw)\}^{-1}] \qquad \forall \begin{cases} 0 \leqslant \epsilon \leqslant 1 & (4.79) \\ \omega \geqslant 0 \end{cases}$$

we will satisfy (4.76). Examining (4.79), we see that $\epsilon = 1$ would be a worst case, since that value makes the left-hand side smallest. Therefore, if we satisfy

$$\overline{\sigma}[G(jw)K(jw)\{I + G(jw)K(jw)\}^{-1}] < \frac{1}{\ell_m(w)} \qquad \forall \ w \geqslant 0 \qquad (4.80)$$

we will always satisfy (4.79). This is the most convenient form of (4.67) to use.

Remember that (4.80) is the condition for satisfying Requirement 2). It is _not_ a conservative requirement if _all_ uncertainties given by (4.65)-(4.66) are to be guarded against. It does, however, impose hard limits on the permissible loop gains. Also, upon examination, we can see that (4.80) is a generalization of one of our familiar SISO requirements. For large uncertainties, $\ell_m(w) \gg 1$, (4.80) becomes

$$\overline{\sigma}[G(jw)K(jw)] < \frac{1}{\ell_m(w)} \qquad \forall \ w \geqslant 0, \ \ell_m(w) \gg 1 \qquad (4.81)$$

which says that small loop gains are required whenever unstructured uncertainties are large.

Finally, Requirement 3), the performance requirement, may be stated mathematically by rewriting (4.47) using $G'(jw)$ instead of $G(jw)$, so that

$$p(w) \leq \underline{\sigma} [I + \{I + L(jw)\}G(jw)K(jw)] \qquad \forall \; w \geq 0, \; L(jw) \qquad (4.82)$$

By the proof in Appendix 4P, this condition is satisfied if

$$\frac{p(w)}{1 - \ell_m(w)} \leq \underline{\sigma} [G(jw)K(jw)] \qquad \begin{array}{l} \forall \; w \geq 0 \\ \ell_m(w) < 1 \\ \underline{\sigma}[G(jw)K(jw)] \gg 1 \end{array} \qquad (4.83)$$

In words, this says that performance objectives can be met in the face of unstructured uncertainties if the nominal loop gains are made sufficiently large to compensate for model variations. Note that if $\ell_m(w)$ is near unity, indicating a fairly high level of uncertainty, to meet strict performance requirements the loop gains would need to be very large. Therefore, uncertainty limits performance, and in order to meet stability robustness conditions high performance is not achievable at high frequencies where $\ell_m(w)$ grows large.

One final function of interest comes from inverting (4.80) to get

$$\ell_m(w) < \frac{1}{\overline{\sigma} [G(jw)K(jw) \{I + G(jw)K(jw)\}^{-1}]}$$

$$= \underline{\sigma}[I + \{G(jw)K(jw)\}^{-1}] \qquad (4.84)$$

This says very directly that stability is guaranteed for all perturbations $L(jw)$ whose maximum singular value falls below the right-hand side of (4.84). In effect, $\underline{\sigma}[I + \{G(jw)K(jw)\}^{-1}]$ is a multivariable generalization of SISO stability margin concepts. This was shown in detail in Chapter 3 of these notes. A major difference from the SISO case is that $\underline{\sigma}[I + \{G(jw)K(jw)\}^{-1}]$ measures stability robustness at the plant outputs only. To reflect uncertainty at the inputs, $\underline{\sigma}[I + \{K(jw)G(jw)\}^{-1}]$ would have to be used. Relationships between the two will be discussed in the next chapter.

4.2.5 σ-Plot Interpretation

Just as in the SISO case, we can graphically represent our performance and stability requirements, here through the use of singular value plots. Note that conditions have been derived for the maximum and minimum singular values only, so only these are shown in Fig 4.5. Again we assume that command following, disturbance rejection, and closed-loop sensitivity reduction are low-frequency concerns, while sensor noise reduction and stability robustness are high-frequency requirements.
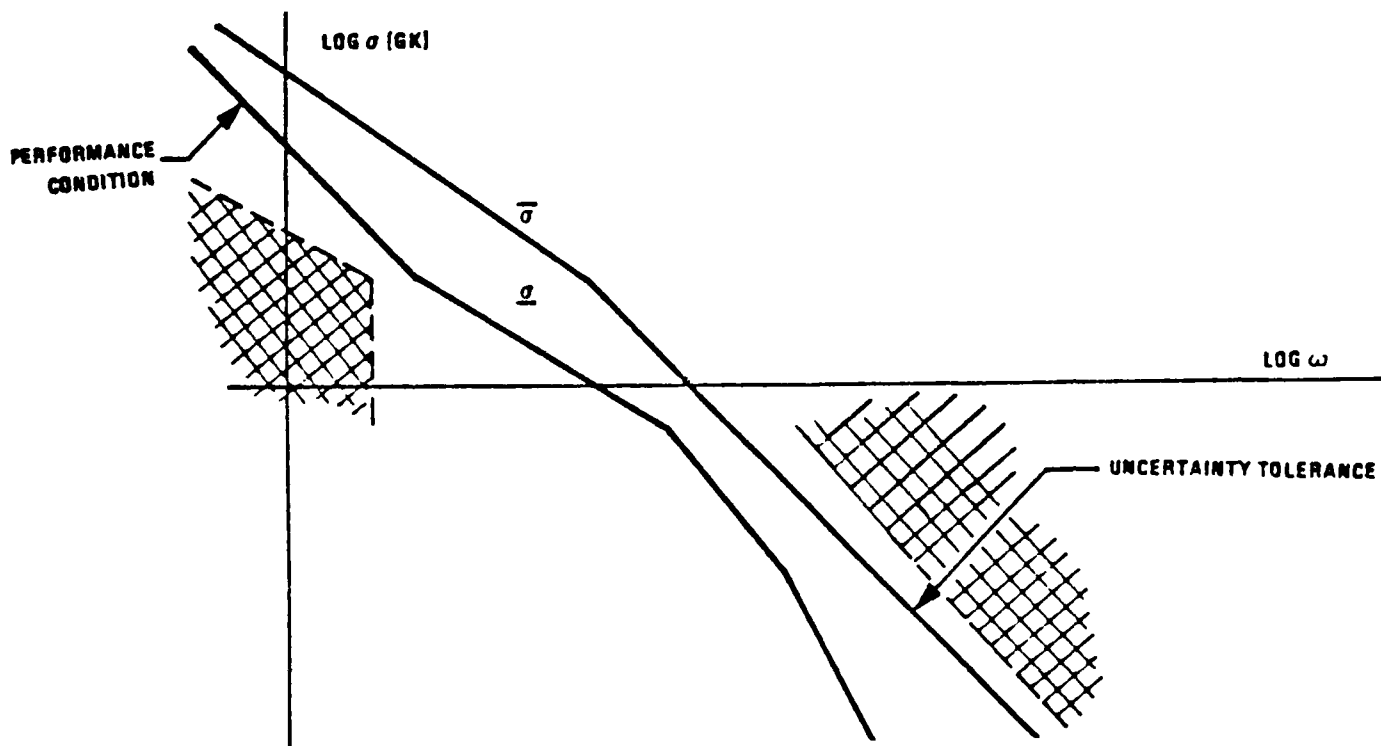
Fig 4.5   The Multivariable Feedback Design Problem

Note that the high-frequency bound is a requirement (stability is mandatory), while the low frequency bound is (mathematically) only desirable. Also note that both depend on $\ell_m(w)$, as they represent stability and performance robustness.

Obviously, a phase plot is not included here. While singular values are an excellent measure of magnitude, they contain no measure of direction (ie, phase). This information is contained in the singular vectors, but not as straightforwardly as SISO phase. Some work has been done interpreting singular vectors [Ref 4-4], but it is not at a useful stage yet. This is not too severe of a limitation, however. When we defined SISO loop shapes, we didn't use phase. Phase information is usually important for evaluating stability (margins) and crossover properties. The phase of a rational function is completely determined by its gain and position of right-half plane poles and zeros, as will be discussed further in the next chapter. Thus, the lack of phase information for a multivariable system is not critical in most cases.

The bandwidth and roll-off near crossover are critical in a multivariable design. The bandwidth of $G(jw)K(jw)$ cannot extend much beyond the crossover of the $\ell_m(w)$ plot. The severity of this constraint depends upon the slope at crossover of $\overline{\sigma}[G(jw)K(jw)]$ and $\underline{\sigma}[G(jw)K(jw)]$; the steeper the better. However, steepness comes at the expense of small stability margins. This will be further discussed in the next chapter.

From (4.25)

$$y*(s) + \delta y(s) = \frac{[g*(s) + \delta g(s)]k(s)}{1 + [g*(s) + \delta g(s)]k(s)} \, r(s) \tag{4A.1}$$

Dividing both sides by $y*(s)$ yields

$$1 + \frac{\delta y(s)}{y*(s)} = \frac{[g*(s) + \delta g(s)]k(s)}{1 + [g*(s) + \delta g(s)]k(s)} \, \frac{r(s)}{y*(s)} \tag{4A.2}$$

Using (4.24), $y*(s)$ on the right-hand side of (4A.2) may be eliminated,

yielding

$$1 + \frac{\delta y(s)}{y*(s)} = \frac{[g*(s) + \delta g(s)]k(s)}{1 + [g*(s) + \delta g(s)]k(s)} \, r(s) \, \frac{1}{r(s)} \, \frac{1 + g*(s)k(s)}{g*(s)k(s)}$$

$$= \frac{[g*(s) + \delta g(s)]}{g*(s)} \, \frac{1 + g*(s)k(s)}{1 + g(s)k(s)} \tag{4A.3}$$

where $[g*(s) + \delta g(s)]$ was replaced by $g(s)$ in the denominator. Subtracting 1

from both sides of (4A.3) yields

$$\frac{\delta y(s)}{y*(s)} = \frac{[g*(s) + \delta g(s)]}{g*(s)} \, \frac{1 + g*(s)k(s)}{1 + g(s)k(s)} - \frac{g*(s)[1 + g(s)k(s)]}{g*(s)[1 + g(s)k(s)]}$$

$$= \frac{g*(s)[1 + g*(s)k(s)] + \delta g(s)[1 + g*(s)k(s)] - g*(s)[1 + g(s)k(s)]}{g*(s)[1 + g(s)k(s)]}$$

$$\tag{4A.4}$$

Looking at the last term in the numerator

$$g*(s)[1 + g(s)k(s)] = g*(s)[1 + \{g*(s) + \delta g(s)\}k(s)]$$

$$= g*(s)[1 + g*(s)k(s)] + g*(s)\delta g(s)k(s) \tag{4A.5}$$

Substituting (4A.5) into (4A.4) yields

4-24

$$\frac{\delta y(s)}{y^*(s)} = \frac{\delta g(s)[1 + g^*(s)k(s)] - g^*(s)\delta g(s)k(s)}{g^*(s)[1 + g(s)k(s)]}$$

$$= \frac{\delta g(s) + \delta g(s)g^*(s)k(s) - g^*(s)\delta g(s)k(s)}{g^*(s)[1 + g(s)k(s)]}$$

$$= \frac{1}{1 + g(s)k(s)} \frac{\delta g(s)}{g^*(s)} \qquad (4A.6)$$

This is the desired result.

Appendix 4B

From (4.82) [dropping functional dependence for brevity]

$$p \leqslant \underline{\sigma}[I + (I + L)GK] = \underline{\sigma}[I + GK + LGK] \tag{4B.1}$$

Factoring I + GK from the right yields

$$p \leqslant \underline{\sigma}[\{I + LGK(I + GK)^{-1}\}(I + GK)] \tag{4B.2}$$

Using $\underline{\sigma}[AB] \geqslant \underline{\sigma}[A]\underline{\sigma}[B]$, we can see that

$$\underline{\sigma}[\{I + LGK(I + GK)^{-1}\}(I + GK)] \geqslant \underline{\sigma}[I + LGK(I + CK)^{-1}] \, \underline{\sigma}[I + GK] \tag{4B.3}$$

Using (4B.3), we can see that (4B.2) is satisfied if

$$p \leqslant \underline{\sigma}[I + LGK(I + GK)^{-1}] \, \underline{\sigma}[I + GK] \tag{4B.4}$$

Now, if we assume $\underline{\sigma}[GK] \gg 1$, (4B.4) becomes

$$p \leqslant \underline{\sigma}[I + LGK(GK)^{-1}] \, \underline{\sigma}[GK] = \underline{\sigma}[I + L] \, \underline{\sigma}[GK] \tag{4B.5}$$

Using the relation $\underline{\sigma}[A + B] \geqslant \underline{\sigma}[A] - \overline{\sigma}[B]$, (4B.5) is satisfied if

$$p \leqslant \{\underline{\sigma}[I] - \overline{\sigma}[L]\}\underline{\sigma}[GK] = \{1 - \overline{\sigma}[L]\}\underline{\sigma}[GK] \tag{4B.6}$$

Since $\overline{\sigma}[L] < \ell_m$, (4B.6) is satisfied if

$$p \leqslant (1 - \ell_m) \, \underline{\sigma}[GK] \tag{4B.7}$$

Assuming $\ell_m < 1$ so that $(1 - \ell_m)$ is non-negative, (4B.7) may be rewritten

$$\frac{p}{1 - \ell_m} \leqslant \underline{\sigma}[GK] \tag{4B.8}$$

This is the desired result.

Chapter 4 References

[4-1] M. Athans, "Lecture Notes on Multivariable Control Systems", LIDS Feport, Massachusetts Institute of Technology, Cambridge, MA, June 1984.

[4-2] M.G. Safonov, Stability and Robustness of Multivariable Feedback Systems, MIT Press, 1980.

[4-3] G. Zames, "On the Input-Output Stability of Time-Varying Nonlinear Feedback Systems - Parts I and II", IEEE Trans. Autom. Contr., Vol AC-11, pp 228-238, Apr 1966 and pp 465-476, July 1966.

[4-4] J. Freudenberg and D.P. Looze, "Phase in Multivariable Feedback Systems", Proceedings of 23rd IEEE Conference on Decision and Control, Las Vegas, NV, Dec 1984.

[4-5] J.C. Doyle, "Multivariable Design Techniques Based on Singular Value Generalizations of Classical Control", AGARD Lecture Series 117, Oct 1981.

5. PERFORMANCE LIMITATIONS FOR MULTIVARIABLE SYSTEMS

The previous chapter developed equations that define a "good" multivariable loop shape. Unfortunately, there are fundamental limitations on the achievable performance of multivariable systems which make the shaping process nontrivial. Most of these limitations are also present in SISO design, such as:

1) the algebraic tradeoff between performance and robustness

2) the functional tradeoff imposed by the Bode gain/phase relations, and

3) limitations due to non-minimum phase zeros.

Another limitation, that of

4) directionality in multiloop systems,

is uniquely multivariable and has no SISO analog. We will now look at all four limitations.

5.1 Trade-Offs Between Performance and Robustness

Again, consider the feedback configuration shown in Fig 5.1. We assume that the nominal system is stable.
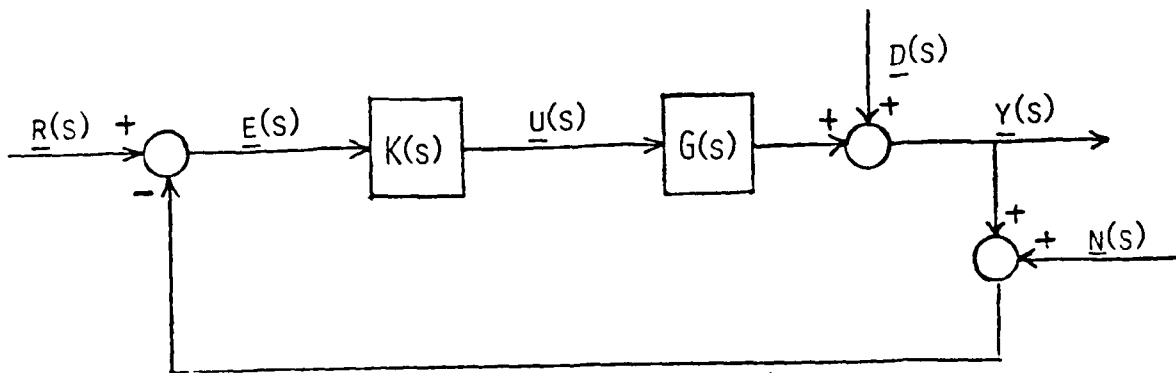
Fig 5.1 Multivariable Feedback System

Let's look at the error equation we derived in the last chapter. From (4.34),

$$e_1(jw) = [I + G(jw)K(jw)]^{-1}[r(jw) - d(jw)]$$
$$+ [I + G(jw)K(jw)]^{-1}G(jw)K(jw)n(jw) \qquad (5.1)$$

For command following and disturbance rejection at any given frequency, the above tells us we must have

$$\overline{\sigma}\{[I + G(jw)K(jw)]^{-1}\} \ll 1 \qquad (5.2)$$

or equivalently

$$\underline{\sigma}[I + G(jw)K(jw)] \gg 1 \qquad (5.3)$$

at that frequency. This requires

$$\underline{\sigma}[G(jw)K(jw)] \gg 1 \qquad (5.4)$$

at that frequency. However, from (5.1) we can also see that for sensor noise reduction we require

$$\overline{\sigma}\{[I + G(jw)K(jw)]^{-1}G(jw)K(jw)\} = \underline{\sigma}\{[I + \{G(jw)K(jw)\}^{-1}]^{-1}\} \ll 1 \quad (5.5)$$

or equivalently

$$\underline{\sigma}[I + \{G(jw)K(jw)\}^{-1}] \gg 1 \qquad (5.6)$$

at frequencies where noise is large. Also, for good robustness properties, equation (4.84) shows that

$$\ell_m(w) < \underline{\sigma}[I + \{G(jw)K(jw)\}^{-1}] \qquad (5.7)$$

Since $\ell_m(w)$ invariably grows large at high frequency, this becomes the same as the requirement in (5.6). To satisfy (5.6)

$$\underline{\sigma}[\{G(jw)K(jw)\}^{-1}] \gg 1 \qquad (5.8)$$

or

$$\overline{\sigma}[G(jw)K(jw)] \ll 1 \qquad (5.9)$$

Obviously, this is the reverse of the requirement in (5.4). This indicates a trade-off -- at any given frequency, it is possible to have $\underline{\sigma}[G(jw)K(jw)] \gg 1$ for command following or disturbance rejection or to have $\overline{\sigma}[G(jw)K(jw)] \ll 1$ for reduction of sensor noise effects and good stability margins, but not both.

Another way to see this is by looking at the relationship between $[I + G(jw)K(jw)]^{-1}$ and $[I + G(jw)K(jw)]^{-1}G(jw)K(jw)$. Introducing terminology from Chapter 2

$$S(jw) = \text{sensitivity matrix}$$

$$= [I + G(jw)K(jw)]^{-1} \tag{5.10}$$

$$T(jw) = \text{complimentary sensitivity matrix}$$

$$= [I + G(jw)K(jw)]^{-1}G(jw)K(jw) \tag{5.11}$$

If we add these functions, we see that

$$S + T = [I + GK]^{-1} + [I + GK]^{-1}GK = [I + GK]^{-1}[I + GK] = I \tag{5.12}$$

Remember that we need loop gains to be large for command following and disturbance rejection. If $G(jw)K(jw)$ is large, so is $[I + G(jw)K(jw)]$, and therefore $S(jw)$ is small. From (5.12) this implies $T(jw)$ is near unity, and looking at (5.5) tells us that noise reduction and margins are poor here. The same argument holds true in reverse if loop gains are small. Thus, command following/disturbance rejection may only be achieved where sensor noise/margins are not critical, and vice versa.

The above conclusion is a limitation of feedback systems, but is not devastating for "typical" systems. Since commands and disturbances usually have most of their energy at low frequency while sensor noise and the need for robustness is large at high frequency, the conflict is minor. However, transition from one region to the other is critical. Here, poor performance and poor stability robustness must be avoided. This will be discussed next.

5.2 Functional Limitations on Transfer Functions

Let's take a look at what the "best" loop transfer function would look like, from a command following/disturbance rejection and noise attenuation/robustness to uncertainties point of view. For ease, let's

call this performance vs. robustness. To achieve the "best" performance, we want loop gains to be as high as possible over a wide frequency range. For robustness, we want them to be low over a wide frequency range. Looking just at SISO for convenience, this implies the loop shape in Fig 5.2.
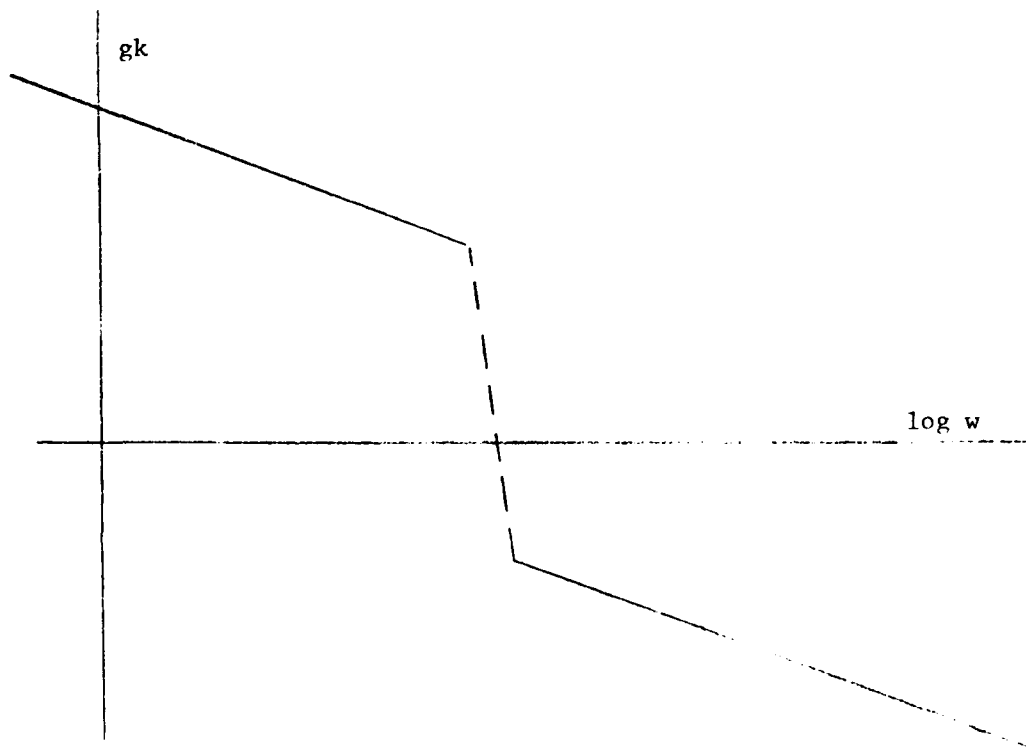
Fig 5.2. An "Ideal" Loop Shape

So what's wrong with this?

For finite dimensional, linear time-invariant transfer functions, Bode (Ref [5-1]) derived relationships between gain and phase, known as the Bode gain-phase relations. Without going into the details, since they involve contour integration of logarithmic and hyperbolic trig functions, these relations show that for a minimum phase SISO transfer function the phase angle near crossover is uniquely determined by the gain. Furthermore, steep attenuation in gain comes only at the expense

of small $|1 + \{g(jw)k(jw)\}^{-1}|$ and $|1 + g(jw)k(jw)|$ values when $|g(jw)k(jw)| \simeq 1$. Therefore, both performance and robustness are poor near crossover if the slope of the loop gain is large.

If the system is non-minimum phase, the right-half plane zeros will reduce total phase at crossover, thus making the problem worse. All of these results have been extended to MIMO systems (Ref [5-2]) (using eigenvalues since singular values are not analytic) and the same properties hold. Therefore, this imposes another limit on achievable performance - loop gains must be reduced gradually before crossover, thus reducing performance near crossover. Also, if $\ell_m(w)$ increases rapidly after crossover, the loop gain may have to be further reduced at lower frequencies.

5.3 Behavior of Non-Minimum Phase Systems

Multivariable non-minimum phase systems are defined by right-half plane transmission zeros. Transmission zeros are defined in Chapter 2 of these notes. They are always undesirable from a feedback point of view. We have already stated in the last section that they reduce the phase angle near crossover and thus reduce stability margins. They cannot be removed from a system through inverse compensation (pole-zero cancellation) since they (as well as any other poles and zeros) are never known exactly. The compensation to remove them would be unstable, and if there was any error in the zero location, the zero would not be cancelled and the compensator would introduce an instability. Thinking of the SISO root locus, the open-loop poles move towards the zeros, and thus a non-minimum phase system goes unstable at some value of gain. This also happens in a multivariable system, and in the frequency domain, loop gains must be small in the frequency range "near" the zero

(Ref [5-3]). We will discuss more ramifications of non-minimum phase

zeros in Chapter 13.

5.4 Directionality in MIMO Systems

The concept of direction in a feedback system is unique to

multivariable systems. Multivariable system signals have a "spatial" as

well as a frequency distribution. For example, some sensors may be

noisier than others, actuators may have different saturation levels,

disturbances may enter only some channels, etc. This leads to the

concept of different bandwidths in various loops. Also, this concept of

varying direction translates into the perturbation matrix L(jw) as well.

The stability tests are tight if all that is known about L(jw) is its

maximum singular value. If we know more about the uncertainty - such as

large in one direction and small in another - then the stability tests

may be sharpened through introducing frequency-dependent weighting

matrices, such as

$$\bar{\sigma}[Q(jw)L(jw)R^{-1}(jw)] < \underline{\sigma}[R(jw)\{I + G(jw)K(jw)\}^{-1}Q^{-1}(jw)] \qquad (5.13)$$

where R(jw) and Q(jw) reflect the known characteristics of the

perturbations. We won't go into any more detail on this here, and the

reader is referred to [5-4] for more details.

This idea of directionality extends one step further. In SISO

systems, inserting uncertainties at the input or at the output of the

plant yields identical results (ie, margins). This is because

g(jw)k(jw) = k(jw)g(jw) when g(jw) and k(jw) are scalar functions. This

is not true in the multivariable case. For MIMO systems, properties of

the system depend upon where the loops are broken. For loop properties

at the output, we use G(jw)K(jw) in all formulas; at the input we use

K(jw)G(jw). Note that in the development in Chapters 7 and 8 we will

concentrate on using $K(jw)G(jw)$ as the loop transfer function, because
we will be looking at input properties. In Chapter 9, we will look at
both. Focusing on stability margins, good margins at one point do not
necessarily imply good margins at another. It _is_ possible to devise a
scheme to fix the margins at one point, then optimize the margins at the
other; more on this may be found in Ref [5-2]. Actually, it may be most
desirable to optimize both margins simultaneously. This requires a
special tool known as the structured singular value (Ref [5-5]), which
was briefly introduced in Chapter 3.

All of these ideas imply a limitation on achievable performance in
a multivariable system. For tight robustness bounds, all loops should
be close together or some transformation will have to be made.
Otherwise, the robustness tests may be quite conservative. If there is
wide separation in the loops, the input and output properties will
differ (possibly radically), and a compromise may have to be made.

Summarizing the entire chapter, feedback design involves tradeoffs.
Analysis and design techniques must make these tradeoffs clear to the
control engineer. As we have already discussed analysis techniques in
Chapter 3, we'll turn our attention toward synthesis. We want a
synthesis method that stabilizes the nominal system and guarantees both
stability and performance of the perturbed system. Also, we require the
tradeoffs to be transparent throughout. In order to build up to the
synthesis method we will develop, we need to start at its most basic
level and modify it accordingly. Thus, the next chapter reviews the
optimal control problem, which forms the basis of our method.

Chapter 5 References

[5-1] H.W. Bode, <u>Network Analysis and Feedback Amplifier Design</u>, D. Van Nostrand, Princeton, 1945.

[5-2] J.C. Doyle, "Limitations on Achievable Performance of Multivariable Feedback Systems", AGARD Lecture Series 117, Sept 1981.

[5-3] I.M. Horowitz, <u>Synthesis of Feedback Systems</u>, Academic Press, N.Y., 1963.

[5-4] M.G. Safonov, "Tight Bounds on the Response of Multivariable Systems with Component Uncertainty", 16th Allerton Conference, Oct 1978.

[5-5] J.C. Doyle, "Analysis of Feedback Systems with Structured Uncertainties," IEE Proceedings, Vol 129, Pt D, No 6, pp 242-250, 1982.

6. A REVIEW OF OPTIMAL CONTROL THEORY

In Chapters 4 and 5, we defined a "good" loop shape and some of the limitations we must face in achieving that shape. In those chapters, we assumed that the nominal closed-loop system was stable. This chapter will give an introduction to optimal control theory, which gives us a synthesis procedure that insures nominal closed-loop stability. In the following chapters, we will examine and modify the procedure so that the goals in Chapter 4 may be achieved. This chapter is by no means a comprehensive study of optimal control -- rather, it is meant to serve as a summary. There are numerous references on optimal control, ranging in difficulty from very basic to highly mathematical and in scope from applications-oriented to theoretically pure. This chapter contains no applications, but does not contain the background theory either. Rather, it attempts to give a generic user-oriented coverage of the required equations, as well as define nomenclature for the remaining chapters. There is a reference list at the end of the chapter containing many of the texts on the subject, where both the theory and many applications may be found.

6.1 The Linear Quadratic Regulator

Suppose that we have the state-space system

$$\dot{x}(t) = Ax(t) + Bu(t) \tag{6.1}$$

where, for now, we make no assumptions on open-loop stability, controllability, etc. We will only consider the time-invariant case here. We wish to minimize the performance index

$$J = \int_0^\infty [x^T(t)Q_c x(t) + u^T R_c u(t)] \, dt \tag{6.2}$$

This performance index, commonly called the quadratic performance index, says that we wish to find a control law $u(t)$ such that the

integral-squared-error of the deviations of the state trajectories from their nominal are kept small without using a great deal of control energy. Q_c and R_c, which are symmetric, real matrices, are chosen by the designer to dictate the relative "importance" of the states and controls.

Obviously, to minimize J we need to insure that J is indeed finite. J will become infinite if uncontrollable, unstable state trajectories are reflected in the performance index. Therefore, if [A, B] is completely controllable, the index J will remain finite. This is actually only a sufficient condition. The necessary and sufficient condition is that [A, B] be stabilizable, which is what we implied by restricting uncontrollable, unstable modes. Under this assumption, only the controllable modes will be moved under feedback (this is obvious from the definition of uncontrollable modes).

Under the assumption of stabilizability, we can always find some feedback law

$$u(t) = -K_c x(t) \tag{6.3}$$

that makes the closed-loop system

$$\dot{x}(t) = Ax(t) + B[-K_c x(t)]$$

$$= [A - BK_c]x(t) \tag{6.4}$$

asymptotically stable and thus results in a finite value of the performance index. Without going into the optimization theory required to prove what the solution is, we will claim that the K_c matrix in (6.3) which minimizes (6.2) is given by

$$K_c = R_c^{-1}B^T P \tag{6.5}$$

where P is the solution to the algebraic Riccati equation

$$0 = A^T P + PA - PBR_c^{-1}B^T P + Q_c \tag{6.6}$$

The above equations require R_c to be positive definite. Also, it may be shown that the minimum value of the performance index is given by

$$J_{min} = x^T(0)Px(0) \tag{6.7}$$

Unfortunately, there is more than one solution to (6.6). In the theoretical development of the problem (which we omitted), the P which produces the minimum value of J given in (6.7) is required to be positive definite (note that all solutions are symmetric, which may be seen by transposing (6.6)). There is only one unique positive definite solution, so this is the one we want. Note that most control software finds only this one, not all possible solutions.

Remember that so far we have only said that there exists a K_c which stabilizes the system. We need to add one more requirement in order to guarantee that the development above will find one. If there are unstable state trajectories which are not "observed" by the performance index, the optimal control law will not attempt to change them and the resulting closed-loop system will not be stable. Alternatively, if all the trajectories do show up in the x^TQ_cx term, closed-loop stability is ensured, since otherwise the index J would be infinite. All the trajectories will appear in x^TQ_cx if Q_c is positive definite, and thus $Q_c > 0$ is a sufficient condition for asymptotic stability. Actually, we can relax the positive definite requirement to positive semidefinite as long as the pair [A, H] is observable, where H is any matrix such that $H^TH = Q_c$ (another way of saying this is that H is a square root of Q). This is easily seen by checking Lyapunov stability criteria, but we will not include the proof here. Usually, we define a system response equation as

$$z(t) = Hx(t) \tag{6.8}$$

6-3

to give a physical meaning to H. This also provides an excellent rationale for choosing Q -- notice that

$$J = \int_0^\infty [x^T Q_c x + u^T R_c u]dt$$

$$= \int_0^\infty [x^T H^T H x + u^T R_c u]dt$$

$$= \int_0^\infty [z^T z + u^T R_c u]dt \qquad (6.9)$$

so that by choosing $Q_c = H^T H$ we are actually requiring regulation of a set of system responses given by (6.8).

Therefore, the requirement of observability of the pair [A, H] is also a sufficient condition for asymptotic stability of the closed-loop system. This may be tightened to a necessary and sufficient condition by requiring detectability of the pair [A, H], since only the unstable modes must be moved. Under a detectability requirement, the requirement that P be positive definite is relaxed to positive semidefinite.

Now we will summarize the results:

Given the stabilizable linear time-invariant plant

$$\dot{x}(t) = Ax(t) + Bu(t) \qquad (6.1)$$

with the performance index

$$J = \int_0^\infty [x^T(t)Q_c x(t) + u^T(t)R_c u(t)]dt \qquad (6.2)$$

where $Q_c = Q_c^T \geq 0$ (positive semidefinite) and $R_c = R_c^T > 0$ (positive definite), a unique optimal control law that minimizes J exists and is given by

$$u(t) = -K_c x(t) \qquad (6.3)$$

with

$$K_c = R_c^{-1} B^T P \qquad (6.5)$$

where P is a constant, symmetric positive semidefinite matrix which is the solution to the algebraic Riccati equation

$$A^T P + PA - PBR_c^{-1}B^T P + Q_c = 0 \qquad (6.6)$$

The closed-loop regulator

$$\dot{x}(t) = [A - BK_c]x(t) = [A - BR_c^{-1}B^TP]x(t) \qquad (6.4)$$

is asymptotically stable if the system given by the state equations
(6.1) and response equations

$$z(t) = Bx(t) \qquad (6.8)$$

is detectable. The minimum value of the performance index is

$$J_{min} = x^T(0)Px(0) \qquad (6.7)$$

6.2 The Kalman Filter

In order to implement the regulator described in the previous
section, we would have to be able to measure <u>all</u> the states in our
system. This is obviously an unrealistic assumption. What we can
measure are outputs, through the sensors in our system. All sensors have
noise associated with them, which means that our measurements are not
perfect. Additionally, real systems will always have some type of
noises or biases affecting them, which will corrupt the state equations.
Therefore, we need a way to reconstruct our state equations and produce
an estimate of them, using our noisy measurements and accounting for the
process noise entering our plant.

We will not go into any probability theory in these notes --
rather, we will assume the reader has a basic level of understanding.
We will consider a stochastic linear system of the form

$$\dot{x}(t) = Ax(t) + Bu(t) + \Gamma\xi(t) \qquad (6.10)$$

$$y(t) = Cx(t) + n(t) \qquad (6.11)$$

where $\xi(t)$ and $n(t)$ are vector random processes called process noise and
measurement noise, respectively. Note that formally the differential
equation in (6.10) is not well defined because of the noise input, but
we will use this form for convenience. The discrete-time case has no

such problem. The processes $\xi(t)$ and $n(t)$ are assumed to be zero-mean, uncorrelated, Gaussian white noises, so that

$$E[\xi(t)] = E[n(t)] = 0 \qquad \forall\ t \qquad (6.12)$$

$$E[\xi(t)\xi^T(\tau)] = Q_0\delta(t-\tau) \qquad (6.13)$$

$$E[n(t)n^T(\tau)] = R_f\delta(t-\tau) \qquad \forall\ t,\tau \qquad (6.14)$$

$$E[\xi(t)n^T(\tau)] = 0 \qquad (6.15)$$

with $Q_0(t)$ and $R_f(t)$ symmetric, positive semidefinite and positive definite matrices, respectively, and δ is the delta function.

What we now wish to do is to produce an estimate, $\hat{x}(T)$, of the state, $x(T)$, at times $T > t_0$, using only the noisy measurement data $\{y(t): t_0 < t < T\}$. We will do this by forming the state error vector

$$e(t) = x(t) - \hat{x}(t) \qquad (6.16)$$

and minimizing the mean-square error

$$e(T) = E[||x(t) - \hat{x}(t)||^2]$$
$$= E[e^T(t)e(t)] \qquad (6.17)$$

We will now skip over the theoretical details and jump to our result. For the time-invariant case, we must assume that $\xi(t)$ and $n(t)$ are wide-sense stationary; the matrices Q_0 and R_f then become constant matrices. Also, we must assume that the observation of the output begins at $t_0 = -\infty$. As long as the observation time is long compared to the dominant time constants of the system, this assumption is reasonably valid.

We will assume that our estimator takes the form of an observer, given by

$$\dot{\hat{x}}(t) = A\hat{x}(t) + Bu(t) + K_f[y(t) - C\hat{x}(t)] \qquad (6.18)$$

The Kalman filter gain matrix, K_f, which minimizes equation (6.17) is given by

$$K_f = \Sigma\, C^T P_f^{-1} \tag{6.19}$$

where Σ is the variance of the error (which, under our assumptions, is constant since $e(t)$ is also stationary), and is found by solving the algebraic variance Riccati equation

$$0 = A\Sigma + \Sigma A^T + Q_f - \Sigma\, C^T R_f^{-1} C \Sigma \tag{6.20}$$

with

$$Q_f = \Gamma Q_o \Gamma^T \tag{6.21}$$

Notice that if $\Gamma = I$ (that is, each state has its own distinct process noise), then $Q_f = Q_o$.

The algebraic variance (filter) Riccati equation shown in (6.20) has several solutions -- the "correct" solution is unique and positive definite. A sufficient condition for Σ to exist as $t_o \rightarrow -\infty$ is that the pair $[A, C]$ be completely observable. This condition may be relaxed to detectability, in which case it is necessary and sufficient and Σ may be positive semidefinite. Given that Σ exists, the error dynamics of the filter are

$$\dot{e}(t) = \dot{x}(t) - \dot{\hat{x}}(t)$$

$$= [Ax(t) + Bu(t) + \Gamma\xi(t)] - [A\hat{x}(t) + Bu(t) + K_f\{y(t) - C\hat{x}(t)\}]$$

$$= Ax(t) + Bu(t) + \Gamma\xi(t) - A\hat{x}(t) - Bu(t)$$
$$\qquad\qquad - K_f[Cx(t) + n(t)] - K_f C\hat{x}(t)$$

$$= [A - K_f C]x(t) - [A - K_f C]\hat{x}(t) + \Gamma\xi(t) - K_f n(t)$$

$$= [A - K_f C]\{x(t) - \hat{x}(t)\} + \Gamma\xi(t) - K_f n(t)$$

$$= [A - K_f C]e(t) + [\Gamma \quad -K_f]\begin{bmatrix}\xi(t)\\n(t)\end{bmatrix} \tag{6.22}$$

Therefore, the poles of $[A - K_f C]$ are the poles of the filter. Obviously, these poles must be stable or the filter will fail to estimate the states (we must have the error going to a small value, not

infinity). A sufficient condition for the filter to be asymptotically stable is that the pair $[A, \Gamma]$ be completely controllable. This may be relaxed to stabilizability, in which case it is a necessary and sufficient condition for stability.

Again, we will summarize our results:

Given the detectable linear time-invariant plant

$$\dot{x}(t) = Ax(t) + Bu(t) + \Gamma\xi(t) \qquad (6.10)$$

$$y(t) = Cx(t) + n(t) \qquad (6.11)$$

with $\xi(t)$ and $n(t)$ being zero-mean, wide-sense stationary, uncorrelated, Gaussian white noises with intensities

$$E[\xi(t)\xi^T(\tau)] = Q_o\delta(t-\tau) \qquad (6.13)$$

$$E[n(t)n^T(\tau)] = R_f\delta(t-\tau) \qquad (6.14)$$

where Q_o is positive semidefinite and R_f is positive definite (both are symmetric). A unique Kalman filter gain matrix which minimizes

$$E[e^T(t)e(t)] \qquad (6.17)$$

where

$$e(t) = x(t) - \hat{x}(t) \qquad (6.16)$$

and $\hat{x}(t)$ is defined by

$$\dot{\hat{x}}(t) = A\hat{x}(t) + Bu(t) + K_f[y(t) - C\hat{x}(t)] \qquad (6.18)$$

is given by

$$K_f = \Sigma C^T R_f^{-1} \qquad (6.19)$$

where Σ is the constant, symmetric, positive semidefinite matrix which is the solution to the algebraic filter Riccati equation

$$0 = A\Sigma + \Sigma A^T + Q_f - \Sigma C^T R_f^{-1} C \Sigma \qquad (6.20)$$

where

$$Q_f = \Gamma Q_o \Gamma^T \qquad (6.21)$$

The filter poles are given by the poles of the error dynamics

6-8

$$\dot{e}(t) = [A - K_fC]e(t) + [\Gamma \quad -K_f]\begin{bmatrix} \xi(t) \\ n(t) \end{bmatrix} \qquad (6.22)$$

which are asymptotically stable iff the pair $[A, \Gamma]$ is stabilizable.

6.3 The Linear Quadratic Gaussian Compensator

Now that we have derived the LQ Regulator, which has the deficiency of assuming all states are available for measurement, and we also have the development of the Kalman filter, which produces an "optimal" estimate of the states, we need to put them together. In this section, we will simply state the problem and its solution.

Given

$$\dot{x}(t) = Ax(t) + Bu(t) + \Gamma\xi(t) \qquad (6.23)$$

$$y(t) = Cx(t) + n(t) \qquad (6.24)$$

$$z(t) = Hx(t) \qquad (6.25)$$

where $\xi(t)$ and $n(t)$ are Gaussian white noise processes with zero means and intensities

$$E[\xi(t)\xi^T(\tau)] = Q_o \delta(t-\tau) \qquad (6.26)$$

$$E[n(t)n^T(\tau)] = R_f \delta(t-\tau) \qquad (6.27)$$

with $Q_o \geq 0$ and $R_f > 0$ (both are symmetric). We wish to find a control law of the form

$$u(t) = i[y(\tau), \tau \leq t] \qquad (6.28)$$

to minimize the criterion

$$J = E\{\lim_{T \to \infty} \frac{1}{T} \int_0^T [z^T(t)z(t) + u^T(t)R_cu(t)]dt\} \qquad (6.29)$$

We must have $[A, B]$ and $[A, \Gamma]$ stabilizable as well as $[A, C]$ and $[A, H]$ detectable. Also, R_c must be symmetric positive definite. The control law which minimizes (6.29) is given by

$$u(t) = -K_c\hat{x}(t) \qquad (6.30)$$

where K_c is the regulator gain matrix given by

$$K_c = R_c^{-1} B^T P \tag{6.31}$$

$$0 = A^T P + PA + Q_c - PBR_c^{-1} B^T P \tag{6.32}$$

$$Q_c = H^T H \tag{6.33}$$

and $\hat{x}(t)$ is the current estimate of the state $x(t)$ based on measurements of $y(\tau)$, $\tau \leqslant t$. This estimate is defined by the Kalman filter

$$\dot{\hat{x}}(t) = A\hat{x}(t) + Bu(t) + K_f[y(t) - C\hat{x}(t)] \tag{6.34}$$

with the Kalman filter gain matrix K_f given by

$$K_f = \Sigma C^T R_f^{-1} \tag{6.35}$$

$$0 = A\Sigma + \Sigma A^T + Q_f - \Sigma C^T R_f^{-1} C\Sigma \tag{6.36}$$

$$Q_f = \Gamma Q_o \Gamma^T \tag{6.37}$$

Under these conditions, the regulator poles, given by

$$\det[sI - A + BK_c] = 0 \tag{6.38}$$

and the filter poles, given by

$$\det[sI - A + K_f C] = 0 \tag{6.39}$$

are guaranteed to be stable. We will now look at the expression for the LQG compensator, that is, the dynamic output feedback compensator made up of the regulator and filter equations. Substituting (6.30) into (6.34) we get

$$\dot{\hat{x}}(t) = A\hat{x}(t) - BK_c\hat{x}(t) + K_f y(t) - K_f C\hat{x}(t)$$

$$= [A - BK_c - K_f C]\hat{x}(t) + K_f y(t) \tag{6.40}$$

Taking Laplace transforms and rearranging yields

$$\hat{x}(s) = [sI - A + BK_c + K_f C]^{-1} K_f y(s) \tag{6.41}$$

Substituting (6.41) into the Laplace transform of (6.30) yields

$$u(s) = -K_c(sI - A + BK_c + K_f C)^{-1} K_f y(s) \tag{6.42}$$

This is the expression for the LQG compensator. We can write the plant transfer function as (omitting the noises for a moment)

$$y(s) = C(sI - A)^{-1} Bu(s) \tag{6.43}$$

Fig 6.1 shows a block diagram of the LQG system.
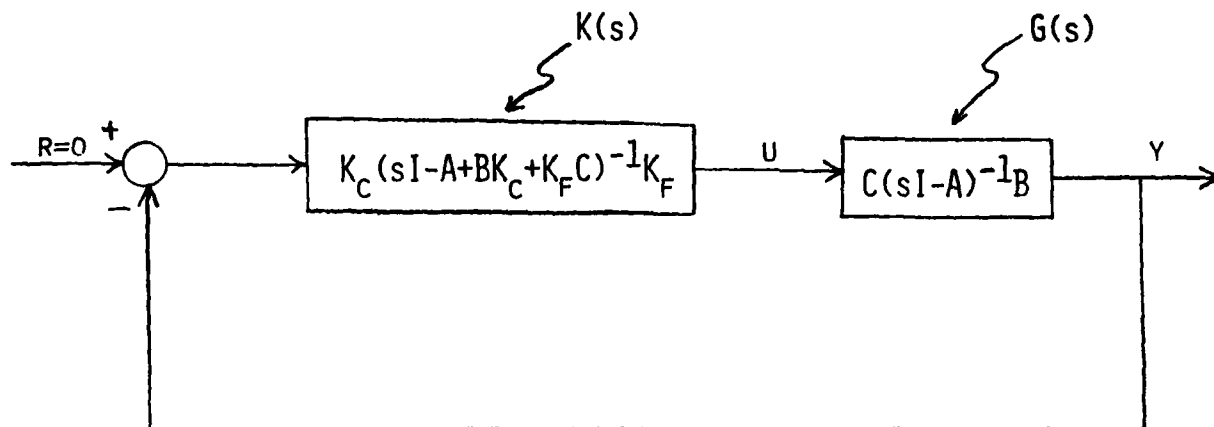
Fig 6.1   Block Diagram of the LQG System

It is easy to show that the poles of the compensator, given by

$$\det[sI - A + BK_c + K_f C] = 0 \qquad (6.44)$$

are not always stable. See the second example in Chapter 8 of these
notes for more discussion on this. We can, however, show that the
closed-loop system is indeed guaranteed to be stable, which is the
crucial requirement.

To show closed-loop stability, we need to look at the eigenvalues
of the closed-loop system. We have two sets of n equations each,
defined by the combination of (6.23) and (6.30), which is

$$\dot{x}(t) = Ax(t) - BK_c \hat{x}(t) + \Gamma \xi(t) \qquad (6.45)$$

and the combination of (6.40) and (6.24), which is

$$\dot{\hat{x}}(t) = [A - BK_c - K_f C]\hat{x}(t) + K_f Cx(t) + K_f n(t) \qquad (6.46)$$

Writing these in state-space form gives

$$\begin{bmatrix} \dot{x}(t) \\ \dot{\hat{x}}(t) \end{bmatrix} = \begin{bmatrix} A & -BK_c \\ K_f C & A - BK_c - K_f C \end{bmatrix} \begin{bmatrix} x(t) \\ \hat{x}(t) \end{bmatrix}$$
$$+ \begin{bmatrix} \Gamma & 0 \\ 0 & K_f \end{bmatrix} \begin{bmatrix} \xi(t) \\ n(t) \end{bmatrix} \qquad (6.47)$$

6-11

The closed-loop LQG poles are therefore given by

$$\det \begin{bmatrix} sI - A & BK_c \\ -K_fC & sI - A + BK_c + K_fC \end{bmatrix} = 0 \qquad (6.48)$$

Unfortunately, stability of the poles is not obvious from (6.48). There is a trick we can do to solve the problem, however. Remember in the last section we defined the estimator error by

$$e(t) = x(t) - \hat{x}(t) \qquad (6.16)$$

so that

$$\dot{e}(t) = \dot{x}(t) - \dot{\hat{x}}(t)$$

$$= [A - K_fC]e(t) + [\Gamma \quad -K_f] \begin{bmatrix} \xi(t) \\ n(t) \end{bmatrix} \qquad (6.22)$$

We can substitute

$$\hat{x}(t) = x(t) - e(t) \qquad (6.49)$$

into (6.45) to obtain

$$\dot{x}(t) = Ax(t) - BK_c[x(t) - e(t)] + \Gamma\xi(t)$$

$$= [A - BK_c]x(t) + BK_ce(t) + \Gamma\xi(t) \qquad (6.50)$$

Now we can write (6.22) and (6.50) in state-space form as

$$\begin{bmatrix} \dot{x}(t) \\ \dot{e}(t) \end{bmatrix} = \begin{bmatrix} A - BK_c & BK_c \\ 0 & A - K_fC \end{bmatrix} \begin{bmatrix} x(t) \\ e(t) \end{bmatrix} + \begin{bmatrix} \Gamma & 0 \\ \Gamma & -K_f \end{bmatrix} \begin{bmatrix} \xi(t) \\ n(t) \end{bmatrix} \qquad (6.51)$$

The eigenvalues of (6.51) must be the same as the eigenvalues of (6.45), because their state vectors are related by a nonsingular linear transformation. Therefore, the closed-loop LQG poles are given by

$$\det \begin{bmatrix} sI - A + BK_c & -BK_c \\ 0 & sI - A + K_fC \end{bmatrix} = 0 \qquad (6.52)$$

Using Schur's formula from Chapter 2, (6.52) may be written as

$$\det[sI - A + BK_c] \cdot \det[sI - A + K_fC] = 0 \qquad (6.53)$$

6-12

Therefore, the closed-loop poles of the overall LQG system are simply the poles of the regulator and the poles of the filter, which we have already shown are guaranteed to be stable. Therefore, LQG compensators always produce stable closed-loop systems.

We have now discussed four sets of poles, which can become confusing if we are not careful. Therefore, we summarize them here, along with the name we will be giving each set from here on:

Regulator poles ---	$\lambda_i[A - BK_c]$	(always stable)
Filter poles ------	$\lambda_j[A - K_fC]$	(always stable)
Compensator poles -	$\lambda_i[A - BK_c - K_fC]$	(not always stable)
Closed-loop poles -	$\lambda_i[A - BK_c], \lambda_i[A - K_fC]$	(always stable)

6.4 Asymptotic Properties of the Regulator and Filter

We will close this chapter by examining properties of the regulator and filter as the control weighting (R_c or R_f) gets very small or very large. This is exactly the same as letting the state weighting get very large or very small, respectively (shown in Appendix 8A). We will not show the full proof here, which is given in Ref [6-1], pp 281-289 and pp 368-370. Rather, we will only state the results.

6.4.1 Asymptotic Regulator Properties

Consider the system given by (6.23) - (6.25). Let the control weighting be

$$R_c = \rho N \qquad (6.54)$$

where $\rho > 0$, $N > 0$. Let

$$G_1(s) = H(sI - A)^{-1}B \qquad (6.55)$$

Then

a) as $\rho \rightarrow 0$, r of the regulator poles approach the values $\hat{z}_i$, $i = 1,2,\ldots,p$, where

$$\hat{z}_i = \begin{cases} z_i & \text{if } \mathrm{Re}(z_i) \leqslant 0 \\ -z_i & \text{if } \mathrm{Re}(z_i) > 0 \end{cases} \tag{6.56}$$

and z_i are the transmission zeros of $G_1(s)$. The remaining $n-p$ poles go to infinity and group into several Butterworth patterns of different orders and different radii.

b) as $\rho \rightarrow \infty$, the n regulator poles approach the values $\hat{\pi}_i$, $i = 1, 2, \ldots, m$, where

$$\hat{\pi}_i = \begin{cases} \pi_i & \text{if } \mathrm{Re}(\pi_i) \leqslant 0 \\ -\pi_i & \text{if } \mathrm{Re}(\pi_i) > 0 \end{cases} \tag{6.57}$$

and π_i are the poles of $G_1(s)$.

It is interesting to note that when control usage is heavily penalized ($\rho \rightarrow \infty$), the optimal regulator will simply move unstable poles to their left-half plane mirror images, and leave stable poles virtually unaffected.

6.4.2 Asymptotic Filter Properties

Again consider the system given by (6.23)-(6.25). Let the measurement noise be represented by

$$R_f = \rho N \tag{6.58}$$

where $\rho > 0$, $N > 0$. Let

$$G_2(s) = C(sI - A)^{-1}\Gamma \tag{6.59}$$

Then

a) as $\rho \rightarrow 0$, p of the filter poles approach the values $\hat{v}_i$, $i = 1, 2, \ldots, n$, where

$$\hat{v}_i = \begin{cases} v_i & \text{if } \mathrm{Re}(v_i) \leqslant 0 \\ -v_i & \text{if } \mathrm{Re}(v_i) > 0 \end{cases} \tag{6.60}$$

and v_i are the transmission zeros of $G_2(s)$. The remaining $n-p$ poles go to infinity and group into several Butterworth patterns of different orders and different radii.

    b)   as $\rho \to \infty$, the n filter poles approach the values $\hat{\pi}_i$, $i = 1,2,\ldots,n$, where

$$\hat{\pi}_i = \begin{cases} \pi_i & \text{if} \quad \text{Re}(\pi_i) \leqslant 0 \\ -\pi_i & \text{if} \quad \text{Re}(\pi_i) > 0 \end{cases} \tag{6.61}$$

Now that we have looked at some general properties of optimal regulators and filters, we will concentrate on specifics. The first aspect we will examine is robustness properties of the regulator, which we take up in the next chapter.

Chapter 6 References

[6-1] H. Kwakernaak and R. Sivan, Linear Optimal Control Systems, Wiley-Interscience, New York, 1972.

[6-2] M. Athans and P. Falb, Optimal Control, McGraw-Hill, New York, 1966.

[6-3] B.D.O. Anderson and J.B. Moore, Linear Optimal Control, Prentice-Hall, N.J., 1971.

[6-4] J.J. D'Azzo and C.H. Houpis, Linear Control System Analysis and Design, McGraw-Hill, New York, 1981.

[6-5] A. Gelb, Applied Optimal Estimation, MIT Press, Cambridge, MA, 1974.

[6-6] P. Maybeck, Stochastic Models, Estimation, and Control, Vol's 1-3, Academic Press, New York, 1979, 1982.

[6-7] D.E. Kirk, Optimal Control Theory: An Introduction, Prentice-Hall, NJ, 1970.

[6-8] T.E. Fortmann and K.L. Hitz, An Introduction to Linear Control Systems, Marcel Dekker, New York, 1977.

[6-9] S.J. Citron, Elements of Optimal Control, Holt, Rinehart, and Winston, New York, 1969.

[6-10] A.E. Bryson and Y-C Ho, Applied Optimal Control, Hemisphere Pub. Co., Washington, 1975.

[6-11] G. Leitmann, The Calculus of Variations and Optimal Control, Plenum Press, New York, 1981.

[6-12] M. Gopal, Modern Control System Theory, Halsted Press, New York, 1984.

[6-13] A.P. Sage and C.C. White, Optimum Systems Control, Prentice-Hall, NJ, 1977.

[6-14] G. Stein and Sandell, "Classical and Modern Methods for Control System Design", Notes for Subject 6.291, Mass. Inst. of Tech., Cambridge, MA, Spring 1979.

[6-15] M. Athans, "Lecture Notes on Multivariable Control Systems", LIDS Report, Mass. Inst. of Tech., Cambridge, MA, June 1984.

[6-16] "Special Issue on the LQG Problem," IEEE Trans Auto. Control, Dec, 1971.

7. GUARANTEED MARGINS OF LINEAR QUADRATIC REGULATORS

A well known property of Linear Quadratic Regulators is that they exhibit guaranteed stability margins. The chapter contains a proof of what these margins are. To do this, we start by using several matrix manipulations on the regulator equations we derived in the last chapter.

7.1 Derivation of the Kalman Inequality

We start by looking at the algebraic Riccati equation for the regulator [note that we will drop the subscript c on Q, R, and K in this chapter since there are no filter equations]

$$PA + A^T P - PBR^{-1}B^T P + Q = 0 \tag{7.1}$$

Using the state equation and feedback law

$$\dot{x} = Ax + Bu \tag{7.2}$$

$$u = -Kx \tag{7.3}$$

we know from the previous chapter that the regulator gain matrix K is given by

$$K = R^{-1}B^T P \tag{7.4}$$

Transposing this yields

$$K^T = PBR^{-1} \tag{7.5}$$

since P and R are symmetric. Using (7.4) and (7.5), the following relation is obvious

$$K^T RK = (PBR^{-1})R(R^{-1}B^T P) = PBR^{-1}B^T P \tag{7.6}$$

Now we can substitute this into (7.1) to yield

$$PA + A^T P - K^T RK + Q = 0 \tag{7.7}$$

Adding and subtracting sP (= Ps) from both sides yields

$$PA - Ps + sP + A^T P - K^T RK + Q = 0 \tag{7.8}$$

Multiplying by (-1) and rearranging gives

$$P(sI - A) + (-sI - A^T)P + K^TRK = Q \tag{7.9}$$

Now, for completely unobvious reasons, multiply both sides of (7.9) on the left by $R^{-\frac{1}{2}}B^T(-sI - A^T)^{-1}$ and on the right by $(sI - A)^{-1}BR^{-1}$, to yield

$$R^{-\frac{1}{2}}B^T(-sI - A^T)^{-1}P(sI - A)(sI - A)^{-1}BP^{-\frac{1}{2}}$$
$$+ R^{-\frac{1}{2}}B^T(-sI - A^T)^{-1}(-sI - A^T)P(sI - A)^{-1}BR^{-\frac{1}{2}}$$
$$+ R^{-\frac{1}{2}}B^T(-sI - A^T)^{-1}K^TRK(sI - A)^{-1}BR^{-\frac{1}{2}}$$
$$= R^{-\frac{1}{2}}B^T(-sI - A^T)^{-1}Q(sI - A)^{-1}BR^{-\frac{1}{2}}$$

or

$$R^{-\frac{1}{2}}B^T(-sI - A^T)PBR^{-\frac{1}{2}} + R^{-\frac{1}{2}}B^TP(sI - A)^{-1}BR^{-\frac{1}{2}}$$
$$+ R^{-\frac{1}{2}}B^T(-sI - A^T)^{-1}K^TRK(sI - A)^{-1}BR^{-\frac{1}{2}}$$
$$= R^{-\frac{1}{2}}B^T(-sI - A^T)^{-1}Q(sI - A)^{-1}BR^{-\frac{1}{2}} \tag{7.10}$$

Notice from (7.4) and (7.5) that

$$R^{-\frac{1}{2}}B^TP = R^{\frac{1}{2}}K \tag{7.11}$$

and

$$PBR^{-\frac{1}{2}} = K^TR^{\frac{1}{2}} \tag{7.12}$$

Substituting these into (7.10) yields

$$R^{-\frac{1}{2}}B^T(-sI - A^T)^{-1}K^TR^{\frac{1}{2}} + R^{\frac{1}{2}}K(sI - A)^{-1}BR^{-\frac{1}{2}}$$
$$+ R^{-\frac{1}{2}}B^T(-sI - A^T)^{-1}K^TRK(sI - A)^{-1}BR^{-\frac{1}{2}}$$
$$= R^{-\frac{1}{2}}B^T(-sI - A^T)^{-1}Q(sI - A)^{-1}BR^{-\frac{1}{2}} \tag{7.13}$$

By divine inspiration (seems that way, anyway), notice that

$$[I + R^{\frac{1}{2}}K(-sI - A)^{-1}BR^{-\frac{1}{2}}]^T[I + R^{\frac{1}{2}}K(sI - A)^{-1}BR^{-\frac{1}{2}}]$$
$$= [I + R^{-\frac{1}{2}}B^T(-sI - A^T)^{-1}K^TR^{\frac{1}{2}}][I + R^{\frac{1}{2}}K(sI - A)^{-1}BR^{-\frac{1}{2}}]$$
$$= I + R^{-\frac{1}{2}}B^T(-sI - A^T)^{-1}K^TR^{\frac{1}{2}} + R^{\frac{1}{2}}K(sI - A)^{-1}BR^{-\frac{1}{2}}$$
$$+ R^{-\frac{1}{2}}B^T(-sI - A^T)^{-1}K^TRK(sI - A)^{-1}BR^{-\frac{1}{2}} \tag{7.14}$$

so that by adding I to each side of (7.13) the resulting equation and (7.14) are equal. Therefore,

$$[I + R^{\frac{1}{2}}K(-sI - A)^{-1}BR^{-\frac{1}{2}}]^T[I + R^{\frac{1}{2}}K(sI - A)^{-1}BR^{-\frac{1}{2}}]$$

$$= I + R^{-\frac{1}{2}}B^T(-sI - A^T)^{-1}Q(sI - A)^{-1}BR^{-\frac{1}{2}} \tag{7.15}$$

Substituting $s = jw$, (7.15) becomes

$$[I + R^{\frac{1}{2}}K(-jwI - A)^{-1}BR^{-\frac{1}{2}}]^T[I + R^{\frac{1}{2}}K(jwI - A)^{-1}BR^{-\frac{1}{2}}]$$

$$= I + R^{-\frac{1}{2}}B^T(-jwI - A^T)^{-1}Q(jwI - A)^{-1}BR^{-\frac{1}{2}} \tag{7.16}$$

It is easy to verify that the left-hand side of (7.16) is Hermitian, and the right-hand side is of the form $I + X^*(jw)QX(jw)$. Both of these facts are shown explicitly in Appendix 7A.

We will adopt the notation $C_1 \geqslant C_2$ for arbitrary Hermitian matrices to indicate that $C_1 - C_2$ is nonnegative. Since $Q \geqslant 0$ from the definition of the state weighting matrix, $X^*(jw)QX(jw) \geqslant 0$. Rewriting (7.16) as

$$[I + R^{\frac{1}{2}}K(-jwI - A)^{-1}BR^{-\frac{1}{2}}]^T[I + R^{\frac{1}{2}}K(jwI - A)^{-1}BR^{-\frac{1}{2}}] - I$$

$$= X^*(jw)QX(jw) \geqslant 0 \tag{7.17}$$

it is obvious that

$$[I + R^{\frac{1}{2}}K(-jwI - A)^{-1}BR^{-\frac{1}{2}}]^T[I + R^{\frac{1}{2}}K(jwI - A)^{-1}BR^{-\frac{1}{2}}] \geqslant I \tag{7.18}$$

The relation in (7.18) is known as the Kalman Inequality.

7.2 Guaranteed Margins for the SISO Case

First, let's look at the SISO case. The Kalman Inequality becomes

$$[1 + r^{\frac{1}{2}}\underline{k}(-jwI - A)^{-1}\underline{b}r^{-\frac{1}{2}}]^T[1 + r^{\frac{1}{2}}\underline{k}(jwI - A)^{-1}\underline{b}r^{-\frac{1}{2}}] \geqslant 1 \tag{7.19}$$

where the underbar denotes vector quantities. The left-hand side can be simplified as follows

$$[1 + r^{\frac{1}{2}}\underline{k}(-jwI - A)^{-1}\underline{b}r^{-\frac{1}{2}}]^T[1 + r^{\frac{1}{2}}\underline{k}(jwI - A)^{-1}\underline{b}r^{-\frac{1}{2}}]$$

$$= [1 + \underline{k}(-jwI - A)^{-1}\underline{b}]^T[1 + \underline{k}(jwI - A)^{-1}\underline{b}]$$

$$= [1 + \underline{k}(jwI - A)^{-1}\underline{b}]^*[1 + \underline{k}(jwI - A)^{-1}\underline{b}]$$

$$= \left|1 + \underline{k}(jwI - A)^{-1}\underline{b}\right|^2 \tag{7.20}$$

Therefore

$$\left|1 + \underline{k}(jwI - A)^{-1}\underline{b}\right|^2 \geqslant 1 \tag{7.21}$$

or

$$\left| 1 + \underline{k}(jwI - A)^{-1}\underline{b} \right| \geqslant 1 \qquad (7.22)$$

Now let's look at a block diagram of the state equations (7.?) and (7.3)
for the SISO case, as shown in Fig 7.1.
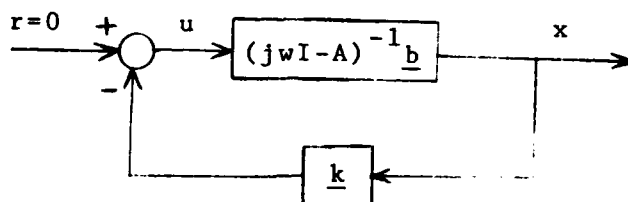
Fig 7.1 SISO Block Diagram for the LQ Regulator

From Fig 7.1, we can see that $1 + \underline{k}(jwI - A)^{-1}\underline{b}$ is the return difference
function for the regulator. Therefore, (7.22) says that the magnitude
of the return difference for a SISO Linear Quadratic Regulator is always
greater than or equal to one. Looking at a polar plot of $\underline{k}(jwI-A)^{-1}\underline{b}$,
this says that the plot must never enter a unit disk centered at the
$-1 + j0$ point. Some typical polar plots are shown in Fig 7.2.

$$a = \underline{k}(jwI-a)^{-1}\underline{b}$$

(a)

(b)

(c)
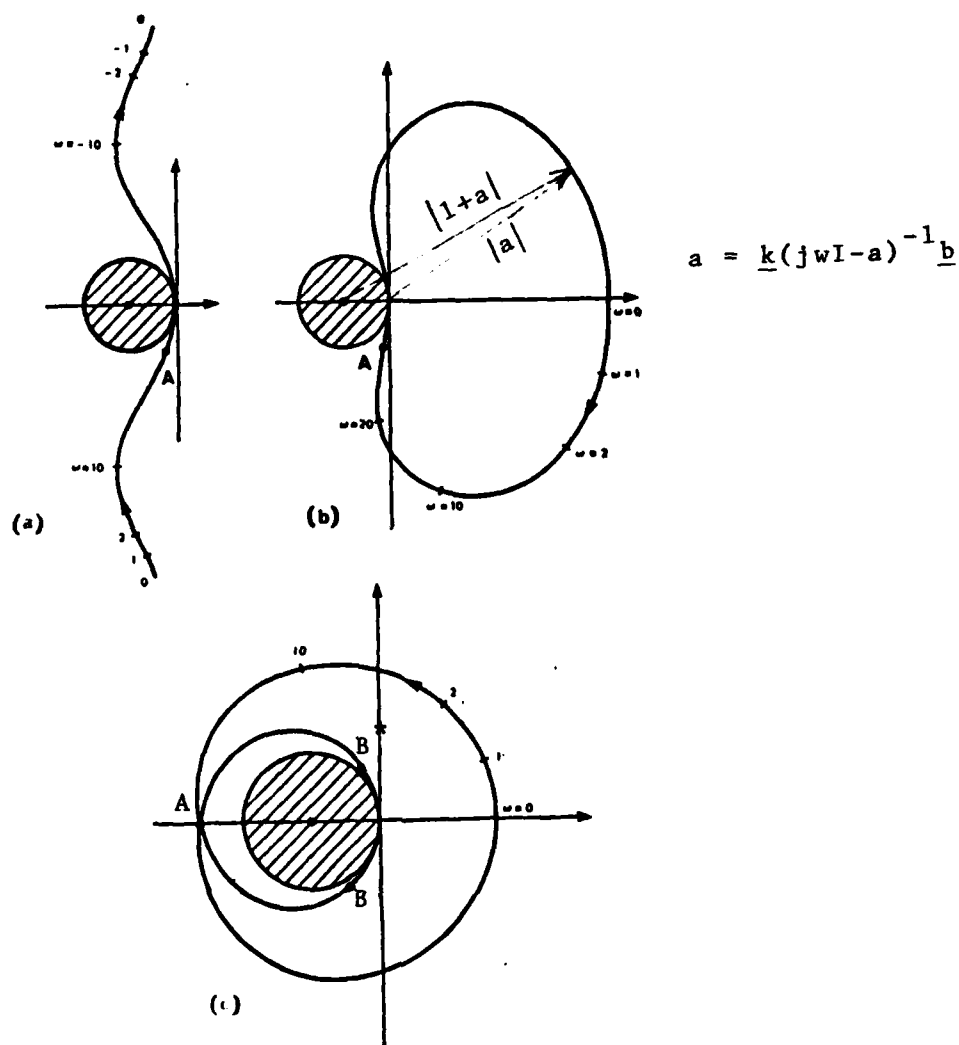
Fig 7.2 Typical polar plots of optimal systems, with disks centered at
          -1 + j0. Note that (c) has two open-loop unstable poles

From these plots, it is easy to verify that the minimum gain margin (GM)
and phase margin (PM) of a Linear Quadratic Regulator are given by

$$\tfrac{1}{2} < GM < \infty \tag{7.23}$$

$$-60° < PM < 60° \tag{7.24}$$

Plot (c) illustrates these limits the best. Obviously, in any of these
plots, the gain may be increased to infinity. If point A in plot (c)
were at the edge of the unit disk (-2+j0 point), which is a worst case,
then the gain could be halved before instability. This yields the

guaranteed (minimum) margin in (7.23). Point B on plot (c) indicates where the polar plot has unit magnitude. Again as a worst case, if B were on the edge of the disk, the angle between B and the negative real axis would be 60°, thus they guaranteed 60° phase margin. The -60° limit is just the margin at the crossing point above the real axis (that is, point B^*).

7.3 Guaranteed Margins for the MIMO Case

Now that we have shown the guaranteed margins for SISO regulators, let's extend this to the MIMO case. First we consider the case where

$$R = \rho I \qquad (7.25)$$

and ρ is a positive scalar. This choice of R is very common and will be used extensively later in these notes. For this choice of R, (7.18) becomes

$$[I + (\rho I)^{\frac{1}{2}} Y (\rho I)^{-\frac{1}{2}}]^* [I + (\rho I)^{\frac{1}{2}} Y (\rho I)^{-\frac{1}{2}}] \geq I \qquad (7.26)$$

where $Y = K(jwI - A)^{-1} B$, and since the ρI terms may be moved to either side of Y, (7.26) is obviously

$$[I + Y]^* [I + Y] \geq I \qquad (7.27)$$

or

$$[I + K(jwI - A)^{-1}B]^* [I + K(jwI - A)^{-1}B] \geq I \qquad (7.28)$$

which is true iff

$$\underline{\sigma}[I + K(jwI - A)^{-1}B] \geq 1 \qquad (7.29)$$

This is proved in Appendix 7B. Notice that the term on the left-hand side of (7.29) is the minimum singular value of the return difference matrix, since $K(jwI - A)^{-1}B$ is again the loop transfer matrix. Looking back to Chapter 3, we see that this equation has the form of (3.40), so that we can define $\alpha_1 = 1$ and plug this value into (3.41) and (3.42) to obtain the gain and phase margins

$$\frac{1}{1 + \alpha_1} < GM < \frac{1}{1 - \alpha_1} \qquad (3.41)$$

or

$$1 < GM < \infty \qquad (7.30)$$

and

$$-2\sin^{-1}(\alpha_1/2) < PM < 2\sin^{-1}(\alpha_1/2) \qquad (3.42)$$

or

$$-60° < PM < 60° \qquad (7.31)$$

This is obviously the same as the SISO result, which is what we expected.

Technically, we still have two more steps before we reach the end. First, we would need to show the margins for any general diagonal R, and then for any general R. The first was shown by Safonov and Athans [7-4], and due to its complexity will not be shown here. Again the guaranteed margins are as in (7.30) and (7.31). Finally, since any general selection for R can always be equivalently replaced by some diagonal choice [7-5], we have the final result. Thus, (7.30) and (7.31) are the guaranteed minimum gain and phase margins for any Linear Quadratic Regulator.

Unfortunately, these results are true in theory only. From an intuitive viewpoint, we should know that gain cannot be increased infinitely for a real system. Let's take a look at why the theory tells us it can, and what the implications of the practical limitations are.

Any full-state feedback design always results in a loop transfer function with one more pole than zero. For a SISO system, this can be seen by rearranging the block diagram so that the compensator has the form $u = k_{eq}y$, as done in Ref [7-6]. It is clear that k_{eq} will have $(n-1)$ zeros, where n is the number of poles of g, thus giving gk_{eq} a

one-pole excess (the zeros of g are the poles of k_{eq}). This can also be extended to the MIMO case. Remember that the LQ Regulator is a full-state feedback design, so it must have this property. This means that the regulator will have high frequency attenuation of the form

$$g(s)k_{eq}(s) = \underline{k}(sI - A)^{-1}\underline{b} \longrightarrow \underline{kb}/s \quad \text{as} \quad s \to \infty \tag{7.32}$$

The above condition is a violation of the Bode-Horowitz condition (Ref [7-7]), which says that for real systems, the following relation must hold

$$\int_0^\infty \ln\left|1 + g(jw)k_{eq}(jw)\right|dw = 0 \tag{7.33}$$

For this to be true, $g(jw)k_{eq}(jw)$ must have at least two more poles than zeros. Therefore, LQ Regulators violate this condition. Does that mean they should be ignored? No, it doesn't. Any real system will always have dynamics we cannot model, and these dynamics will give us the additional roll-off (7.33) requires. These dynamics will cause the plot of $g(jw)'k_{eq}(jw)$ to enter the unit circle centered at $-1 + j0$, where $g'(jw)$ is the real system. This destroys our guaranteed margins. In order to minimize the reduction in stability margins this causes, the bandwidth of $g(jw)k_{eq}(jw)$ must be below the frequency where the unmodelled dynamics become significant. The above arguments can also be extended to the MIMO case. We have already concluded that this is one of the requirements our system must meet, so this is no surprise. The purpose of the discussion was simply to show that the guaranteed margins are for the _model_ of the system, not the real system.

Appendix 7A

1) Show that the left-hand side of (7.16) is Hermitian.

To do this, we must show that

$$\{[I + R^{\frac{1}{2}}K(-jwI - A)^{-1}BR^{-\frac{1}{2}}]^T[I + R^{\frac{1}{2}}K(jwI - A)^{-1}BR^{-\frac{1}{2}}]\}^* \qquad (7A.1)$$

equals the left-hand side of (7.16). Carrying out the * operation

$$(7A.1) = [I + R^{\frac{1}{2}}K(jwI - A)^{-1}BR^{-\frac{1}{2}}]^*[I + R^{\frac{1}{2}}K(-jwI - A)^{-1}BR^{-\frac{1}{2}}]^{T*}$$

$$= [I + R^{-\frac{1}{2}}B^T(-jwI - A^T)^{-1}K^TR^{\frac{1}{2}}][I + R^{\frac{1}{2}}K(jwI - A)^{-1}BR^{-\frac{1}{2}}]$$

$$= [I + R^{\frac{1}{2}}K(-jwI - A)^{-1}BR^{-\frac{1}{2}}]^T[I + R^{\frac{1}{2}}K(jwI - A)^{-1}BR^{-\frac{1}{2}}]$$

$$= \text{l.h.s. of } (7.16) \qquad\qquad\qquad \text{Q.E.D.}$$

2) Show that the right-hand side of (7.16) is of the form
$I + X^*(jw)QX(jw)$.

To do this, define $X(jw)$ as

$$X(jw) = (jwI - A)^{-1}BR^{-\frac{1}{2}} \qquad (7A.2)$$

so that

$$X^*(jw) = R^{-\frac{1}{2}}B^T(-jwI - A^T)^{-1} \qquad (7A.3)$$

Now

$$I + X^*(jw)QX(jw)$$

$$= I + R^{-\frac{1}{2}}B^T(-jwI - A^T)^{-1}Q(jwI - A)^{-1}BR^{-\frac{1}{2}}$$

$$= \text{r.h.s. of } (7.16) \qquad\qquad\qquad \text{Q.E.D.}$$

Appendix 7B

Proposition: $A^*A \geqslant I$ iff $\underline{g}(A) \geqslant 1$ (7B.1)

Proof: If B is Hermitian ($B = B^*$), then there exists a unitary matrix P ($P^*P = I$) such that P^*BP is diagonal (see Ref [7-2]). Now let $B = A^*A$. Then

$$P^*A^*AP = \Lambda \qquad (7B.2)$$

Premultiplying (7B.2) by $(P^*)^{-1}$ and postmultiplying by P^{-1} yields

$$A^*A = (P^*)^{-1}\Lambda P^{-1} = P\Lambda P^* \geqslant I \qquad (7B.3)$$

Remember that Λ can be represented by

$$\Lambda = \text{diag}[\lambda_1, \lambda_2, \ldots, \lambda_n] \qquad (7B.4)$$

There is no loss of generality to assume that $\lambda_1 \geqslant \lambda_2 \geqslant \ldots \geqslant \lambda_n \geqslant 0$, since Hermitian matrices have only positive eigenvalues. Premultiplying by $\underline{x}^*$ and postmultiplying by $\underline{x}$ yields

$$\underline{x}^*P\Lambda P^*\underline{x} \geqslant \underline{x}^*\underline{x} \qquad \underline{x} \in C^n \qquad (7B.5)$$

Now, let's choose

$$\underline{x} = P \begin{bmatrix} 0 \\ 0 \\ . \\ . \\ . \\ 1 \end{bmatrix} \qquad (7B.6)$$

Then

$$\underline{x}^*P\Lambda P^*\underline{x} = [0 \ 0 \ \ldots \ 1] \Lambda \begin{bmatrix} 0 \\ 0 \\ . \\ . \\ . \\ 1 \end{bmatrix} = \lambda_n(P^*A^*AP) = \lambda_n(A^*A)$$

$$= \underline{g}^2(A) \geqslant [0 \ 0 \ \ldots \ 1] \begin{bmatrix} 0 \\ 0 \\ . \\ . \\ . \\ 1 \end{bmatrix} = 1 \qquad (7B.7)$$

Therefore

7-10

$$\underline{g}(A) \geqslant 1 \qquad\qquad (7B.8)$$

This proves that

$$A^*A \geqslant I \Longrightarrow \underline{g}(A) \geqslant 1 \qquad\qquad (7B.9)$$

Now, to conclude the iff proof, we must show that

$$\underline{g}(A) \geqslant 1 \Longrightarrow A^*A \geqslant I \qquad\qquad (7B.10)$$

Instead, we will prove the contrapositive

$$A^*A < I \Longrightarrow \underline{g}(A) < 1 \qquad\qquad (7B.11)$$

which is logically equivalent (see Ref [7-3] for a review of logical

proofs). This proof is trivial -- replace "$\geqslant$" with "$<$" in (7B.3)-(7B.9)

and we have the desired result. This completes the proof.

Chapter 7 References

[7-1] B.D.O. Anderson and J.B. Moore, <u>Linear Optimal Control</u>, Prentice-Hall, N.J., 1971.

[7-2] K. Hoffman and R. Kunze, <u>Linear Algebra</u>, Prentice-Hall, N.J., 1971.

[7-3] R.B. Reisel, <u>Elementary Theory of Metric Spaces</u>, Springer-Verlag, New York, 1983.

[7-4] M.G. Safanov and M. Athans, "Gain and Phase Margin for Multiloop LQG Regulators", IEEE Trans. Auto. Control, Vol AC-22, pp 173-179, Apr 1977.

[7-5] T.E. Bullock and J.M. Elder, "Quadratic Performance Index Generation for Optimal Regulator Design", 10th IEEE Conference on Decision and Control, pp 123-124, 1971.

[7-6] J.J. D'Azzo and C.H. Houpis, <u>Linear Control System Analysis and Design</u>, McGraw-Hill, New York, 1981.

[7-7] I.M. Horowitz, <u>Synthesis of Feedback Systems</u>, Academic Press, New York, 1963.

8. USING OBSERVERS TO RECOVER REGULATOR MARGINS

In this chapter, we will develop a method to "tune" an observer (specifically, a Kalman filter) so that the guaranteed margins of the regulator are nearly achieved. Obviously, this implies that the guaranteed margins of a system with an observer included are not, in general, those of the regulator. We will start by showing that they are not.

8.1 Non-Existence of Guaranteed Margins for an Observer-Based System

A formal proof of non-existence of guaranteed margins for an observer-based system is actually not necessary. Rather, all we need is a counter-example which shows that the guaranteed margins of the LQR do not extend to the observer-in-the-loop case. The observer we will use is the standard Kalman filter, i.e., Linear Quadratic Gaussian (LQG) control. The same type of results can also be shown for the case of a general observer.

Example

Consider the following state space description:

$$\dot{x} = Ax + Bu + \Gamma \xi$$

$$= \begin{bmatrix} -1 & -1 \\ 0 & -1 \end{bmatrix} \begin{bmatrix} x_1 \\ x_2 \end{bmatrix} + \begin{bmatrix} 0 \\ 1 \end{bmatrix} u + \begin{bmatrix} 1 \\ 1 \end{bmatrix} \xi \qquad (8.1)$$

$$y = Cx + n = \begin{bmatrix} 1 & 0 \end{bmatrix} \begin{bmatrix} x_1 \\ x_2 \end{bmatrix} + n \qquad (8.2)$$

$$z = Hx = \begin{bmatrix} 1 & 1 \end{bmatrix} \begin{bmatrix} x_1 \\ x_2 \end{bmatrix} \qquad (8.3)$$

where ξ and n are Gaussian white noises with intensities $\gamma(>0)$ and 1, respectively. Without going into the details, we will let the state weighting matrix Q_c be

$$Q_c = qH^TH = q\begin{bmatrix}1\\1\end{bmatrix}[1 \quad 1] = q\begin{bmatrix}1 & 1\\1 & 1\end{bmatrix} \tag{8.4}$$

where $q > 0$, and let the control weighting R_c be

$$R_c = 1 \tag{8.5}$$

First, we will let $q = \gamma = 1$ and solve the LQG problem. As a refresher, this means we wish to find the regulator and filter gains given by (see Chapter 6)

$$u = -K_c x \tag{8.6}$$

$$K_c = R_c^{-1}B^TP \tag{8.7}$$

$$0 = PA + A^TP + Q_c - PBR_c^{-1}B^TP \tag{8.8}$$

and

$$\dot{\hat{x}} = A\hat{x} + Bu + K_f(y - C\hat{x}) \tag{8.9}$$

$$K_f = \Sigma C^T R_f^{-1} \tag{8.10}$$

$$0 = A\Sigma + \Sigma A^T + Q_f - \Sigma C^T R_f^{-1} C\Sigma \tag{8.11}$$

where $R_f = 1$ (strength of n) and $Q_f = \Gamma\gamma\Gamma^T$. Solving these equations, we get

$$K_c = [0.2361 \quad 0.2361] \tag{8.12}$$

$$K_f = \begin{bmatrix}0.2361\\0.2361\end{bmatrix} \tag{8.13}$$

Note that with $q = \gamma$, the solution matrices are dual (identical but transposed). The open-loop plant has two poles at -1, while the closed-loop LQG system has poles at

$$\lambda\{A_{CL}\} = \{-0.618, -1.618, -0.618, -1.618\} \tag{8.14}$$

8-2

Now we need to examine the stability margins of this system. Since
this is a SISO system, all we really need to do is find these from Bode
or polar plots of the loop transfer function. However, we will follow
the method of Chapters 3 and 7 and find the margins by using $\underline{\sigma}[I + KG]$
instead. You can verify for yourself (if you wish) that the results are
the same. Also note that since this is a SISO system, KG = GK, so the
margins at the input and output of the plant are the same. The
expression for K(s), the LQG compensator, was derived in Chapter 6. The
plot of $\underline{\sigma}[I + KG]$ vs. frequency is shown in Fig 8.1. Note that
$\underline{\sigma}[I + KG] = |1 + kg|$ for a SISO system.
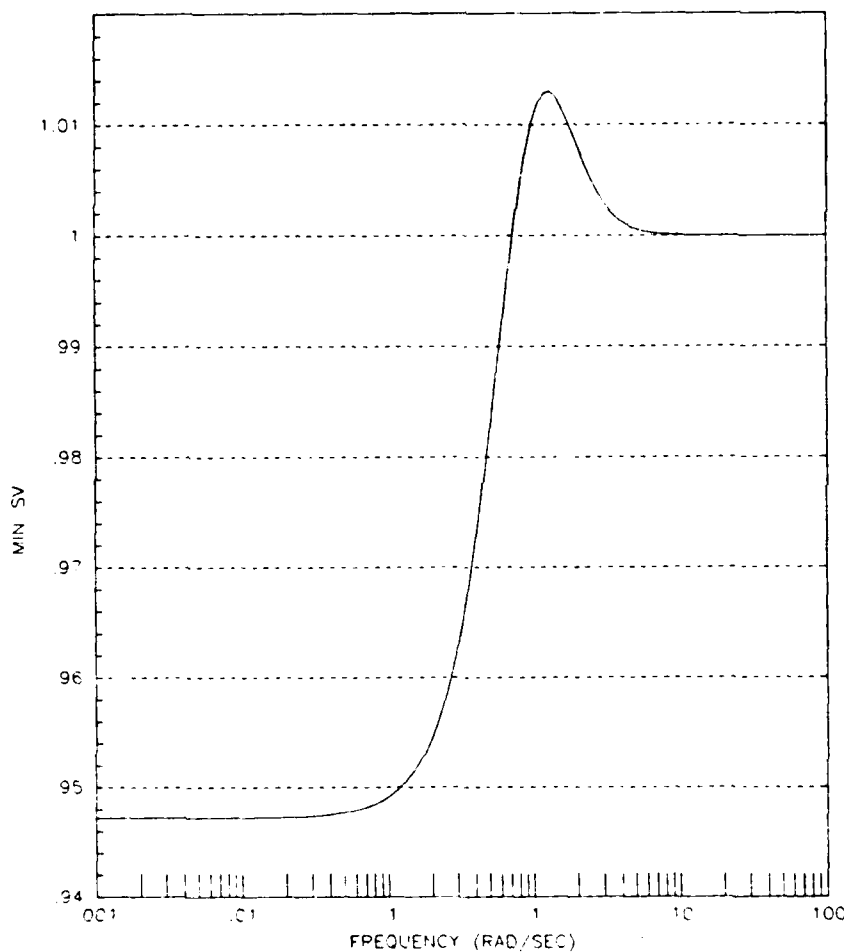
Fig 8.1 $\underline{\sigma}[I + KG]$ vs. Frequency for $\alpha = \gamma = 1$

From this plot we can see that

$$\inf_{\omega} \underline{\sigma}[I + KG] = 0.947 \tag{8.15}$$

which is α_1 by the notation of Chapter 3. Therefore, by (3.41) and (3.42)

$$0.514 < GM < 18.94 \tag{8.16}$$

$$-56.50° < PM < 56.50° \tag{8.17}$$

which obviously violates the guaranteed margins we had before (see Chapter 7).

Now, in an attempt to make the system "better", we can try to speed up the regulator and filter by increasing q and γ to increase K_c and K_f. This is an ad hoc procedure often used to improve performance. We will let q and γ be equal (simply for convenience), and let them have values of 2, 5, 10, and 100. Fig 8.2 shows a superimposing of the plots of $\underline{\sigma}[I + KG]$ for these values of $q = \gamma$, along with $q = \gamma = 1$. Note that the infimum of these plots decreases as $q = \gamma$ increases, which implies the margins decrease. The margins are shown in Table 8.1 for different values of q and γ.

Table 8.1 Gain and Phase Margins for Values of q and γ				
$q = \gamma$	GM		PM	
1	0.514	18.94	-56.5°	56.5°
2	0.546	5.95	-49.2°	49.2°
5	0.667	2.00	-29.0°	29.0°
10	0.801	1.33	-14.2°	14.2°
100	0.986	1.015	-0.8°	0.8°

The table shows that arbitrarily speeding up the regulator and filter (i.e., increasing control power) can actually degrade the system from a stability robustness point of view.
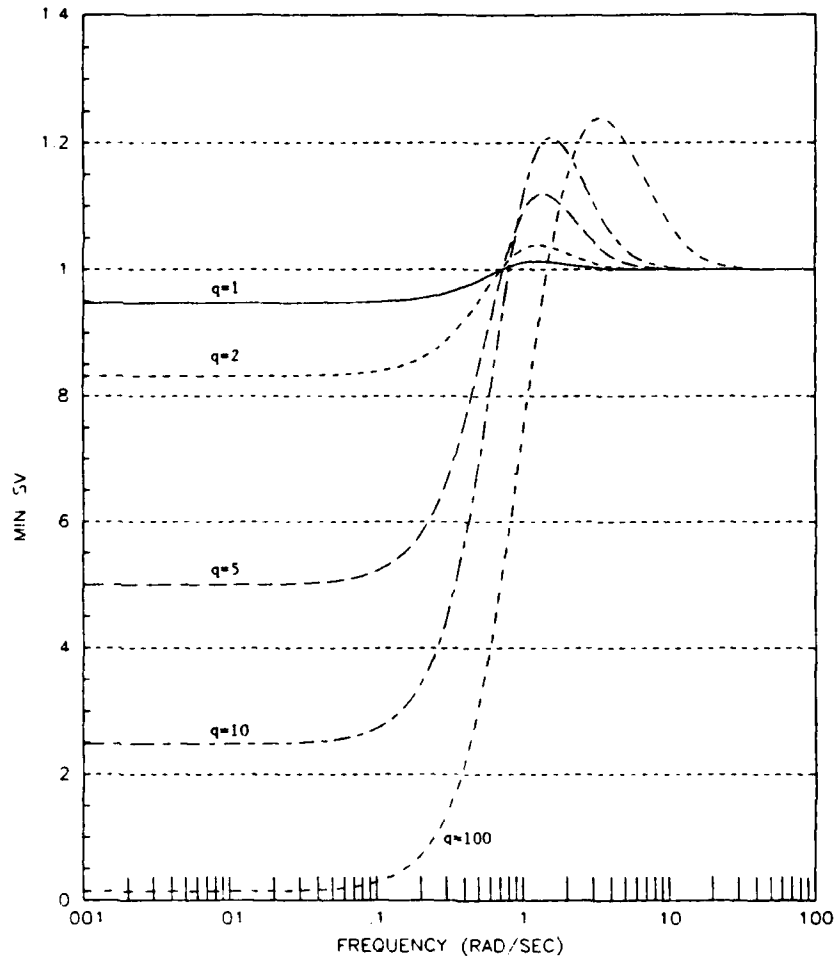
Fig 8.2 $\underline{\sigma}[I + KC]$ vs. Frequency for q = γ = 1, 2, 5, 10, and 100

Let's take a quick look at an interesting point. In this system,
the regulator moves the open-loop poles from {-1, -1} to {-0.618, -1.618}
for q = 1. One may argue that the improvement afforded by the control
system here is minimal. First, that's not the point of the example.
The point is not to design a "good" optimal controller -- rather, we
simply wanted a counter-example to show that there are no guaranteed
margins. Not only are there no guarantees, the margins were shown to be
arbitrarily small for certain controllers. Secondly, if we change A to
-A in (8.1), which makes the open-loop eigenvalues {+1, +1}, the

closed-loop regulator poles for q = 1 are again {-0.618, -1.618}.

Obviously, this _is_ a marked improvement from the open-loop system.

However, Fig 8.3 shows a plot of $\underline{\sigma}[I + KG]$ for this system, which has

$$\inf_{\omega} \underline{\sigma}[I + KG] = 0.0528 \tag{8.18}$$

so that the margins are

$$0.95 < GM < 1.06 \tag{8.19}$$

$$-3.0° < PM < 3.0° \tag{8.20}$$

which are miserable.
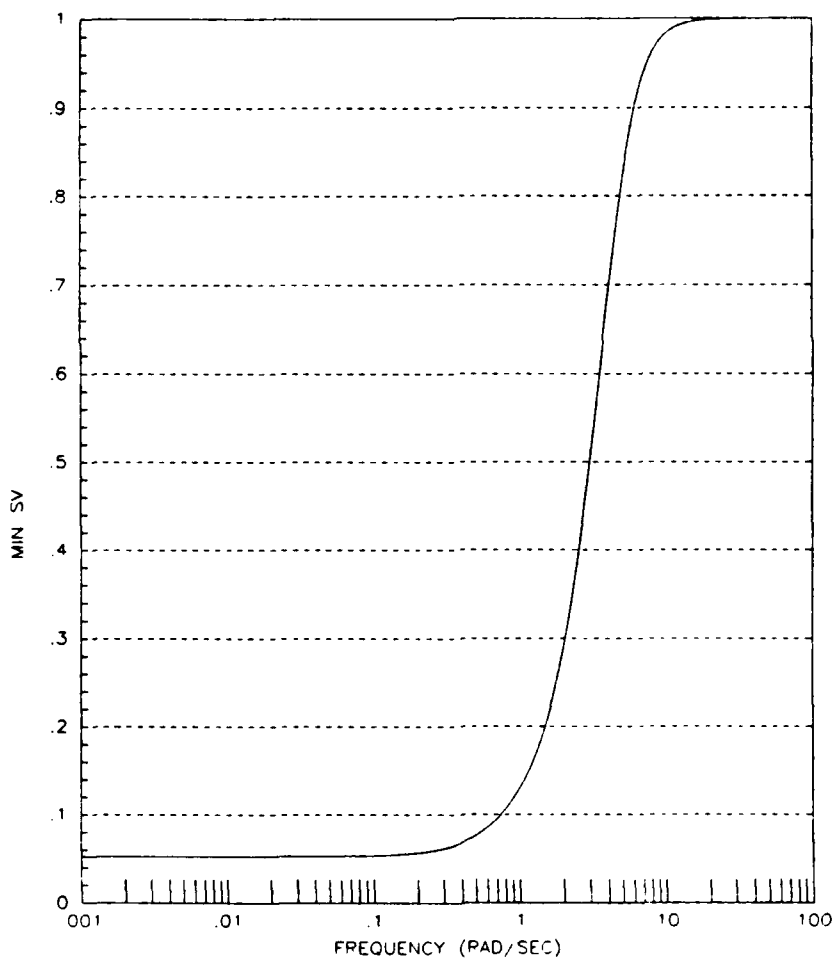
Fig 8.3 $\underline{\sigma}[I + KG]$ vs. Frequency for q = γ = 1, with A = -1.

8-6

This highlights one of the biggest problems with LQG control in the past
-- it has the attraction of being "optimal" and guaranteed closed-loop
stable. Unfortunately, many times it is very sensitive to errors, as
the above system is, and this accounts for many of its past failures
when used on practical systems. In the next section, we will present a
method to "tune" the filter so that it recovers the full-state feedback
properties, which we showed had excellent margins. In the next chapter,
we will couple this with the loop property ideas of Chapters 4 and 5, in
order to incorporate frequency-domain specifications.

8.2 Relationships Between Full-State Feedback and Observer-Based Feedback

First, let's look at a block diagram of a general structure
full-state and observer-based feedback system.

Fig 8.4 Full-State Feedback

Fig 8.5 Observer-Based Feedback

In Fig 8.4, note that H_1 and H_2 are a feedforward and feedback gain matrix, respectively. In Fig 8.5, H_1 and H_2 have the same meaning as above, and K is the observer gain matrix. Now we will state and prove three properties concerning the loop properties of the two systems.

Property 1 - The closed-loop transfer matrices from command signals r to states x are identical in both implementations.

Proof: For the full-state feedback case,

$$x = \Phi Bu'' = \Phi Bu' = \Phi Bu \qquad (8.21)$$

since all loops are intact (i.e., no break at X or XX). Here, Φ is used in place of $(sI - A)^{-1}$. Notice that

$$u = H_1(r - H_2 x) \qquad (8.22)$$

Substituting (8.21) into (8.22) and simplifying yields

$$u = H_1(r - H_2 \Phi Bu)$$

$$= H_1 r - H_1 H_2 \Phi Bu \qquad (8.23)$$

or

$$u = (I + H_1 H_2 \Phi B)^{-1} H_1 r \tag{8.24}$$

Substituting (8.24) into (8.21) yields

$$x = \Phi B (I + H_1 H_2 \Phi B)^{-1} H_1 r \tag{8.25}$$

For the observer-based case,

$$x = \Phi B u'' = \Phi B u' = \Phi B u \tag{8.26}$$

since, once again, all loops are intact. Notice that

$$\hat{x} = \Phi(Bu' + K[y - C\hat{x}]) \tag{8.27}$$

and

$$y = Cx \tag{8.28}$$

so that, substituting (8.28) and (8.26) into (8.27) and simplifying we get

$$
\begin{aligned}
\hat{x} &= \Phi(Bu' + KCx - KC\hat{x}) \\
&= \Phi(Bu' + KC\Phi B u'' - KC\hat{x}) \\
&= \Phi(Bu' + KC\Phi B u'') - \Phi KC\hat{x}
\end{aligned}
\tag{8.29}
$$

or

$$\hat{x} = (I + \Phi KC)^{-1} \Phi[Bu' + KC\Phi B u''] \tag{8.30}$$

Now, since $u' = u''$ in this case

$$
\begin{aligned}
\hat{x} &= (I + \Phi KC)^{-1} \Phi(B + KC\Phi B)u' \\
&= (I + \Phi KC)^{-1}(\Phi + \Phi KC\Phi)Bu' \\
&= (I + \Phi KC)^{-1}(I + \Phi KC)\Phi Bu' \\
&= \Phi Bu'
\end{aligned}
\tag{8.31}
$$

In this case u' also equals u, so that

$$\hat{x} = \Phi Bu \tag{8.32}$$

Looking at the control law,

$$u = H_1(r - H_2\hat{x}) \tag{8.33}$$

and substituting (8.32) into (8.33), we get

$$u = H_1 r - H_1 H_2 \Phi Bu \tag{8.34}$$

or

$$u = (I + H_1 H_2 \Phi B)^{-1} H_1 r \tag{8.35}$$

Now, substituting (8.35) into (8.26) we get

$$x = \Phi B (I + H_1 H_2 \Phi B)^{-1} H_1 r \tag{8.36}$$

which is the same as the full-state feedback result in (8.25). QED

Property 2 - The loop transfer functions from control signals u' to control signals u (loops broken at XX) are identical in both implementations.

Proof: To calculate loop transfer functions, we assume external inputs to be zero; therefore, $r = 0$. Note that here, $u' = u''$, but $u' \neq u$. For the full-state feedback case,

$$u = -H_1 H_2 x \tag{8.37}$$

$$x = \Phi B u'' = \Phi B u' \tag{8.38}$$

and combining these

$$u = -H_1 H_2 \Phi B u' \tag{8.39}$$

For the observer-based case,

$$u = -H_1 H_2 \hat{x} \tag{8.40}$$

Substituting (8.31) into this equation (note that (8.31) is valid here since the only assumption at that point is $u'' = u'$), we get

$$u = -H_1 H_2 \Phi B u' \tag{8.41}$$

which is the same as the full-state feedback result in (8.39). QED

Property 3 - The loop transfer functions from control signals u" to control signals u' (loops broken at X) are, in general, different.

Proof: Note that here, $u' = u$, but $u'' \neq u'$. For the full-state feedback case,

$$x = \Phi B u'' \tag{8.42}$$

and

$$u' = u = -H_1 H_2 x \qquad (8.43)$$

so that

$$u' = -H_1 H_2 \Phi B u'' \qquad (8.44)$$

For the observer-based case, from (8.29) we have

$$\hat{x} = \Phi(Bu' + KC\Phi Bu'') - \Phi KC\hat{x} \qquad (8.45)$$

or

$$(I + \Phi KC)\hat{x} = \Phi(Bu' + KC\Phi Bu'') \qquad (8.46)$$

Note that this is equal to

$$\Phi(\Phi^{-1} + KC)\hat{x} = \Phi(Bu' + KC\Phi Bu'') \qquad (8.47)$$

Notice that Φ^{-1} must exist because

$$\Phi^{-1} = [(sI - A)^{-1}]^{-1} = sI - A \qquad (8.48)$$

Now, premultiplying both sides of (8.47) by $(\Phi^{-1} + KC)^{-1}\Phi^{-1}$ we get

$$\hat{x} = (\Phi^{-1} + KC)^{-1}(Bu' + KC\Phi Bu'')$$

$$= [\Phi^{-1}(I + \Phi KC)]^{-1}(Bu' + KC\Phi Bu'')$$

$$= (I + \Phi KC)^{-1}\Phi(Bu' + KC\Phi Bu'') \qquad (8.49)$$

Now we get clever. From Chapter 2 of these notes,

$$(I + G_2 G_1 F_2 F_1)^{-1} G_2 G_1 = G_2 G_1 - G_2 G_1 F_2 (I + F_1 G_2 G_1 F_2)^{-1} F_1 G_2 G_1 \qquad (2.21)$$

Defining $G_2 G_1 = \Phi$, $F_1 = C$, and $F_2 = K$, we can see that

$$(I + \Phi KC)^{-1}\Phi = \Phi - \Phi K(I + C\Phi K)^{-1} C\Phi \qquad (8.50)$$

Substituting this into (8.49) and simplifying yields

$$\hat{x} = [\Phi - \Phi K(I + C\Phi K)^{-1} C\Phi](Bu' + KC\Phi Bu'')$$

$$= \Phi Bu' - \Phi K(I + C\Phi K)^{-1} C\Phi Bu' + \Phi KC\Phi Bu''$$

$$- \Phi K(I + C\Phi K)^{-1} C\Phi KC\Phi Bu''$$

$$= \Phi B(C\Phi B)^{-1}(C\Phi B)u' - \Phi K(I + C\Phi K)^{-1}(C\Phi B)u'$$

$$+ \Phi K(C\Phi B)u'' - \Phi K(I + C\Phi K)^{-1} C\Phi K(C\Phi B)u''$$

$$= \Phi[B(C\Phi B)^{-1} - K(I + C\Phi K)^{-1}]C\Phi Bu'$$

$$+ \Phi K[I - (I + C\Phi K)^{-1} C\Phi K]C\Phi Bu''$$

$$= \Phi[B(C\Phi B)^{-1} - K(I + C\Phi K)]C\Phi Bu'$$

$$+ \Phi K[(I + C\Phi K)^{-1}\{(I + C\Phi K) - C\Phi K\}]C\Phi Bu''$$

$$= \Phi[B(C\Phi B)^{-1} - K(I + C\Phi K)^{-1}]C\Phi Bu'$$

$$+ \Phi[K(J + C\Phi K)^{-1}]C\Phi Bu'' \qquad (8.51)$$

Note that the only assumption we have made in this development is that $(C\Phi B)^{-1}$ exists. Obviously, $C\Phi B$ is the plant transfer function; therefore, we have assumed the plant to be square and invertible. Later, we will generalize this to non-square plants. The invertibility requirement implies that the plant must have no zeros in the right-half s-plane (i.e., it must be minimum phase).

Now we can write

$$u' = u = -H_1 H_2 \hat{x} \qquad (8.52)$$

from Fig 8.5. Substituting $\hat{x}$ from (8.51) into (8.52), the result is obviously not equal to (8.44) (the full-state feedback result), in general. QED

Now let's look at the ramifications of these three properties:

Property 1 – Input/output properties are the same. This is true because we have assumed a perfect observer.

Property 2 – For loops broken at XX, the robustness, relative stability properties, and disturbance properties are the same. This means that if this set of properties is guaranteed to be good in one implementation, it is guaranteed to be equally good in the other.

Property 3 – For loops broken at X, the above three properties are not the same for each implementation, in general. Guaranteed "goodness" in one implies nothing for the other.

Perhaps you can see the punchline now. The loop-breaking point XX is internal to each of the compensators -- assuming uncertainties here

does not make sense. If we do, we are saying that we don't know if we can build the compensator we design, but we do know the system we are designing it for perfectly. This is the reverse of what we have assumed. Rather, we need to examine loop properties when breaking at X, which is a point external to the compensator and at the plant input. Loop properties at such a point would be related to $[I + K(s)G(s)]$ -- note that for the full-state feedback LQR case, we have proven guaranteed "good" properties for this return difference matrix in Chapter 7. Unfortunately, Property 3 does not allow us to infer that these properties hold for the observer case in general. Therefore, the bottom line is, once again, observer-based feedback does not have guaranteed margins for arbitrary observer gains.

You may have noticed that we keep saying "in general" when we talk about Property 3. Are we implying that there is a way to make the loop properties the same for loops broken at X? Yes there is, and we'll show that next.

8.3 Equating Loop Properties to Recover Robustness

Basically, we have determined that the main problem with using observers (remember that a Kalman filter is an observer) is that the loop properties are different from the full-state feedback case when breaking at point Y in Figs 8.4 and 8.5. Point Y is at the input to the plant, where we know the full-state feedback case has excellent loop properties when the feedback gains are chosen by solving the LQR problem. What we would now like to have is a way to recover these properties when using an observer, by selecting the observer gains properly.

Let's compare the two loop transfer functions. For the full-state

feedback case

$$u' = -H_1 H_2 x \qquad (8.43)$$

$$x = \Phi B u'' \qquad (8.42)$$

while for the observer-based case

$$u' = -H_1 H_2 \hat{x} \qquad (8.52)$$

$$\hat{x} = \Phi[B(C\Phi B)^{-1} - K(I + C\Phi K)^{-1}]C\Phi B u'$$

$$+ \Phi[K(I + C\Phi K)^{-1}]C\Phi B u'' \qquad (8.51)$$

Obviously, for equality of loop transfer functions, we need the transfer functions in (8.42) and (8.51) to be equal. Since we don't want a u' term on the right-hand side of (8.51), we can let

$$B(C\Phi B)^{-1} = K(I + C\Phi K)^{-1} \qquad (8.53)$$

so that the first term in (8.51) vanishes. Equation (8.51) then becomes

$$\hat{x} = \Phi[B(C\Phi B)^{-1}]C\Phi B u''$$

$$= \Phi B u'' \qquad (8.54)$$

This is what we want! That is, if we can choose K so that (8.53) holds, then the loop properties with loops broken at X will be the same for the full-state and observer-based feedback cases. This means that any guarantees that hold for the full-state feedback case will hold for the observer-based case as well.

Next we need a way to choose K so that (8.53) will be satisfied. To do this, we will try to find K as a function of a scalar parameter q such that (note that this q is different from the q in section 8.1)

$$\frac{K(q)}{q} \longrightarrow BW \qquad \text{as} \quad q \longrightarrow \infty \qquad (8.55)$$

where W is any nonsingular matrix. Then

$$K[I + C\Phi K]^{-1} = \frac{K(q)}{q}q[I + C\Phi K(q)]^{-1} = \frac{K(q)}{q}\left[\frac{I}{q} + C\Phi\frac{K(q)}{q}\right]^{-1}$$

$$\longrightarrow BW[C\Phi BW]^{-1} = BWW^{-1}[C\Phi B]^{-1} = B[C\Phi B]^{-1} \quad \text{as } q \longrightarrow \infty \qquad (8.56)$$

which is what we want in order to satisfy (8.53).

Closed-loop stability of the overall system with an observer in the loop requires that the observer error dynamics be stable. We can assure this by requiring the observer to be a Kalman filter for some set of noise statistics. First, we will assume that Γ, the process noise distribution matrix, is identity. From Chapter 6, Kalman filter gains are given by (here with our scalar parameter q included)

$$K_f(q) = \Sigma(q)C^T R_f^{-1} \qquad . \qquad (8.57)$$

where $\Sigma(q)$ is the solution to the filter Riccati equation

$$0 = A\Sigma(q) + \Sigma(q)A^T + Q_f(q) - \Sigma(q)C^T R_f^{-1} C\Sigma(q) \qquad (8.58)$$

Note that we have chosen Q_f to be a function of q also. As in any Kalman filter problem, we must have $Q_f = Q_f^T \geqslant 0$ and $R_f = R_f^T > 0$, and the pairs $[A, Q_f^{\frac{1}{2}}]$ and $[C, A]$ must be stabilizable and detectable, respectively.

In the typical Kalman filter problem, Q_f and R_f are process and measurement noise intensities, respectively. Here we will alter that interpretation slightly. Let Q_o and R_o be the actual process and measurement noise intensities, and define the Riccati weighting matrices as

$$Q_f(q) = Q_o + q^2 BVB^T \qquad (8.59)$$

$$R_f = R_o \qquad (8.60)$$

where V is any positive definite symmetric matrix. Note that the measurement noise weighting is taken as the noise intensity R_o, while the process noise weighting has an additional term added to Q_o. This

8-15

term can be thought of as additional fictitious process noise injected into the system through the inputs to the plant, where we have assumed uncertainties anyway. Also note that, for $q = 0$, we have the standard Kalman filter. Next we will examine what happens as q approaches infinity.

Substituting the weights in (8.59) and (8.60) into the filter Riccati equation (8.58), we get

$$0 = A\Sigma(q) + \Sigma(q)A^T + Q_o + q^2 BVB^T - \Sigma(q)C^T R_o^{-1} C\Sigma(q) \qquad (8.61)$$

Dividing both sides of (8.61) by q^2 we get

$$0 = A(\frac{\Sigma(q)}{q^2}) + (\frac{\Sigma(q)}{q^2})A^T + \frac{Q_o}{q^2} + BVB^T - q^2(\frac{\Sigma(q)}{q^2})C^T R_o^{-1} C(\frac{\Sigma(q)}{q^2}) \qquad (8.62)$$

By the development in Appendix 8A, for a minimum phase system (i.e.. $C\Phi B$ has no right-half plane transmission zeros) with at least as many inputs as outputs, as $q \to \infty$ in (8.62), $\dfrac{\Sigma(q)}{q^2} \to 0$. Therefore, the first

three terms on the right-hand side of (8.62) become small, and

$$q^2(\frac{\Sigma(q)}{q^2})C^T R_o^{-1} C(\frac{\Sigma(q)}{q^2}) \longrightarrow BVB^T \qquad \text{as } q \longrightarrow \infty \qquad (8.63)$$

From (8.57) and (8.60), we see that

$$\begin{aligned}
K_f(q)R_o K_f(q)^T &= [\Sigma(q)C^T R_o^{-1}]R_o[\Sigma(q)C^T R_o^{-1}]^T \\
&= [\Sigma(q)C^T R_o^{-1}]R_o[R_o^{-1}C\Sigma(q)] \\
&= \Sigma(q)C^T R_o^{-1} C\Sigma(q) \qquad (8.64)
\end{aligned}$$

so that

$$\frac{K_f(q)R_o K_f(q)^T}{q^2} = q^2(\frac{\Sigma(q)}{q^2})C^T R_o^{-1} C(\frac{\Sigma(q)}{q^2}) \qquad (8.65)$$

Substituting (8.65) into (8.63) yields

$$\frac{K_f(q)R_o K_f(q)^T}{q^2} \longrightarrow BVB^T \qquad \text{as } q \longrightarrow \infty \qquad (8.66)$$

We will now claim that solutions (remember we are trying to find $K_f(q)$) of (8.66) must be of the form

$$\frac{K_f(q)}{q} \longrightarrow BV^{\frac{1}{2}}R_o^{-\frac{1}{2}} \qquad \text{as } q \longrightarrow \infty \qquad (8.67)$$

To prove this, we substitute (8.67) into the left-hand side of (8.66) and see that

$$\frac{K_f(q)R_o K_f(q)^T}{q \; q} \longrightarrow (BV^{\frac{1}{2}}R_o^{-\frac{1}{2}})R_o(BV^{\frac{1}{2}}R_o^{-\frac{1}{2}})^T$$

$$= BV^{\frac{1}{2}}R_o^{-\frac{1}{2}}R_o R_o^{-\frac{1}{2}}V^{\frac{1}{2}}B^T$$

$$= BVB^T \qquad \text{as } q \longrightarrow \infty$$

which is the right-hand side of (8.66). One more step and we're done. If we now define W as

$$V = V^{\frac{1}{2}}R_o^{-\frac{1}{2}} \qquad (8.68)$$

from (8.67) we will have,

$$\frac{K_f(q)}{q} \longrightarrow BW \qquad \text{as } q \longrightarrow \infty \qquad (8.69)$$

where V is guaranteed to be nonsingular by its definition. Equation (8.69) is exactly equation (8.55). Therefore, choosing the filter weights as shown in (8.59) and (8.60) will yield observer gains that satisfy (8.53) as $q \longrightarrow \infty$, and therefore the loop properties of Figs 8.4 and 8.5 will be identical with loops broken at X, as $q \longrightarrow \infty$.

Let's add one more thing before making some comments. If the plant contains a non-identity process noise distribution matrix Γ, so that

$$\dot{x} = Ax + Bu + \Gamma\xi \qquad (8.70)$$

where

$$E[\xi(t)^T \xi(\tau)] = Q_o \delta(t - \tau) \qquad (8.71)$$

then the weighting matrix Q_f becomes

$$Q_f(q) = \Gamma Q_o \Gamma^T + q^2 BVB^T \qquad (8.72)$$

8-17

This should not be surprising since the standard Kalman filter would have the $\Gamma Q_o \Gamma^T$ term.

Now let's take a look at what we have. By choosing our observer to be a Kalman filter, with weighting matrices as shown in (8.59) and (8.60), we will asymptotically recover (as $q \longrightarrow \infty$) the loop properties of the full-state feedback implementation with loops broken at the input to the plant. If the loop properties of the full-state implementation are good, they will also be good at the input to the plant when a Kalman filter is placed in the loop. Since we have altered the filter's weighting matrices, we may ask if it is still a Kalman filter. The answer is yes, but with strings attached. For $q = 0$, the filter described here is exactly the typical Kalman filter. However, it has no loop recovery properties at all. As q is made larger, the loop properties become closer and closer to that of the full-state feedback case. However, the process noise weighting becomes increasingly different from the assumed process noise intensity, still yielding a Kalman filter but for different noise statistics. Thus, we have a trade-off between loop recovery and accuracy of the filter. This is best shown in a simple example, which we do next.

8.4 Example of Loop Recovery

Consider the simple single-input single-output system described by (Ref [8-3])

$$\dot{x} = Ax + Bu + \Gamma\xi = \begin{bmatrix} 0 & 1 \\ -3 & -4 \end{bmatrix} x + \begin{bmatrix} 0 \\ 1 \end{bmatrix} u + \begin{bmatrix} 35 \\ -61 \end{bmatrix} \xi \qquad (8.73)$$

$$y = Cx + n = \begin{bmatrix} 2 & 1 \end{bmatrix} x + n \qquad (8.74)$$

$$E(\xi) = E(n) = 0 \qquad (8.75)$$

$$E[\xi(t)\xi^T(\tau)] = E[n(t)n^T(\tau)] = \delta(t - \tau)$$

$$\Longrightarrow Q_o = R_o = 1 \qquad (8.76)$$

8-18

The open-loop transfer function for this system is given by

$$C(s) = C(sI - A)^{-1}B = \frac{s + 2}{(s + 1)(s + 3)} \tag{8.77}$$

The controller we will use is an LQ Regulator which minimizes

$$J = E\{\lim_{t \to \infty} \frac{1}{T} \int_0^T [z^T z + u^T R_c u] dt\} \tag{8.78}$$

where we will let

$$z = Hx = 4\sqrt{5} \, [\sqrt{35} \quad 1]x \tag{8.79}$$

so that

$$Q_c = H^T H = 80 \begin{bmatrix} 35 & \sqrt{35} \\ \sqrt{35} & 1 \end{bmatrix} \tag{8.80}$$

and

$$R_c = 1 \tag{8.81}$$

The unorthodox choice of H was made so that the resulting optimal control law would be

$$u = -K_c x = -[50 \quad 10]x \tag{8.82}$$

which produces the closed-loop regulator poles

$$\lambda_{CL_c} = -7.0 \pm j2.0 \tag{8.83}$$

Remember that these come from $\det[sI - A + BK_c] = 0$. In order to be consistent with the notation of Figs 8.4 and 8.5, we let $H_1 = I$ and $H_2 = K_c$. The loop transfer function for the regulator is given by $K_c(sI - A)^{-1}B$. This was shown in Chapters 6 and 7. Figs. 8.6 and 8.7 show a Bode magnitude and a polar plot of this transfer function. We show only the magnitude plot as this is all we would have in a MIMO example (using singular values); note that we could not generate a polar plot for MIMO.
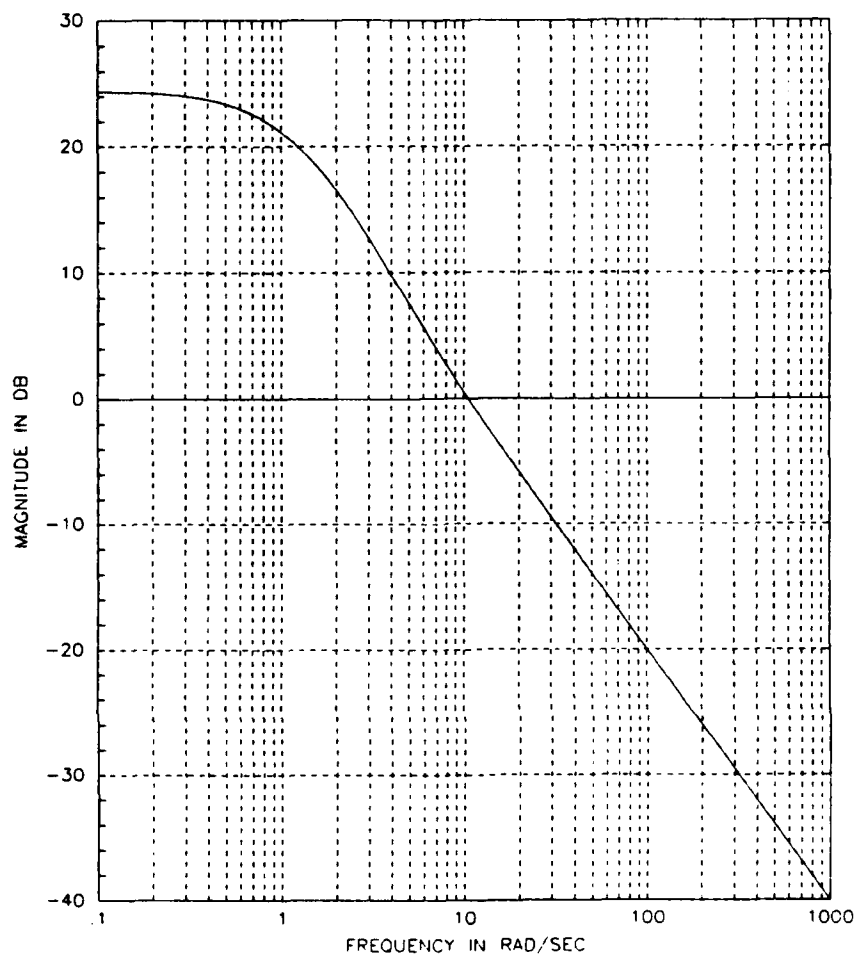
Fig 8.6 Bode Magnitude of the Full-State Regulator System
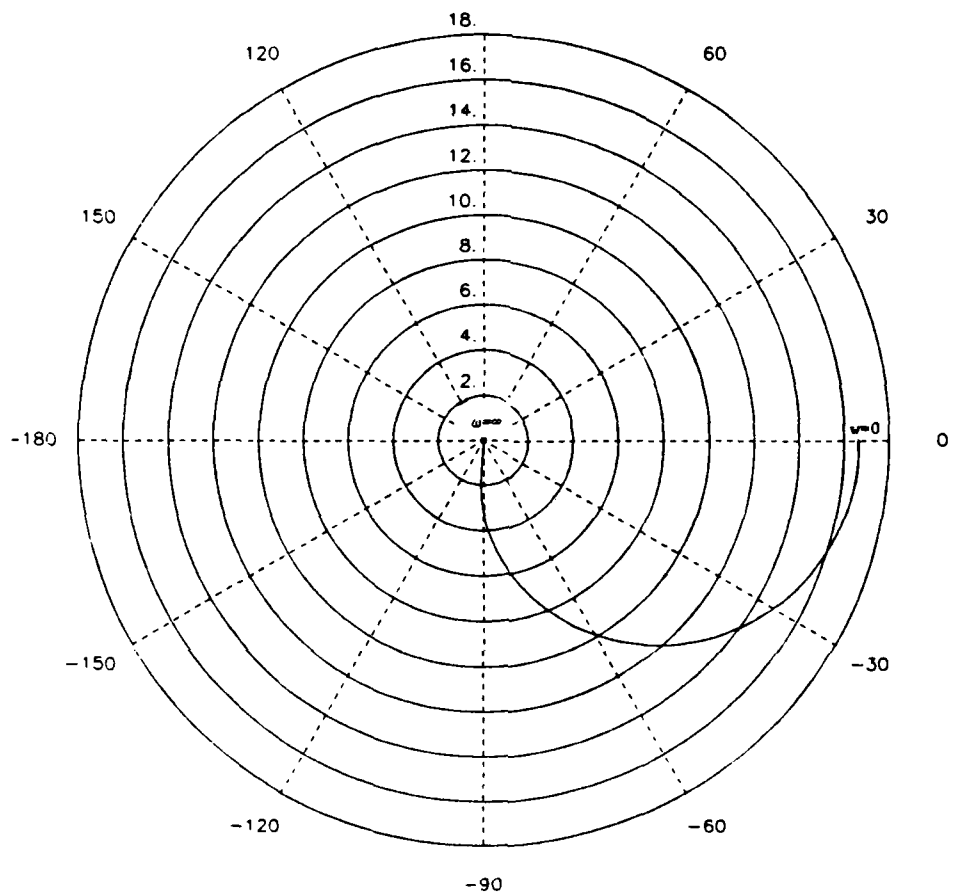
Fig 8.7 Polar Plot of the Full-State Regulator System

Fig 8.8 shows a blow-up of Fig 8.7 at high frequency. Note that the plot does not enter a unit circle centered at $-1 + j0$, and therefore has the promised guaranteed margins. In fact, the gain and phase margins here are $0 < GM < \infty$ and $-85° < PM < 85°$.
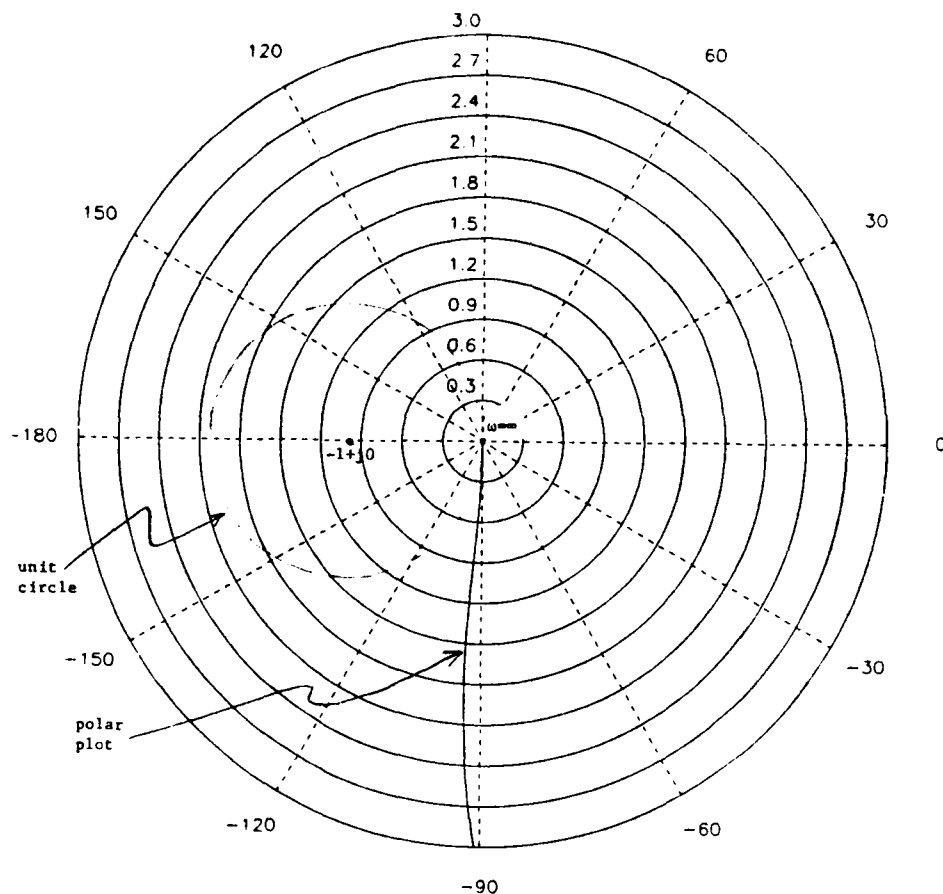
Fig 8.8 High-Frequency Portion of the Full-State Regulator System
Design

Now, since the assumption of availability of all states for feedback is unrealistic, we will add an estimator to reconstruct the states, namely a Kalman filter. Equation 8.82 will therefore remain the same except that x is replaced by $\hat{x}$. In accordance with Chapter 6, we choose Q_f and R_f as

$$Q_f = \Gamma Q_o \Gamma^T = \begin{bmatrix} 35 \\ -61 \end{bmatrix} (1) [35 \quad -61]$$ (8.84)

and

$$R_f = R_o = 1$$ (8.85)

This produces the filter gain matrix

$$K_f = \begin{bmatrix} 30 \\ -50 \end{bmatrix}$$ (8.86)

with filter poles

$$\lambda_{CL_f} = -7.0 \pm j2.0$$ (8.87)

(the same poles as the regulator). Remember that these come from

$det[sI - A + K_f C] = 0$. The loop transfer function for the system with

the filter in the loop (i.e., the LQG loop) is $K(s)G(s)$, where $K(s)$ is

given by

$$K(s) = K_c(sI - A + BK_c + K_f C)^{-1} K_f$$ (8.88)

Again, this was shown in detail in Chapter 6. Note that since this is a

SISO system, $K(s)G(s) = G(s)K(s)$. Figs 8.9 and 8.10 show the Bode

magnitude and polar plot of this LQG loop transfer function.
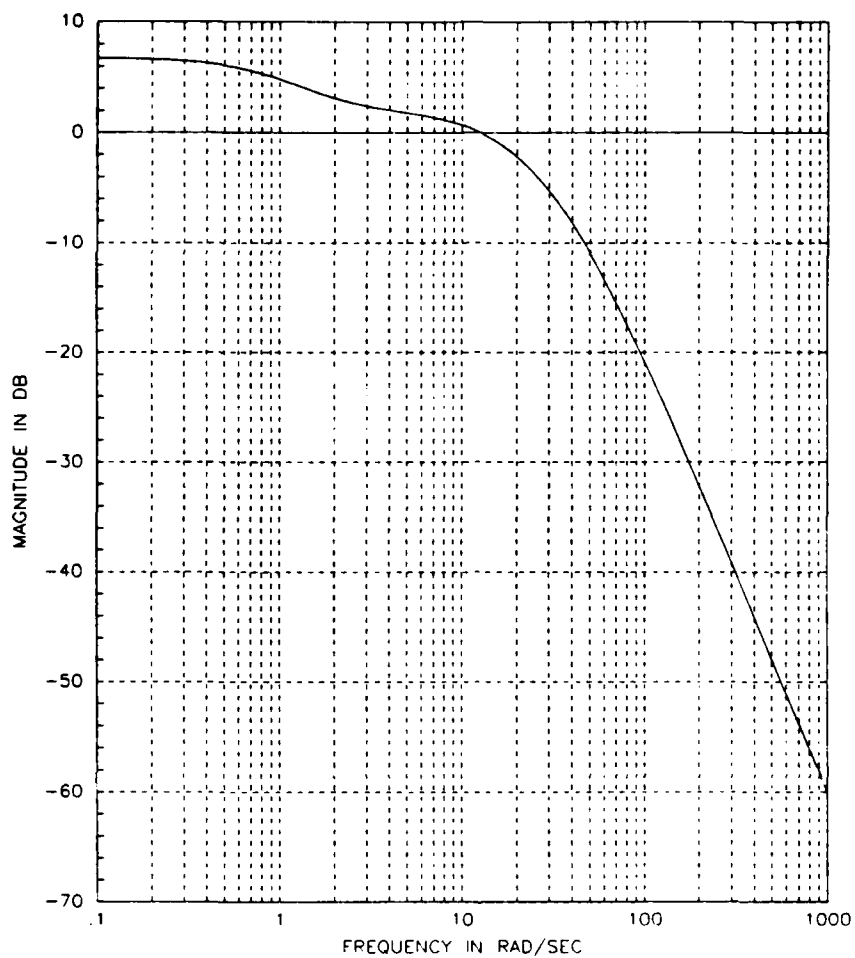
Fig 8.9 Bode Magnitude Plot of the LQG Loop
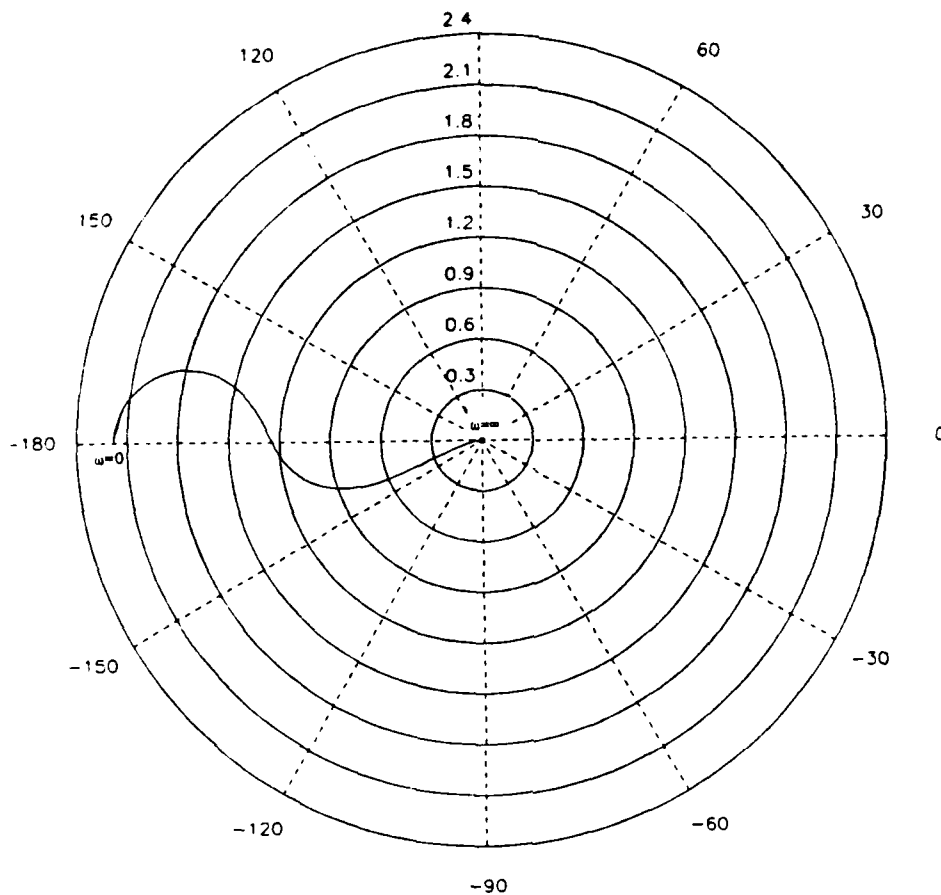
Fig 8.10   Polar Plot of the LQG Loop

Notice that while the bandwidths of the two systems are only slightly different, the margins for the LQG system are much worse. Specifically, the phase margin has been reduced to 15°. From a realistic viewpoint, note that the LQG loop does have the required -40dB/decade roll-off we discussed in Chapter 7, which the regulator loop does not. Therefore, we would like to have a way to retain this 2-pole roll-off property while approaching the desirable margins of the regulator.

To do this, we will use our recovery technique. This example was specially chosen to show the remarkable features of this technique.

Note that our Kalman filter produces an unstable compensator -- the
compensator poles (poles of equation (8.88)) are

$$\lambda_K = \{ -42.7, \ 18.7 \} \tag{8.89}$$

This accounts for the $-180°$ low-frequency phase angle in Fig 8.10. This
happens quite often when using LQG compensators, and in many cases it
should happen. Consider an open-loop system with pole/zero locations as
shown in Fig 8.11.
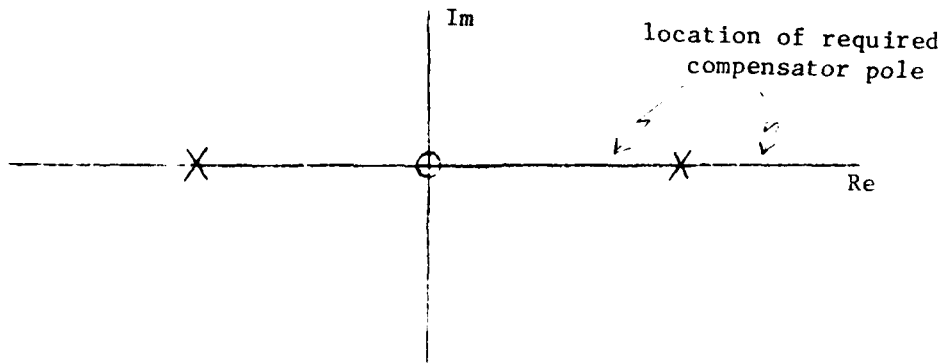
Fig 8.11 Open-Loop Pole/Zero Locations of a System Requiring
Unstable Compensation

Obviously, a dynamic compensator with a pole in the right-half plane
must be added to move the locus into the left-half plane. In our
example, unstable compensation seems unnecessary since the open-loop
plant is stable. However, since all four branches of the locus must go
through the point $-7 \pm j2$ at one value of loop gain (specifically, loop
gain $= 1$), unstable compensation is necessary to achieve this.
Therefore, unstable compensation is "our fault" since we asked for those
root locations.

Now, we let the Q_f matrix take the form as suggested in (8.72)

$$Q_f = \Gamma Q_o \Gamma^T + q^2 BVB^T$$

$$= \begin{bmatrix} 35 \\ -61 \end{bmatrix} (1) [35 \quad -61] + q^2 \begin{bmatrix} 0 \\ 1 \end{bmatrix} (1) [0 \quad 1] \tag{8.90}$$

where q^2 takes on increasingly larger values. Note that since we are free to choose V, and since it's a scalar, we choose it to be unity. We have already seen the results for $q^2 = 0$; they are just the optimal LQG loop (Fig 8.9 and 8.10). First, we'll look at polar plots of K(s)G(s) as $q \longrightarrow \infty$, since they show what's happening very clearly. Fig 8.12 shows the plots for $q^2 = 0$, 100, 500, and 1000.
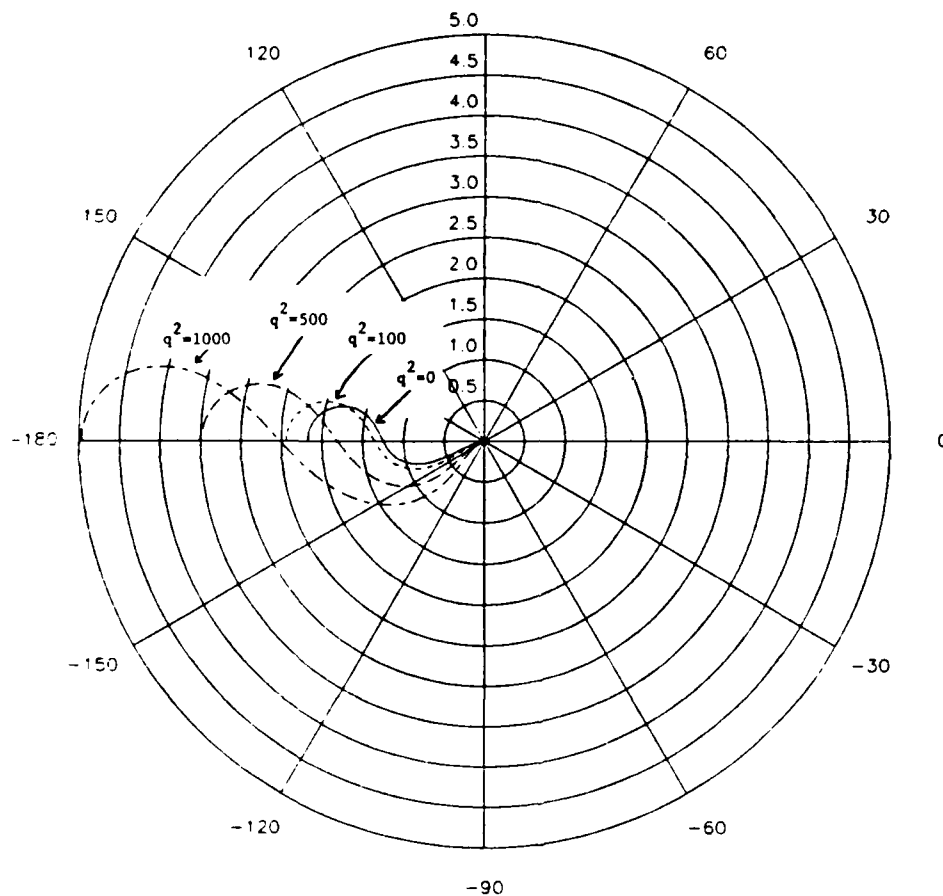
Fig 8.12 Polar Plots for $q^2 = 0$, 100, 500, and 1000

Note that as q^2 increases, the polar plot gets larger and the margins increase (from 15° at $q^2 = 0$ to 45° at $q^2 = 1000$). Fig 8.13 shows polar plots for $q^2 = 0$, 500, 1000, 2500, 3600, 4096, 40000 and 250000, as well as the full-state loop transfer function.
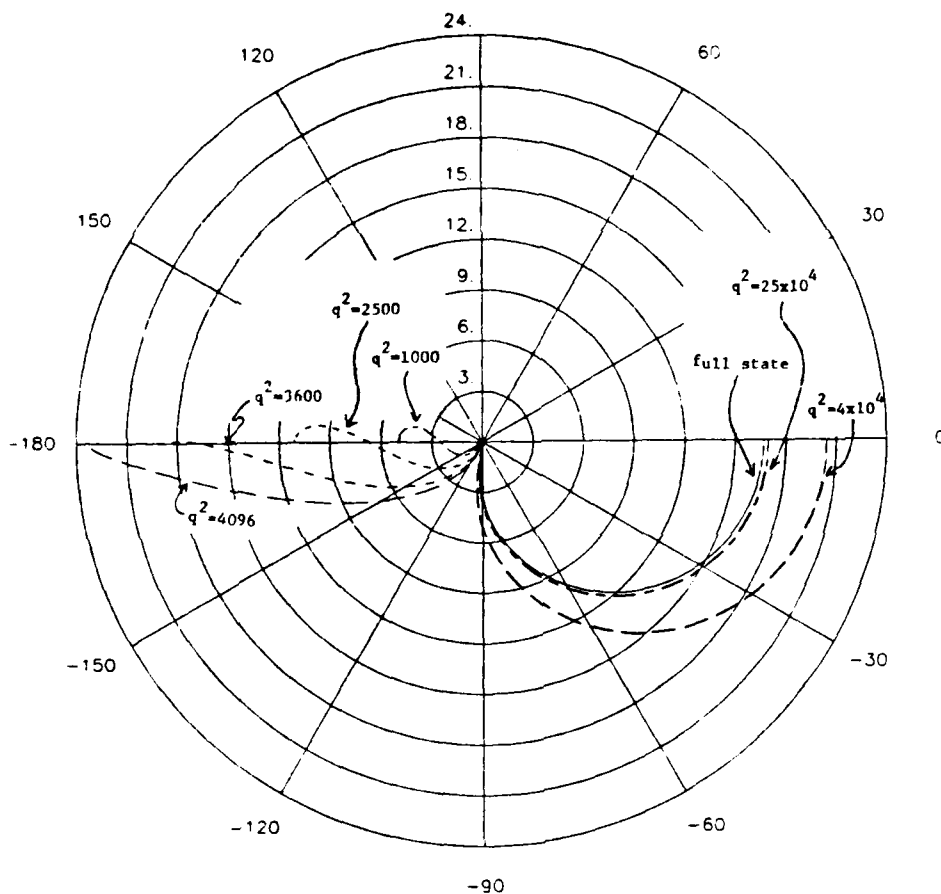
Fig 8.13 Polar Plots for q^2 = 1000, 2500, 3600, 4096, 40000, 250000, and full state

As q^2 increases, the plot continues to get larger and the margins continue to increase. Note that somewhere between q^2 = 3600 and 4096, the plot changes shape so that it remains below the negative real axis. As q^2 increases past 4096, the plot grows larger and larger until at some point (around q^2 = 7500), the system becomes Type 1 and then becomes open-loop stable, so that the low frequency portion moves to the $0°$ axis, but at a very large magnitude. As q^2 is increased further, the plot shrinks, until at q^2 = 250000 it very closely resembles full state. The above described behavior is more easily explained by looking at the compensator poles (roots of $\det[sI - A + BK_c + K_fC] = 0$), as shown in Table 8.2.

8-28

Table 8.2 Poles of the Compensator as $c \longrightarrow \infty$

q^2	Poles of $K(s)$	
0	-42.7	18.7
100	-43.5	16.7
500	-47.4	10.4
1000	-52.5	7.0
2500	-66.0	3.0
3600	-74.6	1.78
4096	-78.2	1.4
5000	-84.3	0.9
6400	-92.0	0.3
8100	-102.0	-0.10
10000	-112.0	-0.44
40000	-210	-1.57
250000	-510	-1.93
1×10^8	-10,010	-1.9998

Now we can see what's really happening. As q^2 is increased, the unstable compensator pole starts moving toward the left-half plane, causing the polar plot to grow. As q^2 increases further, the unstable pole approaches the origin and the plot becomes very large. At some value of q^2 (between 6400 and 8100), the unstable pole moves to the origin, and the system becomes Type 1. For a slightly larger value of q^2, the compensator becomes stable, changing the system back to Type 0 and moving the low-frequency part of the polar plot to the 0° line. As q^2 gets very large, the previously unstable pole moves toward -2, the open-loop (transmission) zero. This causes the polar plot to shrink, and for $q^2 = 250000$, the polar plot of the LQG loop looks almost identical to that of the full-state LQ regulator. Note that the other compensator pole simply becomes faster and faster (moves further into the left-half plane).

Now let's look at the Bode magnitude (singular value) plot. Remember that in a MIMO problem, this would be our only plot. Fig 8.14 show the magnitude plot for $q^2 = 0$, 500, 2500, 8100, 250000 and full state.
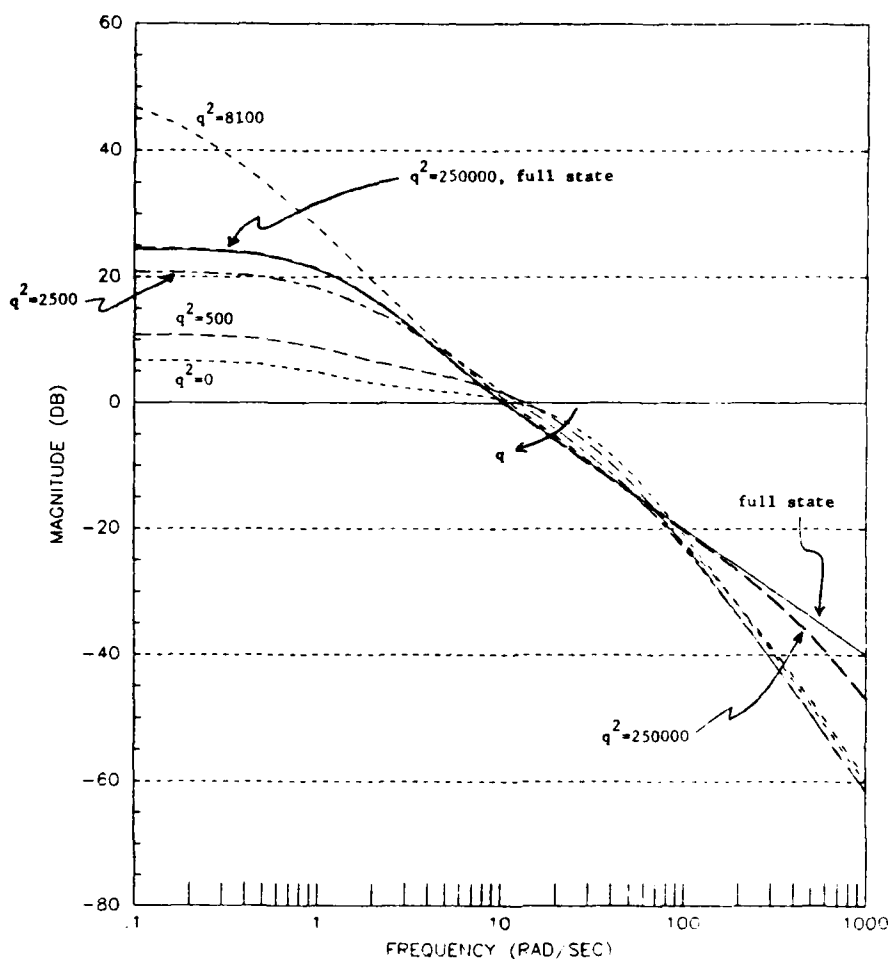
Fig 8.14 Bode Magnitude Plot for $q^2 = 0$, 500, 2500, 8100, 250000
and full state

As q^2 begins to increase, the low-frequency region begins to approach

full state, while the high-frequency region remains virtually unchanged.

As q^2 nears 3000, the low-frequency region almost matches full state,

since the compensator pole at +2 looks like one at -2 from a magnitude

viewpoint. As continues to q^2 increase, the low-frequency region also

increases, diverging from full state. Once q^2 is large enought to move

the compensator pole into the left-half plane, the low-frequency

response lowers until it nearly matches full state. At the same time,

the high-frequency portion of the plot approaches that of full state.

8-30

Note that at $q^2 = 250000$, the LQG loop nearly matches full state, except at very high frequency. Here, the LQG loop exhibits an additional -20dB/decade roll-off, since it has a two-pole roll-off rather than full state's one-pole roll-off. Thus, we have met our objectives. One final point of interest is that recovery is achieved with no increase in bandwidth, which is obviously desirable.

We will conclude this example and chapter with two points. First, in order for recovery to occur, the poles of the compensator must approach the transmission zeros of the plant and infinity. It is easy to see that this is happening by looking at Table 8.2. A slight modification of the development in Appendix 6A or the proof given in Refs [8-1] and [8-2] shows that the filter poles also move towards the plant transmission zeros (or their stable images) and infinity as $q \rightarrow \infty$. Thus, the behavior of the poles in this example is typical. The optimal $(q^2 = 0)$ compensator will not always be unstable; usually, it is not. If it is stable, the "overshoot" behavior seen in Fig 8.14 will not occur.

Secondly, we need to remember that the filter performance degrades as q^2 gets large, so that a trade-off occurs. Ref [8-3], where this example is taken from, shows values of the error covariance matrix $E[(x - \hat{x})(x - \hat{x})^T]$ for several values of q^2. For $q^2 = 10000$, the error covariance matrix entries are 3 to 5 times greater than these of the optimal $(q^2 = 0)$. Whether this is acceptable or not depends on the specific application, and on the importance of robustness. We simply want to point out that the trade-off exists and should be considered when selecting the value of q^2.

Appendix 8A

First, we will state two theorems from Ref [8-1], pp. 306-307 and pp. 370-371. These were first proved in Ref [8-2]. The proof will be omitted here, and interested readers should consult Ref [8-2] for the details.

Theorem A: Consider the linear, time-invariant, stabilizable and detectable system

$$\dot{x} = Ax + Bu \qquad (8A-1)$$

$$z = Hx \qquad (8A-2)$$

where B and H have full rank. Consider the performance index

$$J = \int_0^\infty [z^T(t)Qz(t) + u^T(t)Ru(t)]dt \qquad (8A-3)$$

where $Q \geqslant 0$, $R > 0$. Let

$$R = \rho N \qquad (8A-4)$$

with $N > 0$ and ρ a positive scalar. Let $\bar{P}_\rho$ be the steady-state solution of the Riccati equation

$$0 = H^T QH - \frac{1}{\rho}\bar{P}_\rho BN^{-1}B^T\bar{P}_\rho + A^T\bar{P}_\rho + \bar{P}_\rho A \qquad (8A-5)$$

Then:

1) The limit

$$\lim_{\rho \to 0} \bar{P}_\rho = P_o$$

exists.

2) If $dim(z) \leqslant dim(u)$, $P_o = 0$ iff all the transmission zeros of $G'(s) = H(sI - A)^{-1}B$ are in the left-half plane.

3) If $dim(z) > dim(u)$, then $P_o \neq 0$.

Theorem B: Consider the linear, time-invariant, stabilizable and detectable system

$$\dot{x} = Ax + Bu + \xi \qquad (8A-6)$$

$$v = Cx + n \qquad (8A-7)$$

where C has full rank, ξ and n are zero-mean white noises with intensities $Q > 0$ and $R = \rho N > 0$, respectively. Let $\bar{\Sigma}_\rho$ be the steady-state solution of the filter Riccati equation

$$0 = Q - \frac{1}{\rho}\bar{\Sigma}_\rho C^T N C \bar{\Sigma}_\rho + A\bar{\Sigma}_\rho + \bar{\Sigma}_\rho A^T \qquad (8A-8)$$

Then:

1) The limit

$$\lim_{\rho \to 0} \bar{\Sigma}_\rho = \Sigma_o$$

exists.

2) If $\dim(y) \leqslant \dim(u)$, $\Sigma_o = 0$ iff all the transmission zeros of $G(s) = C(sI - A)^{-1}B$ are in the left-half plane.

3) If $\dim(y) > \dim(u)$, then $\Sigma_o \neq 0$.

For our current application, Theorem B is the one we're interested in. Theorem A was given since this is the one that is proved in detail in Ref [8-2]; Theorem B is its dual. We want $\Sigma_o = 0$, and to get this we must have at least as many inputs as outputs, as well as $C(sI - A)^{-1}B$ being minimum phase. Now we must alter Theorem B to our notation.

First, we want $Q = Q_o + q^2 BVB^T$ and $R = R_o$, where $q \to \infty$. Notice that minimizing

$$J_1 = \int_0^\infty [x^T Q_1 x + u^T \rho R_1 u]dt$$
$$= \rho \int_0^\infty [\frac{1}{\rho}x^T Q_1 x + u^T R_1 u]dt \qquad (8A-9)$$

is the same as minimizing

$$J_2 = \int_0^\infty [\frac{1}{\rho}x^T Q_1 x + u^T R_1 u]dt \qquad (8A-10)$$

since multiplication by a positive scalar does not change the minimization. Now let $\frac{1}{\rho} = q^2$. Therefore, letting $\rho \to 0$ is the same as letting $q \to \infty$. Since we are free to choose Q_1 and R_1, let

$$Q_1 = \frac{Q_o}{q^2} + BVB^T \qquad (8A-11)$$

$$R_1 = R_o \tag{8A-12}$$

Then

$$Q = q^2 Q_1 = Q_o + q^2 B V B^T \tag{8A-13}$$

$$R = R_1 = R_o \tag{8A-14}$$

which is what we want. The Riccati equation in (8A-8) becomes equation (8.61) and $\Sigma_o = 0$ if $C(sI - A)^{-1}B$ is minimum phase. This allows us to conclude

$$\frac{\Sigma(q)}{q^2} \longrightarrow 0 \qquad \text{as } q \longrightarrow \infty \tag{8A-15}$$

Chapter 8 References

[8-1] H. Kwakernaak and R. Sivan, <u>Linear Optimal Control Systems</u>, Wiley-Interscience, New York, 1972.

[8-2] H. Kwakernaak and F. Sivan, "The Maximally Achievable Accuracy of Linear Optimal Regulators and Linear Optimal Filters", IEEE Trans. Auto. Control, Vol AC-17, No 1, pp 79-86, Feb 1972.

[8-3] J.C. Doyle and G. Stein, "Robustness with Observers", IEEE Trans. Auto. Control, Vol AC-24, No 4, pp 607-611, Aug 1979.

[8-4] J.C. Doyle, "Guaranteed Margins for LQG Regulators", IEEE Trans. Auto. Control, Vol AC-23, No. 4, pp 756-757, Aug 1978.

9. PUTTING IT ALL TOGETHER – THE LINEAR QUADRATIC GAUSSIAN WITH LOOP TRANSFER RECOVERY (LQG/LTR) METHODOLOGY

So far we have discussed what a good multivariable loop shape should be, as well as a method which recovers the LQ Regulator loop shape when using an LQG compensator. Now we need to tie these ideas together to produce an overall design methodology. Actually, we will develop one method which has two "versions", depending upon where uncertainties in the system are assumed to be. We will start by restating the LQG problem, but adding a few new assumptions.

9.1 Loop Properties at Various Points in the LQG System

The system dynamics are assumed to be in the form

$$\dot{x} = Ax + Bu + \Gamma\xi \qquad (9.1)$$

$$y = Cx + n \qquad (9.2)$$

where $\dim(u) = m$, $\dim(y) = r$, and ξ and n are Gaussian white noises. We wish to minimize the performance index

$$J = E\{\lim_{T\to\infty} \frac{1}{T} \int_0^T (z^T z + \rho u^T u)dt\} \qquad (9.3)$$

where

$$z = Hx \qquad (9.4)$$

is a desired response equation and ρ is a scalar. There is no loss of generality in assuming this performance index over the "standard" quadratic index

$$J = E\{\lim_{T\to\infty} \frac{1}{T} \int_0^T (x^T Q_c x + u^T R_c u)dt\} \qquad (9.5)$$

Substituting (9.4) into (9.3) yields a Q_c matrix given by $H^T H$, which can produce any desired symmetric positive semidefinite Q_c. Obviously, any R_c matrix may be written as ρN_c, where ρ is a scalar and N_c is symmetric positive definite. Looking at the Riccati equation

$$0 = PA + A^T P + Q_c - \frac{1}{\rho}PBN_c^{-1}B^T P \qquad (9.6)$$

we can redefine

$$\widetilde{B} = BN_c^{\frac{1}{2}} \tag{9.7}$$

where $N_c^{\frac{1}{2}}$ is the square root of N_c (i.e., $N_c = N_c^{\frac{1}{2}}N_c^{\frac{1}{2}}$). Therefore, $R_c = \rho I$ as in (9.3) is general. We will not use the "$\sim$" on the B matrix as in (9.7), but will assume B has been modified if so desired.

The solution to (9.1)-(9.4) is given by

$$u = -K_c \hat{x} \tag{9.8}$$

where

$$K_c = \frac{1}{\rho}B^T P \tag{9.9}$$

and P is the solution to the Riccati equation

$$0 = PA + A^T P + H^T H - PB\frac{1}{\rho}B^T P \tag{9.10}$$

The state estimate $\hat{x}$ is defined by

$$\dot{\hat{x}} = A\hat{x} + Bu + K_f[y - C\hat{x}] \tag{9.11}$$

where

$$K_f = \frac{1}{\mu}\Sigma C^T \tag{9.12}$$

and Σ is the solution to the filter Riccati equation

$$0 = A\Sigma + \Sigma A^T + \Gamma\Gamma^T - \frac{1}{\mu}\Sigma C^T C \Sigma \tag{9.13}$$

$\Gamma\Gamma^T$ is the intensity of the process noise ξ, which again is completely general. μI is the intensity of the measurement noise n, which is general if the non-equal, non-identity portion of R_f is absorbed into C similarly to the development in (9.6) and (9.7). That is, let any R_f be written as μN_f, and redefine

$$\widetilde{C} = N_f^{\frac{1}{2}}C \tag{9.14}$$

Again, we will omit the "$\sim$" in the further development.

Now we need to draw a block diagram representation of the above equations. Fig 9.1 shows the block diagram that's most convenient for our development.

9-2
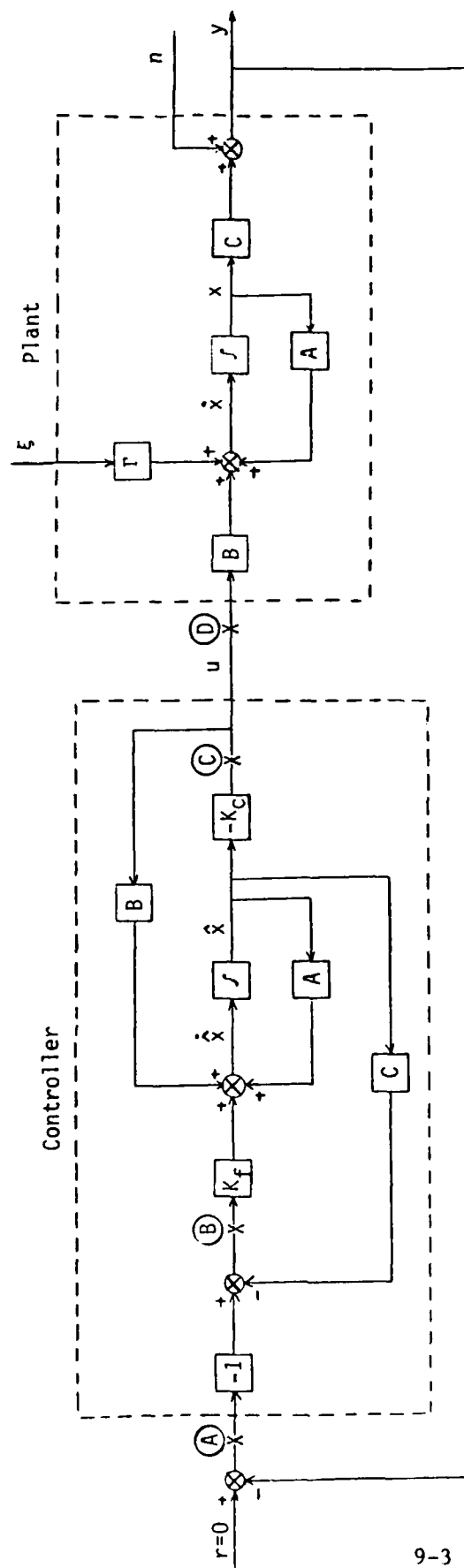
Fig 9.1 Block Diagram of the LQG System

9-3

Now let's look at loop transfer functions at various points in the system. Specifically, we will find the loop transfer at points (A), (B), (C), and (D).

Point (A) - For convenience, we will use a to denote the signal just before the break at point (A), and a' to denote the signal just after. Remember that in calculating loop transfers, we assume that all external inputs are zero. First, we can see that

$$a = -y \qquad (9.15)$$

From (9.1) and (9.2),

$$y = C(sI - A)^{-1}Bu = C\Phi Bu \qquad (9.16)$$

and from (9.8) and (9.11)

$$u = -K_c(sI - A + BK_c + K_fC)^{-1}K_fy \qquad (9.17)$$

Substituting (9.16) and (9.17) into (9.15) we have

$$a = C\Phi BK_c(sI - A + BK_c + K_fC)^{-1}K_fy \qquad (9.18)$$

Notice that

$$y = -a' \qquad (9.19)$$

Therefore, if we use our standard notation

$$G(s) = C\Phi B \qquad (9.20)$$

and

$$K(s) = K_c(sI - A + BK_c + K_fC)^{-1}K_f \qquad (9.21)$$

(9.18) becomes

$$a = -G(s)K(s)a' \qquad (9.22)$$

so that the loop transfer function $T_A(s)$ is

$$T_A(s) = G(s)K(s) \qquad (9.23)$$

Point (B) - Using notation similar to that at point (A),

$$b = y - C\hat{x} \qquad (9.24)$$

Notice that

$$\hat{x} = \Phi[Bu + K_f b'] \tag{9.25}$$

so that using (9.16) and (9.25) in (9.24) we get

$$b = C\Phi Bu - C\Phi[Bu + K_f b']$$

$$= C\Phi Bu - C\Phi Bu - C\Phi K_f b'$$

$$= -C\Phi K_f b' \tag{9.26}$$

Therefore

$$T_B(s) = C\Phi K_f \tag{9.27}$$

Point Ⓒ – We have actually already done this point and point Ⓓ back in Chapter 8 (they were points XX and X, respectively). To be consistent with our notation, we will repeat them here.

$$c = -K_c \hat{x} \tag{9.28}$$

Notice that

$$\hat{x} = \Phi[Bc' + K_f\{y - C\hat{x}\}]$$

$$= \Phi Bc' + \Phi K_f y - \Phi K_f C\hat{x} \tag{9.29}$$

so that

$$\hat{x} = (I + \Phi K_f C)^{-1}[\Phi Bc' + \Phi K_f y] \tag{9.30}$$

Looking at Fig 9.1 we can see that

$$y = C\Phi Bc'$$

so that

$$\hat{x} = (I + \Phi K_f C)^{-1}[\Phi Bc' + \Phi K_f C\Phi Bc']$$

$$= (I + \Phi K_f C)^{-1}[I + \Phi K_f C]\Phi Bc'$$

$$= \Phi Bc' \tag{9.31}$$

Substituting (9.31) into (9.28) we get

$$c = -K_c \Phi Bc' \tag{9.32}$$

so that

$$T_C(s) = K_c \Phi B \tag{9.33}$$

Point Ⓓ – No point in dragging this one out. Here

$$d = u$$

$$= -K(s)y$$

$$= -K(s)G(s)d' \tag{9.34}$$

so that

$$T_D(s) = K(s)G(s) \tag{9.35}$$

Now let's summarize and look at the significance of these four loop transfer functions.

1) The loop transfer function obtained by breaking the LOG loop at point Ⓐ is $G(s)K(s)$. Note that this is equivalent to breaking the loop at the output of the plant.

2) The loop transfer function obtained by breaking the LOG loop at point Ⓑ is $C\Phi K_f$. Repeating (9.11), we see that

$$\dot{\hat{x}} = A\hat{x} + Bu + K_f[y - C\hat{x}] \tag{9.36}$$

The filter operating by itself would be trying to produce an output $\hat{y}$ which closely resembles the input y. It is therefore logical to define the filter output by

$$\hat{y} = C\hat{x} \tag{9.37}$$

Fig 9.2 shows a block diagram of the Kalman filter.
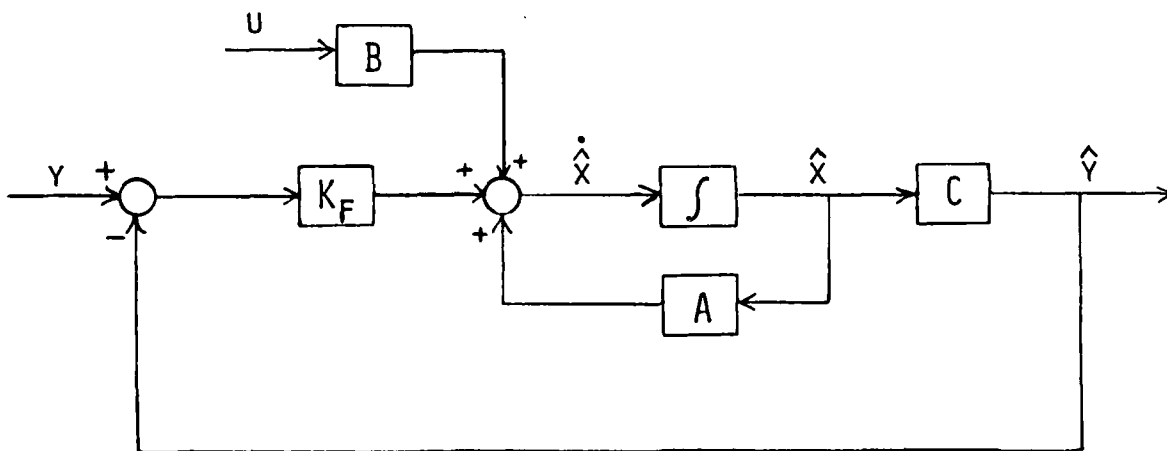
Fig 9.2 Block Diagram of the Kalman Filter

The loop transfer function of the filter is therefore given by (remember that u is an external input)

$$T_{KF}(s) = C\Phi K_f \qquad (9.38)$$

Obviously, this is the loop transfer at point $\widehat{B}$ in the LQG system. By duality to the argument in Chapter 7, this loop transfer function has the same guaranteed robustness properties of the LQ Regulator.

3) The loop transfer function obtained by breaking the LQG loop at point C is $K_c\Phi B$. Note from Chapter 7 that $K_c\Phi B$ is the loop transfer function of the LQ Regulator, which has guaranteed excellent robustness properties.

4) The loop transfer function obtained by breaking the LQG loop at point D is $K(s)G(s)$. Note that this is eqivalent to breaking the loop at the input to the plant.

Here's where we start tying things together. In the last chapter, we developed a method for choosing the filter weights so that the loop transfer function at point $\widehat{D}$ recovered the properties of point $\widehat{C}$. A dual procedure exists for turning the regulator weights so that the properties at point $\widehat{A}$ are matched with those at point $\widehat{B}$. We will call both of these procedures loop transfer recovery. Basically, the overall design procedure consists of two steps, as follows:

Step 1 - Design a full-state feedback law with desirable singular value properties (these were defined in Chapter 4) using the regulator or filter.

Step 2 - Recover these full-state loop shapes via one of the recovery procedures.

9-7

Obviously, the designer must first choose which procedure to use. This is determined by where uncertainties are assumed to enter the system. If the modelling of uncertainties is reflected to the output of the plant, we do a full-state Kalman filter design and recover with the regulator. Conversely, if the uncertainties are modelled so that they enter at the plant input, then we design a full-state LQ Regulator and recover using the Kalman filter. Next we will go through the details of each procedure, adding some new development to simplify the procedure of designing the full-state loop.

9.2 LQG/LTR Design Breaking the Loop at the Plant Input

We will start with this procedure since we have already developed the details of the required recovery procedure in Chapter 8. First, we must design a "good" full-state LQ Regulator loop.

9.2.1 Full-State LQ Regulator Design

We have already defined "goodness" using singular value plots in Chapter 4. Going back to Chapter 7, from (7.16) we have

$$[I + R_c^{\frac{1}{2}} K_c (-jwI - A)^{-1} BR_c^{-\frac{1}{2}}]^T [I + R_c^{\frac{1}{2}} K_c (jwI - A)^{-1} BR_c^{-\frac{1}{2}}]$$
$$= I + R_c^{-\frac{1}{2}} B^T (-jwI - A^T)^{-1} Q_c (jwI - A)^{-1} BR_c^{-\frac{1}{2}} \quad (9.39)$$

This equation is known as the <u>Kalman Equality</u>. Remembering that at the beginning of this chapter we chose to let $Q_c = H^T H$ and $R_c = \rho I$, we can rewrite (9.39) as

$$[I + K_c (jwI - A)^{-1} B]^* [I + K_c (jwI - A)^{-1} B]$$
$$= I + \frac{1}{\rho} [B^T (-jwI - A^T)^{-1} H^T H (jwI - A)^{-1} B]$$
$$= I + \frac{1}{\rho} [H(jwI - A)^{-1} B]^* [H(jwI - A)^{-1} B] \quad (9.40)$$

If we now define $\phi = (jwI - A)^{-1}$ and

$$T_{LO} = K_c \Phi B \quad (9.41)$$

(9.40) becomes

$$[I + T_{LQ}]^*[I + T_{LQ}] = I + \frac{1}{\rho}[H\Phi B]^*[H\Phi B] \qquad (9.42)$$

For these to be equal, the eigenvalues must also be equal, so that

$$\lambda\{[I + T_{LQ}]^*[I + T_{LQ}]\} = \lambda\{I + \frac{1}{\rho}[H\Phi B]^*[H\Phi B]\}$$

$$= 1 + \frac{1}{\rho}\lambda\{[H\Phi B]^*[H\Phi B]\} \qquad (9.43)$$

The last step in (9.43) is a result of the properties given in (2.19) and (2.20). Remembering that singular values are defined by (see (2.31))

$$\sigma_i^2[A] = \lambda_i[A^*A] \qquad (9.44)$$

we can rewrite (9.43) as

$$\sigma_i^2[I + T_{LQ}] = 1 + \frac{1}{\rho}\sigma_i^2[H\Phi B] \qquad (9.45)$$

or

$$\sigma_i[I + T_{LQ}] = \sqrt{1 + \frac{1}{\rho}\sigma_i^2[H\Phi B]} \qquad (9.46)$$

which is valid for all σ_i, and in particular $\underline{\sigma}$ and $\bar{\sigma}$.

9.2.1.1 Performance Properties

Good performance, as we have seen, requires high loop gains at low frequencies. Notice that whenever $\underline{\sigma}[T_{LQ}] \gg 1$, (9.46) becomes

$$\sigma_i[T_{LQ}] \simeq \frac{1}{\sqrt{\rho}}\sigma_i[H\Phi B] \qquad (9.47)$$

This equation holds for all σ_i since all singular values are greater than or equal to $\underline{\sigma}$ by definition. Remember that H and ρ are the tunable parameters in the regulator design. Therefore, H and ρ may be chosen to meet the low frequency performance requirements we described in Chapter 4. That is, at low frequency where the loop gains T_{LQ} are high, (9.47) says that the singular values of $\frac{1}{\sqrt{\rho}}H\Phi B$ are a good approximation to those of T_{LQ}. This is extremely convenient because calculation of T_{LQ} requires solving a Riccati equation, whereas plotting the singular values of $\frac{1}{\sqrt{\rho}}H\Phi B$ does not. Therefore, many different choices of H and ρ may be made with a minimum amount of computation.

H may also be chosen to attempt to bring $\underline{\sigma}[T_{LQ}]$ and $\bar{\sigma}[T_{LQ}]$ closer together (especially at crossover), which typically produces a better design. We will discuss this further in Chapter 11. Once H and ρ have been chosen to produce desirable $\frac{1}{\sqrt{\rho}}\sigma_i[H\Phi B]$, the singular values of T_{LQ} can be calculated to verify the approximation (remember that it is good for low frequency only). As a final note, we add that it may be necessary to append dynamics (especially integrators) to the plant in order to meet the performance specs. We will develop this in detail in the next chapter.

9.2.1.2 Crossover Properties

Looking at (9.46), it is immediately obvious that

$$\sigma_i[I + T_{LQ}] > 1 \qquad \forall \ w \qquad (9.48)$$

In Ref [9-1], Laub proves that this also implies

$$\sigma_i[I + T_{LQ}^{-1}] > \frac{1}{2} \qquad \forall \ w \qquad (9.49)$$

Therefore, by using the gain and phase margin formulas in Chapter 3, we again see that the LQ Regulator loop has excellent crossover properties.

9.2.1.3 Robustness Properties

Looking back to equation (4.84), we have

$$\underline{\sigma}[I + \{G(jw)K(jw)\}^{-1}] > \ell_m(w) \qquad (9.50)$$

T_{LQ} is our loop transfer function, so this equation has the same form as (9.49). Therefore, (9.49) guarantees stability for all unstructured uncertainties reflected to the input of the plant which satisfy $\ell_m(w) < 0.5$. Notice that here $\ell_m(w)$ denotes <u>input</u> multiplicative uncertainty. This guarantee will cover our typical low frequency uncertainties, but we have seen that $\ell_m(w)$ usually grows greater than unity at high frequencies. Therefore, it is necessary to directly manipulate the high frequency behavior of T_{LQ}. Under minimum phase

assumptions on HΦB, the LQ Regulator gains behave such that

$$\sqrt{\rho}\, K_c \longrightarrow WH \qquad \text{as } \rho \to 0 \tag{9.51}$$

where W is an orthonormal matrix (Ref [9-2]). At high frequencies, we can represent jw as

$$s = jc/\sqrt{\rho} \qquad \text{as } \rho \to 0 \tag{9.52}$$

where c is a constant. Therefore

$$T_{LO}(jc/\sqrt{\rho}) = K_c [(jc/\sqrt{\rho})I - A]^{-1} B$$

$$= \sqrt{\rho}\, K_c (jcI - \sqrt{\rho}\, A)^{-1} B$$

$$\implies WH(jcI)^{-1} B = WHB/jc \qquad \text{as } \rho \to 0 \tag{9.53}$$

Note that crossovers, by definition, occur at $\sigma_i [T_{LO}] = 1$. Also note that we can write c as

$$jw = jc/\sqrt{\rho} \qquad c = w\sqrt{\rho} \tag{9.54}$$

Therefore, c at crossover can be written as $w_c\sqrt{\rho}$, where w_c denotes crossover frequency. The maximum crossover frequency corresponds to $\bar{\sigma}[T_{LO}]$, so that (9.53) becomes

$$\bar{\sigma}[T_{LO}]_c = \bar{\sigma}\left[\frac{WHB}{jw_{c_{max}}\sqrt{\rho}}\right] = 1 \tag{9.55}$$

or

$$w_{c_{max}} = \bar{\sigma}[HB]/\sqrt{\rho} \tag{9.56}$$

Note that W vanishes since it is orthonormal (all $\sigma_i = 1$), and the magnitude of j is unity. Equation (9.56) gives us an expression for the maximum crossover frequency of T_{LO}. This frequency cannot be much beyond the frequency where $\ell_m = 1$. Therefore, choices of H and ρ that satisfy our performance requirements must also satisfy

$$w_{c_{max}} < w_\ell \tag{9.57}$$

where w_ℓ is defined as the frequency where $\ell_m = 1$, and $w_{c_{max}}$ is given by (9.56).

Equation (9.53), which says that

$$T_{LQ}(jw) \longrightarrow \frac{WHB}{jw\sqrt{\rho}} \qquad as \quad \rho \rightarrow 0 \qquad (9.58)$$

also shows that an attenuation rate of $1/w$ (-20 dB/decade) is the price
we pay for the excellent margins near crossover. If $\ell_m^{-1}(w)$ attenuates
faster than this, further reduction of $w_{c_{max}}$ may be required to meet the
robustness conditions.

9.2.2 Full-State Loop Transfer Recovery Using the Filter

Now that we have designed our full-state regulator loop to have good
performance properties (Section 9.2.1.1), good crossover properties
(Section 9.2.1.2), and good robustness properties (Section 9.2.1.3), we
need to add a Kalman filter into the system using the recovery technique
developed in Chapter 8. In Chapter 8, we said that our system must be
square -- here we will relax this to $r \geq m$ (equal number or more outputs
than inputs). Also, $C\Phi B$, the open-loop plant, must be minimum phase.
There are two steps in our filter design/recovery procedure:

1) if necessary, append dummy columns to B and zero rows to K_c to
make $C\Phi B$ and $K_c\Phi B$ square (rxr). Note that the dummy columns of B <u>must</u>
be chosen so that $C\Phi B$ remains minimum phase.

2) design the Kalman filter with modified noise intensity matrices

$$Q_f = \Gamma\Gamma^T + q^2 BVB^T \qquad (9.59)$$

$$R_f = \mu I \qquad (9.60)$$

where q is a scalar which takes on a sequence of increasingly larger
values, and V is an arbitrary symmetric positive definite matrix.
Usually, we let $V = I$. As shown in Chapter 8, (modifying (8.52)-(8.54)
to the LQG notation), the loop transfer function of the LQG loop behaves
such that

$$K(s)G(s) \longrightarrow [K_c \Phi B (C \Phi B)^{-1}] C \Phi B = K_c \Phi B \qquad (9.61)$$

as $q^2 \longrightarrow \infty$ in (9.59). Therefore, the LQG loop asymptotically approaches the desired T_{LO} we have just designed. Notice this recovery inverts the plant from the left and thus dictates our minimum phase requirement on the plant.

Note that this procedure corresponds to breaking the loop at point Ⓓ (the plant input) in Fig 9.1, and recovering the loop transfer function of point Ⓒ.

9.3 LQG/LTR Design Breaking the Loop at the Plant Output

All of the development in this section is a dual of the development in Section 9.2. Therefore, we will move much more quickly and leave the verification to the reader.

9.3.1 Full-State Kalman Filter Design

Here we will treat Γ and μ as completely tunable parameters rather that fixed noise intensities. The loop transfer function of the filter is given by

$$T_{KF} = C \Phi K_f \qquad (9.62)$$

Using the Kalman Equality corresponding to the filter, we have the relation

$$[I + T_{KF}][I + T_{KF}]^* = I + \frac{1}{\mu}[C \Phi \Gamma][C \Phi \Gamma]^* \qquad (9.63)$$

Therefore

$$\sigma_i [I + T_{KF}] = \sqrt{1 + \frac{1}{\mu} \sigma_i^2 [C \Phi \Gamma]} \geq 1 \qquad (9.64)$$

At low frequency, where $\sigma_i[T] \gg 1$, this can be simplified as

$$\sigma_i [T_{KF}] \simeq \frac{1}{\sqrt{\mu}} \sigma_i [C \Phi \Gamma] \qquad (9.65)$$

Again, many choices of Γ and μ may be made without solving Riccati equations in order to meet the performance specs. Again, it may be necessary to augment dynamics to the plant in order to meet these specs.

9-13

The same guaranteed margins hold for the Kalman filter as for the LQ

Regulator, so that crossover properties are very good. Finally, as

$\mu \to 0$,

$$\sqrt{\mu}\, K_f \longrightarrow W\Gamma \tag{9.66}$$

where W is again any orthonormal matrix. This implies

$$w_{c_{max}} = \bar{\sigma}[C\Gamma]/\sqrt{\mu} \tag{9.67}$$

Notice that in this procedure, $\ell_m(w)$ is not, in general, the same as in

the previous section. Here it denotes a bound on the uncertainties

entering at the output of the plant, such as sensor dynamics errors.

9.3.2 Full-State Loop Transfer Recovery Using the Regulator

Again, this is a two step procedure:

1) assume $m \geq r$ (equal number or more inputs than outputs). Append

dummy rows to C and zero columns to K_f so that $C\Phi K_f$ and $C\Phi B$ are square

(mxm). The dummy rows of C <u>must</u> be chosen so that $C\Phi B$ remains

minimum phase.

2) design the LQ Regulator with weighting matrices

$$Q_c = H^T H + q^2 C^T V C \tag{9.68}$$

$$R_c = \rho I \tag{9.69}$$

where q is a scalar taking on increasingly larger values and V is an

arbitrary, symmetric positive definite matrix. Then as $q^2 \to \infty$

$$\frac{K_c}{q} \longrightarrow WC \tag{9.70}$$

and

$$G(s)K(s) \longrightarrow C\Phi B[(C\Phi B)^{-1} C\Phi K_f] = C\Phi K_f \tag{9.71}$$

which is the Kalman filter loop T_{KF} we just designed. Notice this

recovery inverts the plant from the right and thus dictates our minimum

phase plant requirement.

This procedure corresponds to breaking the loop at point (A) (plant output) in Fig 9.1, and recovering the loop transfer function of point (B .

9.4 Good News for the Lost

By now, the mass of equations in the preceding chapters probably has you wanting to ignore this method completely. Therefore, the next chapter starts out with a "cookbook" approach to appending dynamics to the plant, then summarizes everything thus far by giving a step-by-step outline of the method, whether breaking at the input or at the output of the plant.

Chapter 9 References

[9-1] A.J. Laub, "Robust Stability of Linear Systems - Some Computational Considerations", LIDS-R-904, Mass. Inst. of Tech., Cambridge, MA, Feb 1979.

[9-2] H. Kwakernaak and R. Sivan, Linear Optimal Control Systems, Wiley-Interscience, New York, 1972.

[9-3] G. Stein, "LQG-Based Multivariable Design: Frequency Domain Interpretation", AGARD Lecture Series 117, Sept 1981.

[9-4] M. Athans, "Lecture Notes on Multivariable Control Systems", LIDS Report, Mass. Inst. of Tech., Cambridge, MA, June 1984.

10. AUGMENTING DYNAMICS AND A STEP-BY-STEP OUTLINE OF LQG/LTR

In this chapter, we give a summary of what we have developed so far. Also, since it is usually necessary in the application of the method, we include the development of how to augment dynamics (typically integrators) to the open-loop plant. To give equal treatment, we will begin with the procedure for breaking the loop at the output to the plant, since we started with the input last chapter.

10.1 Loop Broken at the Output

Here, we assume that all uncertainties in our system are modelled such that they enter at the output to the plant. Therefore, we wish to break the LQG loop at the plant output and examine the loop transfer matrix $G_p(s)K(s)$ to ensure that it will yield

a) good command following

b) good output disturbance rejection

c) good robustness to modelling errors reflected to the plant output

Fig 10.1 shows a block diagram of the LQG system.
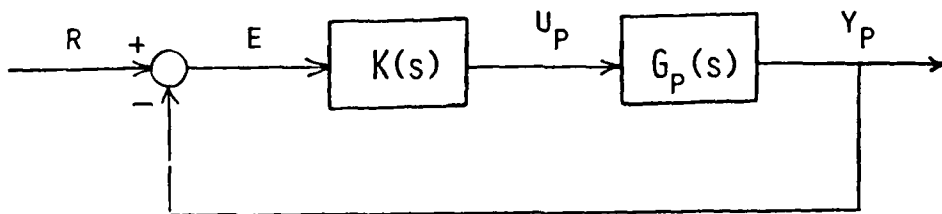
Fig 10.1 MIMO Block Diagram

Note that we have denoted the plant as $G_p(s)$, with the input and output labelled as u_p and y_p, respectively. Fig 10.2 shows a block diagram of our uncertainty representation.
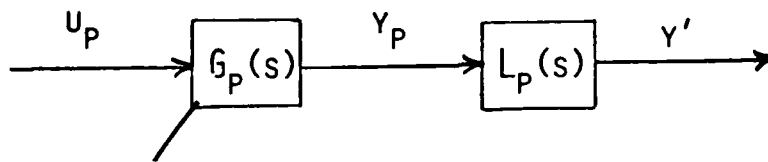
Fig 10.2 Output Multiplicative Uncertainty

Keep in mind that the only places it makes sense to insert uncertainties

is where nature does, i.e., at the input u_p or output y_p to the plant.

LQG is limited in how it can affect the loop shapes of the system.
Since we desire high loop gains at low frequency, and usually want zero
steady-state tracking error, we need integral action in the loop. If
pure integrators are not in the plant to begin with (for aircraft they
usually are not), we need to augment them to our plant. Actually, we
can augment any dynamics we wish to, but integrators are the most common
choice. Let $G_a(s)$ denote the square augmented transfer matrix. For
integrators, this is obviously given by

$$G_a(s) = \frac{1}{s} I \qquad\qquad (10.1)$$

Technically, this is part of the compensator since the designer chooses
it. Now we must decide where to put this transfer function. Let's try
at the input to the plant and see if it makes sense. Fig 10.3 shows the
new block diagram.
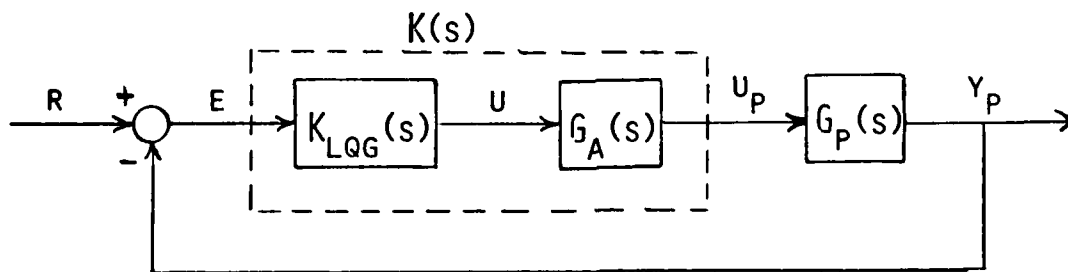
Fig 10.3 Block Diagram of the Input-Augmented LQG System

10-2

Note in Fig 10.3 that we have defined our overall compensator $K(s)$ as

$$K(s) = G_a(s)K_{LQG}(s) \tag{10.2}$$

where $K_{LQG}(s)$ is the LQG compensator we discussed in several previous chapters and will design using LQG/LTR. Therefore, we can define the open-loop augmented plant as

$$G(s) \triangleq G_p(s)G_a(s) \tag{10.3}$$

Note that the input to $G(s)$ is not the physical input $u_p(s)$, but rather the control signal $u(s)$; the output from $G(s)$ is the physical output $y_p(s)$, however. Therefore, it does make sense to break the loop at the output from $G(s)$ in this system. Had we augmented dynamics at the plant output, it would not make sense to break the loop at the output of $G(s)$. Therefore, Fig 10.3 shows the correct choice of augmentation.

In state space form, $G(s)$ becomes

$$\dot{x}(t) = Ax(t) + Bu(t) + \Gamma\xi(t) \tag{10.4}$$

$$y_p(t) = Cx(t) + n(t) \tag{10.5}$$

If the original $G_p(s)$ was defined by the triple (A_p, B_p, C_p) and $G_a(s)$ was defined by (A_a, B_a, C_a), the new triple for $G(s)$ is given by

$$A = \begin{bmatrix} A_p & B_p C_a \\ 0 & A_a \end{bmatrix} \tag{10.6}$$

$$B = \begin{bmatrix} 0 \\ B_a \end{bmatrix} \tag{10.7}$$

$$C = \begin{bmatrix} C_p & 0 \end{bmatrix} \tag{10.8}$$

This is shown in detail in Appendix 10A. Note that this may not yield a minimal realization, and minimization should be done before proceeding. Appendix 10B provides a brief discussion of realizations. Also note that we do not give Γ a specified form here since we will consider it to be completely tunable. If $G_a(s)$ is given by (10.1), then $A_a = \underline{0}$ (the

zero matrix) and $B_a = C_a = I$.

With the problem set up in this form, we first must design a Kalman filter, and then design an LQ Regulator to recover the filter's loop shape. The Kalman Equality gives (see last chapter)

$$(I + T_{KF})(I + T_{KF})^* = I + \frac{1}{\mu}(T_{FOL})(T_{FOL})^* \qquad (10.9)$$

where

$$T_{KF} = C\Phi K_f \qquad (10.10)$$

and

$$T_{FOL} = C\Phi\Gamma \qquad (10.11)$$

Γ and μ are the tunable design parameters. As $\mu \to 0$, the filter gains K_f become large, and therefore so does $\underline{\sigma}[T_{KF}]$ at low frequency. For $\underline{\sigma}[T_{KF}] \gg 1$,

$$\sigma_i[T_{KF}] \simeq \frac{1}{\sqrt{\mu}}\sigma_i[T_{FOL}] \qquad (10.12)$$

Again, this was shown explicitly in Chapter 9. Using this approximation, we may now begin our step-by-step procedure.

STEP 1:

a) Select Γ and μ such that the command following, disturbance rejection, and crossover frequency specs are met by $\frac{1}{\sqrt{\mu}}\sigma_i[T_{FOL}]$. That is, we would like the plots of $\frac{1}{\sqrt{\mu}}\sigma_i[T_{FOL}]$ to meet the low frequency requirements of Fig 10.4. These requirements were derived in detail in Chapter 4. Note that this requires construction of an $\ell_m(w)$ and a $p(w)$ profile. There is no automatic procedure to construct these, and we will discuss them further when we do some examples.
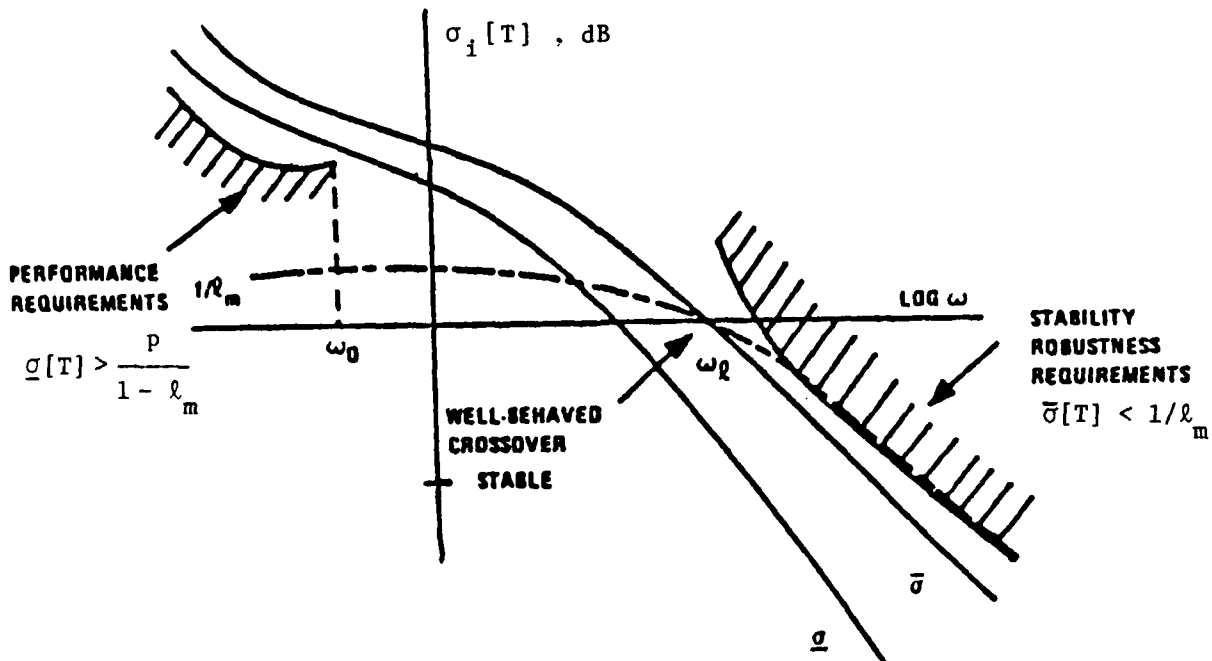
Fig 10.4 Desired Loop Shapes

The approximation between T_{KF} and T_{FOL} is really only good at low frequency, so that Γ and μ should be chosen to meet the low frequency performance bound. We would also like the $\underline{\sigma}$ and $\overline{\sigma}$ plots to be close together, especially near crossover, which can also be affected by changing Γ. A more formal procedure for bringing the plots together is discussed in Chapter 11. Our requirement for good crossover properties is satisfied automatically by the full-state filter. Finally, we must have $w_{c_{max}} = \overline{\sigma}[CT]/\sqrt{\mu}$ less than the frequency where ℓ_m crosses the 0 dB line.

b) After the necessary iterations, plot $\dfrac{1}{\sqrt{\mu}}\sigma_i[T_{FOL}]$ that meets the specs.

c) Save Γ and μ from the step above.

STEP 2:

a) Using the values of Γ and μ in 1c), solve

10-5

$$0 = A\Sigma + \Sigma A^T + \Gamma\Gamma^T - \frac{1}{\mu}\Sigma C^T C\Sigma \qquad (10.13)$$

for Σ.

b) Calculate the filter gain matrix K_f using

$$K_f = \frac{1}{\mu}\Sigma C^T \qquad (10.14)$$

c) Calculate and plot $\sigma_i[T_{KF}]$, where $T_{KF} = C\Phi K_f$. These should match those found in Step 1b) at frequencies below crossover.

d) Calculate and plot

$$\sigma_i[I + T_{KF}] \geq 1 \qquad (10.15)$$

$$\sigma_i[I + T_{KF}^{-1}] \geq \frac{1}{2} \qquad (10.16)$$

These are actually not tests -- they are facts. That is, inequalities (10.15) and (10.16) <u>must</u> hold for any full-state Kalman filter. If violated, you have made a serious error somewhere.

e) Double check for guaranteed robustness by verifying that

$$\ell_m < \underline{\sigma}[I + T_{KF}^{-1}] \qquad (10.17)$$

or

$$1/\ell_m > \bar{\sigma}\{T_{KF}[I + T_{KF}]^{-1}\} \qquad (10.18)$$

holds for all frequency. In practice, (10.18) is better conditioned numerically than (10.17). If this fails, go back to step 1a) and start again, unless the violation is at very high frequency. Remember that when we build this up into an LQG compensator, it will have an additional 20 dB/decade roll-off, so that we <u>may</u> eliminate the violation.

<u>STEP 3</u>:

a) Calculate the transmission zeros of $C\Phi B$, the open-loop plant. If all of them are in the left-half s-plane, we will be able to asymptotically recover the loop shape T_{KF} we just designed. If some are in the right-half s-plane, full recovery is not possible. We will

10-6

discuss this further later. For now, we assume we do have a minimum phase plant.

b) Design a sequence of LQG compensators by designing an LQ Regulator which recovers the properties of the full-state filter. First, solve

$$0 = PA + A^T P + Q_c - PBR_c^{-1}B^T P \qquad (10.19)$$

where

$$Q_c = H^T H + q^2 C^T V C \qquad (10.20)$$

and

$$R_c = \rho I \qquad (10.21)$$

and let $q \to \infty$. H, V, and ρ are free to be chosen by the designer, with V usually set equal to the identity matrix.

Second, calculate the LQ control gain matrix K_c by

$$K_c = R_c^{-1} B^T P \qquad (10.22)$$

c) Calculate the LQG compensator transfer function

$$K_{LQG}(s) = K_c(sI - A + BK_c + K_f C)^{-1}K_f \qquad (10.23)$$

d) Calculate the resulting loop transfer matrix for the loop broken at the plant output

$$
\begin{aligned}
T_o(s) &= G(s)K_{LQG}(s) \\
&= G_p(s)G_a(s)K_{LQG}(s) \\
&= G_p(s)K(s) \qquad (10.24)
\end{aligned}
$$

Calculate and plot $\sigma_i[T_o]$.

e) Compare $\sigma_i[T_o]$ from the previous step with $\sigma_i[T_{KF}]$ from step 2b). If they are sufficiently different (remember that T_o will always be different at high frequency due to an additional 1-pole roll-off), increase q in step 3b) and repeat 3b)-3c). Continue this until reasonable agreement between $\sigma_i[T_o]$ and $\sigma_i[T_{KF}]$ is obtained.

f) Calculate and plot $\sigma_i[I + T_o^{-1}]$. Double-check for guaranteed robustness by verifying that

$$1/\ell_m > \overline{\sigma}\{ T_o[I + T_o]^{-1} \} \tag{10.25}$$

and that the boundaries on Fig 10.4 are not violated by T_o.

g) If all these tests are passed, then

$$K(s) = G_a(s)K_{LQG}(s) \tag{10.26}$$

This ends the procedure for breaking the loop at the output.

10.2 Loop Broken at the Input

This is the mathematical dual of the previous procedure. Here, we reflect our errors to the input of the plant, and must therefore augment our dynamics at the output. However, since the output y_p is what we measure through our sensors, we cannot augment until after we feed back the unaugmented output. Therefore, we move the augmentation to the front of our controller, as shown in Fig 10.5.
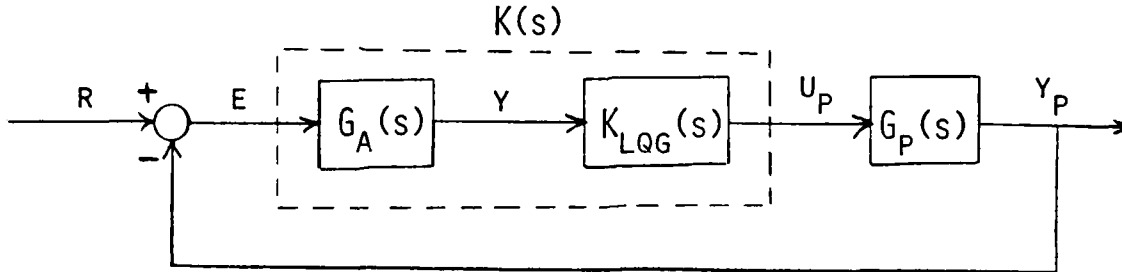
Fig 10.5 Block Diagram of the Output-Augmented LQG System

Looking at Fig 10.5, we can see that

$$K(s) = K_{LQG}(s)G_a(s) \tag{10.27}$$

where $G_a(s)$ represents our augmented dynamics and $K_{LQG}(s)$ is our LQG compensator. We will now let

$$G(s) \triangleq G_a(s)G_p(s) \tag{10.28}$$

and design a compensator for this augmented plant. In state space form, $G(s)$ is given by

$$\dot{x}(t) = Ax(t) + Bu_p(t) + \Gamma\xi(t) \tag{10.29}$$

$$y(t) = Cx(t) + n(t) \tag{10.30}$$

where

$$A = \begin{bmatrix} A_a & B_a C_p \\ 0 & A_p \end{bmatrix} \tag{10.31}$$

$$B = \begin{bmatrix} 0 \\ B_p \end{bmatrix} \tag{10.32}$$

$$C = [C_a \quad 0] \tag{10.33}$$

Again note that this realization may not be minimal, and should be minimized before continuing. Appendix 10A shows the derivation of this realization, and discusses the reworking of the noises.

With the problem set up in this form, first design the LQ Regulator, then design a Kalman filter so that the LQG loop recovers the regulator loop. The Kalman Equality for this case is

$$(I + T_{LQ})^*(I + T_{LQ}) = I + \frac{1}{\rho}(T_{ROL})^*(T_{ROL}) \tag{10.34}$$

where

$$T_{LQ} = K_c \Phi B \tag{10.35}$$

and

$$T_{ROL} = H\Phi B \tag{10.36}$$

H and ρ are the tunable design parameters. As $\rho \to 0$, the regulator gains K_c become large, and at low frequency $\underline{\sigma}[T_{LQ}] \gg 1$. Therefore,

$$\sigma_i[T_{LQ}] \simeq \frac{1}{\sqrt{\rho}}\sigma_i[T_{ROL}] \tag{10.37}$$

We now begin our step-by-step procedure.

STEP 1:

a) Select H and ρ such that the stated command-following, disturbance rejection, and crossover frequency specs are met by $\frac{1}{\sqrt{\rho}}\sigma_i[T_{ROL}]$. That is, we want σ_i high at low frequency to clear our

performance barrier, $\underline{\sigma}$ and $\bar{\sigma}$ close together if possible, and $w_{c_{max}} = \frac{1}{\sqrt{\rho}} \bar{\sigma}[HB]$ to be less than the frequency where ℓ_m crosses 0 dB.

   b)   After the necessary iterations, plot $\frac{1}{\sqrt{\rho}} \sigma_i[T_{ROL}]$ that meets the specs.

   c)   Save H and ρ used in the above step.

STEP 2:

   a)   Using the values of H and ρ from step 1c), solve

$$0 = PA + A^T P + H^T H - \frac{1}{\rho} PBB^T P \tag{10.38}$$

   b)   Calculate the regulator gain matrix K_c using

$$K_c = \frac{1}{\rho} B^T P \tag{10.39}$$

   c)   Calculate and plot $\sigma_i[T_{LQ}]$ using (10.35). These plots should match those found in step 1b) at frequencies below crossover.

   d)   Calculate and plot

$$\sigma_i[I + T_{LQ}] \geqslant 1 \tag{10.40}$$

$$\sigma_i[I + T_{LQ}^{-1}] \geqslant \frac{1}{2} \tag{10.41}$$

as a double-check on your results. These tests are guaranteed to pass.

   e)   Double-check for guaranteed robustness by verifying that

$$1/\ell_m > \bar{\sigma}\{T_{LQ}[I + T_{LQ}]^{-1}\} \tag{10.42}$$

If not, go back to step 1a) and start over, unless the violation is at very high frequency.

STEP 3:

   a)   Calculate the transmission zeros of the open-loop plant, $C\Phi B$. If they are all in the left-half plane, we will be able to recover T_{LQ} when we add our filter.

   b)   Design a sequence of LQG compensators. First, solve

$$0 = A\Sigma + \Sigma A^T + Q_f - \Sigma C^T R_f^{-1} C\Sigma \tag{10.43}$$

where

$$\Omega_f = \Gamma \Gamma^T + q^2 BVB^T \qquad (10.44)$$

and

$$R_f = \mu I \qquad (10.45)$$

and let $q \to \infty$. Γ and μ are the nominal intensities of the process and measurement noises, respectively (often, we allow them to be tunable). V is free to be chosen, and usually taken as the identity matrix.

Second, calculate the Kalman filter gain matrix K_f by

$$K_f = \Sigma C^T R_f^{-1} \qquad (10.46)$$

c) Calculate the LQG compensator transfer function

$$K_{LQG}(s) = K_c (sI - A + BK_c + K_f C)^{-1} K_f \qquad (10.47)$$

d) Calculate the resulting loop transfer matrix for the loop broken at the plant input

$$\begin{aligned}
T_i(s) &= K_{LQG}(s)G(s) \\
&= K_{LQG}(s)G_a(s)G_p(s) \\
&= K(s)G_p(s)
\end{aligned} \qquad (10.48)$$

Calculate and plot $\sigma_i[T_i]$.

e) Compare $\sigma_i[T_i]$ from the previous step with $\sigma_i[T_{LQ}]$ from step 2b). If they are sufficiently different (except at high frequency, where they _must_ be different), increase q in step 3b) and repeat 3b)-3e). Continue this until reasonable agreement between $\sigma_i[T_i]$ and $\sigma_i[T_{LQ}]$ is obtained.

f) Double-check for guaranteed robustness by verifying that

$$1/\ell_m > \bar{\sigma}\{T_i[I + T_i]^{-1}\} \qquad (10.49)$$

and that the boundaries of Fig 10.4 (using the appropriate ℓ_m and p) are not violated by T_i.

g) If all these tests are passed, then

$$K(s) = K_{LQG}(s)G_a(s) \qquad (10.50)$$

This ends the procedure for breaking the loop at the input.

Technically, this is all we need to do an LQG/LTR design. However, some of the steps outlined above are more difficult in practice than they appear. Specifically, choosing either Γ and μ or H and ρ to produce a desired loop shape and to have $\underline{\sigma}$ and $\overline{\sigma}$ close together can be quite difficult and time-consuming. In the next chapter, we will discuss techniques to draw $\underline{\sigma}$ and $\overline{\sigma}$ together at certain frequencies, as well as a technique to do "formal loop shaping".

State Space Representations for Cascaded Systems

First, we will give a general derivation for obtaining a state space representation for two systems cascaded together. Suppose that we have the following block diagram
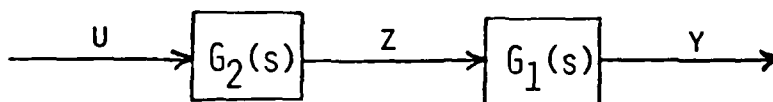
Fig 10A.1 Cascaded Blocks

and we wish to obtain the transfer function

$$G(s) = G_1(s)G_2(s) \tag{10A.1}$$

in state space form, given the state space forms of $G_1(s)$ and $G_2(s)$. Specifically, let $G_1(s)$ be defined by

$$\dot{x}_1 = A_1x_1 + B_1z \tag{10A.2}$$

$$y = C_1x_1 + D_1z \tag{10A.3}$$

and $G_2(s)$ be defined by

$$\dot{x}_2 = A_2x_2 + B_2u \tag{10A.4}$$

$$z = C_2x_2 + D_2u \tag{10A.5}$$

The input to $G(s)$ as defined by (10A.1) would be u, and the output would be y. Therefore, we need to eliminate z. We can do this by substituting (10A.5) into (10A.2) and (10A.3) to obtain

$$\dot{x}_1 = A_1x_1 + B_1C_2x_2 + B_1D_2u \tag{10A.6}$$

$$y = C_1x_1 + D_1C_2x_2 + D_1D_2u \tag{10A.7}$$

Now we can define a new augmented state vector x, given by

$$x = \begin{bmatrix} x_1 \\ x_2 \end{bmatrix} \tag{10A.8}$$

so that

$$\begin{bmatrix} \dot{x}_1 \\ \dot{x}_2 \end{bmatrix} = \begin{bmatrix} A_1 & B_1C_2 \\ 0 & A_2 \end{bmatrix} \begin{bmatrix} x_1 \\ x_2 \end{bmatrix} + \begin{bmatrix} B_1D_2 \\ B_2 \end{bmatrix} u \qquad (10A.9)$$

$$y = \begin{bmatrix} C_1 & D_1C_2 \end{bmatrix} \begin{bmatrix} x_1 \\ x_2 \end{bmatrix} + [D_1D_2] u \qquad (10A.10)$$

Therefore, our new state space matrices would be given by

$$A = \begin{bmatrix} A_1 & B_1C_2 \\ 0 & A_2 \end{bmatrix} \qquad (10A.11)$$

$$B = \begin{bmatrix} B_1D_2 \\ B_2 \end{bmatrix} \qquad (10A.12)$$

$$C = [C_1 \quad D_1C_2] \qquad (10A.13)$$

$$D = [D_1D_2] \qquad (10A.14)$$

Now let's look at how this applies to our augmented dynamics, and what happens to our noise inputs.

<u>Loop Broken at the Output</u> - Here, $G_1(s)$ becomes $G_p(s)$ and $G_2(s)$ becomes $G_a(s)$. However, we have noises associated with $G_p(s)$. Therefore, our new augmented state dynamics become (assuming $D_p = D_a = 0$)

$$\begin{bmatrix} \dot{x}_p \\ \dot{x}_a \end{bmatrix} = \begin{bmatrix} A_p & B_pC_a \\ 0 & A_a \end{bmatrix} \begin{bmatrix} x_p \\ x_a \end{bmatrix} + \begin{bmatrix} 0 \\ B_a \end{bmatrix} u + \begin{bmatrix} \Gamma_p \\ 0 \end{bmatrix} \xi \qquad (10A.15)$$

$$y = [C_p \quad 0] \begin{bmatrix} x_p \\ x_a \end{bmatrix} + n \qquad (10A.16)$$

These obviously produce the A, B, and C matrices given in (10.6)-(10.8). Formally, the new Γ matrix is given by the last term in (10A.15), but since we consider it to be a tunable parameter, we will not impose this structure upon it.

<u>Loop Broken at the Input</u> - This is a bit trickier than the output case. Here, $G_1(s)$ becomes $G_a(s)$ and $G_2(s)$ becomes $G_p(s)$. Again, we have noises associated with $G_p(s)$. Note, however, that the output y

from the augmented system has no measurement noise directly associated
with it – the output y_p (which we wish to eliminate) does. This noise
propagates to y through the x_a states. Therefore, we will assume that
we can define a new noise, again represented by n, which enters the
outputs y instead of y_p. Our new state space then becomes (again
assuming $D_a = D_p = 0$)

$$
\begin{bmatrix} \dot{x}_a \\ \dot{x}_p \end{bmatrix} = \begin{bmatrix} A_a & B_a C_p \\ 0 & A_p \end{bmatrix} \begin{bmatrix} x_a \\ x_p \end{bmatrix} + \begin{bmatrix} 0 \\ B_p \end{bmatrix} u_p + \begin{bmatrix} 0 \\ \Gamma_p \end{bmatrix} \xi \qquad (10A.17)
$$

$$
y = \begin{bmatrix} C_a & 0 \end{bmatrix} \begin{bmatrix} x_a \\ x_p \end{bmatrix} + n \qquad (10A.18)
$$

which gives us the A, B, and C matrices in (10.31)-(10.33).
Technically, the Γ matrix given in (10A.17) should be used in (10.44).
Usually, we let $\Gamma = 0$ in this equation, however, since the q^2 term
overwhelms it. When we simulate the system, we will "move" the noise
back to y_p where it belongs. The value of μ we use in (10.45) is not
that critical, since it can be compensated for by adjusting q^2 (q^2 will
dominate, anyway).

APPENDIX 10B

State Space Realizations

The state space realizations for the cascaded systems described by (10.4)-(10.8), (10.29)-(10.33), and in Appendix 10A may not be minimal. First, let's define a realization. A state space realization of the transfer function G(s) is any quadruple (A, B, C, D) which satisfies

$$G(s)= C(sI - A)^{-1}B + D \qquad (10B.1)$$

We say any quadruple as there are an infinite number of them. There are a variety of methods (which may be found in several texts on linear systems) to find such a set of matrices. A minimal realization of G(s) is one such that the A matrix has the smallest possible dimension. It is easy to prove that a minimal realization (again not unique) must be controllable and observable. If not, there would be pole-zero cancellations, which would account for the additional unnecessary states. Reversing this argument, if we augment our system with dynamics which cause a pole-(transmission)zero cancellation, the realization will be nonminimal and the resulting system will be either uncontrollable, unobservable, or both. This will especially cause problems if integrators are augmented to a system with a zero at the origin. Therefore, a minimal realization of the system should be used in the design.

Computer packages such as MATRIX$_X$ and CONTROL-C will easily find the realization of a transfer function, as well as find a corresponding minimal realization.

Chapter 10 References

[10-1] M. Athans, "Lecture Notes on Multivariable Control Systems", LIDS Report, Mass. Inst. of Tech., Cambridge, MA, June 1984.

[10-2] J. C. Doyle, "Matrix Interpolation Theory and Optimal Control", Ph.D. Dissertation, University of California, Berkeley, Dec 1984.

11. LOOP SHAPING TECHNIQUES

In this chapter, we will briefly present two techniques to aid the designer in choosing the required parameters to shape the filter or regulator loop. Each technique has advantages and disadvantages, which will be pointed out. In general, the designer must choose either Γ and μ to shape the filter loop or H and ρ to shape the regulator loop. The scalars μ and ρ tend to act as "gains" which basically raise or lower the singular value plots without affecting their basic shape. Therefore, the difficult part of the design involves choosing either Γ or H. One method is simply trial and error. This chapter provides two others which the designer can use.

11.1 A Technique for Bringing $\underline{\sigma}$ and $\bar{\sigma}$ Together

This technique can be used in order to draw the maximum and minimum singular values of the loop transfer matrix close together. However, the technique only brings them together over limited frequency ranges, not at all frequencies. Depending on the system, this may or may not be helpful in the design of the system. As usual, dual procedures exist when breaking the loop at the input or output of the plant. Again, we will start with the output.

11.1.1 Loop Broken at the Output

The first assumption we will make is that a bank of integrators is to be augmented to the plant. From Chapter 10, we saw that we must append these to the input of the plant. The two sets of state equations are (ignoring the noises in the plant for brevity)

$$\dot{x}_p = A_p x_p + B_p y_a \qquad (11.1)$$

$$y_p = C_p x_p \qquad (11.2)$$

$$\dot{x}_a = A_a x_a + B_a u \qquad (11.3)$$

11-1

$$y_a = C_a x_a \tag{11.4}$$

Since we have assumed that we augmented integrators, we know that $A_a = 0$ and $B_a = C_a = I$, so that the augmented state equations become

$$\begin{bmatrix} \dot{x}_a \\ \dot{x}_p \end{bmatrix} = \begin{bmatrix} 0 & 0 \\ B_p I & A_p \end{bmatrix} \begin{bmatrix} x_a \\ x_p \end{bmatrix} + \begin{bmatrix} I \\ 0 \end{bmatrix} u \tag{11.5}$$

$$y_p = \begin{bmatrix} 0 & C_p \end{bmatrix} \begin{bmatrix} x_a \\ x_p \end{bmatrix} \tag{11.6}$$

Defining new A, B, and C matrices from the matrices in (11.5) and (11.6), we can derive the expression for $(sI - A)^{-1}$ as

$$(sI - A)^{-1} = \begin{bmatrix} sI & 0 \\ -B_p & sI-A_p \end{bmatrix}^{-1}$$

$$= \begin{bmatrix} \dfrac{I}{s} & 0 \\ (sI-A_p)^{-1}\dfrac{B_p}{s} & (sI-A_p)^{-1} \end{bmatrix} \tag{11.7}$$

You can easily verify that (11.7) is correct, if you wish. Now, remember that the loop we are trying to shape is

$$T_{FOL} = C\Phi\Gamma = C(sI - A)^{-1}\Gamma$$

$$= \begin{bmatrix} 0 & C_p \end{bmatrix} \begin{bmatrix} \dfrac{I}{s} & 0 \\ (sI-A_p)^{-1}\dfrac{B_p}{s} & (sI-A_p)^{-1} \end{bmatrix} \begin{bmatrix} \Gamma_1 \\ \Gamma_2 \end{bmatrix} \tag{11.8}$$

Note that we have written Γ, the process noise distribution matrix, in partitioned form to match the dimensions. Remember we assume that Γ is completely tunable, so this is perfectly legal. Carrying out the multiplication in (11.8), we get

11-2

$$T_{FOL} = C_p(sI - A_p)^{-1}\frac{B_p}{s}\Gamma_1 + C_p(sI - A_p)^{-1}\Gamma_2 \qquad (11.9)$$

Should we desire to tighten the spread of singular values of T_{FOL} at low frequency, we can examine (11.9) at small w (replace s with jw). Obviously, for small w,

$$(jwI - A_p)^{-1} \simeq -A_p^{-1} \qquad (11.10)$$

so that (11.9) becomes

$$T_{FOL} \simeq -C_p A_p^{-1}\frac{B_p}{jw}\Gamma_1 - C_p A_p^{-1}\Gamma_2 \qquad (11.11)$$

Since w is small, the first term dominates. Let's choose

$$\Gamma_1 = -(C_p A_p^{-1} B_p)^{-1} \qquad (11.12)$$

Then (11.11) becomes

$$T_{FOL} \simeq \frac{I}{jw} - C_p A_p^{-1}\Gamma_2 \qquad (11.13)$$

Now, for arbitrary Γ_2, T_{FOL} will look like a bank of pure integrators at low frequency, and the singular values will all be nearly identical. Note that (11.12) actually says

$$\Gamma_1 = G(0)^{-1} \qquad (11.14)$$

that is, the inverse of the plant at $w = 0$. Also note that we could let $\Gamma_2 = 0$ in (11.13), which may produce a matching of singular values over a larger frequency range. To get an approximate match at low frequency, however, we only need to choose

$$\Gamma = \begin{bmatrix} G(0)^{-1} \\ \Gamma_2 \end{bmatrix} \qquad (11.15)$$

where Γ_2 is arbitrary.

Now let's look back to (11.9). If we let w be large,

$$(jwI - A_p)^{-1} \simeq \frac{I}{jw} \qquad (11.16)$$

11-3

so that (11.9) becomes

$$T_{FOL} \simeq C_p B_p \frac{\Gamma_1}{(jw)^2} + C_p \frac{\Gamma_2}{(jw)} \qquad (11.17)$$

At high frequency, the second term dominates. Therefore, let

$$\Gamma_2 = C_p^T (C_p C_p^T)^{-1} \qquad (11.18)$$

We make this strange choice since C_p is rarely square and we don't want to use pseudoinverses. Using (11.18) in (11.17), we get

$$T_{FOL} \simeq C_p B_p \frac{\Gamma_1}{(jw)^2} + \frac{I}{jw} \qquad (11.19)$$

At high frequency, the first term is small compared to the second, so that the singular values at high frequency will be nearly identical for arbitrary Γ_1. Here, we <u>cannot</u> let $\Gamma_1 = 0$, as doing so would remove our low frequency integral action. This is easy to see by looking at (11.9), where the integral action is clearly contained in the first term. In general, therefore, we need to let

$$\Gamma = \begin{bmatrix} \Gamma_1 \\ C_p^T (C_p C_p^T)^{-1} \end{bmatrix} \qquad (11.20)$$

with arbitrary (but nonzero) Γ_1 to get high frequency matching.

We could also try a union of the two choices, that is, let

$$\Gamma = \begin{bmatrix} G(0)^{-1} \\ C_p^T (C_p C_p^T)^{-1} \end{bmatrix} \qquad (11.21)$$

This should produce singular value matching at both low and high frequency. However, at frequencies inbetween, the match may be very poor due to the additional "nonmatched" term in (11.13) and (11.19).

Remember that our real goal was to match the singular values near crossover. Realize that neither low nor high frequency matching, nor a union of the two, may produce this. Whether it does or not depends upon

the structure of the particular example. Also note that the high
frequency matching alone may not work at all, in the long run. By high
frequency matching, we mean matching the singular values of T_{FOL} at high
frequency. What we really need to be matched are the singular values of
T_{KF}. In the previous two chapters we showed that the singular values of
T_{FOL} and T_{KF} are guaranteed to be approximately equal, but _only_ at low
frequency. Therefore, matching $\sigma_i[T_{FOL}]$ at high frequency alone
guarantees nothing as far as $\sigma_i[T_{KF}]$ is concerned.

11.1.2 Loop Broken at the Input

Again we assume that we have augmented a bank of integrators, but
this time at the output to the plant. Therefore, our state equations
are

$$\dot{x}_p = A_p x_p + B_p u_p \tag{11.22}$$

$$y_p = C_p x_p \tag{11.23}$$

$$\dot{x}_a = A_a x_a + B_a y_p \tag{11.24}$$

$$y = C_a x_a \tag{11.25}$$

Since we are augmenting integrators, we know that $A_a = 0$ and $B_a = C_a = I$,
so that the augmented state equations become

$$\begin{bmatrix} \dot{x}_p \\ \dot{x}_a \end{bmatrix} = \begin{bmatrix} A_p & 0 \\ IC_p & 0 \end{bmatrix} \begin{bmatrix} x_p \\ x_a \end{bmatrix} + \begin{bmatrix} B_p \\ 0 \end{bmatrix} u_p \tag{11.26}$$

$$y = \begin{bmatrix} 0 & I \end{bmatrix} \begin{bmatrix} x_p \\ x_a \end{bmatrix} \tag{11.27}$$

Defining new A, B, and C matrices from (11.26) and (11.27), we can
derive the expression for $(sI - A)^{-1}$ as

$$(sI - A)^{-1} = \begin{bmatrix} sI-A_p & 0 \\ -C_p & sI \end{bmatrix}^{-1} = \begin{bmatrix} (sI-A_p)^{-1} & 0 \\ \frac{C_p}{s}(sI-A_p)^{-1} & \frac{I}{s} \end{bmatrix} \tag{11.28}$$

The loop we are trying to shape is

$$T_{ROL} = H\Phi B = H(sI - A)^{-1}B$$

$$= [H_1 \quad H_2] \begin{bmatrix} (sI-A_p)^{-1} & 0 \\ \frac{C_p}{s}(sI-A_p)^{-1} & \frac{I}{s} \end{bmatrix} \begin{bmatrix} B_p \\ 0 \end{bmatrix} \tag{11.29}$$

where we have written H in partitioned form. Carrying out the multiplication in (11.29) we get

$$T_{ROL} = H_1(sI - A_p)^{-1}B_p + H_2\frac{C_p}{s}(sI-A_p)^{-1}B_p \tag{11.30}$$

Without going through the details, for low frequency matching we need to choose

$$H = [H_1 \quad G(0)^{-1}] \tag{11.31}$$

with H_1 arbitrary and $G(0)^{-1}$ the inverse of the plant at $w = 0$. For high frequency matching, we must choose

$$H = [(B_p{}^T B_p)^{-1}B_p{}^T \quad H_2] \tag{11.32}$$

where H_2 is arbitrary, but must be nonzero to retain the low frequency integral action. Again, the union of the two, that is

$$H = [(B_p{}^T B_p)^{-1}B_p{}^T \quad G(0)^{-1}] \tag{11.33}$$

may be chosen to match singular values at low _and_ high frequency. Again, we caution that none of the above procedures guarantee desirable results around crossover.

11.2 Formal Loop Shaping

The above technique for matching the singular values at low or high frequency is obviously limited. We cannot specify the entire loop shape using that technique; we can only dictate the behavior over limited frequency ranges. The technique we will now present, called formal loop shaping, gives us a way to specify all of the loop shapes over the

critical frequency range. There is possibly a severe penalty we pay to do this, however -- it requires the augmentation of additional states. We will start with the plant broken at the output.

11.2.1 Formal Loop Shaping at the Output

Looking back to Chapter 9, we saw that for low frequency, where the loop gains are high,

$$\sigma_i [T_{KF}] = \sigma_i [C\Phi K_f] \simeq \frac{1}{\sqrt{\mu}} \sigma_i [C\Phi\Gamma] \qquad (11.34)$$

As we have seen before, the "shape" of T_{KF} under this approximation is dictated by $C\Phi\Gamma$, and μ becomes a "gain" parameter which raises or lowers the singular value plots. For convenience, let's represent $C\Phi\Gamma$ by $W(s)$. If $W(s)$ is simply some shape we have in the back of our mind, then Γ may be found by trial and error or by the previous procedure in this chapter. If, however, we can represent it as a transfer function matrix, which we will call $W_d(s)$, we can avoid using trial and error.

Let's assume that we know exactly what our loop shapes should look like -- better than that, let's assume that we can represent them with a state space realization

$$W_d(s) = C_d(sI - A_d)^{-1}B_d \qquad (11.35)$$

There should <u>never</u> be a D_d matrix here, as the loop shapes must be strictly proper (more poles than zeros). Also, remember that the $W_d(s)$ we choose must be realizable using a Kalman filter (should have integral action if you have augmented integrators and have a 1-pole excess).

Obviously, to do a realization we must first have a transfer function $W_d(s)$. If we know what we want $\sigma_i [W_d(s)]$ to look like, there are two "missing" pieces of information needed to construct a unique transfer function. They are:

1) phase information

2) cross-coupling information

The first is not a major problem. It makes sense to assume a transfer
function that is minimum phase. The Kalman filter design procedure will
not place a zero in the right-half plane anyway. Therefore, the phase
information is not really needed.

The second missing piece is a bigger problem. There is no way to
determine unique individual multiloop transfer functions from singular
value plots -- that is, there are many transfer functions which produce
the same singular value plots. One easy way around this is to assume
that $W_d(s)$ is diagonal. Then, each $\sigma_i[W_d(s)]$ plot is nothing but a SISO
Bode magnitude plot for each diagonal function. This is the approach we
will take. Constructing transfer functions from Bode magnitude plots of
minimum phase systems is relatively simple, and documented in most
classical control texts.

What we will do is augment the desired dynamics $W_d(s)$ to the output
of the plant. Since these dynamics enter the system via the process
noise (obvious since Γ is involved), we will drive these dynamics by ξ.
Fig 11.1 shows the block diagram.
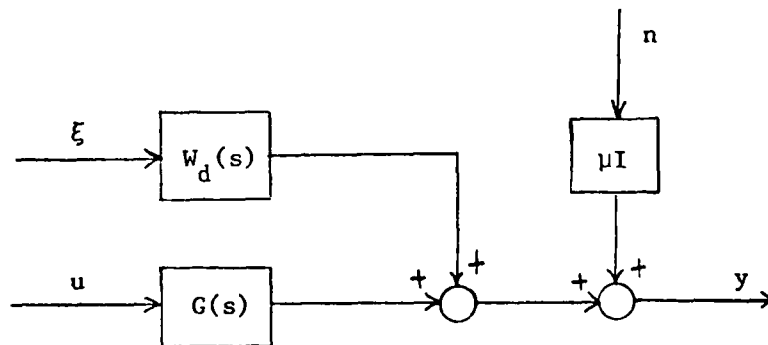
Fig 11.1 Augmenting Desired Dynamics to the Plant Output

Note that we are showing the process noise entering at the output of the

plant. Also, we show the noise n as being unit intensity, but being

multiplied by μI, which is equivalent to our old representation. From

Fig 11.1,

$$y = G(s)u + W_d(s)\xi + \mu In \qquad (11.36)$$

From our original development

$$\dot{x} = Ax + Bu + \Gamma\xi \qquad (11.37)$$

$$y = Cx + \mu In \qquad (11.38)$$

so that

$$y = C\Phi Bu + C\Phi\Gamma\xi + \mu In \qquad (11.39)$$

Comparing (11.36) and (11.39), and remembering that $G(s) = C\Phi B$, we can

see that

$$W_d(s) = C\Phi\Gamma \qquad (11.40)$$

which is exactly what we want when we take the singular values of each

side of (11.40). Now let's look further at the state space block

diagram for this system, as seen in Fig 11.2.
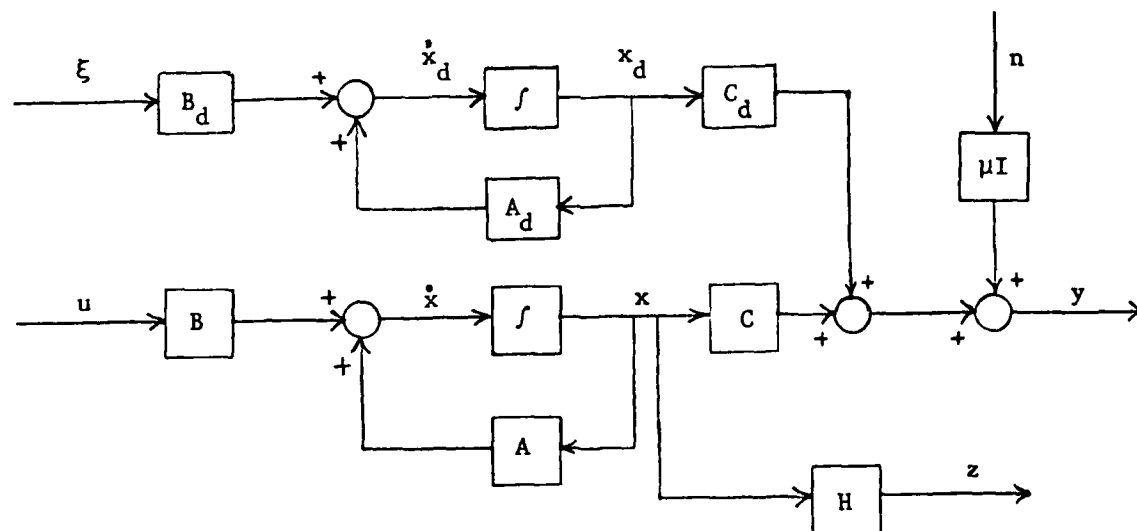
Fig 11.2 State Space Block Diagram of the Output Augmented System

The resulting equations are

$$\dot{x} = Ax + Bu \qquad (11.41)$$

$$\dot{x}_d = A_d x_d + B_d \xi \tag{11.42}$$

$$y = Cx + C_d x_d + \mu In \tag{11.43}$$

$$z = Hx \tag{11.44}$$

which may be written in augmented form as

$$\begin{bmatrix} \dot{x} \\ \dot{x}_d \end{bmatrix} = \begin{bmatrix} A & 0 \\ 0 & A_d \end{bmatrix} \begin{bmatrix} x \\ x_d \end{bmatrix} + \begin{bmatrix} B \\ 0 \end{bmatrix} u + \begin{bmatrix} 0 \\ B_d \end{bmatrix} \xi \tag{11.45}$$

$$y = \begin{bmatrix} C & C_d \end{bmatrix} \begin{bmatrix} x \\ x_d \end{bmatrix} + \mu In \tag{11.46}$$

$$z = \begin{bmatrix} H & 0 \end{bmatrix} \begin{bmatrix} x \\ x_d \end{bmatrix} \tag{11.47}$$

Therefore, we define a new system given by

$$\dot{\tilde{x}} = \tilde{A}\tilde{x} + \tilde{B}u + \tilde{\Gamma}\xi \tag{11.48}$$

$$y = \tilde{C}\tilde{x} + \mu In \tag{11.49}$$

$$z = \tilde{H}\tilde{x} \tag{11.50}$$

where $\tilde{A}$, $\tilde{B}$, $\tilde{C}$, $\tilde{\Gamma}$, and $\tilde{H}$ are given by the corresponding matrices in (11.45)-(11.47).

Notice that (trivially obvious due to block-diagonal form of the $\tilde{A}$ matrix in (11.45))

1) the modes of A_d are uncontrollable from u

2) the modes of A_d are unobservable from z

3) the system is completely observable from y

4) the modes of A are uncontrollable from ξ

Conditions 1) and 2) pose no problem to our Kalman filter design, since the designer chooses A_d and we choose it to be stable. Therefore, A_c will be stabilizable from u and detectable from z. Condition 3) is obviously no problem. However, condition 4) may be a problem. If any

11-10

of the modes of the plant are unstable, then the system would not be stabilizable from ξ. First, we will assume that we have a stable plant. Then we will return to the unstable plant case.

11.2.1.1 Stable Plant

For this case, the $\tilde{\Gamma}$ matrix is given by

$$\tilde{\Gamma} = \begin{bmatrix} 0 \\ B_d \end{bmatrix} \tag{11.51}$$

so that

$$Q_f = \tilde{\Gamma}\tilde{\Gamma}^T = \begin{bmatrix} 0 & 0 \\ 0 & B_d B_d^T \end{bmatrix} \tag{11.52}$$

and

$$R_f = \mu I \tag{11.53}$$

For the recovery procedure, we must use

$$\begin{aligned} Q_c &= \tilde{H}^T\tilde{H} + q^2\tilde{C}^T\tilde{C} \\ &= [H \quad 0]^T[H \quad 0] + q^2[C \quad C_d]^T[C \quad C_d] \\ &= \begin{bmatrix} H^T H & 0 \\ 0 & 0 \end{bmatrix} + q^2 \begin{bmatrix} C^T C & C^T C_d \\ C_d^T C & C_d^T C_d \end{bmatrix} \end{aligned} \tag{11.54}$$

and

$$R_c = \rho I \tag{11.55}$$

Note that in (11.54) we have let the tunable V matrix be identity -- this is not required, it just makes it easier to show the results.

11.2.1.2 Unstable Plant

In this case, the system is not stabilizable from ξ, which is required for the optimal control procedure. Therefore, we rewrite the plant transfer function G(s) as

$$G(s) = B_p(s)^{-1}G_{ms}(s) \tag{11.56}$$

where $G_{ms}(s)$ is minimum phase and stable, and $B_p(s)$ is an all-pass

11-11

filter, that is

$$B_p(jw)B_p(jw)^* = I \qquad \forall\ w \qquad\qquad (11.57)$$

For us, the plant will already be minimum phase, so we simply need to factor out the unstable poles. This is easy, since all the transfer functions have a common denominator. Assuming that we have unstable poles at $s_i = p_i$ (p_i positive), the all-pass filter will have the form

$$B_p^{-1}(s) = \frac{\underset{i}{\pi}(s + p_i)}{\underset{i}{\pi}(s - p_i)}\ I \qquad\qquad (11.58)$$

and $G_{ms}(s)$ will be identical to $G(s)$ except that all $(s - p_i)$ terms will be replaced by $(s + p_i)$ terms.

We can now redraw Fig 11.1 so that our noise ξ enters the system before B_p^{-1}, as shown in Fig 11.3.
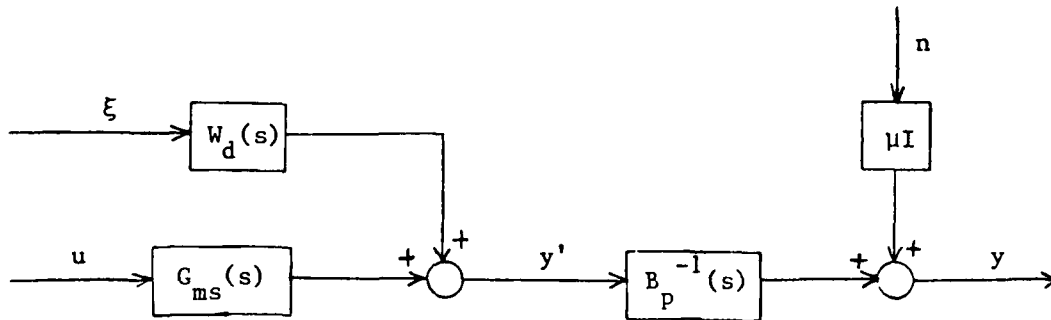
Fig 11.3 Output-Augmented Dynamics for an Unstable Plant

Note that y' looks much like the y in the stable plant case, if we use $G_{ms}(s)$ instead of $G(s)$. We will realize $G_{ms}(s)$ by

$$G_{ms}(s) = C_{ms}(sI - A_{ms})^{-1}B_{ms} \qquad\qquad (11.59)$$

so that the augmented state space becomes

$$\begin{bmatrix} \dot{x} \\ \dot{x}_d \end{bmatrix} = \begin{bmatrix} A_{ms} & 0 \\ 0 & A_d \end{bmatrix}\begin{bmatrix} x \\ x_d \end{bmatrix} + \begin{bmatrix} B_{ms} \\ 0 \end{bmatrix}u + \begin{bmatrix} 0 \\ B_d \end{bmatrix}\xi \qquad\qquad (11.60)$$

$$y' = [\ C_{ms} \quad C_d\ ] \begin{bmatrix} x \\ x_d \end{bmatrix} \tag{11.61}$$

Adding the equation

$$y = B_p^{-1} y' + \mu In \tag{11.62}$$

and the fact that

$$y' = G_{ms} u + W_d \xi \tag{11.63}$$

we get

$$y = B_p^{-1} G_{ms} u + B_p^{-1} W_d \xi + \mu In \tag{11.64}$$

Remember that we defined $G(s) = B_p^{-1} G_{ms}$, so that comparing (11.64) with (11.39) we see that $C\Phi\Gamma = B_p^{-1} W_d$. Taking singular values of both sides

$$\sigma_i [C\Phi\Gamma] = \sigma_i [B_p^{-1} W_d] = \sigma_i [W_d] \tag{11.65}$$

since $B_p(s)$ is all-pass, which by definition (see (11.57)) has all singular values equal to unity. Therefore, this augmentation gives us what we want.

We are not quite done. The augmentation in (11.60)-(11.61) is not what we want, since the output is y'. We need y as the output so we must extend the augmentation to include $B_p^{-1}(s)$. $B_p^{-1}(s)$ may be realized by

$$B_p^{-1}(s) = C_{ap}(sI - A_{ap})^{-1} B_{ap} + D_{ap} \tag{11.66}$$

We will _always_ have a D_{ap} term since an all-pass _always_ has equal order numerator and denominator. Fig 11.4 shows a block diagram of $B_p^{-1}(s)$, in the position it appears in our system.
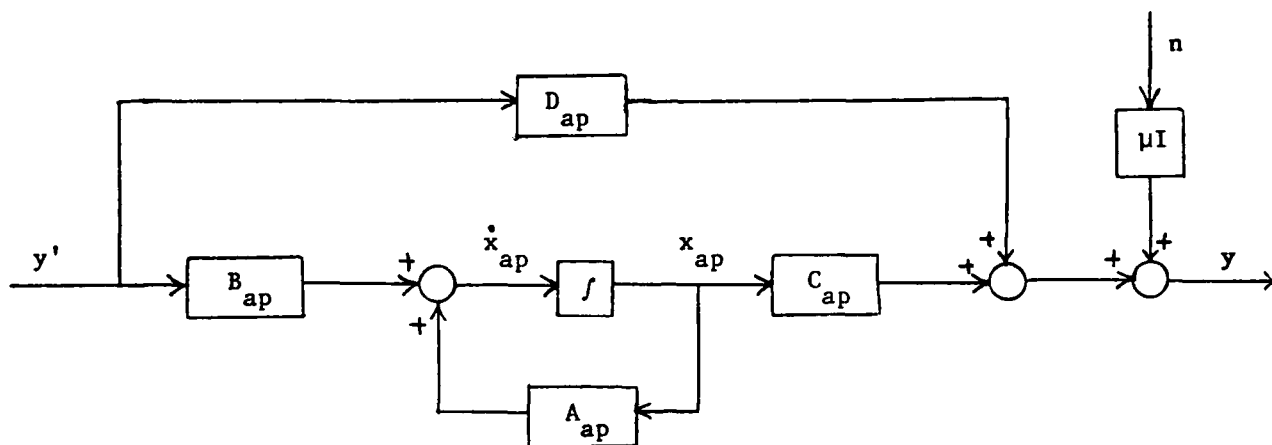
Fig 11.4   Block Diagram of $B_p(s)^{-1}$

Using this figure and (11.61), we can see that

$$\dot{x}_{ap} = A_{ap}x_{ap} + B_{ap}y'$$
$$= A_{ap}x_{ap} + B_{ap}C_{ms}x + B_{ap}C_dx_d \qquad (11.67)$$

$$y = C_{ap}x_{ap} + D_{ap}y' + \mu In$$
$$= C_{ap}x_{ap} + D_{ap}C_{ms}x + D_{ap}C_dx_d + \mu In \qquad (11.68)$$

Now, combining (11.60), (11.67), (11.68), and our response equation

$z = Hx$, we get

$$\begin{bmatrix} \dot{x} \\ \dot{x}_d \\ \dot{x}_{ap} \end{bmatrix} = \begin{bmatrix} A_{ms} & 0 & 0 \\ 0 & A_d & 0 \\ B_{ap}C_{ms} & B_{ap}C_d & A_{ap} \end{bmatrix} \begin{bmatrix} x \\ x_d \\ x_{ap} \end{bmatrix} + \begin{bmatrix} B_{ms} \\ 0 \\ 0 \end{bmatrix} u + \begin{bmatrix} 0 \\ B_d \\ 0 \end{bmatrix} \xi \qquad (11.69)$$

$$y = \begin{bmatrix} D_{ap}C_{ms} & D_{ap}C_d & C_{ap} \end{bmatrix} \begin{bmatrix} x \\ x_d \\ x_{ap} \end{bmatrix} + \mu In \qquad (11.70)$$

$$z = \begin{bmatrix} H & 0 & 0 \end{bmatrix} \begin{bmatrix} x \\ x_d \\ x_{ap} \end{bmatrix} \qquad (11.71)$$

This system is stabilizable from u and ξ and detectable from y and z.

Therefore, we choose

11-14

$$O_f = \begin{bmatrix} 0 \\ B_d \\ 0 \end{bmatrix} \begin{bmatrix} 0 & B_d^T & 0 \end{bmatrix} = \begin{bmatrix} 0 & 0 & 0 \\ 0 & B_d B_d^T & 0 \\ 0 & 0 & 0 \end{bmatrix} \tag{11.72}$$

and

$$O_c = \begin{bmatrix} H & 0 & 0 \end{bmatrix}^T \begin{bmatrix} H & 0 & 0 \end{bmatrix}$$

$$+ q^2 \begin{bmatrix} D_{ap}C_{ms} & D_{ap}C_d & C_{ap} \end{bmatrix}^T V \begin{bmatrix} D_{ap}C_{ms} & D_{ap}C_d & C_{ap} \end{bmatrix} \tag{11.73}$$

with R_f and R_c as before ((11.53) and (11.55)).

11.2.2 Formal Loop Shaping at the Input

For breaking the loop at the input to the plant, we wish to shape the singular value plots of T_{LO}, given by

$$\sigma_i[T_{LQ}] = \sigma_i[K_c \Phi B] \simeq \frac{1}{\sqrt{\rho}} \sigma_i[H\Phi B] \tag{11.74}$$

where the approximation is good at low frequency. Again, ρ is a scaling or gain parameter as far as the singular value plots are concerned, so we will represent $H\Phi B$ by $W_d(s)$, where $W_d(s)$ is a minimum phase diagonal transfer function realized by

$$W_d(s) = C_d(sI - A_d)^{-1} B_d \tag{11.75}$$

We will augment these dynamics with those of the plant through our desired responses z, as seen in Fig 11.5.
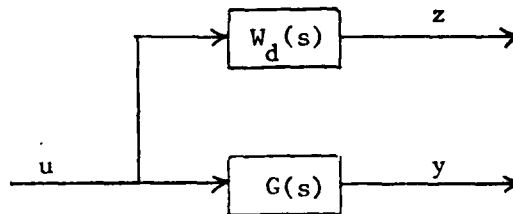
Fig 11.5 Augmenting Desired Dynamics From the Plant Input

Note that since we are trying to shape the regulator alone, we omit the noises entering the system for a moment. From our original system

$$\dot{x} = Ax + Bu \tag{11.76}$$

11-15

$$z = Hx \tag{11.77}$$

so that

$$x = \Phi Bu \tag{11.78}$$

and therefore

$$z = H\Phi Bu \tag{11.79}$$

From Fig 11.5,

$$z = W_d(s)u \tag{11.80}$$

so that, equating (11.79) and (11.80), we see that

$$W_d(s) = H\Phi B \tag{11.81}$$

By taking singular values of both sides of (11.81) we see that the singular values of $W_d(s)$ will be the same as those of $H\Phi B$, which is what we want. Now, using the realization in (11.75), we can write

$$\dot{x}_d = A_d x_d + B_d u \tag{11.82}$$

$$z = C_d x_d \tag{11.83}$$

so that by augmenting this with our original system (and replacing the noises we omitted)

$$\begin{bmatrix} \dot{x} \\ \dot{x}_d \end{bmatrix} = \begin{bmatrix} A & 0 \\ 0 & A_d \end{bmatrix} \begin{bmatrix} x \\ x_d \end{bmatrix} + \begin{bmatrix} B \\ B_d \end{bmatrix} u + \begin{bmatrix} \Gamma \\ 0 \end{bmatrix} \xi \tag{11.84}$$

$$y = \begin{bmatrix} C & 0 \end{bmatrix} \begin{bmatrix} x \\ x_d \end{bmatrix} + \mu In \tag{11.85}$$

$$z = \begin{bmatrix} 0 & C_d \end{bmatrix} \begin{bmatrix} x \\ x_d \end{bmatrix} \tag{11.86}$$

Assuming that we have a stable plant, this system is stabilizable from u and ξ and detectable from y and z. Therefore, we can do our LQG/LTR design using

$$Q_c = \begin{bmatrix} 0 & C_d \end{bmatrix}^T \begin{bmatrix} 0 & C_d \end{bmatrix} = \begin{bmatrix} 0 & 0 \\ 0 & C_d C_d^T \end{bmatrix} \tag{11.87}$$

11-16

$$R_c = \rho I \tag{11.88}$$

$$Q_f = \begin{bmatrix} \Gamma \\ 0 \end{bmatrix} [\Gamma^T \quad 0] + q^2 \begin{bmatrix} B \\ B_d \end{bmatrix} V[B^T \quad B_d^T] \tag{11.89}$$

$$R_f = \mu I \tag{11.90}$$

If we have an unstable plant, A will not be detectable from z. Therefore, we must again break our plant into an all-pass factor and a minimum phase stable plant, given by

$$G(s) = G_{ms}(s)B_p^{-1}(s) \tag{11.91}$$

This is shown in Fig 11.6.
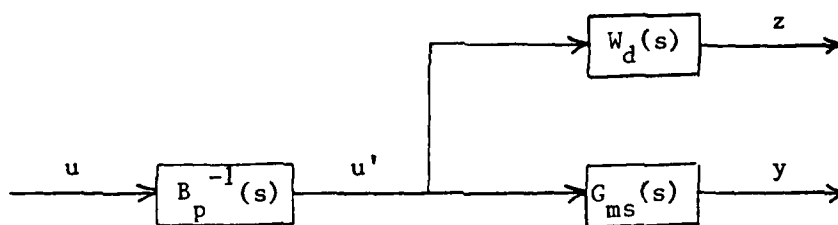
Fig 11.6 Input-Augmented Dynamics for an Unstable Plant

If the realization of $B_p^{-1}(s)$ is given by

$$B_p^{-1}(s) = C_{ap}(sI - A_{ap})^{-1}B_{ap} + D_{ap} \tag{11.92}$$

then

$$\dot{x}_{ap} = A_{ap}x_{ap} + B_{ap}u \tag{11.93}$$

$$u' = C_{ap}x_{ap} + D_{ap}u \tag{11.94}$$

Changing u to u' in (11.84), then substituting (11.94) into the resulting equations yields the new augmented state space

$$\begin{bmatrix} \dot{x} \\ \dot{x}_d \\ \dot{x}_{ap} \end{bmatrix} = \begin{bmatrix} A_{ms} & 0 & B_{ms}C_{ap} \\ 0 & A_d & B_dC_{ap} \\ 0 & 0 & A_{ap} \end{bmatrix} \begin{bmatrix} x \\ x_d \\ x_{ap} \end{bmatrix} + \begin{bmatrix} B_{ms}D_{ap} \\ B_dD_{ap} \\ B_{ap} \end{bmatrix} u + \begin{bmatrix} \Gamma \\ 0 \\ 0 \end{bmatrix} \xi \tag{11.95}$$

$$y = [C_{ms} \quad 0 \quad 0] \begin{bmatrix} x \\ x_d \\ x_{ap} \end{bmatrix} + \mu In \tag{11.96}$$

$$z = \begin{bmatrix} 0 & C_d & 0 \end{bmatrix} \begin{bmatrix} x \\ x_d \\ x_{ap} \end{bmatrix} \qquad (11.97)$$

The system is now fully stabilizable and detectable. Equations
(11.87)-(11.90) may be used to do the LQG/LTR designs after substituting
the corresponding matrices from (11.95)-(11.97).

After doing a minimal realization of the desired loop transfer
matrix W_d (and B_p^{-1}), the matrices Γ and H are completely known. This
avoids having to select them by trial and error methods, which is the
main advantage of this method. We caution that the major penalty
associated with this technique is the amount of dynamics which must be
augmented to the system. This could be considered excessive, depending
upon the example. Also, formal loop shaping tends to invert the stable
dynamics of the plant, and indiscriminant use of the technique could be
dangerous. It is a good idea to try to include as much of the original
dynamics of the plant in the desired loop shapes as possible, in order
to reduce the inversion.

Chapter 11 References

[11-1] G. Stein and M. Athans, "The LQG/LTR Procedure for Multivariable Feedback Control Design", 1984 American Control Conference, San Diego, CA., June 1984 (paper available for the authors).

[11-2] K. A. Lively, "Multivariable Control System Design for a Submarine", MIT Thesis, LIDS-TH-1379, Mass. Inst. of Tech., Cambridge, MA., May 1984.

12. SOLVING THE L_2/H_2 OPTIMIZATION PROBLEM USING LQG/LTR

This chapter does not contain any additions or extensions to what we have covered thus far. Rather, it poses the LQG/LTR methodology in a more mathematical framework, by showing that it is one way to solve a formal L_2/H_2 optimization problem.

12.1 The L_2/H_2 Optimization Problem

First, let's redraw the generic MIMO control system block diagram, as shown in Fig 12.1.
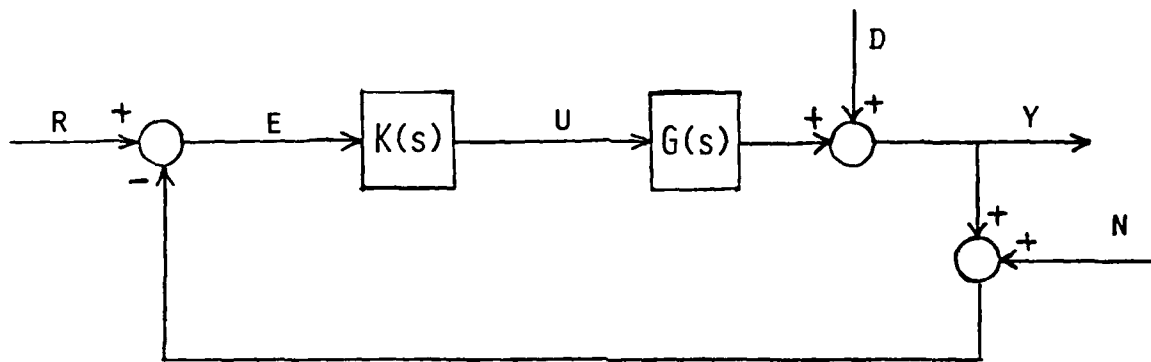
Fig 12.1 Generic MIMO Control System

Looking back to equation (4.32), the expression for the output is given by

$$y = G(s)K(s)[I + G(s)K(s)]^{-1}\{r - n\} + [I + G(s)K(s)]^{-1}d \qquad (12.1)$$

Now we define the output sensitivity function, $S_o(s)$, as

$$S_o(s) = [I + G(s)K(s)]^{-1} \qquad (12.2)$$

and the complimentary output sensitivity function, $T_o(s)$, as

$$T_o(s) = G(s)K(s)[I + G(s)K(s)]^{-1} \qquad (12.3)$$

Note that this is different from the $T_o(s)$ we defined in Chapter 10. Using (12.2) and (12.3) in (12.1), we get

$$y = T_o(s)[r - n] + S_o(s)d \qquad (12.4)$$

For good command following and disturbance rejection, we must have $S_o(s)$ small. Remember that our robustness requirement from (4.80) requires

12-1

$$\bar{\sigma}[T_o(s)] < \frac{1}{\ell_m} \qquad (12.5)$$

where ℓ_m grows large at high frequency. From (12.4) and the above we can see that $T_o(s)$ must be small for sensor noise rejection and robustness to high frequency errors. Therefore, our two main objectives may be stated as:

1) make $S_o(s)$ small whenever $d(s)$ or $r(s)$ is large

2) make $T_o(s)$ small whenever $\ell_m(w)$ or $n(s)$ is large

Obviously, these objectives require both $S_o(s)$ and $T_o(s)$ to be small over certain frequency ranges. However,

$$S_o(s) + T_o(s) = [I + G(s)K(s)]^{-1} + G(s)K(s)[I + G(s)K(s)]^{-1}$$
$$= [I + G(s)K(s)][I + G(s)K(s)]^{-1} = I \qquad (12.6)$$

Therefore, both <u>cannot</u> be small at the same frequency. This was also seen explicitly back in Chapters 4 and 5. The final conclusion is that we must perform some type of trade-off between these two objectives. We will state this trade-off between $S_o(s)$ and $T_o(s)$ as a formal optimization problem next.

Back in Chapter 2, equation (2.62), we saw that

$$\bar{\sigma}^2[M] \leq tr[MM^*] \qquad (12.7)$$

where M is any matrix and $tr[\cdot]$ denotes trace of the matrix. Therefore, if we make $tr[MM^*]$ small, $\bar{\sigma}^2[M]$ will be small, which says that M is small. Since we desire a trade between $S_o(s)$ and $T_o(s)$, we can use a weighting matrix $W(s)$ to dictate their relative importance at any frequency. The formal L_2/H_2 optimization problem then becomes:

Given $G(s)$, $W(s)$ and the definitions of $S_o(s)$ and $T_o(s)$, find a stabilizing compensator $K(s)$ which minimizes

$$J = \frac{1}{2\pi} \int_0^\infty \{tr[S_o WW^* S_o^*] + tr[T_o T_o^*]\} dw \qquad (12.8)$$

If we let

$$M(s) = [S_o(s)W(s) \quad T_o(s)]$$ (12.9)

then

$$MM^* = [S_o WW^* S_o^* + T_o T_o^*]$$ (12.10)

Taking the trace of both sides of (12.10), and realizing that

$$tr[A + B] = tr[A] + tr[B]$$ (12.11)

we can see that (12.8) may be written as

$$J = \frac{1}{2\pi} \int_0^\infty tr[MM^*]dw$$ (12.12)

which conforms with the definition of the L_2/H_2 norm we gave in Chapter 2. Now let's see if we can use the LQG/LTR formulation as a means of solving this optimization problem.

12.2 L_2/H_2 Optimization Via LQG/LTR

In general, the solution $K(s)$ to the L_2/H_2 optimization problem we just defined need not be finite dimensional or strictly proper (more poles than zeros). Obviously, we desire $K(s)$ to have these properties. Therefore, we will restrict $G(s)$ and $W(s)$ to be finite dimensional and strictly proper in order to generate a sequence of finite dimensional, strictly proper compensators which minimize (12.8) in the limit. For most applications, this poses no restriction on the plant $G(s)$ since it has these characteristics anyway. Therefore, we only restrict $W(s)$. We will define what we mean by "in the limit" shortly.

Consider our typical system

$$\dot{x} = Ax + Bu + \Gamma\xi$$ (12.13)

$$y = Cx + \mu I\eta$$ (12.14)

$$z = Ux$$ (12.15)

We assume that ξ and η are unit intensity here, since Γ and μ may be used to adjust their effective intensities. The LQG performance index we wish to minimize is

$$J_{LOG} = E\{\lim_{T \to \infty} \frac{1}{T} \int_0^\infty [z^T z + \rho^2 u^T u] dt\} \qquad (12.16)$$

Notice that we are using ρ^2 here instead of ρ so that we avoid square root signs later -- this is simply for convenience. That is, ρ^2 is the _same_ as ρ used to be. We let Γ, μ, H and ρ be completely tunable parameters. From (12.13) we have

$$x(s) = \Phi B u(s) + \Phi \Gamma \xi(s) \qquad (12.17)$$

where

$$\Phi = (sI - A)^{-1} \qquad (12.18)$$

Using (12.17) in the Laplace transformed versions of (12.14) and (12.15) we get

$$y(s) = C\Phi B u(s) + C\Phi \Gamma \xi(s) + \mu In(s) \qquad (12.19)$$

$$z(s) = H\Phi B u(s) + H\Phi \Gamma \xi(s) \qquad (12.20)$$

Writing these in augmented matrix form, we have

$$\begin{bmatrix} y(s) \\ z(s) \end{bmatrix} = \begin{bmatrix} C\Phi B & C\Phi\Gamma & \mu I \\ H\Phi B & H\Phi\Gamma & 0 \end{bmatrix} \begin{bmatrix} u(s) \\ \xi(s) \\ n(s) \end{bmatrix} \qquad (12.21)$$

Using the fact that we are designing a dynamic output feedback controller, we can write our feedback law as

$$u(s) = -K(s)y(s) \qquad (12.22)$$

Using our typical plant transfer function notation

$$G(s) = C\Phi B \qquad (12.23)$$

we can use (12.22) and (12.23) in (12.19) to obtain

$$y(s) = -G(s)K(s)y(s) + C\Phi\Gamma\xi(s) + \mu In(s) \qquad (12.24)$$

or

$$y(s) = [I + G(s)K(s)]^{-1} C\Phi\Gamma\xi(s) + [I + G(s)K(s)]^{-1} \mu In(s) \qquad (12.25)$$

Now, substituting (12.22) into (12.20), we can see that

$$z(s) = -H\Phi BK(s)y(s) + H\Phi\Gamma\xi(s) \qquad (12.26)$$

Substituting (12.25) into (12.26), we get

$$z(s) = -H\Phi BK(s)[I + G(s)K(s)]^{-1}C\Phi\Gamma\xi(s)$$

$$- H\Phi BK(s)[I + G(s)K(s)]^{-1}\mu In(s) + H\Phi\Gamma\xi(s) \qquad (12.27)$$

Finally, substituting (12.25) into (12.22), we get

$$u(s) = -K(s)[I + G(s)K(s)]^{-1}C\Phi\Gamma\xi(s)$$

$$- K(s)[I + G(s)K(s)]^{-1}\mu In(s) \qquad (12.28)$$

Now we can write (12.27) and (12.28) in augmented matrix form as

(multiplying both sides of (12.28) by ρ first)

$$\begin{bmatrix} z(s) \\ \rho u(s) \end{bmatrix} = P(s) \begin{bmatrix} \xi(s) \\ n(s) \end{bmatrix} \qquad (12.29)$$

where

$$P(s) = \begin{bmatrix} H\Phi\Gamma - H\Phi BK(I + GK)^{-1}C\Phi\Gamma & -\mu H\Phi BK(I + GK)^{-1} \\ -\rho K(I + GK)^{-1}C\Phi\Gamma & -\mu\rho K(I + GK)^{-1} \end{bmatrix} \qquad (12.30)$$

Most of this probably seems pointless so far. However, notice that

$$\begin{bmatrix} z^T & \rho u^T \end{bmatrix} \begin{bmatrix} z \\ \rho u \end{bmatrix} = z^T z + \rho^2 u^T u \qquad (12.31)$$

which is the integrand in (12.16). Using Parseval's theorem on (12.16) and the relation given in (12.29), J_{LQG} becomes

$$J_{LQG} = \frac{1}{2\pi} \int_0^\infty tr[PP^*]dw \qquad (12.32)$$

Now we can see that (12.32) looks like (12.12). In other words, if we can choose H, Γ, μ, and ρ in $P(s)$ so that (12.32) equals (12.12), we will solve the L_2/H_2 optimization problem using LQG/LTR.

12.2.1 Weighting Choice One

Let's choose Γ and μ so that

$$\frac{1}{\mu} C\Phi\Gamma = W(s) \qquad (12.33)$$

where $W(s)$ is a weighting function (we will soon see that it is the same

12-5

one as in (12.8)). Also, let $H = C$ and $\rho \to 0$. Then $P(s)$ becomes

$$P(s) = \begin{bmatrix} C\Phi\Gamma - C\Phi BK(I + GK)^{-1}C\Phi\Gamma & -\mu C\Phi BK(I + GK)^{-1} \\ -\rho K(I + GK)^{-1}C\Phi\Gamma & -\rho\mu K(I + GK)^{-1} \end{bmatrix}$$

$$= \begin{bmatrix} \mu W - \mu GK(I + GK)^{-1}W & -\mu GK(I + GK)^{-1} \\ -\rho\mu K(I + GK)^{-1}W & -\rho\mu K(I + GK)^{-1} \end{bmatrix}$$

$$\longrightarrow \mu \begin{bmatrix} [I - GK(I + GK)^{-1}]W & -GK(I + GK)^{-1} \\ 0 & 0 \end{bmatrix} \tag{12.34}$$

as $\rho \to 0$. Notice that

$$I - GK(I + GK)^{-1} = [I + GK][I + GK]^{-1} - GK[I + GK]^{-1}$$

$$= [I + GK - GK][I + GK]^{-1}$$

$$= (I + GK)^{-1} \tag{12.35}$$

so that (12.34) becomes

$$P(s) \longrightarrow \mu \begin{bmatrix} (I + GK)^{-1}W & -GK(I + GK)^{-1} \\ 0 & 0 \end{bmatrix} \tag{12.36}$$

Using the definitions of S_o and T_o in (12.2) and (12.3), we can see that (12.36) is actually

$$P(s) \longrightarrow \mu \begin{bmatrix} S_o(s)W(s) & -T_o(s) \\ 0 & 0 \end{bmatrix} \tag{12.37}$$

This is almost identical to the definition of $M(s)$ in (12.9). What we actually need to show is that, in the limit as $\rho \to 0$,

$$\mathrm{tr}[MM^*] = \mathrm{tr}[S_o WW^* S_o^*] + \mathrm{tr}[T_o T_o^*] = \mathrm{tr}[PP^*] \tag{12.38}$$

From (12.37)

$$\mathrm{tr}[PP^*] = \mathrm{tr}\left\{ \mu^2 \begin{bmatrix} S_o W & -T_o \\ 0 & 0 \end{bmatrix} \begin{bmatrix} (S_o W)^* & 0 \\ -T_o^* & 0 \end{bmatrix} \right\}$$

$$= \mathrm{tr}\left\{ \mu^2 \begin{bmatrix} S_o WW^* S_o^* + T_o T_o^* & 0 \\ 0 & 0 \end{bmatrix} \right\} \tag{12.39a}$$

or

$$tr[PP^*] = \mu^2\{tr[S_oWW^*S_o^*] + tr[T_oT_o^*]\} \qquad (12.39b)$$

The μ^2 term would come out of the integrand and would not affect the minimization (i.e., the solution $K(s)$). Therefore, the given choices of H, Γ, μ, and ρ do cause (12.32) to have the form of an L_2/H_2 optimization problem.

Now let's examine the weightings. Remember that (from Chapter 9)

$$\sigma_i[T_{KF}] \simeq \frac{1}{\sqrt{\mu}}\sigma_i[T_{FOL}] \qquad (12.40)$$

or

$$\sigma_i[C\Phi K_f] \simeq \frac{1}{\sqrt{\mu}}\sigma_i[C\Phi\Gamma] \qquad (12.41)$$

Looking at the choice in (12.33), we can see that the singular values of W(s) are simply the singular values of the Kalman filter loop transfer function scaled by the constant $\sqrt{\mu}$. Also, notice that in the loop-broken-at-the-output recovery procedure, we normally choose (as seen in Chapter 9)

$$Q_c = H^TH + q^2C^TC \qquad (12.42)$$

$$R_c = \rho I \qquad (12.43)$$

and let $q\rightarrow\infty$. Here, we let

$$Q_c = H^TH = C^TC \qquad (12.44)$$

and choose R_c as in (12.43), but we let $\rho\rightarrow 0$. These are equivalent in the limit since Q_c goes to ∞ proportionally to C^TC in (12.42), and we have already shown that $Q_c\rightarrow\infty$ is equivalent to $R_c\rightarrow 0$ (see Appendix 8A).

The overall conclusion of this section is that by choosing the LQG/LTR parameters as shown, the resulting compensator will minimize an L_2/H_2 optimization problem in the limit as $\rho\rightarrow 0$. This is the "in the limit" we discussed earlier, and we should note that the resulting compensator is only L_2/H_2 optimal in the limit. Also note that this

choice of weights is equivalent to the LQG/LTR procedure with the loop broken at the plant output.

12.2.2 Weighting Choice Two

Hopefully you can guess that this choice of weights will be equivalent to LQG/LTR breaking the loop at the plant input. Here we choose H and ρ such that

$$\frac{1}{\rho} H\Phi B = W(s) \tag{12.45}$$

and let $\Gamma = B$ and $\mu \rightarrow 0$. Then P(s) becomes

$$P(s) = \begin{bmatrix} H\Phi B - H\Phi BK(I + GK)^{-1}C\Phi B & -\mu H\Phi BK(I + GK)^{-1} \\ -\rho K(I + GK)^{-1}C\Phi B & -\mu\rho K(I + GK)^{-1} \end{bmatrix}$$

$$= \begin{bmatrix} \rho W - \rho WK(I + GK)^{-1}G & -\mu\rho WK(I + GK)^{-1} \\ -\rho K(I + GK)^{-1}G & -\mu\rho K(I + GK)^{-1} \end{bmatrix}$$

$$\longrightarrow \rho \begin{bmatrix} W[I - K(I + GK)^{-1}G] & 0 \\ -K(I + GK)^{-1}G & 0 \end{bmatrix} \tag{12.46}$$

as $\mu \rightarrow 0$. Using the first identities in (2.21), we can write

$$K(I + GK)^{-1}G = [I + KG]^{-1}KG \tag{12.47}$$

Also notice that

$$I - [I + KG]^{-1}KG = [I + KG]^{-1}[I + KG] - [I + KG]^{-1}KG$$

$$= [I + KG]^{-1}[I + KG - KG] = [I + KG]^{-1} \tag{12.48}$$

Therefore, (12.46) may be rewritten as

$$P(s) \longrightarrow \rho \begin{bmatrix} W(I + KG)^{-1} & 0 \\ -(I + KG)^{-1}KG & 0 \end{bmatrix} \tag{12.49}$$

Analogous to the definitions of S_o and T_o, which are output related, we can define the __input__ sensitivity function

$$S_i(s) = [I + KG]^{-1} \tag{12.50}$$

and the __input__ complimentary sensitivity function

12-8

$$T_i(s) = [I + KG]^{-1}KG \qquad (12.51)$$

Using this terminology, we can rewrite (12.49) as

$$P(s) \to \rho \begin{bmatrix} WS_i(s) & 0 \\ -T_i(s) & 0 \end{bmatrix} \qquad (12.52)$$

Now, forming $tr[PP^*]$, we get

$$tr[PP^*] = tr\left\{\rho^2 \begin{bmatrix} WS_i & 0 \\ -T_i & 0 \end{bmatrix}\begin{bmatrix} (WS_i)^* & -T_i^* \\ 0 & 0 \end{bmatrix}\right\}$$

$$= tr\left\{\rho^2 \begin{bmatrix} WS_i S_i^* W^* & -WS_i T_i^* \\ -T_i S_i^* W^* & T_i T_i^* \end{bmatrix}\right\}$$

$$= \rho^2\{tr[WS_i S_i^* W^*] + tr[T_i T_i^*]\} \qquad (12.53)$$

The ρ^2 term will not affect the minimization, so that the given choices of H, Γ, ρ, and μ do cause (12.32) to have the form of an L_2/H_2 optimization problem, except that here we are trading off the loop properties at the plant input. Using the plant input, the M(s) matrix in (12.9) would become

$$M(s) = [W(s)S_i(s) \qquad T_i(s)] \qquad (12.54)$$

so we can see that (12.53) is consistent with this.

Let's examine the weightings we have chosen. From Chapter 9,

$$\sigma_i[T_{LO}] = \sigma_i[K_c \Phi B] \simeq \frac{1}{\sqrt{\rho}}\sigma_i[H\Phi B] \qquad (12.55)$$

Looking at the choice of W(s) in (12.45), we can see that singular values of W(s) are simply the singular values of the regulator loop transfer function scaled by the constant $\sqrt{\rho}$. Also, in the input-breaking LQG/LTR procedure, we usually choose

$$Q_f = \Gamma\Gamma^T + q^2 BB^T \qquad (12.56)$$

with $q \to \infty$ and

$$R_f = R_c \qquad (12.57)$$

12-9

In the procedure discussed in this chapter, we let

$$O_f = BB^T \qquad (12.58)$$

and

$$R_f = \mu I \qquad (12.59)$$

with $\mu \to 0$. Again, the similarity should be obvious. Also, note that the LOG/LTR solution is only L_2/h_2 optimal in the limit as $\mu \to 0$.

This essentially completes all of the theoretical development we will do towards describing the LOG/LTR method. In the next chapter, we will present an aircraft example which will hopefully clarify some of the theory, show how well it does or does not work in practice, and highlight some interesting points in the application of the method.

Chapter 12 References

[12-1] G. Stein and M. Athans, "The LQG/LTR Procedure for Multivariable Feedback Control Design", 1984 American Control Conference, San Diego, CA., June 1984 (paper available from authors).

13. DRONE LATERAL ATTITUDE CONTROL EXAMPLE

To truly understand what LQG/LTR does and how it works we need to do some examples. In this example, we will design several controllers for lateral attitude control of a drone aircraft.

13.1 Example Set-Up

The plant, which is taken from Ref [13-1], is given by

$$\dot{x} = Ax + Bu + \Gamma\xi \tag{13.1}$$

$$y = Cx + n \tag{13.2}$$

where

$$
A = \begin{bmatrix}
-0.08527 & -0.0001423 & -0.9994 & 0.04142 & 0 & 0.1862 \\
-46.86 & -2.757 & 0.3896 & 0 & -124.3 & 128.6 \\
-0.4248 & -0.06224 & -0.06714 & 0 & -8.792 & -20.46 \\
0 & 1 & 0.0523 & 0 & 0 & 0 \\
0 & 0 & 0 & 0 & -20 & 0 \\
0 & 0 & 0 & 0 & 0 & -20
\end{bmatrix}
\tag{13.3}
$$

$$
B = \begin{bmatrix}
0 & 0 \\
0 & 0 \\
0 & 0 \\
0 & 0 \\
20 & 0 \\
0 & 20
\end{bmatrix}
\tag{13.4}
$$

$$
C = \begin{bmatrix}
1 & 0 & 0 & 0 & 0 & 0 \\
0 & 0 & 0 & 1 & 0 & 0
\end{bmatrix}
\tag{13.5}
$$

$$x = \lceil \beta \quad \dot{\phi} \quad \dot{\psi} \quad \phi \quad \delta_e \quad \delta_r \rceil^T \qquad (13.6)$$

and

$$u = \lceil \delta_{e_c} \quad \delta_{r_c} \rceil^T \qquad (13.7)$$

The states and inputs in (13.6) and (13.7) are, in order: sideslip

angle, roll rate, yaw rate, roll angle, elevon surface deflection,

rudder surface deflection, elevon servo command, and rudder servo

command. The nominal Γ matrix will not be specified, except its

dimension, which is (6x2). The strengths of ξ and n are assumed to be

unity.

Note that we have assumed that we can measure sideslip and roll

angle. These angles will also be the responses we will try to control,

so that our response equation

$$z = Hx \qquad (13.8)$$

has H = C. The maneuver we will try to design a controller for will be

a step command in roll angle with no change in sideslip.

The open-loop plant, CΦB, has the eigenvalues shown in Table 13.1,

and one transmission zero at -158.15.

Table 13.1 Eigenvalues of the Plant, $\lambda(A)$	
Spiral Mode	-0.0360
Dutch Roll (unstable)	$0.1884 \pm 1.0511i$
Roll Convergence	-3.2503
Elevon Actuator	-20.0
Rudder Actuator	-20.0

The singular value plot of CΦB is shown in Fig 13.1. Notice that the

plant has widely separated singular values at low frequency, does not

exhibit integral action, and has a natural maximum bandwidth of about 12

rad/sec.

13-2
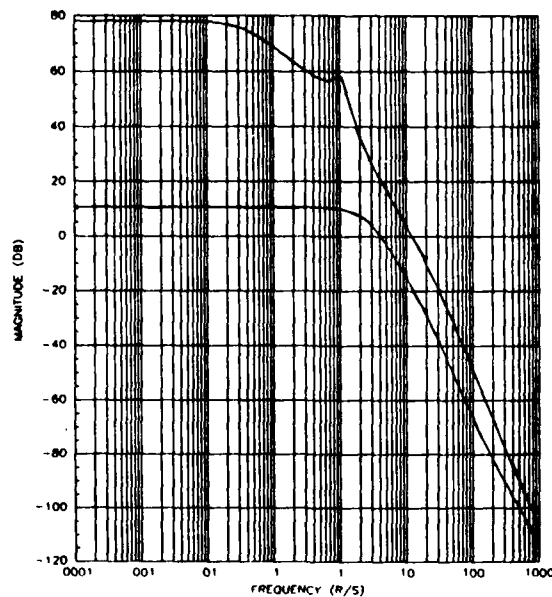
Fig 13.1 Singular Values of the Plant

The last things we need to establish are our performance and robustness requirements. Mathematically, this translates into defining the scalar functions $p(w)$ and $\ell_m(w)$. For $p(w)$, we shall assume that we require our loop transfer to have at least 20 dB gain at $w \leqslant 0.1$ rad/sec. We will also require tracking of our commands so that (formally) integral action is necessary, and will impose a restriction of 10 rad/sec for the maximum crossover frequency of our system. For our robustness requirements, we assume that our model is reasonably accurate (to within 10% of the true plant) up to 2 rad/sec, then our uncertainty grows without bound at a rate of 20 dB/decade. This produces the $\ell_m(w)$ curve shown in Fig 13.2.
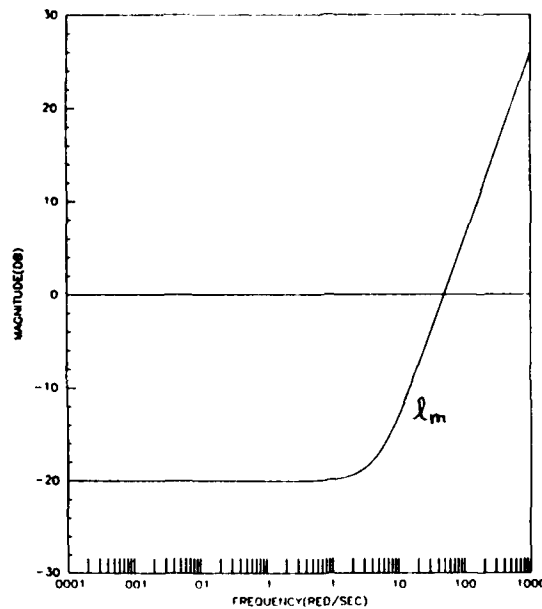
Fig 13.2 Uncertainty Profile

We assume that this $\ell_m(w)$ represents either input or output

multiplicative perturbations. Putting these requirements on performance

and stability together, we come up with the loop transfer function

"barriers" shown in Fig 13.3.
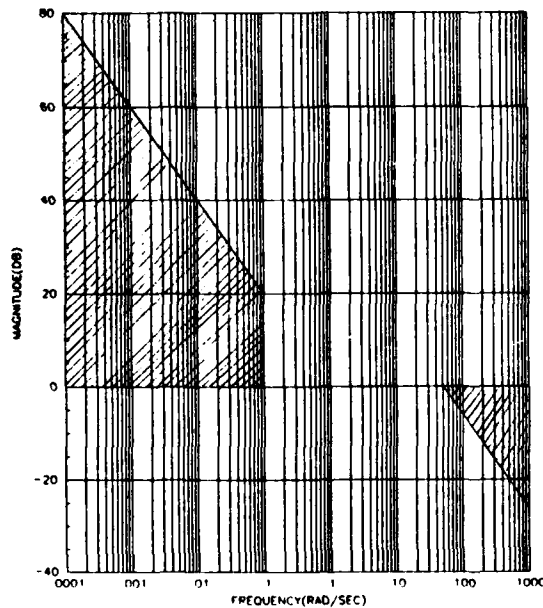
Fig 13.3 Performance and Stability Barriers

Recall that the low frequency performance barrier is actually a

performance robustness barrier and is not $p(w)$. From (4.83), it is

13-4

given by

$$\text{performance barrier (p.b.)} = \frac{p(w)}{1 - \ell_m(w)} \qquad (13.9)$$

Since Fig 13.2 shows that $\ell_m(w)$ is a constant from $0 \le w \le 0.1$, the denominator of (13.9) is constant. Transforming (13.9) to decibels we see that

$$p.b. = 20\log[p(w)] - 20\log[1 - \ell_m(w)]$$
$$= 20\log[p(w)] + 0.91 \text{ dB} \qquad (13.10)$$

Thus, the barrier shown in Fig 13.3 is shifted upwards by 0.91 dB over the actual $p(w)$. In the figure, the difference is hardly noticeable.

13.2 Design With Output Uncertainties

We will now proceed to design several controllers for our plant, assuming first that we are modelling uncertainties at the output of the plant. Realize that since the system is square, we can design at the output or at the input. First, even though we cannot possibly meet our performance specs, we will design a controller without augmenting integrators. This yields some interesting results which are worth commenting on. Next, we will augment integrators to the plant, and then look at several designs using singular value matching and one where we arbitrarily choose Γ.

13.2.1 Unaugmented Design

As a refresher, recall that here we must choose μ and Γ so that $\frac{1}{\sqrt{\mu}} \sigma_i[C\Phi\Gamma]$ has a desirable loop shape at low frequency. Also recall that Γ affects the shape while μ simply raises or lowers the plots. After several choices of Γ, it becomes obvious that little improvement over $\Gamma = B$ (i.e., the open-loop plant) is possible. It seems that any attempt to raise the $\underline{\sigma}$ plot (see Fig 13.1) increases the bandwidth far

beyond the desired 10 rad/sec. Therefore, the choice of $\Gamma = B$ was made.
Since the open-loop plant had a maximum bandwidth greater than 10
rad/sec, μ was chosen to be greater than unity, in order to lower the
plots. The choice of $\mu = 5$ was made, which yields a maximum crossover
of just under 9 rad/sec.

Now that μ and Γ have been selected, we can calculate the filter
gain matrix K_f. Doing this, and plotting $\sigma_i[C\Phi K_f]$, we can compare these
plots with those found in the previous step. This is shown in Fig 13.4.
The solid line plots are $\frac{1}{\sqrt{\mu}}\sigma_i[C\Phi\Gamma]$ (from here on called T_{FOL}) and the
dotted line plots are $\sigma_i[C\Phi K_f]$ (from here on called T_{KF}).
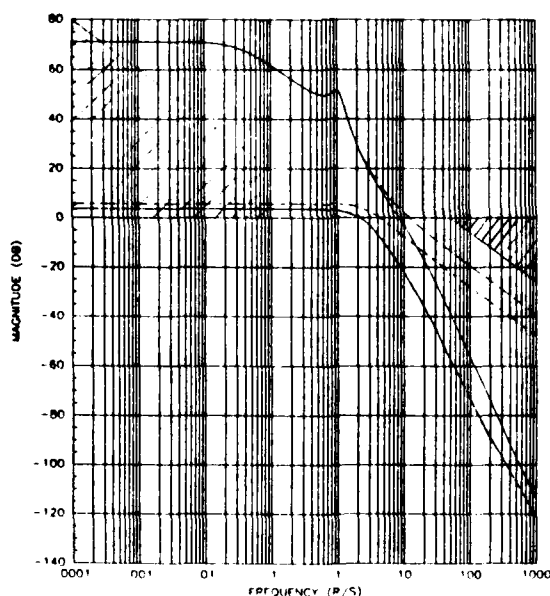
Fig 13.4 Singular Values of T_{FOL} and T_{KF}, Unaugmented Case

Note that there is close agreement between the two sets of plots at low
frequency. Actually, there is a small mismatch between the σ plots, but
this should be expected since the loop gain is _not_ high there, which is
required for equality. At high frequency, where the singular values
become small, the plots diverge. Note that the crossover of T_{KF} is just

above 10 rad/sec, which means we do not meet our bandwidth spec. Technically, μ should be increased slightly and the process repeated, but since we're close (and won't keep this design anyway), we'll proceed with $\mu = 5$.

Finally, notice that while we are below our robustness boundary at high frequency, we are not even close to meeting our performance spec (we _still_ would not meet it even if we didn't require integral action). We should see the consequences of this when we finish the design and look at time responses.

Now that we have designed our full state filter, we must try to recover this loop shape using the regulator. This requires selection of H, ρ, and the recovery parameter q^2. For convenience, we will _always_ choose $\rho = 1$ in this section. Since our measured variables are also those we wish to control, $H = C$ is the most logical choice for H, and we will make this choice throughout this section also. Since for recovery we must choose

$$Q_c = H^T H + q^2 C^T C \qquad (13.11)$$

and since $H = C$, we are already beginning to recover at $q^2 = 0$. Only the actual choice of q^2 is left to be made. Without going through the different choices, the value $q^2 = 10^5$ yields excellent recovery, and the plots of T_{KF} (solid) versus GK (dotted) are shown in Fig 13.5. Notice that the maximum bandwidth is slightly less than in the full state case, but is still just barely above 10 rad/sec.
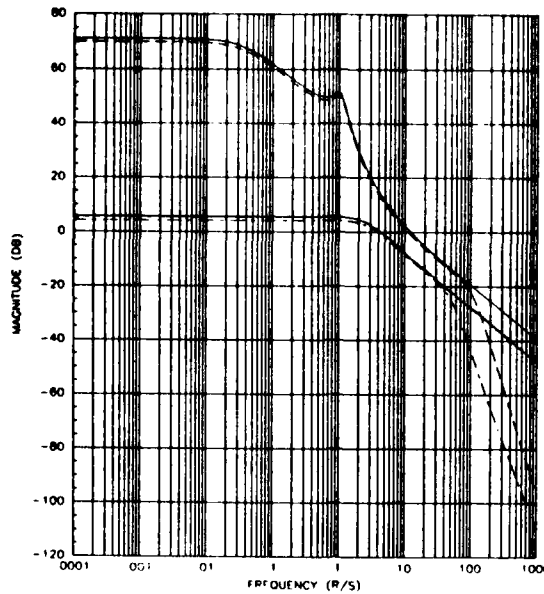
Fig 13.5 Singular Values of T_{KF} and GK, Unaugmented Design

Table 13.2 Data for the Unaugmented Output Design

$$\mu = 5 \qquad \Gamma = B \qquad \sigma^2 = 10^5$$

$$\text{zeros}(C\Phi\Gamma) = [\ -158.15 \ ]$$

$$\text{zeros}(C\Phi K_f) = \begin{bmatrix} -2.68 \\ -8.37 \\ -19.23 \\ -19.98 \end{bmatrix}$$

$$\text{poles(filter)} = \begin{bmatrix} -2.62 \pm j2.05 \\ -6.00 \pm j6.48 \\ -20.00 \\ -20.37 \end{bmatrix}$$

$$\text{poles(regulator)} = \begin{bmatrix} -26.79 \pm j42.72 \\ -52.49 \pm j89.63 \\ -51.17 \\ -104.69 \end{bmatrix}$$

$$K_f = \begin{bmatrix} 4.20 & -1.19 \\ -18.17 & 55.81 \\ -9.92 & -0.60 \\ -1.19 & 10.49 \\ 0.0181 & -0.333 \\ 0.1149 & 0.338 \end{bmatrix}$$

$$K_c = \begin{bmatrix} 215.1 & -4.665 & -7.895 & -233.2 & 6.708 & -2.554 \\ 231.5 & 3.723 & -7.453 & 213.5 & -2.554 & 6.869 \end{bmatrix}$$

$$\text{zeros}[K(s)] = \begin{bmatrix} -2.55 \\ -7.52 \\ -19.55 \\ -19.99 \end{bmatrix} \qquad \text{poles}[K(s)] = \begin{bmatrix} -27.45 \pm j44.04 \\ -52.68 \pm j95.65 \\ -54.16 \\ -114.7 \end{bmatrix}$$

13-8

Table 13.2 shows some of the interesting specifics about this design. We will not make any comments on the various poles and zeros here, since they will be commented on a great deal in the next design. It is interesting to note that the only regulator gains that are getting large are those in the first and fourth columns, which correspond to those multiplying the response variables β and ϕ.

The last and possibly most important thing we need to examine are the system responses to given commands. The roll and sideslip responses to a unit step command in roll angle (zero commanded sideslip) are shown in Fig 13.6. Notice that both settle out to their commanded values in about one second, the maximum overshoot in roll angle in about 17%, and the maximum sideslip angle is only about 0.05 degrees.
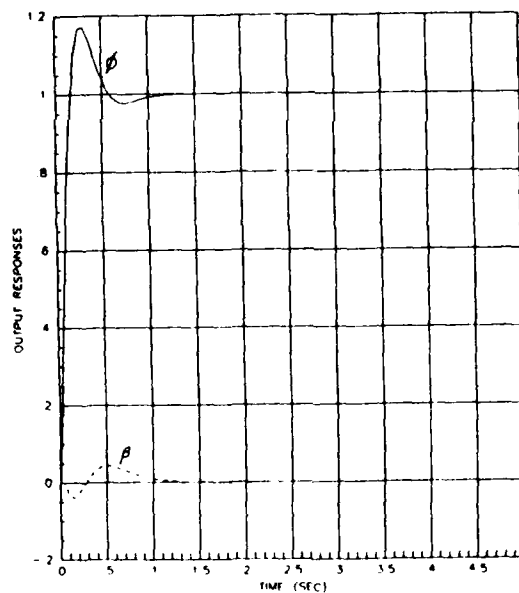
Fig 13.6 Time Responses to a Roll Command, Unaugmented Design

Hopefully, you are slightly surprised. These responses are quite good, yet the loop shapes of GK are poor (don't meet performance specs). To see what is happening, let's reverse the command (command unit step sideslip angle with zero commanded roll). These responses are shown in

Fig 13.7. These are miserable. The sideslip angle response has a 7%

steady state error, while the roll angle settles out at -0.7 degrees

rather than the command zero.
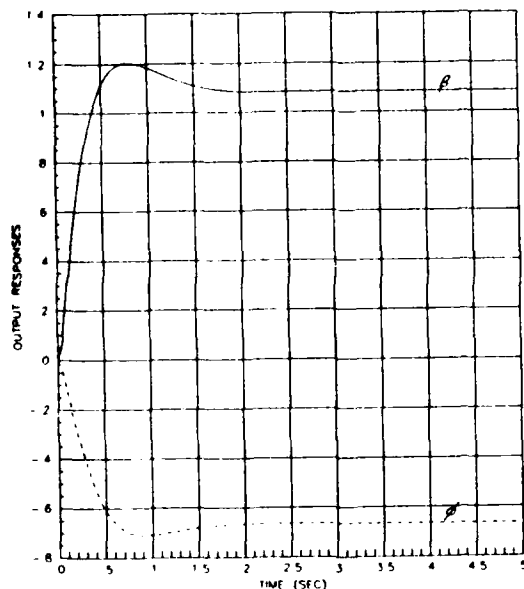
Fig 13.7 Time Responses to a Sideslip Command, Unaugmented Design

It seems that, in this example, $\bar{\sigma}[GK]$, which has very high gain at low

frequency, dominates the roll command loop while $\underline{\sigma}[GK]$ (which is very

low) dominates the sideslip command channel. Realize that commanding

sideslip at this flight condition is silly, but still illustrates the

point. Therefore, if a roll command with small sideslip is all we are

concerned about, this design is not too bad. In general, however, it is

quite poor and should be discarded.

13.2.2 Augmented Designs

Obviously, in order to meet our performance specs we must augment

integrators to our plant so that we have integral action in both loops.

Following the augmentation procedure in Chapter 10, we augment a bank

of integrators in front of the plant. The new augmented plant has the

singular value plots shown in Fig 13.8. This will be the "plant" we use

13-10

to design several controllers for in the next subsections.
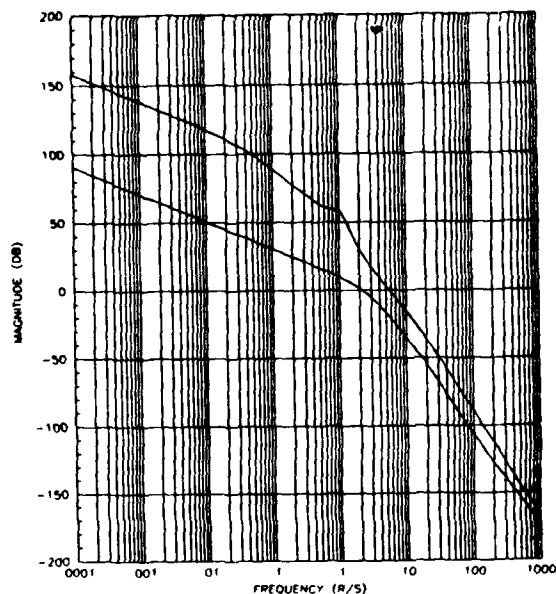
Fig 13.8   Singular Values of the Augmented Plant

13.2.2.1   Low and High Frequency Matching

First, we will "go for it." That is, we will choose Γ so that we get singular value matching at both low and high frequency, as detailed in Chapter 11. To really see what happens here, we need to look at the poles and zeros of each transfer function we produce throughout the design.

As a refresher, to achieve high and low frequency matching we must choose Γ as

$$\Gamma = \begin{bmatrix} G(0)^{-1} \\ C_p{}^T(C_p C_p{}^T)^{-1} \end{bmatrix} \tag{13.12}$$

Adjustment of the scalar μ so that the maximum bandwidth of T_{FOL} is close to 10 rad/sec produces a value of $\mu = 0.01$. The plot of T_{FOL} is shown in Fig 13.9 for these choices. Note that all specs are met, and the plots look like I/s except for a "rise" and a "dip" near 1 rad/sec.

13-11
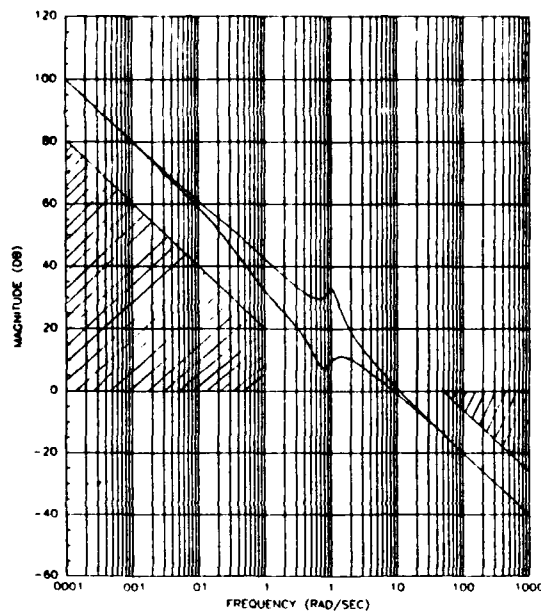
Fig 13.9 Singular Values of T_{FOL}, Hi-Low Matching

This easily explained by examining the poles and zeros of $C\Phi\Gamma$. They are

$$\text{zeros}(C\Phi\Gamma) = \begin{bmatrix} -0.075 \\ 0.168 \pm j0.737 \\ -3.14 \\ -19.96 \\ -19.99 \end{bmatrix} \tag{13.13}$$

$$\text{poles}(C\Phi\Gamma) = \begin{bmatrix} -0.036 \\ 0.188 \pm j1.05 \\ -3.25 \\ -20.0 \\ -20.0 \\ 0.0 \\ 0.0 \end{bmatrix} \tag{13.14}$$

Obviously, the poles are just those of the plant plus the augmented

integrators. Examination of (13.13) and (13.14) shows that the poles

and zeros of $C\Phi\Gamma$ nearly "cancel" each other, except for the integrator

poles and a mismatch in the complex pole-zero pair. The mismatch in the

complex pairs is why we see a rise and dip in Fig 13.9. The rise

corresponds to the pole frequency of 1.067 rad/sec and the dip to the

zero frequency of 0.756 rad/sec. The fact that only the integrators

effectively remain yields the overall I/s behavior of the singular value

13-12

plots.

Note that this selection for Γ yields a nonminimum phase $C\Phi\Gamma$. This occurs because the plant is open-loop unstable and we are trying to invert the plant. Realize that plant inversion _is_ what we are asking for since we want the singular values to be matched and look like I/s. The Kalman filter can _never_ be nonminimum phase. Therefore, we should expect to see these zeros mirrored to their stable images when we compute $C\Phi K_f$.

Now we'll compute K_f using the Γ and μ we just chose. Doing this and overlaying the plots in Fig 13.9 with those of $C\Phi K_f$ yields Fig 13.10.
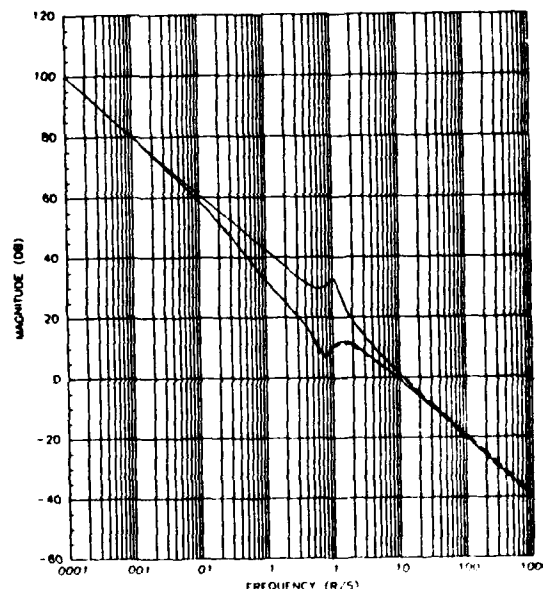
Fig 13.10 Singular Values of T_{POL} and T_{KF}, Hi-Low Matching

Obviously, the two plots are nearly identical. The poles of $C\Phi K_f$ are obviously the same as those of $C\Phi\Gamma$, so all we need to look at are the zeros of $C\Phi K_f$, given by

$$\text{zeros}(C\Phi K_f) = \begin{bmatrix} -0.074 \\ -0.144 \pm j0.714 \\ -3.18 \\ -20.00 \\ -20.02 \end{bmatrix} \tag{13.15}$$

These are literally identical to those of (13.13), except that the
nonminimum phase complex pair in (13.13) is nearly mirrored into the
left-half plane in (13.15). Obviously, this only slightly alters the
σ-plots since the magnitude of right-half vs. left-half plane poles
(zeros) is the same. Obviously, T_{KF} meets our specs.

Now the trouble begins. The next step is to "close the loop" on
the filter and compute the filter poles. The zeros of any system are
invariant under feedback, so that the zeros of the filter are given by
(13.15). The filter poles (poles of $[A - K_f C]$) are given by

$$
\text{filter poles} = \begin{bmatrix}
-0.074 \\
-0.184 \pm j0.732 \\
-3.05 \\
-20.00 \\
-20.08 \\
-10.02 \pm j1.41
\end{bmatrix}
\tag{13.16}
$$

Remember that these will be poles of the overall closed-loop system.
Obviously, the complex poles and the pole near the origin are not at all
desirable. Since there are zeros very close to them, their residuals
will be small (small contributions), but they will take a long time to
die out and the response is very oscillatory. Is this a fluke? No, not
really.

Looking back to Fig 9.2, we see that the closed-loop filter is just
$C\Phi K_f$ with unity feedback around it. Therefore, we can construct a
"root-locus" using the poles and zeros of $C\Phi K_f$ to determine the filter
poles. Unfortunately, a MIMO root-locus does not follow all the rules
of a SISO root-locus, and it is not worth going into the MIMO locus
here. The important point can be made without the actual locus. Since
all of the zeros lie very close to the plant poles (except the two zeros
at ∞), the plant poles will go to the zeros and therefore will not move
very much (the only poles that move very far are due to the integrators,

13-14

which go towards the zeros at ∞). Therefore, the closed-loop filter poles are almost identical to the stable images of the open-loop plant poles. In general, any time we choose Γ (and/or K_f) to invert the plant, the poles and zeros on the filter locus will be close together for each pole we try to invert. Therefore, even for a "low gain" filter, the closed-loop filter poles will be very close to the "inverted" open-loop poles (or their stable images). If the open-loop poles or their stable images are undesirable from a closed-loop point-of-view, we should not try to invert them.

Just for fun, let's finish the design. Choosing $q^2 = 10^5$ we get the regulator poles

$$\text{regulator poles} = \begin{bmatrix} -7.72 \pm j15.49 \\ -12.92 \pm j28.77 \\ -20.22 \pm j5.07 \\ -31.61 \pm j11.7 \end{bmatrix} \qquad (13.17)$$

which, even though some are lightly damped, are fast enough to present no problem. The singular values of T_{KF} and GK are shown in Fig 13.11, and show a high degree of recovery.
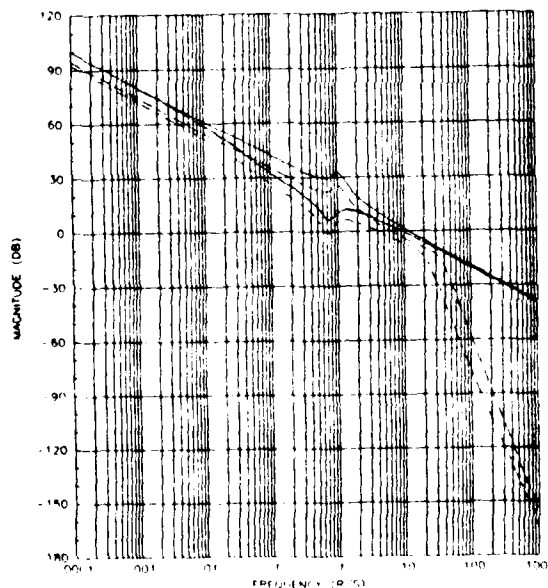
Fig 13.11 Singular Values of T_{KF} and GK, Hi-Low Matching

13-15

Actually, the recovery parameter q^2 would have to be increased if excellent recovery was desired, but in this case the results are only slightly altered by doing so. Joining the regulator and filter together produces an LQG compensator with poles and zeros

$$\text{zeros}[K(s)] = \begin{bmatrix} -0.074 \\ -0.105 \pm j0.704 \\ -3.18 \\ -20.00 \\ -20.01 \end{bmatrix} \tag{13.18}$$

$$\text{poles}[K(s)] = \begin{bmatrix} -7.43 \pm j19.09 \\ -11.26 \pm j32.85 \\ -25.47 \pm j9.37 \\ -38.65 \pm j17.0 \\ 0.0 \\ 0.0 \end{bmatrix} \tag{13.19}$$

Closing the loop on our overall system, we get the closed-loop zeros and poles

$$\text{zeros(closed-loop)} = \begin{bmatrix} -158.15 \\ -0.074 \\ -0.105 \pm j0.704 \\ -3.18 \\ -20 \\ -20 \end{bmatrix} \tag{13.20}$$

$$\text{poles(closed-loop)} = [\text{ poles of regulator (Eq (13.17))} \\ \text{plus poles of filter (Eq (13.16)) }] \tag{13.21}$$

Now, we look at the punchline. Fig 13.12 shows the time responses of β and ϕ to a unit step ϕ-command. While the sideslip response is excellent, the roll response is highly oscillatory and takes a long time to settle down. Obviously, a poor design.
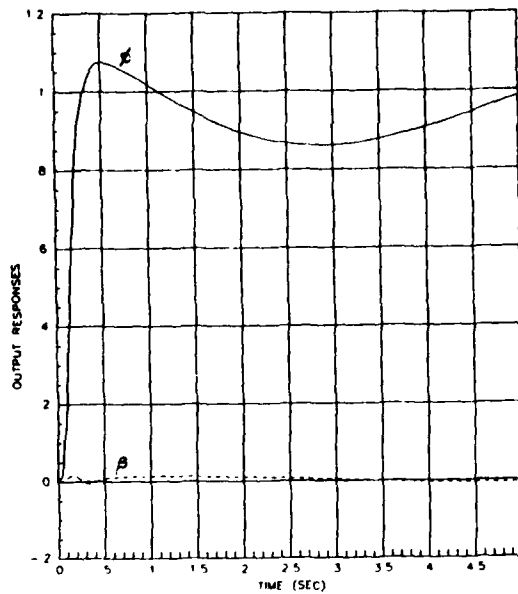
Fig 13.12 Time Resonses for a Roll Command, Hi-Low Matching

13.2.2.2 Low Frequency Matching

Since high and low frequency matching did not work well, let's try just low frequency matching. To accomplish this, we choose

$$\Gamma = \begin{bmatrix} C(0)^{-1} \\ 0 \end{bmatrix} \tag{13.22}$$

and $\mu = 0.01$. The resulting zero of $C\Phi\Gamma$ is simply the transmission zero of the plant (-158.15), so that this choice of Γ does <u>not</u> try to invert the plant. Computing $C\Phi K_f$ using this μ and Γ, and computing the singular values of T_{FOL} and T_{KF} produces the plots in Fig 13.13 (the T_{FOL} plots are solid lines).

13-17
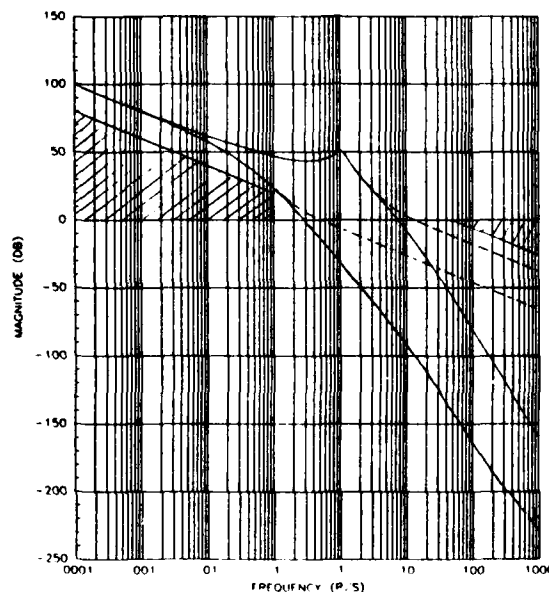
Fig 13.13 Singular Values of T_{FOL} anf T_{KF}, Low Matching

As expected, the plots match well where the gain is large, but at high frequency T_{KF} levels out from T_{FOL} since T_{KF} has only a 1-pole roll-off.

This is also seen by looking at the zeros of $C\Phi K_f$, shown in Table 13.3.

Table 13.3 Data for Low Frequency Matching, Output Design

$$\mu = 0.01 \qquad \Gamma = [\; G(0)^{-1} \quad 0\,]^T \qquad q^2 = 10^6$$

$$\text{poles(filter)} = \begin{bmatrix} -0.16 \pm j0.25 \\ -3.78 \pm j6.56 \\ -0.32 \\ -8.20 \\ -19.96 \\ -20.00 \end{bmatrix}$$

$$\text{zeros}(C\Phi\Gamma) = [\; -158.15 \;]$$

$$\text{zeros}(C\Phi K_f) = \begin{bmatrix} -0.19 \pm j0.14 \\ -4.61 \pm j6.56 \\ -20.00 \\ -20.04 \end{bmatrix}$$

$$\text{poles(regulator)} = \begin{bmatrix} -10.24 \pm j21.7 \\ -17.02 \pm j39.1 \\ -25.33 \pm j8.43 \\ -41.26 \pm j16.1 \end{bmatrix}$$

$$K_f = \begin{bmatrix} -0.121 & -2.756 \\ 0.044 & 0.979 \\ 0.500 & -0.003 \\ -0.466 & 83.911 \\ -0.160 & 0.266 \\ -0.003 & 12.956 \\ -0.120 & -2.719 \\ 0.044 & 0.966 \end{bmatrix} \qquad K_c = \begin{bmatrix} 71.62 & -21.35 \\ -21.35 & 73.16 \\ 737.28 & 685.13 \\ -42.56 & 36.43 \\ -73.42 & -68.28 \\ -735.65 & 677.10 \\ 139.62 & -77.78 \\ -76.76 & 145.21 \end{bmatrix}^T$$

$$\text{zeros}[K(s)] = \begin{bmatrix} -0.19 \pm j0.14 \\ -4.00 \pm j2.99 \\ -20.00 \\ -20.01 \end{bmatrix}$$

Notice that while Γ does not try to invert the plant, the resulting value of K_f produces a pair of complex zeros near the imaginary axis. This should signal potential problems. When we close the filter loop, the resulting poles are shown in Table 13.3. Note that there is a low frequency, poorly damped complex pair as well as a low frequency real pole.

Setting $q^2 = 10^6$ produces the recovery plot in Fig 13.14. T_{KF} plots are shown as solid lines, while GK plots are dashed.
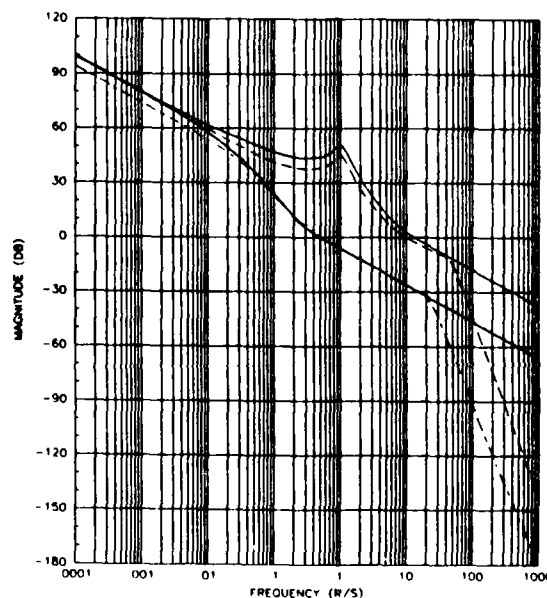
Fig 13.14 Singular Values of T_{KF} and GK, Low Matching

Recovery is excellent at frequencies up to crossover, then additional roll-off is added by the LQG compensator. The regulator poles, compensator zeros, and gain matrices are also shown in Table 13.3. Finally, the time responses due to step commands in roll and sideslip are shown in Figs 13.15 and 13.16, respectively. The roll-to-roll command response has a large overshoot, but is otherwise well behaved. The sideslip-to-roll command response, on the other hand, is small but takes a long time to settle. The sideslip command responses are

terrible, but since a sideslip command controller is not our objective
this may not be important. Still, we can do better.
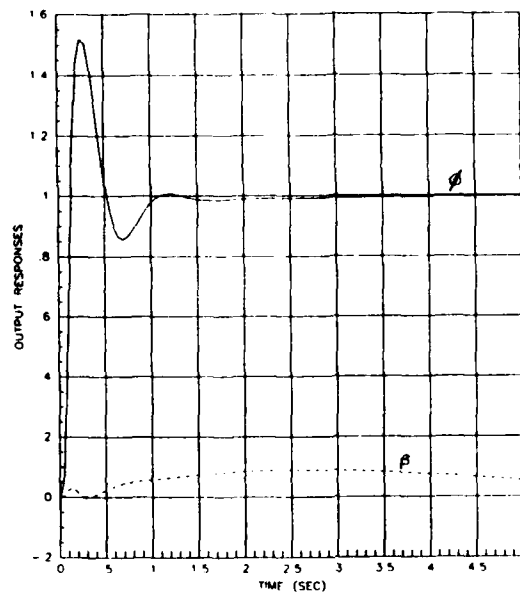
Fig 13.15   Time Responses for a Roll Command, Low Matching
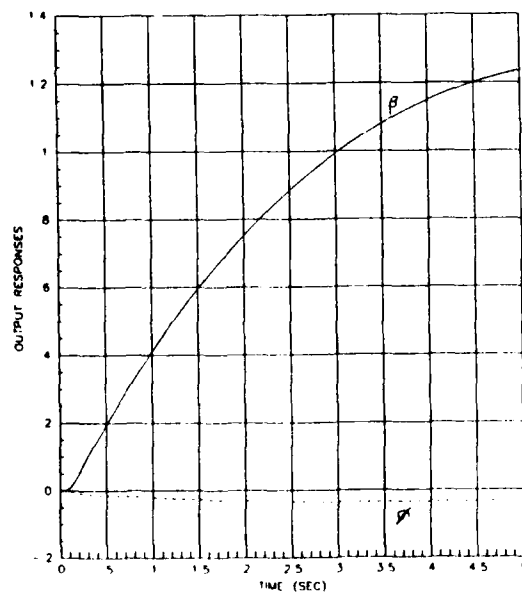
Fig 13.16   Time Responses for a Sideslip Command, Low Matching

13.2.2.3 High Frequency Matching

Now we will try using only high frequency matching. To accomplish
this, we must choose

13-20

$$\Gamma = \begin{bmatrix} \Gamma_1 \\ C_p^{\ T}(C_p C_p^{\ T})^{-1} \end{bmatrix}$$ (13.23)

where Γ_1 is arbitrary but non-zero. For convenience, Γ_1 was chosen to be I_2. Choosing $\mu = 0.1$ produces a bandwidth of just under 10 rad/sec, as shown in the solid curves in Fig 13.17. Obviously, we do get high frequency matching, and our specs are met.
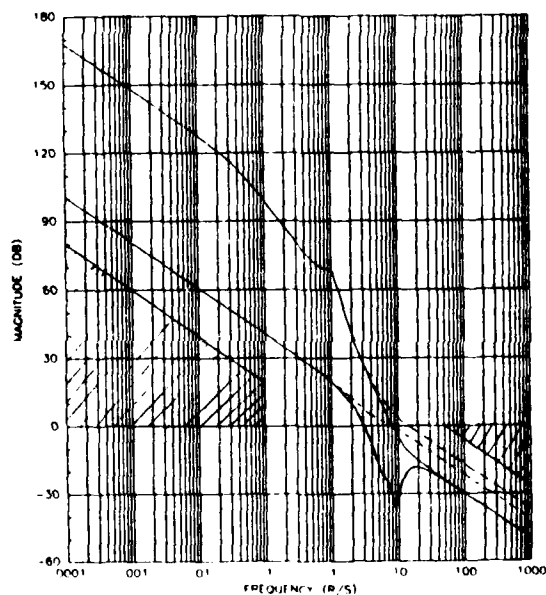
Fig 13.17 Singular Values of T_{FOL} and T_{KF}, Hi Matching

13-21

Table 13.4 Data for High Frequency Matching, Output Design

$$\mu = 0.1 \qquad \Gamma = [\; I_2 \quad C_p^T(C_p C_p^T)^{-1}\;]^T \qquad q^2 = 10^6$$

$$\text{zeros}(C\Phi\Gamma) = \begin{bmatrix} 0.126 \pm j9.34 \\ 1.230 \pm j5.58 \\ -21.27 \\ -24.27 \end{bmatrix} \qquad \text{poles(filter)} = \begin{bmatrix} -1.50 \pm j3.07 \\ -3.62 \pm j7.15 \\ -4.18 \\ -10.35 \\ -19.74 \\ -19.97 \end{bmatrix}$$

$$\text{zeros}(C\Phi K_f) = \begin{bmatrix} -1.84 \pm j2.04 \\ -4.56 \pm j4.57 \\ -20.08 \\ -20.15 \end{bmatrix}$$

poles(regulator) = same as in Table 13.3

$$K_f = \begin{bmatrix} 1.977 & -2.469 \\ 2.469 & 1.977 \\ 8.302 & -0.605 \\ -17.222 & 92.111 \\ -29.938 & -4.418 \\ -0.605 & 13.907 \\ 1.641 & -2.427 \\ 2.455 & 1.686 \end{bmatrix} \qquad K_c = \text{same as in Table 13.3}$$

$$\text{zeros}[K(s)] = \begin{bmatrix} -1.68 \pm j1.59 \\ -4.07 \pm j3.58 \\ -20.01 \\ -20.04 \end{bmatrix}$$

Table 13.4 shows the zeros of $C\Phi\Gamma$ for this case. Here we see two right-half plane complex pairs, both of which are lightly damped and at high frequency. The pair at $(0.126 + j9.338)$ looks like a real problem, since it is near the imaginary axis. However, it is at high frequency (near the crossover region) and, as may be seen in Fig 13.17, is predominantly affecting σ plot (the "dip" in σ). Therefore, when we use this choice of μ and Γ, the resulting singular values plots of $C\Phi K_f$ (shown as dotted lines in Fig 13.17) do not have this dip. This is also easy to see by noticing the zeros of $C\Phi K_f$, shown in Table 13.4. Here, both troublesome complex pairs of zeros are "moved" to much better locations, since T_{FOL} approximates T_{KF} only where the gains of T_{FOL} are high.

13-22

The resulting filter poles are also shown in Table 13.4. These are well behaved with damping ratios near 0.5. Choosing $q^2 = 10^6$, we get the recovery plot shown in Fig 13.18, where the solid lines are T_{KF}.
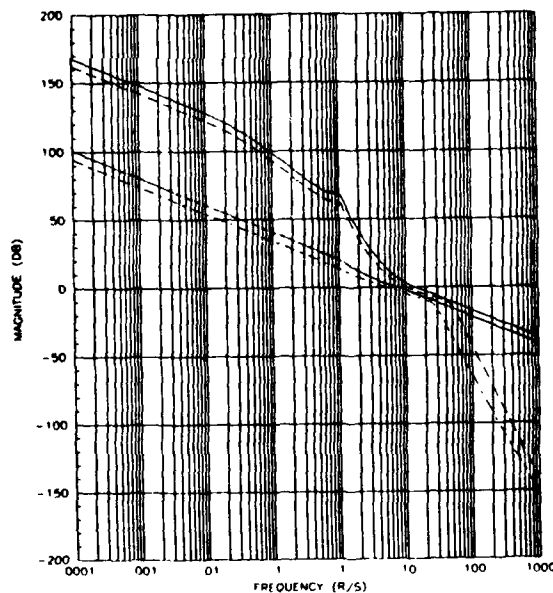
Fig 13.18   Singular Values of T_{KF} and GK, Hi Matching

Again, recovery is excellent and the bandwidth has been lowered to 10 rad/sec (notice that T_{KF} actually violated the bandwidth spec). The remaining poles, zeros, and gain matrices are shown in Table 13.4. Simulating our overall system, we get the roll command responses shown in Fig 13.19.
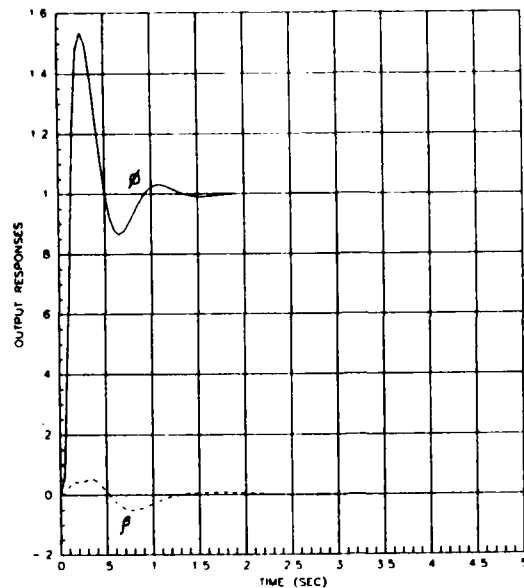
Fig 13.19   Time Responses for a Roll Command, Hi Matching

The overshoot on the roll response is large (55%), but could be reduced

using a prefilter. This design is not bad. However, it may seem

pointless to go through the high frequency matching technique when it is

not really possible to get T_{FOL} and T_{KF} to match at high frequency.

Therefore, we will try one more choice, which will produce literally the

same results as this one, but which is a more logical choice for Γ.

13.2.2.4   "Arbitrary" Γ Selection

As this is the design we will select as the "best," more details

will be shown throughout the design process. In this case, we will make

the "easiest" and most common selection for Γ, that is ,Γ = B. Looking

back to Fig 13.8, notice that the singular values of $C\Phi B$ for our

augmented system are not that bad; that is, by increasing the gain

(decreasing μ) we can increase the bandwidth and easily meet our specs.

Typically, this is what a designer would choose first, since it requires

no real trial-and-error selection for Γ.

First, we will choose Γ = B (remember that the B here is the

13-24

augmented system's input matrix) and $\mu = 0.2$. Using these values to compute K_f, we get the plots of T_{FOL} and T_{KF} shown in Fig 13.20 (T_{FOL} in solid lines).
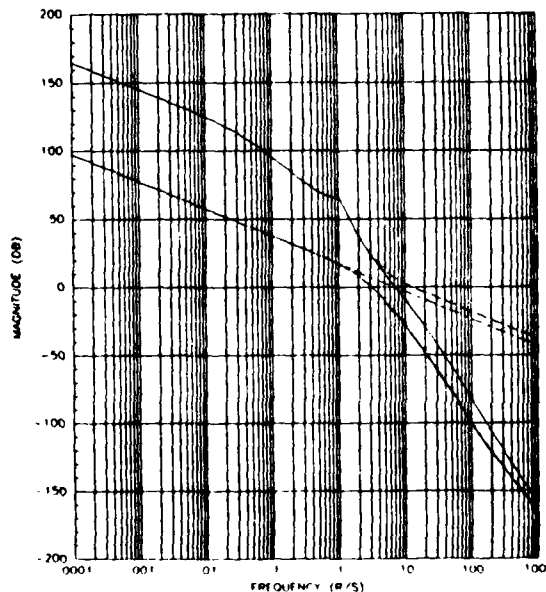
Fig 13.20   Singular Values of T_{FOL} and T_{KF}, $\Gamma = B$, $\mu = 0.2$

Notice that even though T_{FOL} has a maximum crossover frequency below 10 rad/sec, T_{KF} exceeds it. Since T_{KF} doesn't satisfy our bandwidth spec, we must increase μ. Increasing μ to 0.3 generates the plots of T_{FOL} and T_{KF} shown in Fig 13.21. The maximum crossover is still just above 10 rad/sec, but when we recover this loop shape the bandwidth should reduce. The increase in μ from 0.2 to 0.3 causes a roughly 20% decrease in the individual elements of K_f, thus illustrating the benefit of using less control power.
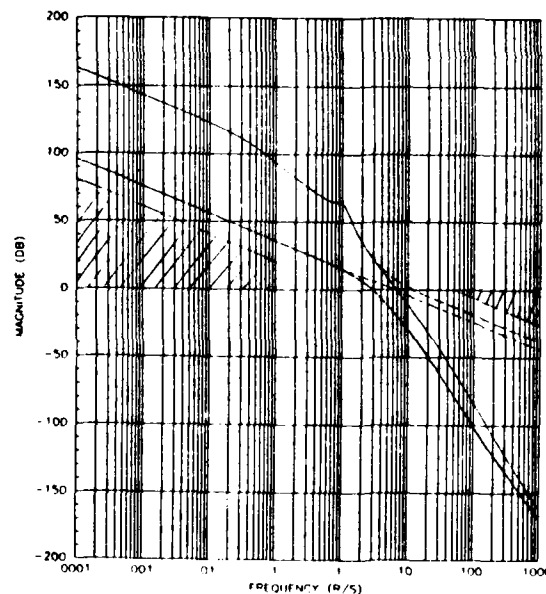
Fig 13.21   Singular Values of T_{FOL} and T_{KF}, $\Gamma = B, \mu = 0.3$

Table 13.5   Data for Augmented = B Output Design

$$\mu = 0.3 \qquad \Gamma = B \qquad q^2 = 10^6$$

$\text{zeros}(C\Phi\Gamma) = [\ -158.15\ ]$

$\text{zeros}(C\Phi K_f) = \begin{bmatrix} -1.92 \pm j1.46 \\ -4.07 \pm j3.41 \\ -20.00 \\ -20.02 \end{bmatrix}$

$\text{poles(filter)} = \begin{matrix} -1.92 \pm j2.66 \\ -3.31 \pm j5.89 \\ -3.49 \\ -7.15 \\ -19.98 \\ -20.02 \end{matrix}$

poles(regulator) = same as in Table 13.3

$K_f = \begin{bmatrix} 0.818 & -1.633 \\ 1.633 & 0.818 \\ 6.547 & -1.221 \\ -19.074 & 68.314 \\ -22.491 & 2.677 \\ -1.221 & 11.637 \\ 0.817 & -1.620 \\ 1.628 & 0.804 \end{bmatrix}$

K_c = same as in Table 13.3

$\text{zeros}[K(s)] = \begin{matrix} -1.72 \pm j1.16 \\ -3.56 \pm j2.73 \\ -20.00 \\ -20.00 \end{matrix}$

$\text{poles}[K(s)] = \begin{matrix} -9.00 \pm j25.0 \\ -14.10 \pm j44.2 \\ -29.85 \pm j12.0 \\ -50.00 \pm j23.10 \\ 0.0 \\ 0.0 \end{matrix}$

The zeros of $C\Phi\Gamma$ and $C\Phi K_f$ for our choices of μ and Γ are shown in Table 13.5. All of the zeros of $C\Phi K_f$ are in "desirable" locations and have good damping. Closing the filter loop produces the filter poles shown in Table 13.5. These are also well behaved, so we'll proceed with the recovery. Several choices of q^2 were made, ranging from 0 to 10^8. By looking at <u>both</u> the recovery plots <u>and</u> the time responses a good value of q^2 may be chosen. For $q^2 = 10^6$, which was the final selection, the recovery plots are shown in Fig 13.22. The plot of GK (shown as dashed lines) does meet all of our specs. The resulting filter poles, compensator poles and zeros, and gain matrices K_c and K_f are shown in Table 13.5.
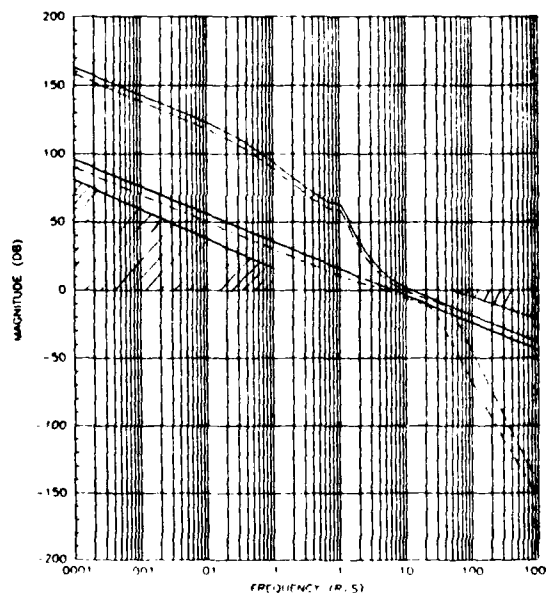
Fig 13.22   Singular Values of T_{KF} and GK, $\Gamma = B$, $\mu = 0.3$

Now let's take a good look at our design. Notice that so far we have not been showing any of our robustness tests, gain and phase margins, or control input histories. This was simply to conserve space. Here, we will examine them. Figs 13.23 and 13.24 show the plots of $\sigma_i [I + T_{KF}]$ and $\sigma_i [I + (T_{KF})^{-1}]$, respectively. Notice that the singular

13-27

values of the filter return difference in Fig 13.23 are always at or
above 0 dB, as guaranteed by the Kalman Equality. Similarly, the plots
in Fig 13.24 never go below -6 dB, which again is guaranteed.
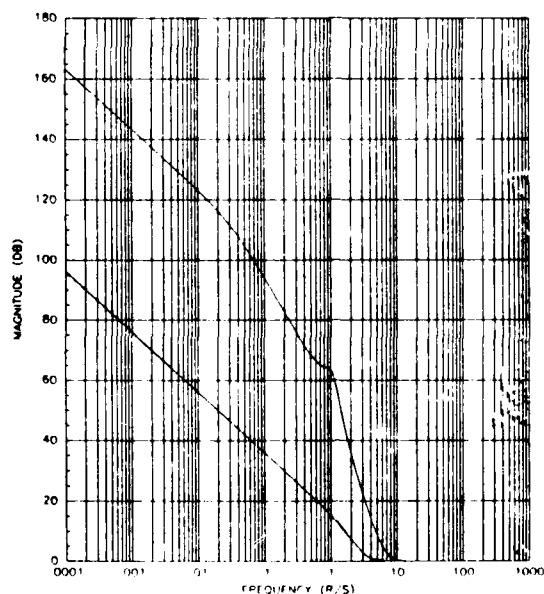
Fig 13.23   Singular Values of $I + T_{KF}$, $\Gamma = B$, $\mu = 0.3$
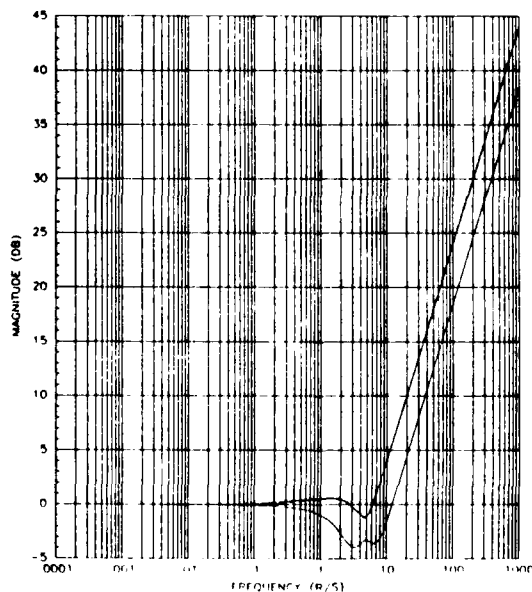
Fig 13.24   Singular Values of $I + (T_{KF})^{-1}$, $\Gamma = B$, $\mu = 0.3$

13-28

To check for robustness in our filter, we compare the plots of $\ell_m(w)$ and $\underline{\sigma}[I + (T_{KF})^{-1}]$ in Fig 13.25. Obviously, $\ell_m(w)$ is less than $\underline{\sigma}$ at all frequencies, so we pass the test.
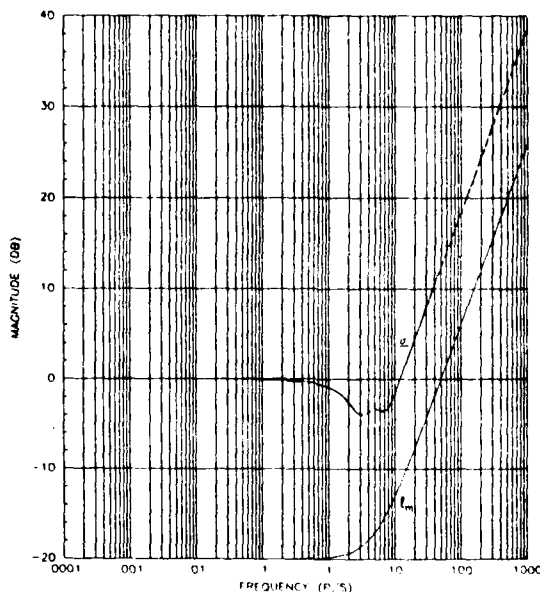
Fig 13.25 Singular Values of ℓ_m and $\underline{\sigma}[I + (T_{KF})^{-1}]$, $\Gamma = B$, $\mu = 0.3$

Now let's examine our actual loop transfer function, GK. Fig 13.26 shows a comparison of $\ell_m(w)$ and $\sigma[I + (GK)^{-1}]$.
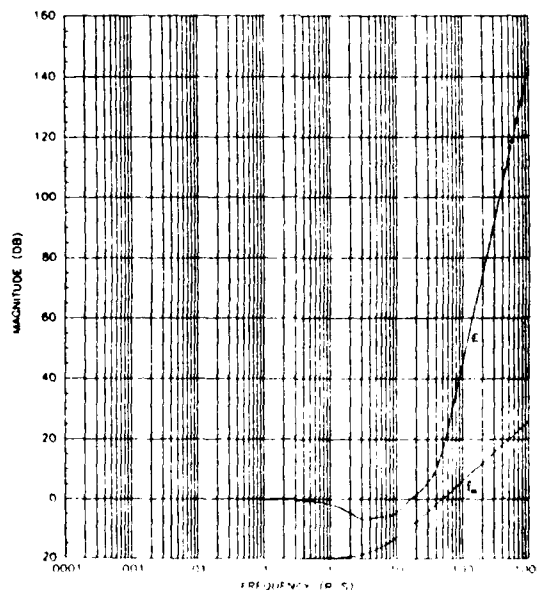
Fig 13.26 Singular Values of ℓ_m and $\underline{\sigma}[I + (GK)^{-1}]$, $\Gamma = B$, $\mu = 0.3$

Since $\ell_m(w)$ is below $\underline{\sigma}[I + (GK)^{-1}]$ at all frequencies, we are guaranteed that the closed-loop system will remain stable in the face of all output uncertainties bounded by ℓ_m (actually, all bounded by $\underline{\sigma}[I + (GK)^{-1}]$). From Fig 13.26 and a plot of $\underline{\sigma}[I + GK]$ (not shown), we can compute the MIMO gain and phase margins of our system. These were found to be

$$-5.26 \text{ dB} \leq GM \leq 6.58 \text{ dB} \tag{13.24}$$

$$-30.8° \leq PM \leq 30.8° \tag{13.25}$$

If these are considered to be too low, then q^2 would need to be increased.

Now let's examine our time responses. Fig 13.27 shows the response of sideslip and roll angle to a unit step roll command. We can see that we have perfect staedy-state tracking, a settling time in both responses of about 1.5 seconds, a maximum overshoot of 50% in our roll response, and a maximum sideslip angle of less than 0.1 degrees. The corresponding control histories are shown in Figs 13.28 and 13.29. Fig 13.28 shows a maximum elevon deflection of -2.2 degrees and Fig 13.29 shows a maximum rudder deflection of -1.2 degrees. The "bad" aspects of these responses are relatively high surface deflection rates and a large overshoot in roll respons'. Let's try to fix these.
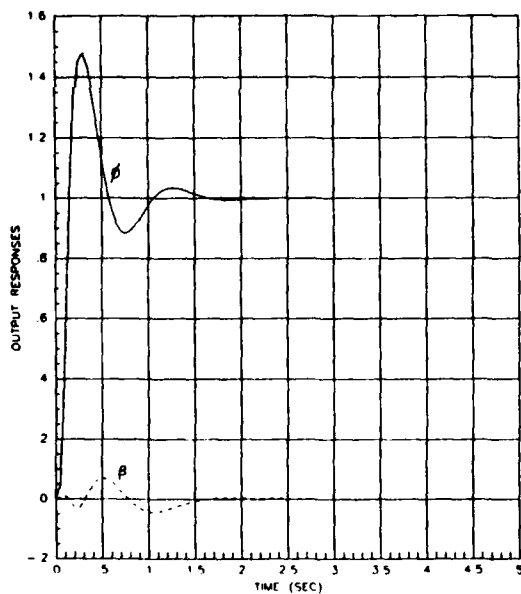
Fig 13.27 Time Responses for a Roll Command, $\Gamma = B$, $\mu = 0.3$
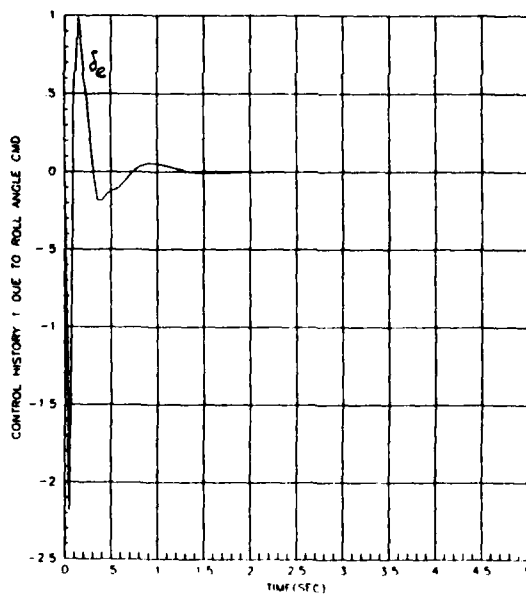
Fig 13.28 Elevon Surface Deflection due to a Roll Command
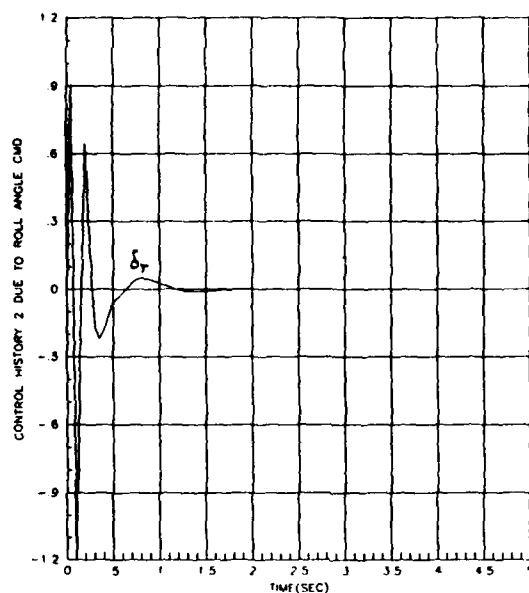
Fig 13.29 Rudder Surface Deflection due to a Roll Commmand

To improve the response, we will add a diagonal prefilter to our system, as shown in Fig 13.30.
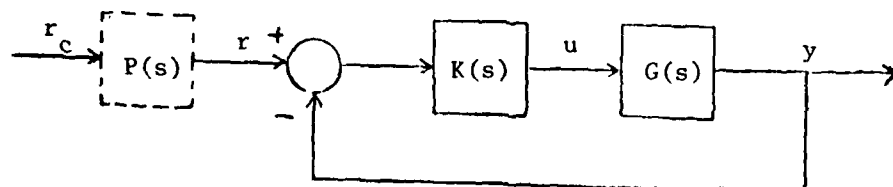
Fig 13.30 System With an Added Prefilter

Here, we will choose P(s) as

$$P(s) = \begin{bmatrix} \dfrac{4}{s+4} & 0 \\ \\ 0 & \dfrac{4}{s+4} \end{bmatrix} \tag{13.26}$$

to slow down our responses and decrease the overshoot. The roll angle

13-32

response to a unit step roll command (now r_c in Fig 13.30) is shown in
Fig 13.31. Now we can see that the maximum overshoot has been reduced
to roughly 6% with little increase in settling time. The sideslip
response is shown in Fig 13.32, which shows excellent decoupling with a
maximum deviation of less than 0.04 degrees. The elevon surface
deflection is shown in Fig 13.33, and shows a maximum deflection of only
-0.26 degrees. The maximum rate is less than 4 deg/sec. Fig 13.34
shows the rudder deflection, which has a maximum deflection of about 0.1
degrees, and a maximum rate of 2 deg/sec. All of these figures are
reasonable and well withing the limits of the aircraft. This was
considered to be a very good controller design, with excellent
robustness properties.
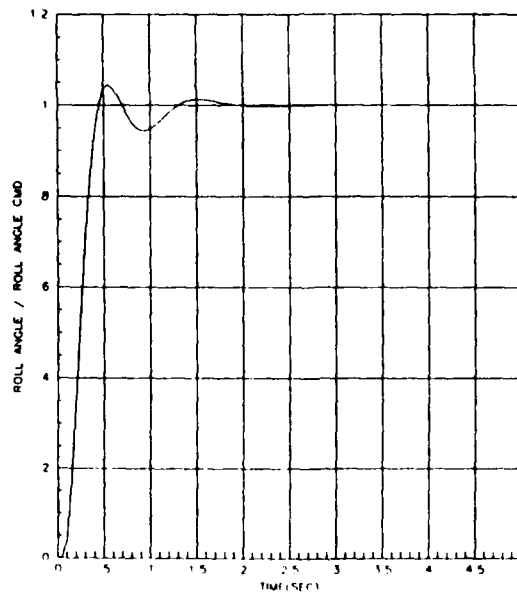
Fig 13.31   Roll Response to a Prefiltered Roll Command
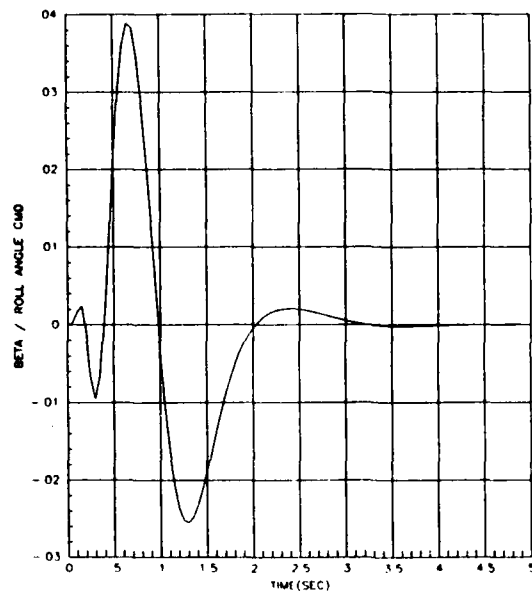
Fig 13.32 Sideslip Response to a Prefiltered Roll Command
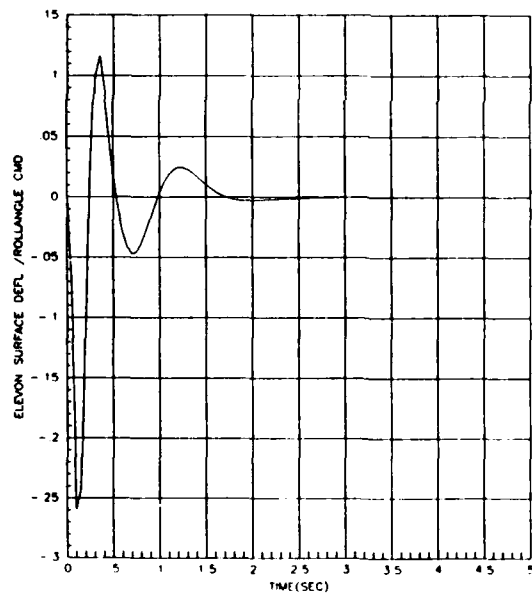
Fig 13.33 Elevon Surface Deflection due to a Prefiltered Roll Command
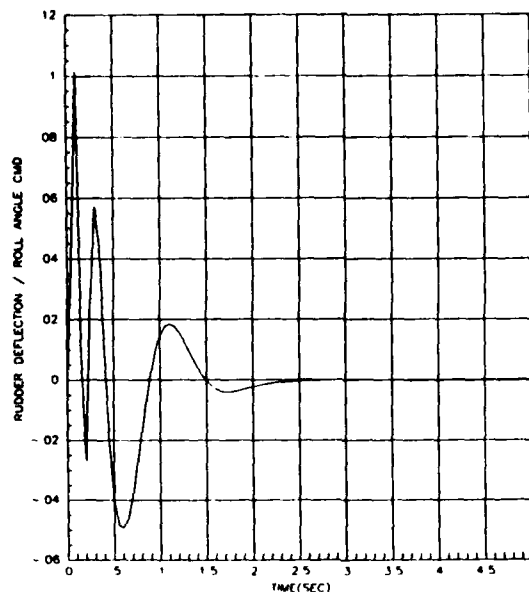
13-34

Fig 13.34   Rudder Surface Deflection due to a Prefiltered Roll Command

13.3 Design With Input Uncertainties

Now we will design two controllers for the case where we break the loop at the input to our plant. As a reminder, we said that we will assume that our input multiplicative uncertainties are the same as those at the output; therefore, $\ell_m(w)$ is defined by Fig 13.2 for this case. We will also assume that out performance requirements are the same here as they were at the output, so that Fig 13.3 shows the barriers our input loop transfer functions (T_{ROL}, T_{LQ}, and KG) must not intersect. We will make some comments on the meaning and validity of our performance requirements in the upcoming example.

13.3.1 Low Frequency Matching

First, we will look at a design where we have augmented integrators at the plant output and choose H to achieve low frequency matching. This requires H to be chosen as

$$H = [H_1 \quad G(0)^{-1}] \tag{13.27}$$

13-35

where H_1 is arbitrary. Since we can choose H_1, and it weights the plant states, we will choose

$$H_1 = \begin{bmatrix} 0 & 0 & 0 & 0.05 & 0 & 0 \\ 0.5 & 0 & 0 & 0 & 0 & 0 \end{bmatrix} \qquad (13.28)$$

so that roll and sideslip are regulated well. The strange choice of values in (13.28) comes from two factors. First, sideslip was weighted 10 times as heavily as roll, since sideslip seems to be predominantly controlled by the minimum singular value in the output cases. Secondly, the 0.05 value for roll weighting was chosen so that when B postmultiplies H to form T_{ROL}, the product of H and B will yield a unity value (since B has 20's in it). Adjustment of ρ so that the largest singular value of T_{ROL} (here defined as $\frac{1}{\sqrt{\rho}} \sigma_1[H\Phi B]$) crosses 0 dB near 10 rad/sec yields $\rho = 0.01$. The resulting plot of T_{ROL} is shown as solid curves in Fig 13.35.
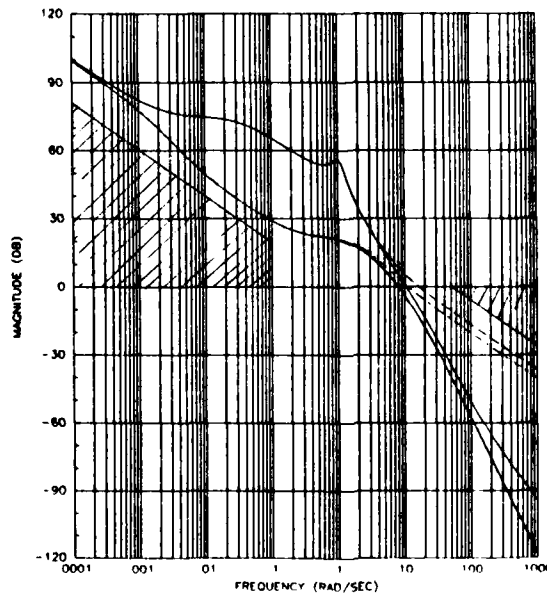
Fig 13.35 Singular Values of T_{ROL} and T_{LO}, Low Matching

Both our performance and robustness specs are met by T_{ROL}, so we can use these choices of ρ and H to calculate K_c. Doing so produces the plots of T_{LQ} (defined as $_1[K_c\Phi B]$) shown as dotted lines in Fig 13.35. T_{LQ} obviously still meets the specs. Table 13.6 shows the zeros of $H\Phi B$ and those of $K_c\Phi B$ for this design. Notice that two low frequency zeros appear. Luckily, the resulting regulator poles (also shown in Table 13.6) almost perfectly cancel these, so that their contribution may be insignificant if a compensator zero (zero of $K(s)$) is also there.

Table 13.6   Data for Low Frequency Matching, Input Design

$$\rho = 0.01 \qquad H = [\ H_1 \quad G(0)^{-1}\ ] \qquad q^2 = 10^6$$

$$\text{zeros}(H\Phi B) = \begin{bmatrix} 0.00713 \\ -0.204 \\ -158.15 \end{bmatrix} \qquad \text{poles(regulator)} = \begin{bmatrix} -0.00713 \\ -0.203 \\ -6.19 \pm j6.10 \\ -6.95 \pm j8.20 \\ -20.36 \\ -20.72 \end{bmatrix}$$

$$\text{zeros}(K_c\Phi B) = \begin{bmatrix} -0.00712 \\ -0.201 \\ -7.90 \\ -8.88 \\ -18.95 \\ -19.32 \end{bmatrix}$$

$$\text{poles(filter)} = \begin{bmatrix} -10.24 \pm j21.74 \\ -17.02 \pm j39.13 \\ -25.33 \pm j8.43 \\ -41.26 \pm j16.11 \end{bmatrix}$$

$$K_c = \begin{bmatrix} 3.148 & 4.286 \\ -0.066 & 0.033 \\ -0.534 & -0.714 \\ -0.429 & 0.246 \\ 0.513 & 0.079 \\ 0.079 & 0.721 \\ 2.918 & -0.237 \\ -0.001 & -0.001 \end{bmatrix}^T \qquad K_f = \begin{bmatrix} 1.31\times10^3 & 1.94\times10^2 \\ 7.03\times10^3 & 1.11\times10^5 \\ -1.77\times10^4 & -4.58\times10^3 \\ 2.02\times10^2 & 4.38\times10^3 \\ 1.81\times10^3 & -4.43\times10^3 \\ 2.63\times10^3 & 4.23\times10^3 \\ 5.12\times10^1 & 2.74\times10^0 \\ 2.74\times10^0 & 9.36\times10^1 \end{bmatrix}$$

$$\text{zeros}[K(s)] = \begin{bmatrix} -0.00712 \\ -0.193 \\ -4.53 \\ -6.53 \\ -19.81 \\ -19.95 \end{bmatrix}$$

Now we must recover T_{LO} by designing our filter. For convenience, we choose $\Gamma = B$ so that our recovery is starting out in the right direction (remember that we must choose $O_f = \Gamma\Gamma^T + q^2 BB^T$). Choosing a different Γ has little effect on the overall results. Choosing $q^2 = 10^6$ produces the KG plots shown in Fig 13.36 (T_{LO} plots are solid lines, KG dashed). Notice that our specs are met by KG. Are these specs truly meaningful?
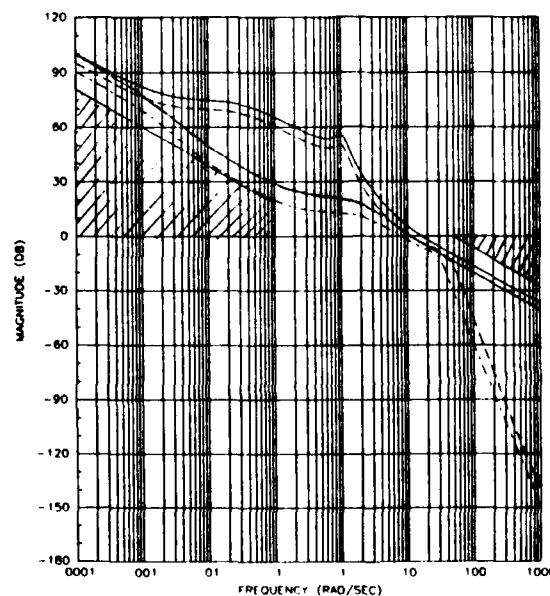

Fig 13.36 Singular Values of T_{LO} and KG, Low Matching

For loop-breaking at the input, the answer may be, "not really." The robustness requirements definitely do make sense, since they represent input multiplicative perturbations. However, the performance requirements are intended to reflect command following requirements. That is, we wish our outputs to follow our commands. This requires GK to be large at our command frequencies, as shown in Chapter 4. Notice that we are looking at KG in our input designs, which is not equal to GK, in general. Therefore, requiring KG to be large at low frequency

13-38

may not give us good command following, if the corresponding GK does not

meet the specs. The whole problem here is that our robustness

requirements are reflected to the plant input, while our performance

requirements naturally reflect to the output. The singular value is

inadequate for the "multiple location uncertainties" just described.

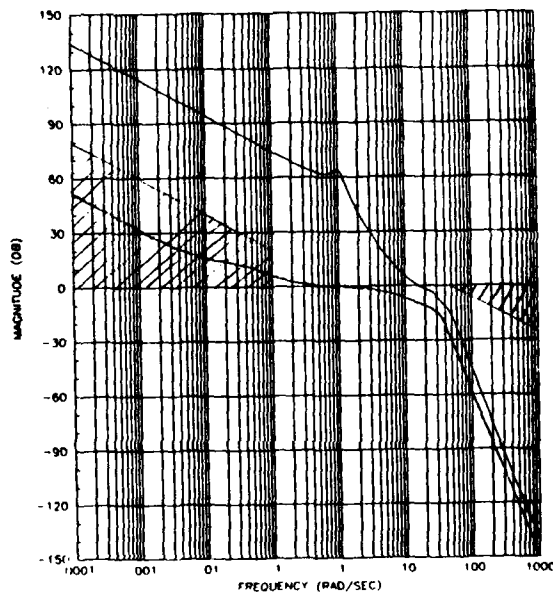Let's look at GK for this example, which is shown in Fig 13.37.

Fig 13.37 Singular Values of GK, Low Matching

Notice that GK does not meet the performance specs. We should see some

effects from this in our system time responses. Finishing the design

gives us the remaining data in Table 13.6. Note that while the

regulator (and thus closed-loop) pole at -0.00713 is almost exactly

cancelled by a zero at -0.00712, the pole at -0.201 is "missed" by the

zero at -0.193, so we may expect some slow transients.
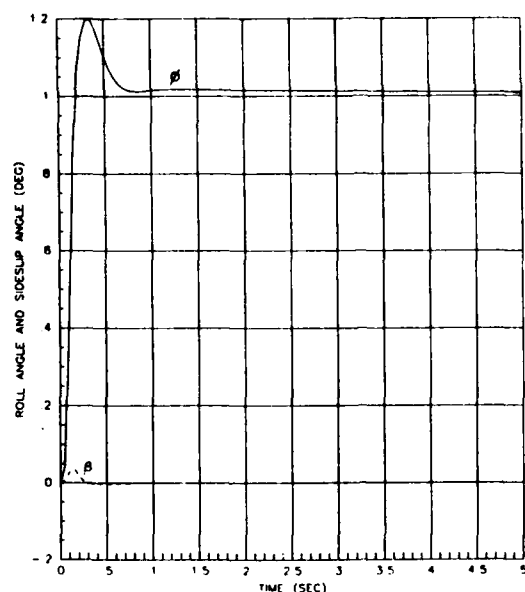
Fig 13.38   Time Responses for a Roll Commmand, Low Matching

Fig 13.38 shows the sideslip and roll responses to a unit step roll command.   These responses are very nice!   Where did the result of GK not meeting our specs go?   Fig 13.39 shows the responses due to a sideslip command.   Obviously, this is where our spec violation is manifested. This again shows some of the peculiarities of a MIMO system.   As far as whether this is a good design or not depends on whether or not commanding sideslip is important.   Technically, since GK does not meet our specs, we should redesign.

13-40
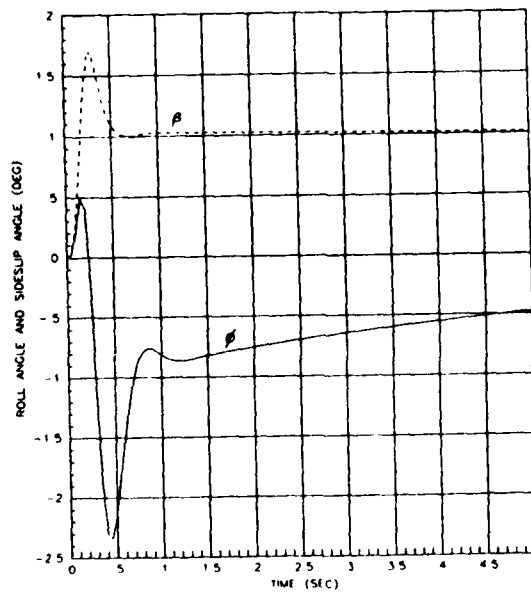
Fig 13.39 Time Responses to a Sideslip Command, Low Matching

13.3.2 "Arbitrary" H Selection

In this final example, we will again augment with integrators, but here we will choose H arbitrarily. Again, since the singular value plots of CΦB are not bad, and since we want to control our measured variables, we will choose F = C (the <u>augmented</u> C matrix, that is). Choosing ρ = 1 produces the plot of T_{ROL} shown in Fig 13.40 (shown as solid lines). The specs are met, but the maximum bandwidth is below 10 rad/sec. This is deliberate; using this ρ and H produces the plots of T_{LO} also shown in Fig 13.40, for which the maximum crossover frequency is very close to 10 rad/sec.
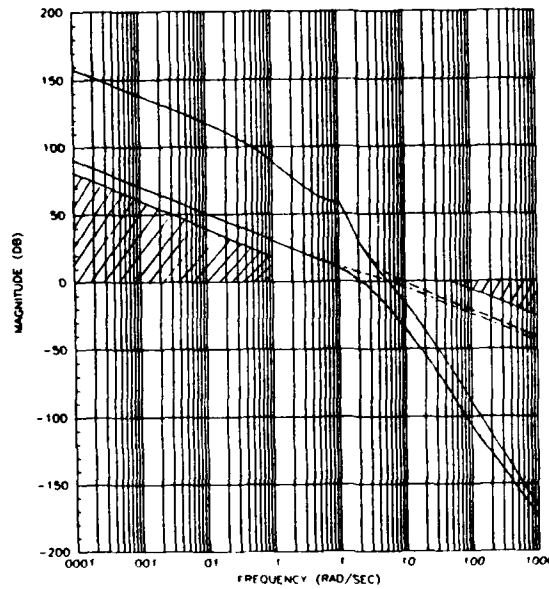
Fig 13.40 Singular Values of T_{ROL} and T_{LO}, $H = C$

Obviously, this was a result of trial-and-error, not gifted insight.

The zeros of $H\Phi B$ and $K_c\Phi B$ are shown in Table 13.7, as well as the

resulting regulator poles. Notice that these are in desirable

locations.

Table 13.7   Data for Augmented H = C Input Design

$$\rho = 1 \qquad H = C \qquad q^2 = 10^6$$

zeros(HϕB) = [-158.15]

poles(regulator) = $\begin{bmatrix} -1.76 \pm j2.06 \\ -2.72 \pm j4.81 \\ -2.79 \\ -5.88 \\ -20.00 \\ -20.00 \end{bmatrix}$

zeros($K_c\phi$B) = $\begin{bmatrix} -1.64 \pm j0.93 \\ -3.49 \pm j2.72 \\ -20.00 \\ -20.01 \end{bmatrix}$

$$K_c = \begin{bmatrix} 0.941 & -0.053 & -0.255 & -0.340 & -0.370 & -0.059 & -0.787 & 0.616 \\ 0.492 & 0.031 & -0.227 & 0.224 & -0.059 & 0.366 & 0.616 & 0.787 \end{bmatrix}$$

K_f = same as in Table 13.6

poles(filter) = same as in Table 13.6

zeros[K(s)] = $\begin{bmatrix} -1.50 \pm j0.72 \\ -3.14 \pm j2.23 \\ -20.00 \\ -20.00 \end{bmatrix}$ poles[K(s)] = $\begin{bmatrix} -9.05 \pm j24.77 \\ -14.66 \pm j42.87 \\ -29.60 \pm j11.91 \\ -47.89 \pm j21.65 \end{bmatrix}$
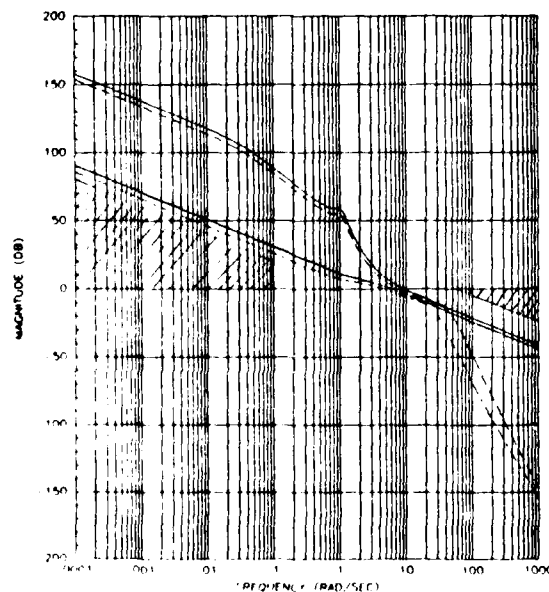

Fig 13.41   Singular Values of T_{LO} and KG, H = C

13-43

Fig 13.41 shows the recovery plots. The solid lines are T_{LQ}, and the dashed lines are KG. Obviously, our specs are met. Actually, the maximum bandwidth is only 8 rad/sec, so ρ could be decreased if so desired. Looking at a plot of GK as shown in Fig 13.42, we see that it also has high gain at low frequency, so we don't expect the problems we saw in the last design. The remaining data for this example is given in Table 13.7.
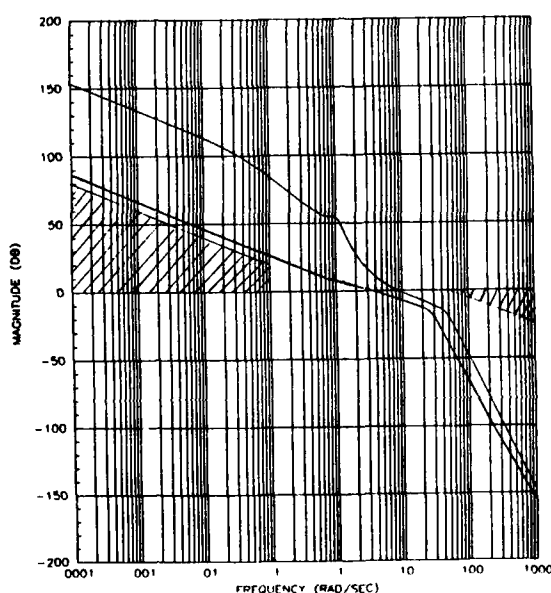

Fig 13.42   Singular Values of GK, H = C

The roll and sideslip responses to a roll command are shown in Fig 13.43. Other than a large overshoot in roll, they are very nice. Fig 13.44 shows the responses to a sideslip command. The roll response is quite large, but considerably better than before.
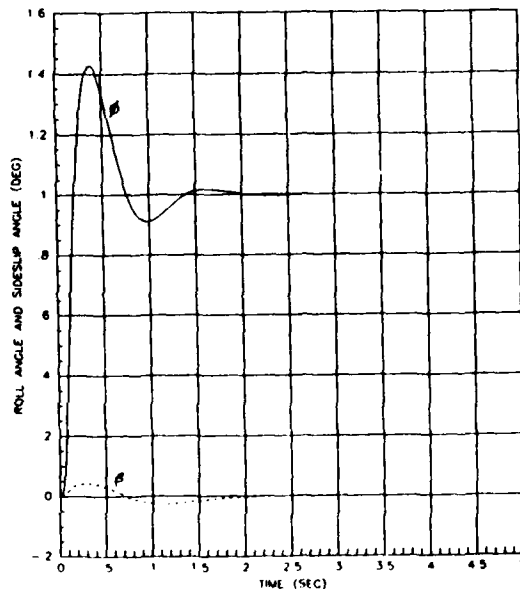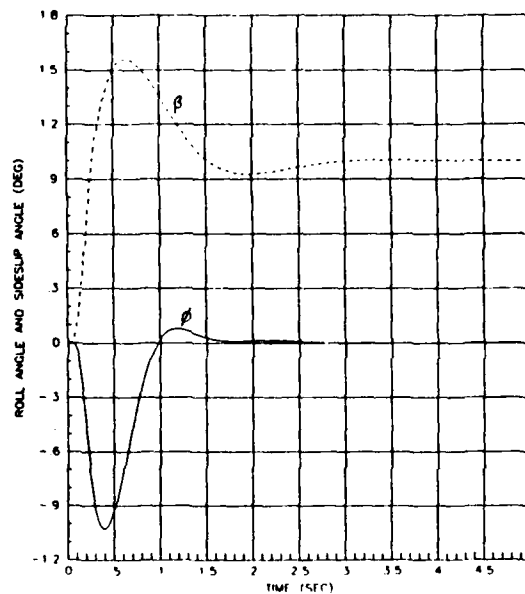
Fig 13.43 Time Responses to a Roll Command, H = C

Fig 13.44 Time Responses to a Sideslip Command, H = C

We chose this as our "best" case. To reduce the overshoot in roll

in Fig 13.43, a prefilter as given in (13.26) was added to the system.

The resulting responses are shown in Fig 13.45, which show a reduction

in overshoot to 12%. The corresponding surface deflections are shown in

Fig 13.46, which are quite reasonable for the aircraft. Finally, Fig 13.47 shows a comparison of $\ell_m(w)$ and $\underline{\sigma}[I + (KG)^{-1}]$, which clearly passes the robustness test. The corresponding gain and phase margins are very close to those given in the output design best case (equations (13.24) and (13.25)).
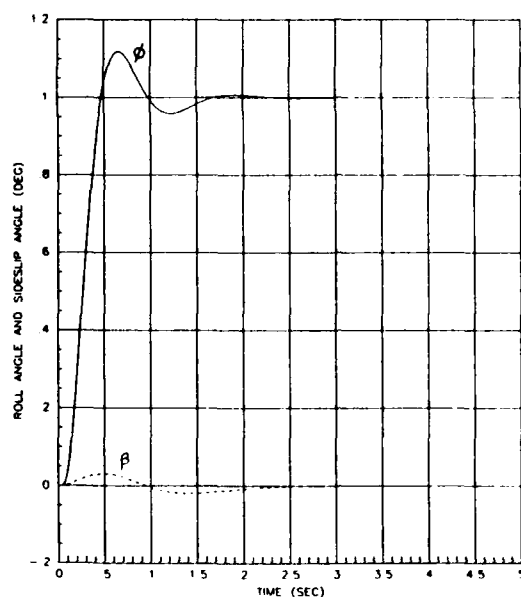

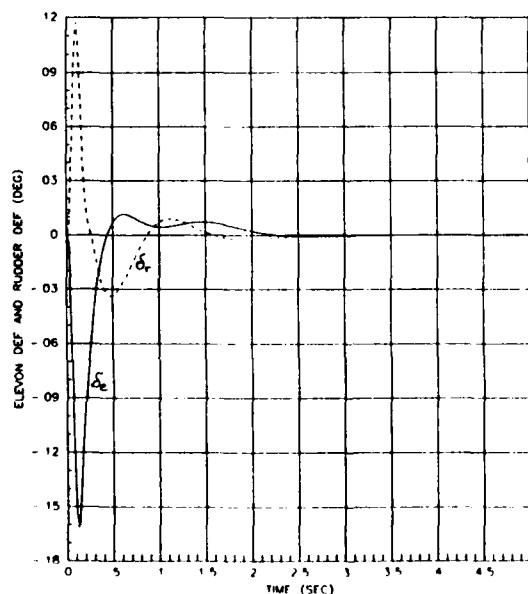Fig 13.45   Time Responses to a Prefiltered Roll Command, H = C

Fig 13.46   Control Surface Deflections due to a Prefiltered Roll Command
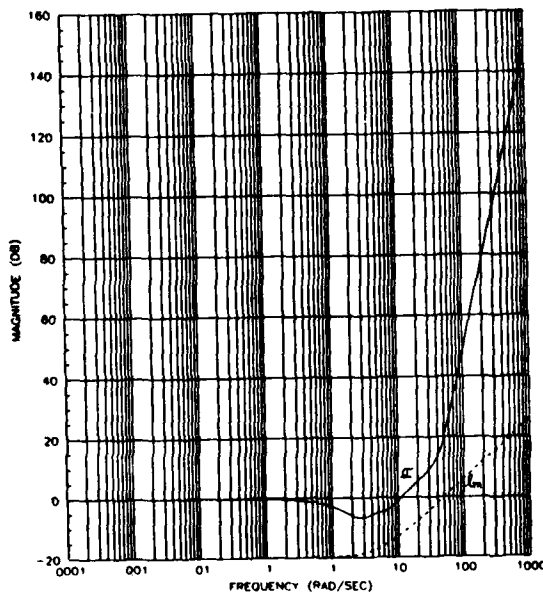
Fig 13.47 Singular Values of ℓ_m and $\underline{\sigma}[J + (KG)^{-1}]$

This concludes the example. The major point of the input breaking case was to show that requiring KG to meet performance bounds does not, in general, imply good command following. In the output breaking case, several points were made. First of all, the LQG/LTR method will do approximate plant inversion to produce desired loop shapes. The designer must be aware of this and not ask for loop shapes which require inversion of poles or zeros in "undesirable" s-plane locations. Coupled to this, it is important to look at both time and frequency domain information while doing the design. Overall, the method is extremely straightforward and easy to use, and will produce excellent results if the designer makes intelligent demands on the method. As a final disclaimer, none of these designs should be considered as final flight-ready controllers -- they are simply to illustrate the method. Actually, much better designs are possible, and we, the authors, challenge you to better them.

13-47

[13-1]   V. Mukhopadhyay and J. R. Newsome, "A Multiloop System Stability Margin Study Using Matrix Singular Values," Journal of Guidance Control and Dynamics, Vol 7, Sept-Oct, 1984, pp 582-587.

14. SUMMARY AND CONCLUSIONS

In these notes, we have attempted to provide a fairly comprehensive treatment of the LQG/LTR methodology. Chapter 2 reviewed some of the necessary mathematics and developed some of the required tools from multivariable linear systems theory. Chapter 3 then introduced the basic ideas behind multivariable robustness analysis, in both the frequency and time domains. Chapters 4 and 5 presented the concepts of using singular values to define a good multivariable loop shape, and discussed some of the limitations a designer must face in trying to achieve a given loop shape. The remaining chapters concentrate on developing the LQG/LTR method. After a brief review of optimal control in Chapter 6, Chapter 7 proves that all Linear Quadratic Regulators have guaranteed minimum gain and phase margins of $\frac{1}{2} < GM < \infty$ and $-60° < PM < 60°$, respectively. Unfortunately, since we can never measure all of our states in practice, and since the full-state feedback controller is unrealistic in the sense that it violates the Bode-Horowitz condition, we find that we must design an observer to estimate our states. Chapter 8 shows that a general observer has no guaranteed margins, but by cleverly choosing our estimator weights we can asymptotically recover our full-state margins. Using a Kalman filter for the observer, Chapters 9 and 10 formalize this procedure, to produce the LQG/LTR methodology. Chapter 11 then provides some useful tricks for producing desired loop shapes, while Chapter 12 formalizes the method mathematically and shows it is a specialized solution to an L_2/H_2 optimization problem. Chapter 13 then presents a detailed example for an aircraft.

Now let's examine some of the advantages and limitations of the
method. On the advantages side, the method is very powerful yet easily
finds (due to readily available computer software) the solution to an
important optimization problem. From a practical viewpoint, the method
allows performance requirements and uncertainty information to be
specified in the frequency domain. The resulting controller is
guaranteed to remain stable for all possible uncertainties within the
user-defined set. The trade-offs the designer must make along the way
are easily visible, and since the calculations are actually done in the
time domain, information on pole-zero locations is easy to obtain.

The limitations of the method hopefully have been highlighted
throughout the chapters. Many of them stem from the inherent
limitations of multivariable systems. First, through the example, we
have seen that lightly damped/low frequency poles or zeros in the plant
may cause problems with the closed-loop system response. The designer
must be aware of what random use of the method will do under these
conditions. As pointed out in [14-1], although the method is applicable
to nonminimum phase plants full state recovery is not possible. The
loop transfer function $G(s)$ will not converge to the full state loop
transfer function, rather, it will converge to the solution of a L_2/H_2
optimization problem. One of the biggest limitations of LQG/LTR as it
has been developed so far is that all uncertainties and performance
requirements must be reflected to one point in the system, whereas in
reality uncertainties may enter the system in different ways at various
points. Additionally, performance requirements are generally readily
modeled at the plant output. Also, the frequency domain does not lend

itself to real parameter variations using the singular value. These limitations could be overcome by using the structured singular value which allows multiple uncertainties rather than the singular value. Unfortunately, the LQG/LTR method has not been extended to using the structured singular value (it may be possible to do so).

To wrap things up, we would like to mention some other techniques to design a robust multivariable controller. This list is by no means comprehensive. One method, developed in Ref [14-2], allows stable factor uncertainties and uses a factorization approach to synthesize a robust controller. More on the factorization approach may be found in the excellent book by Vidyasagar [14-3]. An iterative method using an LQG formulation is presented in Ref [14-4] to design robust controllers when uncertainties in the state, input, and measurement distribution matrices are present. Uncertainties are expressed in terms of interval matrices in Ref [14-5], which then develops an iterative solution scheme. Quantitative feedback theory is used to shape loop transmissions in Ref [14-6], where uncertainties and performance specifications are transformed into templates that are used in conjunction with Nichols charts.

The methods in the previous paragraph deal primarily with uncertainties that are represented as real parameter variations. Another group of methods primarily using norm-bounded uncertainties are based on formal optimization procedures. For example, L_2/H_2 optimization (which we have not fully discussed in this report) can be used to recover the full state loop transfer function. The advantage of such an approach is that the controller uses lower gains (thus, lower actuator power) as opposed to the high gains obtained through LQG/LTR.

14-3

A detailed description of this particular optimization problem is the subject of upcoming papers by the authors. Another control system design method based upon $\infty/H\infty$ optimization is well described in [14-7] and its references. A new technique, informally called "μ-synthesis" (also discussed in [14-7]) by Doyle, may bridge the gap by allowing multiple uncertainties as well as real and norm-bounded uncertainty representations. We encourage you to examine these methods yourself and become involved in this growing area of research.

References

[14-1] G. Stein and M. Athans, "The LQG/LTR Procedure for Multivariable Feedback Control Design", 1984 American Control Conference, San Diego, CA., June 1984 (paper available from the authors).

[14-2] M. Vidyasagar and H. Kimura, "Robust Controllers for Uncertain Linear Multivariable Systems", Proc. IFAC World Congress, Budapest, Hungary 1984.

[14-3] M. Vidyasagar, Control System Synthesis: A Factorization Approach

[14-4] R. K. Yedavalli, "Time Domain Control Design for Robust Stability of Linear Regulators - Application to Aircraft Control", American Control Conference, Boston, MA, June 1985.

[14-5] R. J. Evans and Xie Xianya, "Robust Regulator Design", Int. J. Control, Vol. 41, No. 2, 1985, pp 461-476.

[14-6] I. M. Horowitz, "Quantitative Feedback Theory", IEE Proceedings, Vol. 129, November 1982.

[14-7] J. C. Doyle, "Matrix Interpolation Theory and Optimal Control", Ph.D. Dissertation, University of California, Berkeley, Dec 1984.